

**All-in-one microsystem for long-term cell culturing and  
real-time chip-level lensless microscopy**

Dissertation  
zur Erlangung des Grades  
der Doktorin der Naturwissenschaften  
der Naturwissenschaftlich-Technischen Fakultät  
der Universität des Saarlandes

von

Wei Li

Saarbrücken  
2017



Tag des Kolloquiums: 17.01.2018

Dekanin/Dekan: Univ.-Prof. Dr. rer. nat. Guido Kickelbick

Mitglieder des  
Prüfungsausschusses: Univ.-Prof. Dr. rer. nat. Günter R. Fuhr  
Univ.-Prof. Dr. rer. nat. Helmut Seidel  
  
Univ.-Prof. Dr. rer. nat. Andreas Schütze  
  
Dr. Samuel Grandthyll



# Erklärung

Hiermit versichere ich an Eides statt, dass ich diese Arbeit nur unter Verwendung der angegebenen Quellen und Hilfsmittel eigenständig angefertigt habe.

Saarbrücken, June 29, 2017

Wei LI



# Peer-reviewed Publications

## Related to the thesis:

- W. LI, Thorsten Knoll, Hagen Thielecke, "On-chip integrated lensless microscopy module for optical monitoring of adherent growing mammalian cells", Proc. IEEE EMBS 2010, Buenos Aries, Argentina, Oral Presentations in regular session and student paper competition  
*Student paper competition finalist Prize*  
*IEEE EMB and US NSF sponsored, 32<sup>nd</sup> IEEE EMBC, 2010*
- W. LI, Thorsten Knoll, Adam Sossala, Heiko Büth, Hagen Thielecke, "On-chip integrated fluorescent microscopy/Spectroscopy module for cell-based sensors", Proc. SPIE BIOS 2011, San Francisco, USA, Oral presentation
- Y. Kohl, Y. Xu, A. Shah, W. Li, K. Riehemann, H. von. Briesen, S. Wagner, T. Velten and T. Knoll, "Miniaturized Incubator Microscope for long-term Cultivation, Imaging and Characterization of Cells in-vitro", Lab chip, 2015 (submitted)

## Publications before:

- W.J. Wang, X.L. Liu, W. LI, etc. "A Blue-violet Enhanced BDJ Photo-detector and its Applications in the Probe Chip Measurements of the LEDs for Solid-state Lighting", Sensors & Actuators: A. Physical, 136, 168-172, 2007
- X. L. Liu, W. J. Wang, H. R. Ren, W. LI, etc. "Water Quality Monitoring using a Novel Colorimetric Method Based on a Semiconductor Optical Wavelength Sensor", Measurement, 42(1), 51-56, 2009
- W. LI., K. L. H. R. Ren etc. "Color measurement for RGB white LEDs in solid-state lighting using a BDJ photodetector", Displays, 30, 107-113, 2009



# Acknowledgements

*Firstly, I would like to appreciate Prof. Fuhr, Dr. Velten and Dr. Thielecke. Thanks for giving me the opportunity, guidance and great help along my study and working in Fraunhofer IBMT. I also would like to appreciate the support and inspiration from my colleagues.*

*For whom I really want to appreciate are my parents in China, for all you have given me all the time out of your best, and my parents-in-law here, for your support and encourage out of love. Especially my husband, for your company, understanding, and encourage helping me facing difficulties. You are always my source of happiness and inspirations.*



## Abstract

The study is to concept, develop and evaluate an all-in-one microsystem with combined long-term animal cell culturing and real-time chip-level lensless microscopy functions suitable for applications in cell biology studies, and at the point-of-use. The microsystem consists of a 5 megapixel CMOS image sensor, a disposable microchip for cell culture, heating elements and LED illumination. The overall size is only 40 mm x 40 mm x 50 mm. The disposable microchip for cell culture is composed of a polymer microfluidic interface and a silicon micro-cavity chip with a 1  $\mu\text{m}$  thick 1 mm x 1 mm transparent  $\text{Si}_3\text{N}_4$  bottom membrane, which is directly placed onto the image sensor surface. Under the collimated LED illumination, the optical resolution of the lensless imaging module is only dependent on the digital resolution of the image sensor, which amounts to 3.5  $\mu\text{m}$  (double pixel pitches). The imaging quality is proven comparable to a 4x optical microscope without image computation or processing. Both the morphologies of different cell cultures (L929, A549 and T47D) and the single cells with colorimetric staining can be clearly visualized in real time. With the additional deposition of an interference filter on the image sensor surface, fluorescence spreading cells in culture are observed on the chip under a common blue LED illumination. The temperature for the incubating module is controlled at  $37\pm 0.2^\circ\text{C}$  in the room environment. Mammalian cells (L929 and A549) are cultured with conventional culture medium and monitored under the time-lapse lensless microscopy by the all-in-one microsystem up to 5 days outside a laboratory incubator. Very fast operational processes, such as cell loading, passaging and staining, have been readily carried out and monitored in real-time by the platform. Besides cell cultures in monolayer, the formation of 3D clusters of L929 cells has also been demonstrated and recorded under time-lapse lensless microscopy by using the all-in-one microsystem.

## Abstract (German)

Das Ziel der vorliegenden Dissertation ist die Konzeption, Entwicklung und Evaluation eines All-in-One-Mikrosystems mit der Kombination aus Langzeit Kultivierung von Tierzellen und Echtzeit Linsenloser Mikroskopie Funktionen auf Chip Level, die für Anwendungen in zellbiologischen Studien sowie für Point-of-use geeignet sind. Das Mikrosystem besteht aus einem 5 Megapixel CMOS-Bildsensor, einem Einweg-Mikrochip für die Zellkultur, Heizelementen sowie einer LED-Beleuchtung. Die Gesamtgröße beträgt nur 40 mm x 40 mm x 50 mm. Der Einweg-Mikrochip für die Zellkultur besteht aus einer polymeren, mikrofluidischen Grenzfläche und einem Silizium-Mikrohohlraum-Chip mit einer 1 µm dicken und 1 mm x 1 mm transparenten Si<sub>3</sub>N<sub>4</sub>-Bodenmembran, die direkt auf die Bildsensoroberfläche aufgesetzt wird. Unter der kollimierten LED-Beleuchtung ist die optische Auflösung des linsenlosen Abbildungsmoduls nur von der digitalen Auflösung des Bildsensors abhängig, was 3,5 µm beträgt (Doppelpixelabstände). Die Bildqualität ist vergleichbar mit einem 4x optischen Mikroskop ohne Bildberechnung oder Verarbeitung. Sowohl die Morphologien verschiedener Zellkulturen (L929, A549 und T47D) als auch die einzelnen Zellen mit farbmeterischer Färbung können in Echtzeit deutlich sichtbar gemacht werden. Mit der zusätzlichen Abscheidung eines Interferenzfilters auf der Bildsensoroberfläche werden fluoreszenzverteilende Zellen in Kultur auf dem Chip unter einer gemeinsamen blauen LED-Beleuchtung beobachtet. Die Temperatur für das Inkubationsmodul wird bei  $37 \pm 0,2$  °C in der Raumumgebung festgelegt. Säugetierzellen (L929 und A549) werden mit herkömmlichem Kulturmedium kultiviert und unter der Zeitrasterlinsenmikroskopie durch das All-in-One-Mikrosystem bis zu 5 Tage außerhalb eines Laborinkubators überwacht. Sehr schnelle operative Prozesse wie z. B. Zellbeladung, Durchfluss und Färbung wurden in Echtzeit durch die Plattform durchgeführt und überwacht. Neben den Zellkulturen in der Monoschicht wurde auch die Bildung von 3D-Clustern von L929-Zellen in Zeitraster bei lichtempfindlicher Mikroskopie unter Verwendung des All-in-One-Mikrosystems nachgewiesen und aufgezeichnet.

# Table of Contents

TABLE CAPTIONS .....	IV
ABBREVIATIONS .....	V
SYMBOLS .....	VII
<b><u>1 INTRODUCTION .....</u></b>	<b><u>1</u></b>
<b>1.1 PROBLEM DESCRIPTION.....</b>	<b>1</b>
<b>1.2 CRITICAL REVIEW OF THE RELATED STATE-OF-THE-ARTS.....</b>	<b>3</b>
1.2.1 <i>IN VITRO</i> CELL CULTURE TECHNIQUE.....	3
1.2.2 LIVE CELL IMAGING TECHNIQUE .....	6
1.2.3 MICROSYSTEMS FOR CELL CULTURE AND CELL-BASED ASSAY .....	16
1.2.4 ON-CHIP LENSLESS IMAGING METHODS.....	21
<b>1.3 OBJECTIVES OF THE STUDY AND APPROPRIATE SOLUTIONS .....</b>	<b>28</b>
1.3.1 GOAL AND OBJECTIVES OF THE STUDY .....	28
1.3.2 WORKING PLAN OF THE STUDY .....	29
<b><u>2 THEORIES AND ANALYSIS .....</u></b>	<b><u>30</u></b>
<b>2.1 SUSTAINING PHYSIOLOGICAL ENVIRONMENT OUT OF INCUBATOR .....</b>	<b>30</b>
<b>2.2 PARAMETER CALCULATIONS FOR OPERATING STAND-ALONE MICROFLUIDICS .....</b>	<b>31</b>
<b>2.3 OPTICAL CONFIGURATIONS APPLIED BY STANDARD MICROSCOPY .....</b>	<b>34</b>
<b>2.4 THEORETICAL RESOLUTION OF “VERY NEAR-FIELD” SHADOW IMAGING.....</b>	<b>36</b>
<b><u>3 MATERIALS AND METHODS.....</u></b>	<b><u>40</u></b>
<b>3.1 ESTABLISHING A STAND-ALONE MICROFLUIDIC INCUBATING SYSTEM FOR CELL CULTURE .....</b>	<b>40</b>
3.1.1 MODIFICATION TO A PLASTIC MICRO-CHANNEL SLIDE BASED SETUP.....	40
3.1.2 FLOW RATE DETERMINATION FOR THE ESTABLISHED MICRO-CHANNEL SLIDE BASED MICROFLUIDIC SYSTEM .....	43
3.1.3 TEMPERATURE CONTROL FOR THE MICRO-CHANNEL BASED SLIDE .....	45

<b>3.2</b>	<b>CONSTRUCTING A COMPACT “DESKTOP” AUTOMATIC MICROSCOPE FOR TIME-LAPSE CELL IMAGING..</b>	<b>46</b>
3.2.1	OPTICAL AND MECHANICAL CONSTRUCTION OF THE COMPACT MICROSCOPE.....	46
3.2.2	ELECTRONICS AND CONTROLLER FOR THE HARDWARE AUTOMATION .....	51
3.2.3	CONTROL SOFTWARE FOR THE AUTOMATED IMAGING FUNCTIONS .....	52
<b>3.3</b>	<b>REALIZATION OF THE “VERY NEAR-FIELD” SHADOW IMAGING CONFIGURATION.....</b>	<b>55</b>
3.3.1	MEMS MICROCHIPS WITH TRANSPARENT BOTTOM MEMBRANE.....	55
3.3.2	PROCESSING AND MODIFICATIONS TO THE IMAGE SENSORS .....	58
<b>3.4</b>	<b>ESTABLISHING A STAND-ALONE CELL CULTURE MICROSYSTEM ADAPTED TO THE “VERY-NEAR FIELD” SHADOW IMAGING .....</b>	<b>63</b>
3.4.1	INTEGRATION OF MICROFLUIDICS WITH MICRO-CAVITY CHIPS.....	63
3.4.2	PARYLENE C COATING ON THE Si/PDMS MICROFLUIDIC CHIP .....	66
3.4.3	TEMPERATURE CONTROL FOR THE CELL CULTURE INSIDE THE Si/PDMS MICROFLUIDIC SYSTEM ....	67
<b>3.5</b>	<b>PREPARATION OF CELL CULTURES .....</b>	<b>72</b>
<b>4</b>	<b><u>EXPERIMENTS .....</u></b>	<b><u>73</u></b>
<b>4.1</b>	<b>TESTING THE STAND-ALONE CELL INCUBATING SYSTEM .....</b>	<b>73</b>
4.1.1	MICRO-CHANNEL BASED STAND-ALONE CELL CULTURE MICROFLUIDIC SETUP .....	73
4.1.2	PREPARATION OF THE MICROFLUIDICS.....	76
4.1.3	OPERATIONS OF CELL CULTURE WITH THE MICROFLUIDIC SYSTEM.....	76
<b>4.2</b>	<b>TESTING THE COMPACT MICROSCOPE SYSTEM .....</b>	<b>78</b>
4.2.1	IMAGING SETUP OF THE COMPACT AUTOMATIC MICROSCOPE.....	78
4.2.2	TEST OF THE IMAGING ABILITY OF THE “DESKTOP” MICROSCOPE .....	79
4.2.3	STABILITY TEST OF THE “DESKTOP” MICROSCOPE FOR TIME-LAPSE IMAGING .....	79
4.2.4	IMAGING GFP CELLS BY THE “DESKTOP” MICROSCOPE .....	80
<b>4.3</b>	<b>TESTING THE “VERY-NEAR FIELD” SHADOW IMAGING MODULE .....</b>	<b>82</b>
4.3.1	LENSLESS “VERY-NEAR FIELD” SHADOW IMAGING SETUP .....	82
4.3.2	TESTING THE OVERALL OPTICAL RESOLUTION OF THE “VERY-NEAR FIELD” SHADOW IMAGING SYSTEM .....	83
4.3.3	TESTING OF THE “VERY-NEAR FIELD” COLOR SHADOW IMAGING OF CELLS.....	84
4.3.4	TESTING THE “VERY-NEAR FIELD” FLUORESCENCE IMAGING OF CELLS.....	85
<b>4.4</b>	<b>TESTING THE ALL-IN-ONE CELL CULTURE-SHADOW IMAGING MICROSYSTEM .....</b>	<b>86</b>
4.4.1	ALL-IN-ONE CELL CULTURE-IMAGING MICROSYSTEM SETUP.....	86
4.4.2	PREPARATION OF THE MICROFLUIDICS OF THE ALL-IN-ONE MICROSYSTEM .....	88
4.4.3	SEEDING CELLS INTO THE ALL-IN-ONE MICROSYSTEM .....	89
4.4.4	INCUBATING CELLS INSIDE THE ALL-IN-ONE MICROSYSTEM .....	89
4.4.5	LIVE-DEAD STAINING OF CELL CULTURE IN THE ALL-IN-ONE MICROSYSTEM .....	90
4.4.6	PASSAGING ADHERENT CELLS CULTURED IN THE ALL-IN-ONE MICROSYSTEM .....	91
4.4.7	3D CELL CULTURE BY THE ALL-IN-ONE MICROSYSTEM.....	91
<b>5</b>	<b><u>RESULTS.....</u></b>	<b><u>92</u></b>

<b>5.1</b>	<b>CELLS CULTURED IN THE STAND-ALONE INCUBATING SYSTEM .....</b>	<b>92</b>
5.1.1	TIME-LAPSE IMAGES OF CELL CULTURE IN A SINGLE CHANNEL .....	92
5.1.2	TIME-LAPSE IMAGES OF CELL CULTURES IN DOUBLE CHANNELS .....	95
<b>5.2</b>	<b>PERFORMANCE OF THE “DESKTOP” AUTOMATIC MICROSCOPE .....</b>	<b>98</b>
5.2.1	IMAGING QUALITY OF THE “DESKTOP” AUTOMATIC MICROSCOPE .....	98
5.2.2	STABILITY OF THE AUTOMATIC MICROSCOPY OPERATION .....	100
5.2.3	IMAGES OF CELL CULTURES BY THE “DESKTOP” MICROSCOPIC OPTICS .....	100
<b>5.3</b>	<b>IMAGING CAPABILITIES OF THE “VERY-NEAR FIELD” SHADOW IMAGING CONFIGURATION .....</b>	<b>102</b>
5.3.1	IMAGING QUALITY OF THE “VERY-NEAR FIELD” SHADOW IMAGING .....	102
5.3.2	“VERY-NEAR FIELD” SHADOW IMAGES OF DIFFERENT CELL MORPHOLOGIES .....	105
5.3.3	“VERY-NEAR FIELD” SHADOW IMAGES OF LIVE-DEAD STAINING OF CELLS .....	108
5.3.4	“VERY-NEAR FIELD” FLUORESCENT IMAGES OF VIABILITY TEST OF CELLS.....	110
<b>5.4</b>	<b>CELL CULTURE AND TESTING BY THE ALL-IN-ONE CELL CULTURE-SHADOW IMAGING MICROSYSTEM ....</b>	<b>117</b>
5.4.1	REAL-TIME SHADOW IMAGES OF FAST CELL LOADING PROCESS .....	117
5.4.2	CELL RESPONSES BY TEMPERATURE ADJUSTMENT.....	120
5.4.3	REAL-TIME SHADOW IMAGES OF LIVE-DEAD COLORIMETRIC STAINING .....	122
5.4.4	CELL CULTURE AND HARVESTING BY THE ALL-IN-ONE MICROSYSTEM.....	123
5.4.5	3D CELL CULTURE AND TIME-LAPSE IMAGING BY THE ALL-IN-ONE MICROSYSTEM.....	128
<b>6</b>	<b><u>DISCUSSIONS .....</u></b>	<b><u>131</u></b>
<b>6.1</b>	<b>“MICRO INCUBATOR” OR A STAND-ALONE MICROFLUIDIC CELL INCUBATING SYSTEM .....</b>	<b>131</b>
<b>6.2</b>	<b>COMPACT “DESKTOP” AUTOMATIC MICROSCOPE .....</b>	<b>132</b>
<b>6.3</b>	<b>REAL-TIME CHIP-LEVEL LENSLESS MICROSCOPE .....</b>	<b>132</b>
<b>6.4</b>	<b>ALL-IN-ONE CELL CULTURING-IMAGING MICROSYSTEM:.....</b>	<b>133</b>
<b>6.5</b>	<b>OUTLOOKS OF THE STUDY .....</b>	<b>134</b>
6.5.1	ENGINEERING WORKS TO THE SINGLE ALL-IN-ONE CELL CULTURE-MICROSCOPY DEVICE.....	134
6.5.2	REALIZATION OF AN ALL-IN-ONE CELL CULTURE-MICROSCOPY ARRAY-FORMED INSTRUMENT .....	135
<b>7</b>	<b><u>CONCLUSIONS .....</u></b>	<b><u>136</u></b>
	<b><u>REFERENCES .....</u></b>	<b><u>138</u></b>

# Table Captions

Table 2.1	Physical and chemical environment comparison
Table 2.2	Corresponding thickness of a transparent material for a given optical resolution
Table 3.1	Ibidi micro-channel specifications
Table 3.2	Barrier properties of materials for microfluidics
Table 3.3	Price list of the optical and mechanical components for constructing the “desktop” automatic microscope
Table 3.4	Callendar-Van Dusen Equation (IEC751 Class B)
Table 4.1	Calibration of the fluorescence imaging of the “desktop” microscope

# Abbreviations

AI	Analog Input
AO	Analog Output
AOI	Angel of Incidence
A549	Human lung adenocarcinoma epithelial cell line
CCD	Charge-Coupled Device (digital image sensor)
CMOS	Complementary Metal Oxide Semiconductor (image sensor)
CHO	Chinese Hamster Ovary cell line
CLCC	Ceramic Leaded Chip Carrier ceramic
CNC	Computer Numerical Control
DAQ	Data Acquisition
DFR	Dry Film Resist
DI	Digital Input
DO	Digital Output
FEM	Finite Element Method
FCS	Fetal Calf Serum
FITC	Fluorescein Isothiocyanate
FDA	Fluorescein Diacetate
FP	Fluorescent Proteins
FWHM	Full Width Half Maximum
GFP	Green Fluorescence Protein
GPU	Graphic Processing Unit
HEPES	4-(2-hydroxyethyl)-1-piperazineethanesulfonic acid
IR	Infrared
ID	Inner Diameter
ITO	Indium Tin Oxide
LED	Light Emitting Diode
L929	mouse fibroblast cell line cell line
LWD	Long Working Distance
MAX	Measurement & Automation Explorer
MCU	Microcontroller Unit
MEMS	Micro electro mechanical system
NA	Numerical Aperture
NP	Nano Particle
OD	Outer Diameter
OP	Operational Amplifier
PDMS	Polydimethylsiloxane (silicone rubber)
Parylene	Poly-para-xylylenes
PECVD	Plasma Enhanced Chemical Vapor Deposition
PGMEA	1-Methoxy-2-propyl acetate)
PID	Proportion-Integration-Differentiation
PSF	Point Spread Function
RA	Right Angel
RIE	Reactive Ion Etching
RTD	Resistive Temperature Detector
SU-8	a commonly used epoxy-based negative photoresist
T47D	human breast columnar epithelial tumor cells

TSCs  
UV

Timestamp Counters  
Ultra Violet

# Symbols

$T_{macro}$	medium turnover time of conventional cell culture
$h$	height of the micro-channel
$w$	width of the micro-channel
$L$	length of the micro-channel
$t_r$	time scale of the cell reaction or substance consumption
$t_d$	time scale of the lateral diffusion process
$t_c$	time scale of convection flow
$\sigma$	cell density on the micro-channel floor
$\Delta S$	unit area of the micro-channel floor
$K_m$	unit cellular mass consumption rate
$C_0$	initial concentration of the substance
$D$	diffusivity of the substance
$\bar{v}$	average flow velocity
$T_{micro}$	medium turnover time of cell culture in microsystems
$Q$	flow rate
$\tau$	shear stress
$\mu$	viscosity of the liquid
$z$	coordinate along the micro-channel height
$v$	liquid velocity
$\tau_{single}$	shear stress on one single cell on the micro-channel floor
$\tau_{population}$	shear stress on cell population on the micro-channel floor
$R$	optical resolution
$b_{min}$	the minimum resolved dimension by the optical system
$\lambda$	wavelength of the illumination
$s$	mask-to-wafer distance in the optical lithography
$n_{air}$	refractive index of the air
$d_i$	thickness of the interlayered optical material
$n_i$	refractive index of the interlayered optical material
$d_{max}$	theoretically allowed maximum thickness of the interlayered optical material



# 1 Introduction

## 1.1 Problem description

*In vitro* animal cell culture together with cell-based assays is not only an essential tool in life science and clinical researches, but has been also increasingly applied in biotechnological and pharmaceutical industries. For example, mammalian cells are widely used in drug screening, regenerative medicine. Chicken embryo cells, which are the most frequently used avian cells, are important in stem cells research and vaccine production [1] [2]. Fish cells have found potential sensing applications in eco-and food-toxicity tests [3]. Different cell types require different physiological environments. Mammalian cells need to be cultured in an incubator with 37°C, more than 95 % humidity and 5–10 % CO<sub>2</sub> atmosphere. The optimal temperature for chicken embryo cells is 37–39°C [4]. Fish cells are usually kept at 15–21°C (coldwater fishes) or 25–35°C (warmwater fishes) [5]. Insect cell lines grow best at 26–28 °C [6]. Conventionally, the cell culture is bathed into the “bulky” medium layer (of several millimeters) and cultured in the same static medium for three to four days inside a large incubator. The incubator provides a specific temperature and gaseous condition, usually optimized for mammalian cells. Culture vessels are only taken out for necessary microscopy inspections, since any environmental changes could interfere with cell growth or cell activity. Characterization of cells is based on their collective responses, but individual dynamic cellular responses could not be recorded. Usually, many testing conditions need to be carried out, each with multiple culture samples, in order to generate statistically relevant results. Conventional cell culture not only consumes not only large amounts of reagents and laboratory materials, but also requires a great deal of repeated laboratory work. With the rapid developments in the life science and pharmaceuticals related fields, there is an increasing need for systems that can provide non-invasive real-time monitoring of cell cultures which are sustained in more refined and flexible culturing environments for long-term investigations.

Live cell imaging technique has been developed and commercially available for the real-time observation and characterization of living cells in culture. This technique is a combination of the microscopy and the incubating functions. It can be a microscope-based system equipped with a scaled incubator; or an incubator-based system, inside of which the optical imaging components are installed. In more advanced fully automatic cell culture systems based on the sterile bench, robotic arms are further integrated for vessel transportation and liquid handling. Since the humid acid incubating environment is detrimental to those mechanical, optical and electronic instruments, the live cell imaging

## 1. Introduction

systems are practically aimed for recording special fast cellular events with high optical resolution microscopy and fine temporal resolution, but are not ideal for long-term investigations. Moreover, these systems are rather bulky, expensive and associated with high running costs.

Microfabrication technologies provide possibilities of the fabrication of miniaturized cell culture systems with more refined and controllable microenvironments. There have been many reports about cells cultured in planar as well as 3D structures by using microchips of various designs. Additionally, on-chip integrated biosensors can provide on-line monitoring as well as subsequent cellular analysis by electrochemical or optical methods in a simple and inexpensive manner. Such systems can be applied in analytical chemistry and biological related disciplines [7]-[12]. However, besides other periphery supporting parts for a microchip, the imaging of a microchip still relies on the optical microscope to ensure a proper sampling, observation and verification of cell responses. Since for building a standard microscope, expensive optical elements need to be precisely and stably arranged with certain distances, it will be not easy to scale down an optical microscope to the level comparable with that of a microchip.

With the rapid advancement of digital imaging technology in semiconductor image sensors, many works have been focused on the development of compact and low-cost so called “lensless” or “lensfree” systems for imaging cells and microfluidics without using optical lens. In brief, the cell sample is placed directly in contact or close to the image sensor surface [13] [14], and therefore, the best optical resolution of the shadow image will be the digital resolution (amounts to double pixel pitches) of the image sensor, and the distance between the object and the image sensor will also have an influence on the resolution due to the optical diffraction effect [15] [16]. To achieve a better imaging quality, complicated image acquisition methods, illumination schemes and complicated computational imaging reconstruction algorithms have been developed. However, the computing algorithms can vary according to different samples, and the image processing speed is often impossibly supportive of observing cells and microfluidics operations in real time [13] [17]-[19]. Moreover, the integration of such lensless imaging configuration with miniaturized cell culture systems has not been well addressed for the long-term investigations where biocompatibility, disposability and stability issues need to be considered.

Therefore, the goal of this thesis is to concept, develop and evaluate an all-in-one microsystem with combined long-term animal cell culturing and real-time microscopy functions suitable for applications in cell biology and point-of-use diagnosis. Cell culture operations, such as liquid handling, incubating and processing, can be readily carried out outside a laboratory incubator by this miniaturized cell culture system, and individual cell activities can be monitored and characterized for long-term investigations.

## 1.2 Critical review of the related State-of-the-arts

Before describing the study in detail, the corresponding state-of-the-art will be briefly introduced and critically reviewed in this chapter. In the following paragraphs, *in vitro* cell culture technique, live cell imaging technique and related various instruments, microsystems applied in cell culture and processing, as well as novel on-chip lensless cell imaging methods will be addressed respectively. By focusing on practical problems, technical hurdles and opportunities with cell culture and cell-based assays, the roadmap of the thesis will gradually become more specific and clear.

### 1.2.1 *In vitro* cell culture technique

Compared to direct and specific target-based biochemical measurements, cell-based models have emerged as a more physiological alternative in recent years. Cell-based sensors utilize biological cells as the transduction element. External stimuli or changes in cellular microenvironment can perturb the physiological activities of biological cells. Based on these cellular phenotypes, it allows for the screening, monitoring, and measurement of the functionality or toxicity of compounds, and also allows probing the presence of pathogens or toxins in clinical, environmental, or food samples. Cell based assays have become an indispensable approach for functional sensing and diagnostics. They represent approximately half of all screenings currently performed in the pharmaceutical and biotechnological industries and academic researches. A major focus of cell culture technology has been in developing cell-based high-throughput screening (HTS) platforms capable of providing higher value data on potential drug targets and advancing cell biology [20]-[22].

#### 1.2.1.1 Physiological environment essential for cell culture *in vitro*

Cell culture needs to be performed in a sterile manner. Cells are usually kept in culturing media to sustain the essential physiological environment for them. This environment should be provided with specific and stable physiochemical conditions. Besides requirements of temperature and osmotic pressure, most animal cells also require the pH condition in the range of 7.2–7.4. There are two buffering systems available for the medium pH value regulation:  $\text{CO}_2/\text{HCO}_3^-$ , and HEPES. The former has been very commonly used and needs to be maintained in an atmosphere of 5–10%  $\text{CO}_2$ . HEPES (4-(2-hydroxyethyl)-1-piperazineethanesulfonic acid) is not required a controlled gaseous atmosphere. But HEPES is not well accepted by many biologists, because of its potential toxic effects to cells at higher concentrations [23]. Ambient light could cause the production of  $\text{H}_2\text{O}_2$  in the HEPES solution [24]. Generally, the animal cell culture uses bicarbonate/ $\text{CO}_2$  buffering system. Meanwhile, an incubator is required not only for maintaining a proper atmospheric condition, but also to provide the optimal temperature and humidity level for the cultured cells bathed in culture medium. This environment is necessary for cell growth but harsh for electrical, optical and mechanical instruments.

## 1. Introduction

### 1.2.1.2 Optical microscopy for the observation and characterization of cells in culture

The optical microscope is nowadays still the essential tool for the observation and characterization of cells in both qualitative and quantitative ways. The use of microscopy in biological research was introduced in the middle 17th century and is today still used on daily basis in most biological laboratories [25]. Though other electrical monitoring methods like impedance measurements for both cell layer and single cell have been developed, to calibrate or verify the results, optical microscopy is still required as a standard complementary [26] [27]. Light microscopy is often used to provide information such as cell morphology, proliferation, and motility if with time-lapse image sequence. Plenty of colorimetric staining reagents are available for on-site diagnosis of cell status such as necrosis, apoptosis and differentiation. As the great progress in the development of synthetic fluorescent dyes and fluorescent proteins, the scope of the fluorescence microscopy has been extended from individual cells to the intracellular molecular level. Besides end-point assays, transfected fluorescent proteins (FP) with a selection of diverse colors makes possible the real-time analysis of selectively visualized molecular events (by expression, redistribution, translocation) with fluorescent reporters' fusion in living cells [28]-[30].

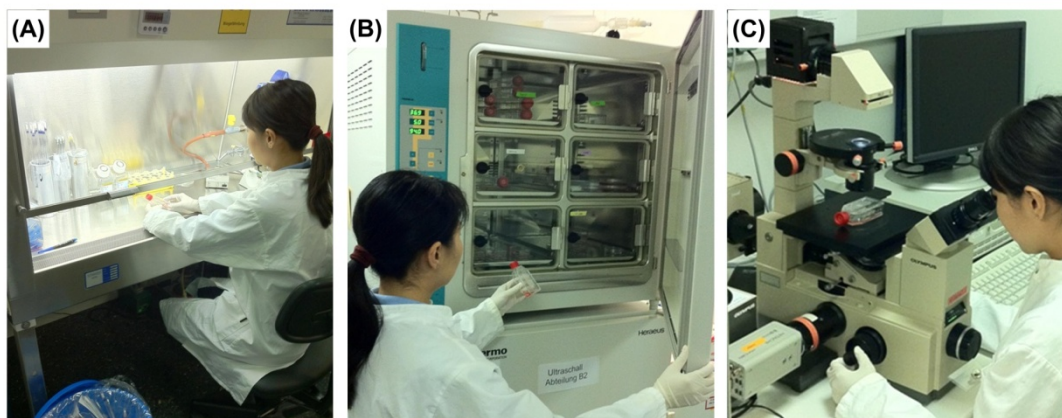


**Figure 1.2.1** Photographs showing general operations required for cell culture in the lab: (A) liquid handling, (B) incubating, and (C) microscopy of adherent mammalian cells culture in a flask. (The photographs were taken in the cell culture lab 1 of Fraunhofer IBMT, St. Ingbert, Germany, 2011)

### 1.2.1.3 Cell culture operations

Cell culture and assays so far are still operated manually in most biological and clinical laboratories. Briefly speaking, cell culture in lab generally requires three kinds of operations: (A) liquid handling in a sterile laminar flow bench; (B) cells culturing in an incubator and (C) cell observation under an optical microscope. The operations are shown in the photographs in Figure 1.2.1. Cells are seeded manually in plastic culture flasks, petri dishes or multi-well plates (6, 12, 24, and 96- format) with cell culture treated substrate,

filled with nutrient buffer (about 3-5 mm in depth). For instance, with mammalian cells, these vessels need to be placed inside a standard CO<sub>2</sub> incubator (37°C, 95% or more humidity and 5% CO<sub>2</sub>). After a day or so, cells in culture will be shortly taken out and observed under a microscope. As to the above described cell culture operations, following issues should be noticed and improved:

### **Uncontrollable culturing microenvironment for cells**

During the 3 to 4 days of culture there is no medium change. Mass transportation is mainly aided mainly by convection flow because of the liquid-air interface in macro-scale culture vessels [31]. The physiochemical environment of culture medium for cells is degrading along the culture time and not reproducible or predictable in perspective of single cells. Compared to cells *in vivo*, the nutrients supply and waste removal are realized via circulation networks, and the mass transportation for most cells in tissue is dominated by diffusion around their microenvironments [8].

### **Inflexible on-line imaging of cells**

Observations of cell responses by taking culturing vessels out of the incubator can influence the experiment and could cause stress to cells. Slight variation in environmental parameters can have a significant impact on assay performance [32]. Therefore, the times and duration of the observations should be minimized. This does not allow for the tracking of dynamic responses of individual cells, and special cellular events could be often missed. The results are therefore analyzed based on the collective responses of cell populations imaged on different testing points.

### **Time and cost inefficiency**

To find the end-point of an assay, usually many conditions (dosing concentration, exposure duration) are needed to be tested, and under each testing condition, multiple culture samples are required to generate results statistically. Usually the experiments need to be carried out in several batches to gradually narrow down the conditional parameters before approaching to the end-point. Therefore, conventional cell culture and cell-based assays consume not only large quantity of reagents and laboratory consumable materials, but also a great deal of repeated labor work and time is required. Cell culture and cell-based assays have never been an easy and efficient task.

## 1. Introduction

### 1.2.2 Live cell imaging technique

Live cell imaging technique has been developed and commercially available for the real-time observation and characterization of living cells in culture. This technique is a combination of the microscopy and the incubating functions. Continuous optical microscopy observation of living cells in culture has been extended to hours or even to days. The dynamic cell responses and behaviors can be characterized and analysis in real time. Although there are many commercially available systems with various designs, the instrumental configurations can be generally characterized here in three types:

1. Microscope-based system
2. Incubator-based system
3. Sterile bench-based fully automatic system.

#### 1.2.2.1 Microscope-based system

This kind of system is based on an automatic microscope fitted with a scaled incubator for sustaining cells cultured in petri dishes. Some components and accessories of the microscopy system are motorized. The imaging procedures of cells are programmed running repeatedly at one or more testing points.

##### **Stage-top incubator**

The incubator part can be scaled down to just fit in the translational sample stage of an automatic microscope. A stage-top incubator is shown in Figure 1.2.2 (A). The physiological environment is confined to the culture chamber. There are not only products from microscope manufacturers but also many aftermarkets third party products can be selected that are designed to fit microscope configurations from those main manufacturers.

In Figure 1.2.2 (B) and (C), the general construction of a stage-top incubator and its cross-sectional diagram are illustrated respectively. From top to bottom the incubator chamber is mainly composed of: (1) Clear glass top heater: at the very top of the incubator comes the clear glass heater for direct heating of the culturing chamber from above. It could bear a uniform transparent conductive coating of ITO (Indium tin oxide) material or could be embedded with very thin metal wires arranged in a tortuous pattern, which are all to ensure the homogeneous electrical heating field on glass. Meanwhile the glass heater on top can prevent liquid condensation on top of the chamber unit and thus a clear field of view is provided for microscopy. The glass heater could be in rectangular or round shaped according to different culturing vessel configurations. (2) Humidity tank: on this part, constant CO<sub>2</sub>-air flow is introduced into the chamber from a side port. Sterile water is kept in the water bath along the inner rim of the tank and is heated while working by another heater underneath the bath to provide humidified environment around the culturing chamber. This kind of forced humidification lasts, for example, 2 days with 40 ml water in the bath unit [33]. The water can be supplied from another side port so that the long-term incubation over 2 days is possible for continuous imaging under microscopes. Another

method is to introduce gas mixture into a heated scrubbing bottle filled with DI (De-ionized) water (Figure 1.2.2 (D)), the bottle standing on the humidifier controller for carrying humidity with the gas mixer into the chamber. The (1) and (2) parts can be designed into one unit as shown in Figure 1.2.2 (D) left, a humidity-CO<sub>2</sub> cover with its controller. (3) Dish adaptor: the dish adaptor is used to fix the culturing vessel e.g. a petri dish, chamber slide or microplate in the incubating chamber. A series of dish adaptors are available for standard culturing vessels of different sizes and shapes. (4) Heating insert: beneath the dish adaptor is the heating insert for heating the chamber from bottom. The shape and size of the heating insert varies according to different sample stage configurations. (5) Objective heater: They are also made of anodized black aluminum. Rings of different diameters are available to fit different objective sizes. It is used for heating microscope objectives to reduce loss of temperature in the observation area. The cross-sectional diagram of the incubator unit can be seen in Figure 1.2.2 (C) for a clearer illustration of its construction. Each objective heater is equipped with a built-in heating element, including temperature sensor for the close-loop temperature control. The heating system achieves a resolution of the 0.1°C PID (Proportional-Integral-Derivative) control algorithm. Generally, 3 to 4 independent channels for heating control can be provided, plus CO<sub>2</sub> concentration and humidity feeding and monitoring modules. These help the system sustain proper temperature, humidity and gaseous conditions for cells enclosed in the chamber.

Besides applications in live cell imaging, such compact stage-top systems are more often applied in experiments requiring extended temperature range or quick temperature changes. For example, electrophysiology measurements and fish cells culturing are generally implemented in lower temperatures; in the characterization of protein folding mutants, the temperature level is quickly changed automatically by program. Such systems are not only equipped with heating but also cooling temperature control. The surface temperature can be raised from ambient up to 45 °C by using a top glass heater. The cooling system is realized by circulating temperable liquid through the controlled components to conduct heat away. Constituents of the cooling incubating system are presented in Figure 1.2.2 (D). CO<sub>2</sub> and humidity are provided from ambient temperature. The electrical heating elements in the heating insert and objective heater are replaced by flowing temperable liquid, and tubes for liquid inlet and outlet are in place of the electrical cables. Temperature sensors are integrated inside the components for a close-loop control of the temperature by varying the flow rate of the temperable liquid.

## 1. Introduction

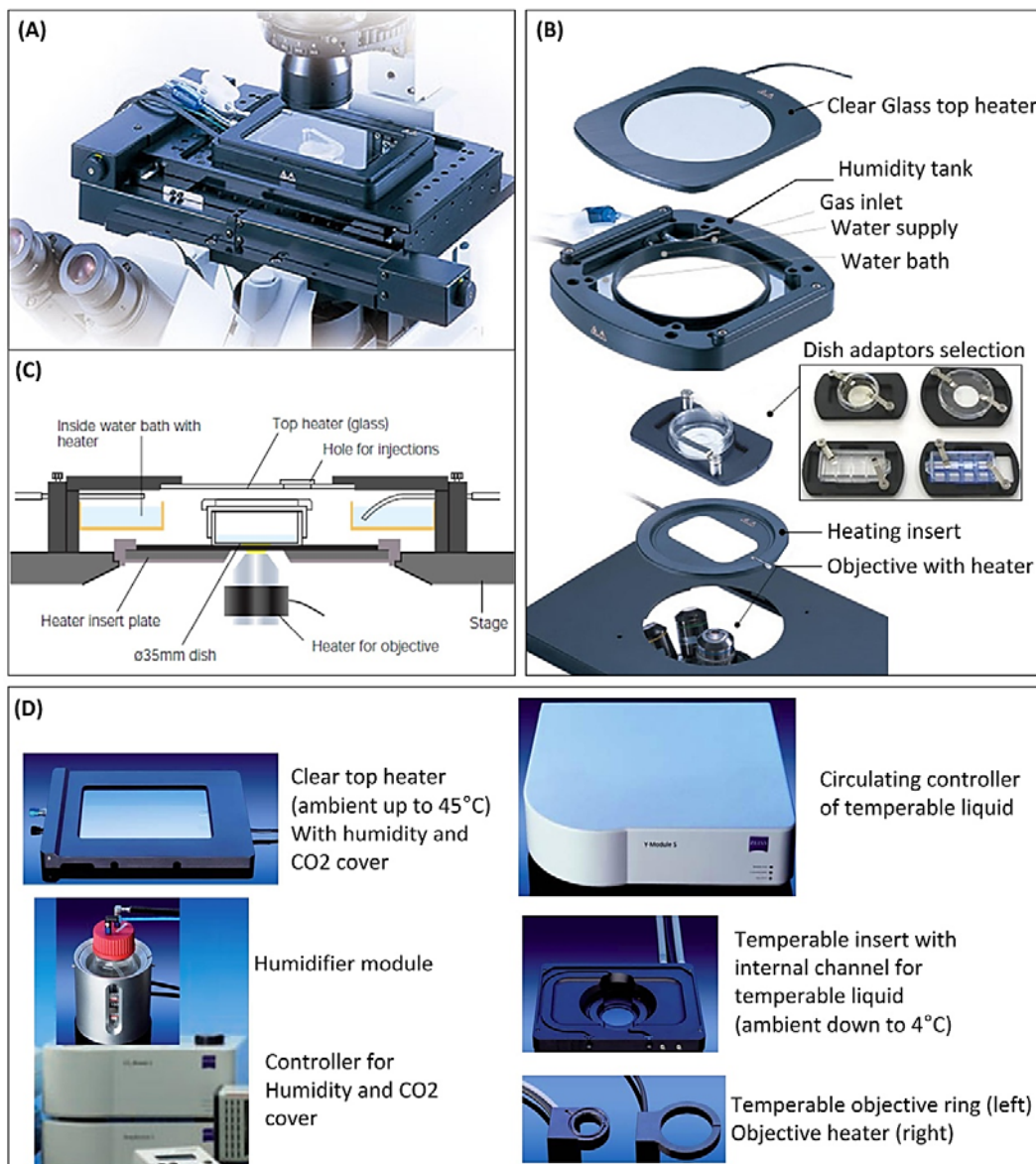


**Figure 1.2.2** (A) A representative stage-top incubator installed on an automatic microscope and (B) General construction of a stage-top incubator chamber with variable dish adaptors [[http://spectraservices.com/mm5/pdf/INU\\_catalog.pdf](http://spectraservices.com/mm5/pdf/INU_catalog.pdf), 2012]; (C) cross-sectional diagram of the stage-top incubator construction [33]; (D) Stage-top incubating system with cooling function [[https://fcam.uni-frankfurt.de/files/documents/60-4-0001\\_e.pdf](https://fcam.uni-frankfurt.de/files/documents/60-4-0001_e.pdf), 2012].

### Large climate chamber incubator

Microscope integrated with a large chamber incubator is a better solution for experiments conducted at a more stable and uniform temperature. The diagram of a live cell imaging system composed of an automatic microscope and a large chamber incubator (also as here called “Environmental control chamber”) is presented in Figure 1.2.3. The optical and mechanical components along the microscopy optical path are thermally isolated by the

large chamber. This can effectively prevent fluctuations in the ambient temperature, which would have effects on focus stability of the microscopy imaging. This kind of setup is the most popular live cell imaging solution for experiments with mammalian cells cultured at 37°C.

Diagrams of assembled components for such most popular systems are presented in Figure 1.2.3(A). The whole system is based on an automatic microscope. The main opto-mechanical parts are covered with a large transparent (the sample placing process can be easily observed when the operator manipulates through the access ports) climate chamber, inside which proper physiological environment is sustained by bulky peripheral components. The CO<sub>2</sub>-supplying module, structured as those used for stage-top incubators but more powerful, can be equipped with a gas flow meter controlling premixed CO<sub>2</sub>/air bombs, or can be equipped with a digital gas mixer to produce e.g. 5% CO<sub>2</sub> from 100% CO<sub>2</sub> bottle. The in-chamber temperature and CO<sub>2</sub> sensors continuously monitors the CO<sub>2</sub> concentration, according to which the flow rate is adjusted by the controller. The gas is carried with heated water vapor and introduced into the chamber (Figure 1.2.2 (B)).

Generally, a reduced humidity level (~70%) is recommended to implement in the chamber for slowing down the corrosion process that can happen on opto-mechanical instruments emerged in the weak acid gaseous environment. Experiments are limited to hours in such an environment that is compromised for cell culture and detrimental to enclosed instruments. The achievable temperature range of the large chamber incubator is from ambient to 40°C. It normally needs 2 to 3 hours of warm-up period before starting the experiment to wait until all the incubation values (temperature, humidity and CO<sub>2</sub> concentration) have been reached in the large space. The time it takes will differ depending on the configuration. This complete system with all its many bulky supporting and controlling subsystems is expensive and takes up much space. Many laboratories are not able to afford the expensive instrumental price and high running costs. Besides, the system is not optimized for usage over days considering technical as well as economic reasons. As for experiments over days, additional stage-top incubator or perfusion chamber is preferred to confine optimized gaseous and humidity environment only on microscope stage, while the large chamber incubator provides temperature condition for both cells in culture and surrounding air space. As shown in Figure 1.2.3 (C), an operator is installing some culturing pod onto the stage inside a large chamber incubator. The practical operation with microfluidic cell culture systems with tubing and pumps can be very hindered by this large chamber with small openings. The “incubator” chamber is also not easy to be sterilized with microscope components and motorized stage inside.

## 1. Introduction

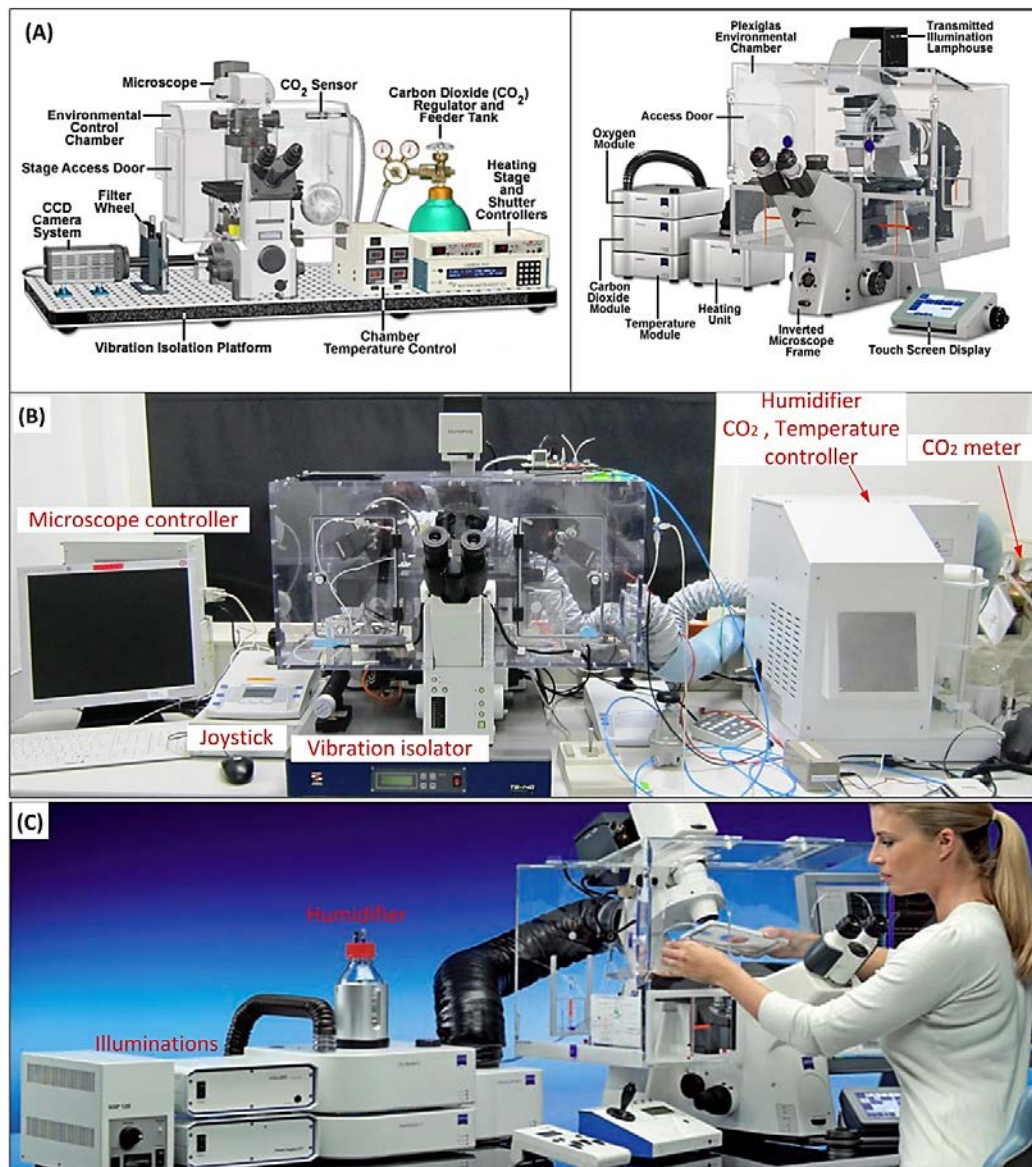


**Figure 1.2.3** (A) Diagrams of live cell imaging configuration based on an automatic optical microscope integrated with a large chamber incubator [left: <https://www.microscopyu.com/applications/live-cell-imaging/the-automatic-microscope>, 2012; right: <http://zeiss-campus.magnet.fsu.edu/articles/livecellimaging/imagingsystems.html> 2012]; (B) Photograph of a live cell imaging system installed in an exclusively reserved laboratory (The photograph was taken in the dark room of Fraunhofer IBMT, St. Ingbert, Germany, 2011); (C) Additional on-stage incubator or perfusion chamber is required besides of a passive humidifier deployed large chamber incubator for preventing culture drying out over days [[https://fcam.uni-frankfurt.de/files/documents/60-4-0001\\_e.pdf](https://fcam.uni-frankfurt.de/files/documents/60-4-0001_e.pdf), 2012].

The live cell imaging instrument is constructed based on an automatic microscope, which is a complicated system including not only optical elements but also mechanical and

electronical parts. Fast and precise optical and fluorescence microscopy can be carried out repeatedly for multiple testing points. The automated microscopy procedures, as shown in Figure 1.2.4, includes: stage positioning (servo motor close loop controlled motorized stage), auto axial focusing (piezoelectric objective auto focusing), fluorescence filter wheel shifting (microprocessor controlled), illuminations control, exposure control (mechanical/digital shutter) and image acquisition (camera control) and storage. The timescale intervals of the time-lapse imaging can range from milliseconds to tens or hundreds of minutes. The continuous recording of individual cells can be realized.

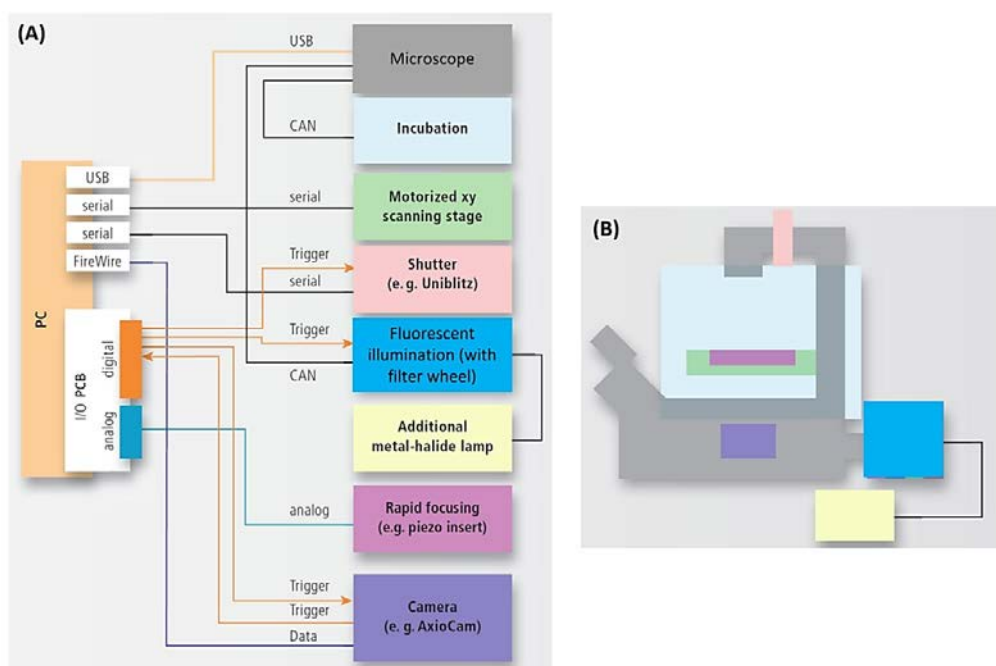


**Figure 1.2.4** System architecture of an automatic microscope-based live cell imaging system from Zeiss Cell Observer: (A) components diagram and hardware interface, and (B) the corresponding optical and mechanical system configuration [[https://fcam.uni-frankfurt.de/files/documents/60-4-0001\\_e.pdf](https://fcam.uni-frankfurt.de/files/documents/60-4-0001_e.pdf), 2012].

The automatic microscope system is very expensive (~100,000 Euros) and along with considerable running cost. But it is often worth the investment as for the multi-user services in core facilities. The system is more suitable for recording those fast-cellular events lasting for several hours with refined time resolution, but is not practical and cost efficient to apply in the first batch of cell-based screening to find the end-point of the assay.

#### Desktop time-lapse imaging system

In such desktop time-lapse imaging system, the design is mainly based on a microscope with on-stage incubator. But to realize an even more compact and professional instrument dedicated for high content imaging for live cells, the whole system is enclosed, as shown in Figure 1.2.5, to substitute the requirement of dark room. The ocular part is also removed.

## 1. Introduction

Instead, the sample is observed using digital imaging application on a desktop monitor on the outside. The physiological climate for biological sample is confined in a small chamber. Compared to the automatic microscopy systems integrated with stage-top or large climate chamber incubators, the system is more flexible and faster in optical imaging and mechanical scanning operations for high content imaging, like fluorescence and even confocal. But usually the microscopy objective to sample moving range is only several millimeters. So, this system is not suitable to multi-channel observation of cells. The physical configuration of such a system determines that only one culturing condition can be monitored. Otherwise, multiple such instruments must be purchased to conduct the experiment in a high throughput way.

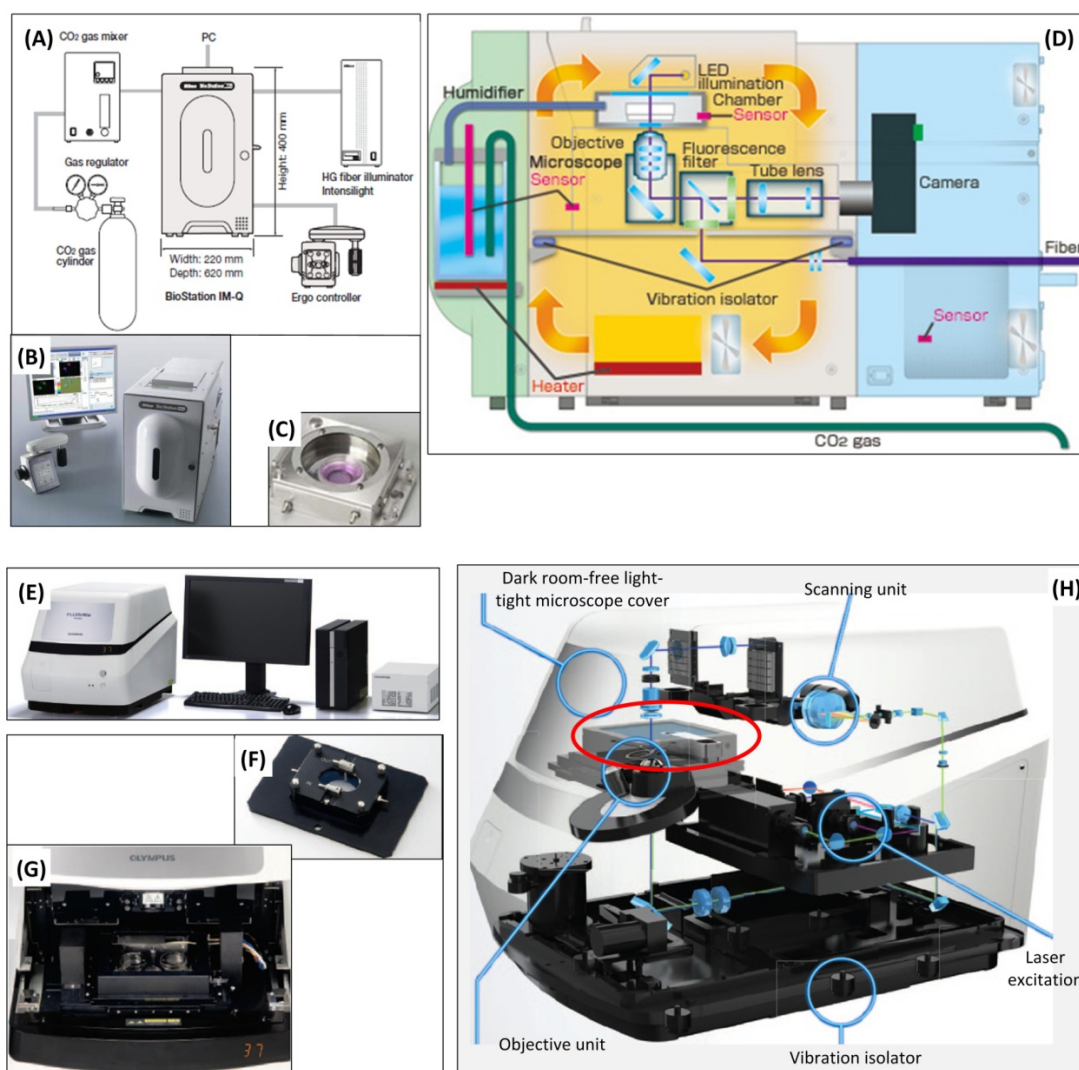


**Figure 1.2.5 (A) Nikon BioStation IM\_Q system diagram with peripheral components, (B) Demonstrated desktop instrument with joystick and monitor, (C) A specially designed culture vessel with fluidic and humidity ports and (D) Inner operational diagram presentation [https://www.nikoninstruments.com/Products/Live-Cell-Screening-Systems/BioStation-IM-Q, 2011]; (E) Olympus FV10i-LIV Live Cell Time-Lapse Confocal**

**Imaging Station demonstrated desktop system components, and (F) Small incubator for cell culture, which is situated inside the system as shown in (G). (H) Inner operational diagram presentation and the incubator is marked inside the red circle**

[[https://www.olympus-lifescience.com/en/laser-scanning/fv10i-liv/#!cms\[tab\]=%2Flaser-scanning%2Ffv10i-liv%2Ffeatures](https://www.olympus-lifescience.com/en/laser-scanning/fv10i-liv/#!cms[tab]=%2Flaser-scanning%2Ffv10i-liv%2Ffeatures), 2011].

### 1.2.2.2 Incubator-based system

Besides the above presented automatic microscopy systems, there are also incubator-based systems from SANYO [34], Nikon Biostation CT and Olympus LCV110U. Subsystems for automatic culturing vessel transportation and optical imaging are enclosed. This makes the overall size of such equipment even larger. Cells grow in conventional or specially designed petri dishes or flasks that are installed in a rotatable wheel or stack-structured racks to facilitate the automatic mechanical and optical operations. This configuration provides cells with an ideal environment for implementing time-lapse experiments over days.

However, it brings greater challenges to mechanical and optical systems and the whole system integration because of the highly humid environment inside the CO<sub>2</sub> incubator. For instance, the illuminator, objectives and digital camera of the SANYO system are placed and protected in a stainless-steel case that used for the moisture isolation. The optical objective is also protected by an additional glass lid sealed with an O-ring. The observation distance is thus increased and long working distance optical components are essential for achieving good image quality [34]. Therefore, much effort in designing and engineering for such systems is still required.

### 1.2.2.3 Sterile bench-based fully automatic system

Either the microscope-based or incubator-based system is still semi-automated for the cell culture operation. To facilitate high throughput pharmaceutical screening, quality production in the biotechnology industry and a large quantity of cell cultures for tissue engineering, fully automatic cell culture systems have been developed based on the configuration of a sterile bench. Besides of the automatic microscopy procedures, operations of liquid handling and transportation of culturing vessels are made automatically by robotic arms. On-line monitoring and hands-free operation are aimed to better control the quality and reproducibility of cell cultures and cell-based screening. Transportation of culture vessels and even liquid handling operations by robotic arms are integrated into automatic cell culture systems. The overall and detailed parts of such fully automatic systems are presented in Figure 1.2.6.

With the increasing system volume and complexity of the integration level, the price and related running cost and maintenance effort for the live cell imaging system will also greatly increase. In most cases, it is far beyond the affordability of many biological or biomedical research groups, so the application area is so far mainly confined in the national research centers or production lines of pharmaceuticals and biomedical industry. However, the

## 1. Introduction

“combinational method” of live cell imaging technique is with inherent limitation. Because of the harsh environment required by the incubating function, the stability of the electronic, mechatronic and optical parts of the system is a problem. Even such advanced fully automatic systems are not working stable enough, but they can also occasionally break down.

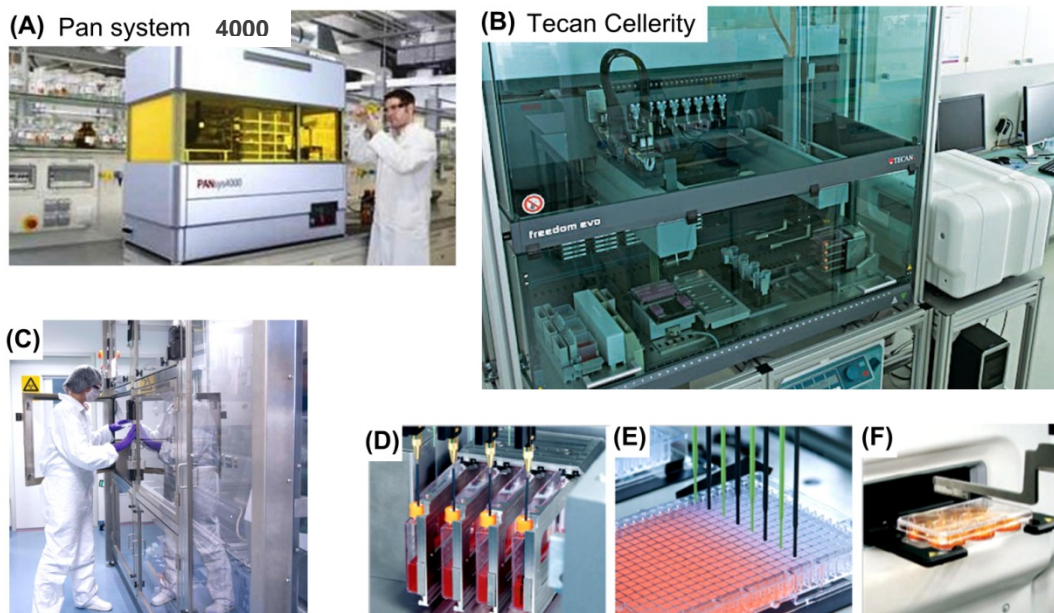


**Figure 1.2.6** Photographs of automatic cell culture systems. **(A)** Overview of a running system placed in the industry production line [<http://www.pan-biotech.de/automatisierte-zellkultur/pansys-4000>, 2011]; **(B)** System in a testing lab environment. Bio-safety cabinet encloses all parts supporting long-term cell maintenance without contamination [[http://ww3.tecan.com/mandant/files/doc/282/BR\\_Automating\\_cell\\_biology\\_processes\\_395992\\_V1-1.pdf](http://ww3.tecan.com/mandant/files/doc/282/BR_Automating_cell_biology_processes_395992_V1-1.pdf), 2011]; **(C)** Materials exchange from a running system managed by an operator working in a sterile lab environment [Fraunhofer IBMT Jahresbericht 2010]; **(D)** Behind the glass shield in (B), a closer look of the automatic liquid handling operations (dispensing/aspiration) with cell culture vessels, **(E)** with a 384-well microplate and **(F)** Transportation of a microplate into the optical testing device, the port of which is protected from outer environment [[http://ww3.tecan.com/mandant/files/doc/282/BR\\_Automating\\_cell\\_biology\\_processes\\_395992\\_V1-1.pdf](http://ww3.tecan.com/mandant/files/doc/282/BR_Automating_cell_biology_processes_395992_V1-1.pdf), 2011].

However, disadvantages of these systems are:

- Expensive and bulky: a transparent heating plate can cost several thousand Euros. The price of solely one automatic microscopy system (with fluorescence microscopy module) can be as much as  $\sim 100.000$  Euros. The main part together with its supporting sub-systems is heavy and generally takes up half of a laboratory room. The high instrumental and running costs exclude it out of many biological laboratories. Automatic cell culture system

is generally deployed in core research centers or industries, well-trained technicians and sterilized rooms are required;

- Compromised environment: a reduced humidity level is used to protect mechanical, optical and electronic instruments. However, the humidity can still often make the fully automatic culture system unstable. The climate box is not easily to be sterilized with microscopy parts inside. The temperature field, especially along the direction of the hot air flow, is not uniform, and usually is optimized for mammalian cells at 37 °C but not for other animal cells culturing;
- Non-optimal for long-term cell culture: in practice, the live cell imaging systems are aimed for recording special cellular events with high optical resolution microscopy and fine temporal resolution. The duration of the experiment is generally within several hours. Usually, the end-point of the assay has been already determined in advance by conventional cell culture and testing operations;
- Incompatible with microfluidic chips: like conventional incubators, the climate box or chamber makes it also very troublesome or impossible to work with microfluidic cell culture systems with complicated periphery parts.

## 1. Introduction

### 1.2.3 Microsystems for cell culture and cell-based assay

Microsystems technology has opened a new era for cell biology. Micro- and nano-scale engineered surfaces can be employed to mimic the complex extra-cellular matrix. Microfluidics can be employed for regulating the transport of fluidics and soluble factors. The flow patterns around cells, as well as the corresponding spatial and temporal gradients of soluble factors, are possible to be calculated [35] [36]. “Considerable progress has been made in the design and use of novel microfluidic devices for culturing cells and for subsequent treatment and analysis” [8]. Microsystems promise to provide high throughput testing (e.g. drug screening) with much lower sample consumption [37] and the integration with other analytical methods into robust and portable diagnostic devices [35] [38]. Microchips have found various applications not only in cell counting, cell detection but also in cytotoxicity assays, migration assays as well as in stem cell studies [12] and other biochemical and biomolecular analysis [39]. The microsystem has shown its advantages not only in 2D but also in 3D cell culture that are used for tissue engineering and regenerative medicines [11].

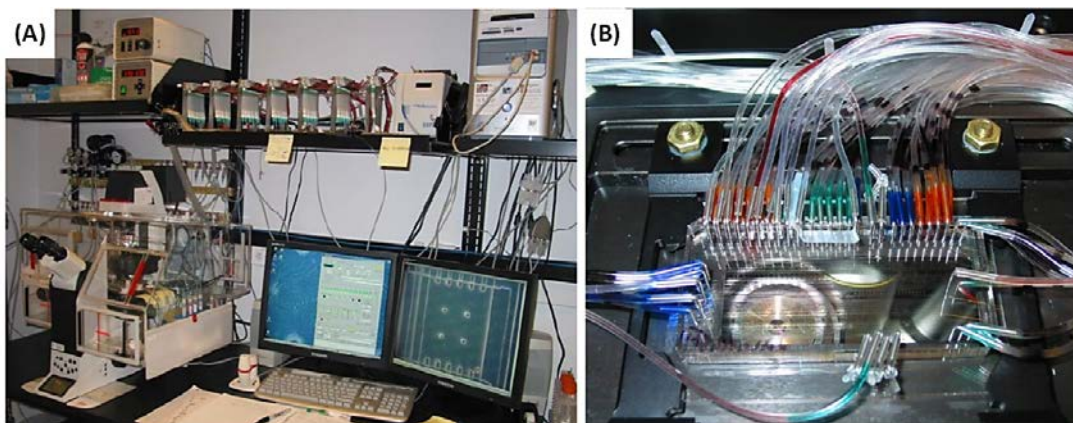


**Figure 1.2.7** Photos of the complete microfluidic cell culture system. (A) View of the complete system showing the microscope with a climate chamber, the solenoid valves that drive the on-chip valves, and the computer that controls all the operations; (B) Close-up view of a fully-connected microfluidic chip on the microscope stage [40].

#### 1.2.3.1 Microsystem configurations and operations for cell culture

The microsystem for culturing cells usually includes a microchip on which “micro-culture vessels” and microfluidic channels are connected to outer tubings, pumps and other controllers. The microchip itself is small but the microsystem is usually large, as shown in Figure 1.2.7 showing one practical experimental setup of a fully automated microfluidic system addressing 96 separate micro-chambers fixed onto an automatic microsystem with a climate box [40]. An incubator or a climate box is usually required for sustaining the physiological environment of cells inside the microchip, while some microchips were

integrated with transparent ITO (Indium tin oxide) heating modules and using CO<sub>2</sub>-independent medium or by continuously flowing preheated medium for sustaining cell growth outside the incubator [41]-[44].

Transferring conventional cell culture to microsystem has never been an easy task. There have been many reported works and products covering microfluidic systems for mammalian cells culturing. There is, however, a lack of thorough characterizations of the physiological microenvironment in those microchips. Diverse non-standard protocols for cell culture in chips of different designs make it difficult to compare and evaluate the results regarding conventional *in vitro* experiments. They have not been well accepted and applied by the biological community. Generally, microsystems of different designs can be configured into three types with corresponding operational methods for culturing cells:

**Type 1:** Gas-permeable system + conventional medium + Incubator/Climate box

Most cell culture microsystems are within this category. The microchip is often made of materials like PDMS (Polydimethylsiloxan). Silicone tubings are often used for the easy connection between the microchip and the microfluidics. Conventional culture medium with safe CO<sub>2</sub>/HCO<sub>3</sub><sup>-</sup> buffering system is preferred. Since silicone tubings exhibit a high permeability of gas and water, the microchip must be placed inside an incubator or a climate box, and its periphery supporting parts for running the microchip are placed outside nearby. If using a conventional incubator, the microchip should be taken out every time for the observation. If the microchip is placed onto the stage of an automatic microscope with a climate box, the microchip itself and periphery parts should be properly fixed inside the narrow and crowded climate box.

To get rid of incubators and to facilitate the continuous observation of cells on conventional microscopes that usually do not come with climate chamber, a few stand-alone microsystems have been reported for cell incubating in the room environment requiring no standard incubators. Those stand-alone microsystems can be further classified into the following two types:

**Type 2:** Gas-permeable system + heating element + CO<sub>2</sub>-independent medium

The microchip of type 1 is additionally integrated with transparent ITO heating elements. CO<sub>2</sub>-independent culture medium containing HEPES buffering system is employed. The flow rate should be set relatively high in order to prevent the liquid from evaporation if the microchip material is not provided with good sealing properties [41] [44].

**Type 3:** Gas-tight system + heating element + conventional culture medium

Microchips are made of materials such as plastics, silicon, and glass in order to greatly reduce any gas leakage or water evaporation from the microchip. Transparent ITO heating elements are integrated with the microchip to provide it with proper incubating temperature. The conventional culture medium is

## 1. Introduction

preheated and continuously flowing into the microchip to provide necessary nutrients for the growth of cells [42] [43]. Most microsystems related to cell culture still require microscopes and incubators. Microsystems are small but have to adapt to bulky incubators and microscopes. Transferring conventional cell culture from an incubator into a microsystem has not been an easy task. Non-standard medium and non-standard culture protocols described in type 2 and type 3 have not been well accepted by the biological society, and needs further improvement and investigation. The optical configuration of a standard microscope is also not easy to be scaled down to a microchip level. Those are still the bottleneck to fully realize the compactness, cost efficiency and high throughput manner that the microsystem has promised.

### 1.2.3.2 Microchip geometry design optimized for cell culture

The aim of microfluidic cell culture systems is to establish a controllable and reproducible *in vitro* cellular microenvironment. As to be called microsystem, at least one dimension of a microfluidic channel or chamber should be within  $\sim 100$  micrometers. With such small dimensions comparable with that *in vivo*, microfluidic behaves quite different from that in the macro-scale static condition. There are two features pertinent to microfluidics: **laminar flow and diffusion dominant mass transportation**, both of which can be controlled and predicted [45].

The most common design of a microchip is simple channel geometry. This design is easy to be fabricated and has been well characterized. But a drawback is that the shear stress experienced by cells adhering to the bottom floor of the micro-channel increases directly with the flow rate of culture medium. Several studies have already shown that shear stress can have not only a range of negative effects on cells, but also could lead to biased information on functional cellular analysis even at low shear stress range of less than  $10 \text{ dyn/cm}^2$  (corresponding to  $1.0 \text{ Pa}$ ) [46]. Inspired by the *in vivo* microenvironment, soluble nutrients are supplied by convective flow, while the mass exchange with cells is mainly realized by diffusion process. One promising method is by using micro-groove or micro-well structures in the chip design [47]-[49]. This design principle greatly minimizes shear stress that could be harmful to cells while maintaining adequate medium perfusion supply. By using this structure, the shear stress values inside all the grooves are greatly reduced compared to those in the mainstream. Another advantage of a micro-grooved structure is that the samples inside micro-wells and microfluidic channels are separated in two stacked layers. This vertical structure simplifies the design and is provided with higher well density compared to those planer low shear stress designs [50].

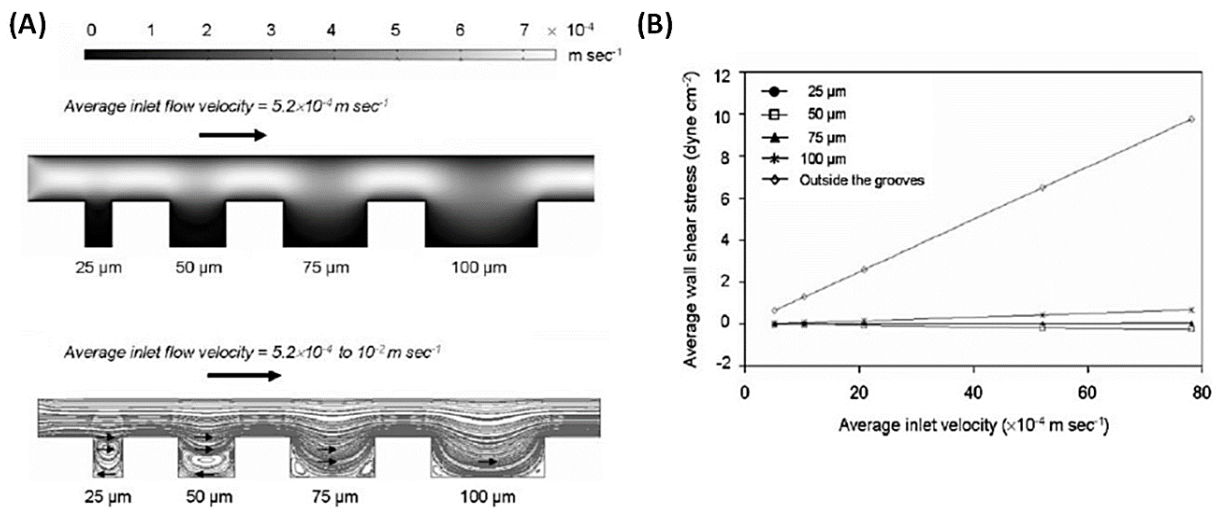


Figure 1.2.8 (A) Velocity profiles in a micro-groove channel. Velocity contours for micro-grooves of different widths, showing higher penetration for grooves of larger widths. And below are the streamline patterns for grooves of different widths; (B) The linear relationship between the shear stress and the inlet velocity. The average shear stress on the floor was simulated outside and inside the microgrooves of different aspect ratios [47].

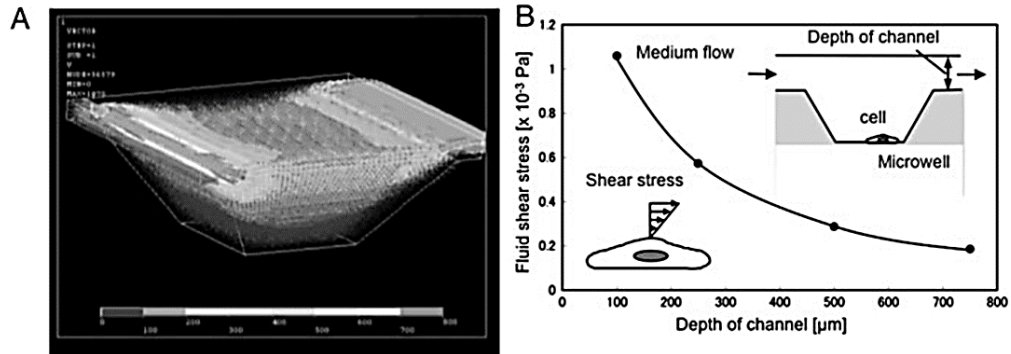


Figure 1.2.9 Flow analysis in a micro-well. (A) The typical flow pattern in the micro-well, with shading indicating velocities (light, relatively high velocities; dark, lower velocities); (B) The calculated shear stress values with different micro-channel depths from 100 to 750 μm with the same inlet velocity [48].

The simulation results of Manbachi in 2008 as shown in Figure 1.2.8 (A) indicate that turbulence can occur in rectangular shaped micro-grooves with high aspect ratio [47]. In contrast, there is no dead corner of a microchip design by using funnel-shaped micro-well structures [48], which is easier and cost effective to be fabricated. Inside the well, as shown in Figure 1.2.9, laminar flow can be obtained [48]. By the simulation result as shown in Figure 1.2.8 (B), the shear stress on the bottom of the grooves increases linearly with the

## 1. Introduction

inlet velocity, but the shear stress values have been greatly reduced compared to those outside the grooves [47]. Similarly, by the simulation result of the micro-well structure, as shown in Figure 1.2.9 (B), the flow velocity at the bottom side becomes very small compared with the upper layer. As the height of the upper microfluidic channel increases, the shear stress by simulation exerted on cells at bottom side decreases [48].

Microsystem technology has provided new possibilities for cell culture and for subsequent cellular treatment and analysis. Continuous medium micro-flow and properly designed micro-scale geometries, of which micro-grooved/well structure is a simple and optimized example, have better represented the *in vivo* cellular microenvironment. Microsystem provides a more controllable and stable microenvironment than conventional cell culture in flasks or petri dishes. However, transferring conventional cell culture to microsystem is not an easy task. Microscopes and incubator are very inconvenient and inflexible for the operation of complicated microfluidic systems. Compared to using controversial CO<sub>2</sub>-independent medium, the scheme of getting rid of incubators by using a gas- and vapor-tight microchip with conventional culture medium should be more easily accepted by the biological society. However, to realize a stand-alone microsystem for cell culture, the system configuration and operational protocol still need to be carefully investigated.

### 1.2.4 On-chip lensless imaging methods

Besides of standard microscopes, recently reported lensless imaging methods or lensless microscopy such as contact/shadow imaging and computational image reconstruction methods have presented the possibility that cells and microfluidics will be imaged in a very compact and cost-efficient way. In the following paragraphs, those lensless on-chip imaging methods as well as on-chip fluorescence imaging methods will be briefly introduced and reviewed.

#### 1.2.4.1 Contact/Shadow imaging

A simple approach to construct a miniaturized imaging system with micro-scale resolution is by integrating an image sensor array under the sample of interest directly [51][52]. The image is acquired under collimated illumination through objects or by capturing light emitted from luminous objects using a CCD or CMOS image sensor array. This kind of approach is referred to as “contact imaging” [16] or “shadow imaging” [52]. In contrast to conventional imaging methods, a contact/shadow imaging system is by placing the object very close to the image sensor plane without using any image-forming optical lens. Therefore, artifacts of the contact/shadow images come from the diffraction effect raised by the distance of the object from the sensor surface, as well as the pixelation effect raised by the digital sensor array [16] [52].

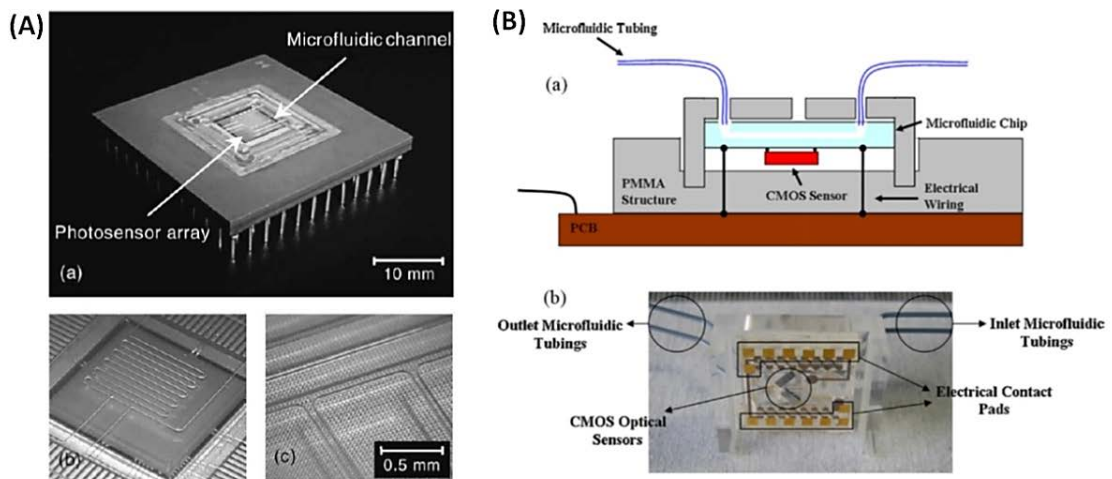


**Figure 1.2.10** (A) Photographs of an integrated micro-electrophoretic chip on a packaged photo sensor array chip. The acrylic microfluidic chip is fabricated by stereolithographic process. The distance between the bottom of the micro-channel and the photo sensor surface is  $500\ \mu\text{m}$  [53]; (B) The CMOS image sensor is coupled onto the microfluidic glass chip by using solder reflow flip-chip bonding. The glass chip bottom plate is  $100\ \mu\text{m}$  in thickness [54].

## 1. Introduction

To realize shadow imaging, the samples need to be brought into a very close distance from the sensor surface. Integration of the microchip with a packaged image sensor with electronic connections needs careful design and a lot of engineering effort. Examples of microchip and image sensor integration are presented in Figure 1.2.10. Because of the physical confinement of image sensor package and the thickness of microchip substrate, samples still have a distance of 500  $\mu\text{m}$  (Figure 1.2.10 (A)) and 100  $\mu\text{m}$  (Figure 1.2.10 (B)) respectively from the image sensor surface [53] [54]. In an earlier report, a gas permeable membrane (Opticell™) of 300  $\mu\text{m}$  thickness is glued as both the cover and substrate of the microchip, which leads to the sample having a distance of 300  $\mu\text{m}$  from the image sensor [52]. Furthermore, the time course of signals from active pixels of the image sensor have been analyzed to generate information such as moving speed, moving direction and concentration of testing samples in microfluidics. [53]-[56] [52]

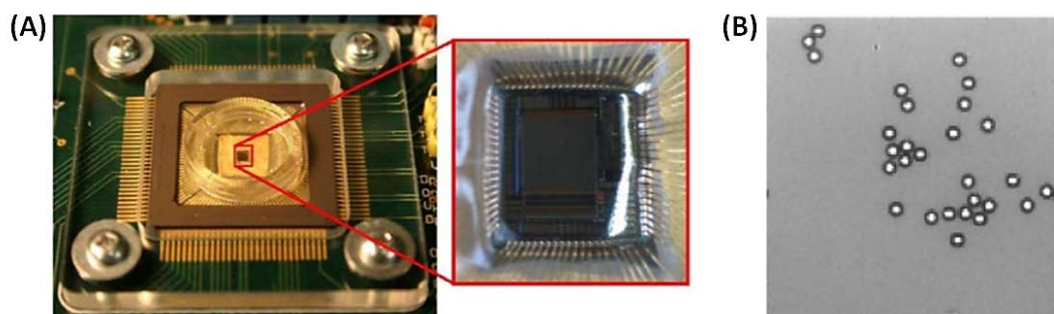


**Figure 1.2.11 (A) Photograph of the contact imaging device based on a packaged image sensor. The bonded wires of the electronic connection and the image sensor surface are protected by vulcanizing silicone sealant in room temperature. A glass culture chamber wall is glued on top surface; (B) Contact imaging of 45  $\mu\text{m}$  polystyrene microbeads. Pixel size of the image sensor is 7  $\mu\text{m}$  [57].**

It would be preferable if the contact imager can be applied in lab-on-chip systems for samples preparation, manipulation and single cells monitoring [58]. Practically, “in order to test the contact imager with cultured cells directly coupled to the chip surface, the chip must be further packaged both to protect the bond pads and wires from being corroded and shorted by cell culture medium and to protect cells from toxic materials in the chip packaging” [59]. In the case presented in Figure 1.2.11 (A), silicone sealant is applied with a syringe on the sensor surface and electronic connections. The thickness of the sealant on the surface is unknown. Polystyrene microbeads with a diameter of 45  $\mu\text{m}$  are imaged in solution and the image acquired from the image sensor array (pixel size is 7  $\mu\text{m}$ ) is shown in Figure 1.2.11 (B). The transparent microbead is intuitively visualized as a dark circular outlined with a bright center. It is stated that this bright center is due to the optical effect of the sphere, which causes light to be focused directly below the bead [57]. The contact/shadowing imaging method is simple and is preferable to monitor the operations

and sample activities inside the microfluidics without complicated computational reconstruction process, i.e. “*what you see is what you get*” in real time.

However, the imaging potential of this method has not yet been well developed. It has been demonstrated by Fischer and Zingsheim in 1981 that the resolution of the contact imaging is determined not by the wavelength of the illumination but by the distance between the sample plane and the image plane. Under visible illumination, the contact imaging resolution of a planer metal pattern onto the photoresist or a film of dye layer has been achieved down to 100 nm [60] [61]. However, in general conditions, ideal “contact” by vacuum is not possible. Once the sample leaves the recording surface and as the distance increases, the projection will become more blurred and distorted by the optical diffraction effect. As the pixel size of high resolution CMOS image sensors (for instance, Aptina AR1335 1/3.2-inch CMOS active-pixel digital image sensor with a pixel array of 4208 x 3120) has been fabricated down to 1.1  $\mu\text{m}$ , the practical question for the further development of shadow imaging comes to: how close has the sample to be brought to the image sensor surface that the diffraction effect will become insignificant compared to the image sensor pixel size. The optical resolution of shadow imaging method in the “very-near field” needs to be carefully characterized.

#### 1.2.4.2 Lensless/Lensfree computational image reconstruction

Recently, computational image reconstruction method has been brought into this on-chip imaging area to overcome the resolution limits resulted from diffraction and pixelation effects in order to achieve sub-micrometer optical resolution. There have been two kinds of experimental configurations supporting such reconstruction method:

- (1) One kind of experimental device is similar to the contact mode configuration, called “**e-petri**” with specimens in direct contact with the optical sensor surface. The micro-lens array and if required color filter array on the image sensor pixels are removed in order to further reduce the space between sample and image sensor thus eliminating the diffraction effect to the most. Adherent cells are directly cultured on the sensor surface within a glued outer well. The whole system has been placed inside a 37°C CO<sub>2</sub> incubator for extended period monitoring of cells in culture. In order to improve the imaging resolution of the digital image sensor down to sub-micrometers, specimens can be illuminated from different angels. The underlined image sensor takes interval images at each illumination angel for the further image reconstruction. As shown in Figure 1.2.12 (A)-(F), samples are illuminated by LEDs (Light Emitting Diode) array or simply by a smartphone screen, which is programmed lighting in different areas [62]-[64]. Another structure of the contact mode is called **optofluidic** microscope. It uses microfluidic flow “scanning” of suspended samples under collimated illumination in order to improve the imaging resolution by image reconstruction. In references [65] and [66], this method has been used for the imaging of *Caenorhabditis elegans* and cells flowing over the image sensor. The sensor surface is planarized and further fabricated with a

## 1. Introduction

line of micro-apertures or Fresnel zone plates on individual pixels. However, the latter optofluidic “scanning” method is not 100% stable because of the occasionally happened sample rotations along the microflow directions.

- (2) The second kind of experimental configuration is so called “Digital holographic lensfree microscopy”, which is using partially coherent illumination [13] [14]. Samples are sandwiched by two coverslips and placed onto the image sensor. There is a small distance of a couple of millimeters from the sensor surface. Holographic patterns are then recorded by the image sensor under programmed variable illumination settings [67]. The diagram of the very compact lensfree holographic microscope and its inside optical construction [67] are shown in Figure 1.2.12 (G) and (H). The operation in the holographic method is relatively simple and easy to be kept sterilized.

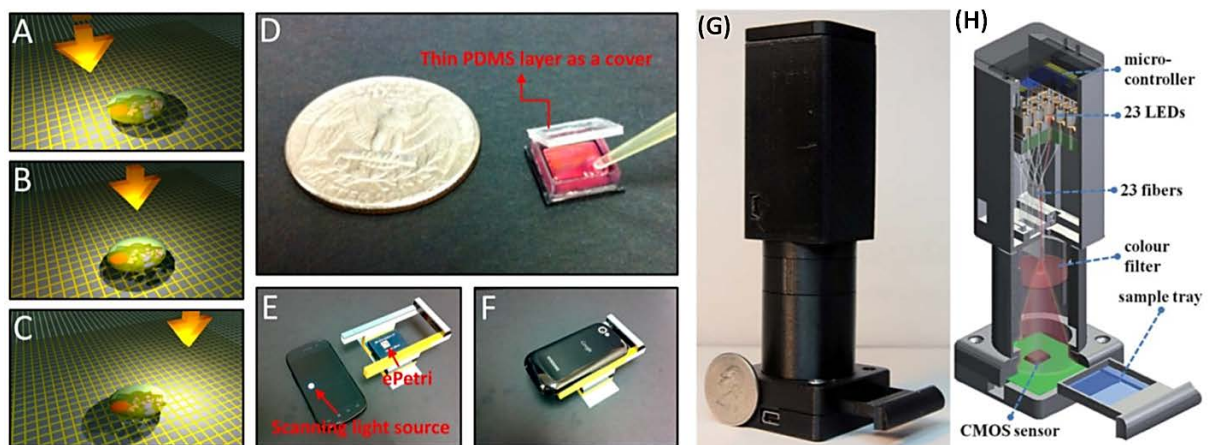


**Figure 1.2.12** Principle of super-resolution and “e-Petri dish” prototype. (A–C) “With the incremental tilt/shift of the illumination, the target specimens’ shadow will incrementally shift across the sensor pixels” [62]; (D) The ePetri prototype. The microchip was placed inside an incubator. A thin PDMS layer is used as a cover to eliminate the media evaporation and to support CO<sub>2</sub> exchange; (E–F) A smartphone screen is programmed to be used as the scanning light source [62]; (G) and (H) The diagram of the lensfree holographic microscope weighing 95 g. Each of the 23 LEDs is controlled by an MCU (Micro Controller Unit) and sequentially switched on and off to create shifted holographic image sequences [67].

Accordingly, two kinds of reconstruction steps are needed to visualize an object’s image. One step is termed as “pixel super-resolution” or “sub-pixel resolution”, which is used to overcome the resolution limitation due to the pixel size. The scheme of the contact-mode “e-petri” or the digital holographic lensfree microscopy is to capture sub-pixel shifted image sequences (typically ~10–100) of the same static object under the illumination of different shifting angles [14]. The digital holographic microscopy requires additional computational reconstruction to compensate the diffraction effect raised by the small distance between

the objects and the imager [14]. Rayleigh–Sommerfeld or Fresnel-Kirchhof optical wave propagation algorithm based on scalar diffraction theory is applied to digitally undo the diffraction effect. This algorithm can only be applied in case of coherent or partially coherent illumination of spherical or planar wave front [13]. Sub-micrometer optical resolution can be achieved by both contact-mode and holographic computational imaging method.

In the holographic method, the selection of algorithms and modifications are dependent on physical optical configurations and samples' optical properties. For example, to compensate intrinsic artifacts of color microscopy, imaging must be captured at several sample-to-sensor distances [13] [17]. In the contact-mode computational imaging method, the distance from the sample to the imaging detector is very critical. "Pixel super-resolution" algorithm is therefore not applied to "standing" cells, for example, cells just be seeded or dividing cells [17]. For color imaging of both methods, red, green and blue channels have to be illuminated sequentially, and constructed images of each channel are then combined to form a full-color image [17]-[19]. Additional procedures further increase the data acquisition and computational time. For instance, in the contact type, the data acquisition time is 20 seconds and the computational time is 2-3 minutes. It is estimated that the data processing time could be cut off less than 1 second by using GPU (Graphic Processing Unit) in the computer [19]. However, the overall processing speed will be still not fast enough for observing cells and microfluidics operations in real time.

So far, the computational lensless imaging is not intuitive enough to ensure users to have "*what you see is what you get*" in real time. The sub-pixel resolution computational imaging is more suitable for end-point diagnosis. Likewise, the developing trends of such lensless computational imaging is toward Global health and cell phone based Telemedicine applications in the wide field diagnosing of blood cells, semen and tissue as well as in the ecology monitoring of waterborne parasites and microorganisms [68]-[70] [19]

#### 1.2.4.3 On-chip fluorescence cell imaging

The bulky and expensive optics employed by the fluorescence microscopy or spectrometry devices makes it difficult to realize compact and economical on-chip integration. Fluorescence contact imaging has been proven to be one of the most promising methods. The samples are placed in the proximate distance of a CCD or a CMOS image sensor with a fluorescence emission filter between them [57] [71] [72]. The near-field imaging method features much higher collection efficiency for the emitted fluorescent photons compared to the far-field imaging geometry with intermediary optics. In the microarray diagnostics, compatible resolution ( $\sim 100 \mu\text{m}$  spot) has been provided by using image sensors [73] [74]. A wide selection of optical filter technologies was reviewed for the integrated fluorescence sensors [75]. Interference filters, dye-doped filters, total internal reflection and cross-polarizing filtering schemes have been integrated with CMOS image sensors or organic photodetectors. The functionality of these systems was demonstrated as on-chip microfluidic fluorescent spectrometers [76]-[80]. In one example, fluorescent microbeads

## 1. Introduction

clusters were observed. A resolution of down to 10  $\mu\text{m}$  was achieved by using computational imaging de-convolution algorithm [79]. In another example, fluorescence living cells were imaged with a resolution of 13  $\mu\text{m}$  by fabrication absorbance filter and very complicated silo-filter on a CMOS image sensor [63].

As to the fluorescence microscopy for biological cells, the blocking capability of the filter for the excitation illumination should be better than 0.001% (-50dB). While for its transmittance should be as much as possible, normally at least 80% of the emitted fluorescent light. The interference filter is so far considered as the best choice for making filter cubes and split mirrors in the fluorescence microscopy because of its superior spectral and physical stability even under harsh environments [57] [71] [81]. In a former example of constructing an on-chip fluorescence microscopy, an extra interference filter was glued onto an image sensor. However, small air bubbles in the glue would often impair the blocking ability in parts of the field of view [71]. The filtering performance would be improved by depositing the filter with a thickness of several  $\mu\text{m}$  directly onto the sensor surface. Although the fabrication of the interference filter by coating dozens of thin layers is relatively expensive, the unit price would be greatly reduced by batch coating process on wafers ( $\sim 100$  Dies/wafer) of image sensors or other microchips.

Fluorescence emits to all directions. It is spatially and temporally incoherent, so it is not suitable for holographic recording. The wave propagation algorithms cannot provide focusing. In those lensless fluorescence imaging systems, the point-spread function of free space propagation is applied for the de-convolution process. Holographic digital reconstruction or pixel super-resolution techniques mentioned above cannot be used here. The received fluorescence emission on the image sensor is out of focus and much weaker compared to that projected holographic patterns in the holographic lensfree imaging. Even with additional "sparse signal recovery techniques (based on compressive sampling)", sub-micrometer optical resolution cannot be achieved but with an actual resolution of 3–4  $\mu\text{m}$  [14], and the reason is mostly the reduced signal-to-noise ratio [13] [14] [82]. For the contact typed computational imaging, a grid of tightly focused laser spots generated by a uniformly laser-illuminated lenslet (microlens) grid is required. This focused grid is then used to perform high-resolution scanning ( $\sim 1$   $\mu\text{m}$ ) of the sample. By using this method, Shuo Pang [83] has achieved a resolution of 1.2  $\mu\text{m}$  after reconstructing in the imaging of cells. However, the bulky illumination module is very complicated and needs to be precisely aligned.

Those on-chip lensless imaging systems have presented the possibility of the imaging of cells in a microchip in a very compact and inexpensive way. Although the sub-micrometer optical resolution has been achieved, the computational imaging reconstruction method is not flexible enough to cope with on-line monitoring and characterization of living cells. According to different microscopy methods or optical properties of samples, the optical configuration, illumination schemes, the selection and modification of computing algorithms for the image reconstruction can vary. Moreover, the data acquisition and computational speed have not been fast enough for the user to observe microfluidics and

cells in real time while his/her operation [13] [17]-[19]. Therefore, the computational imaging is more suitable towards end-point diagnosis in the field. The contact/shadowing imaging method is simple and intuitive enough to ensure users to have “*what you see is what you get*” in real time, but the imaging capability has not been fully realized and the image forming mechanism still needs further investigation and characterization. Cell culture and cell-based assays often require flexible imaging capabilities for cell morphology visualization as well as colorimetric or fluorescent characterization down to single cells level. Reported lensless imaging systems have not presented the readiness to meet all those requirements. Additionally, much effort should be applied on how to integrate the imaging methods properly with long-term cell culture microsystem in terms of biocompatibility, disposability and stability issues.

### **1.3 Objectives of the study and appropriate solutions**

There is an increasing need for systems that can provide non-invasive real-time monitoring of cell cultures for long-term investigations. Although live cell imaging instruments have been long in the market, the high price limits their popularization. Miniaturized cell culture systems have presented great advantages over conventional method. However, the imaging of a microchip still relies on the expensive and large optical microscope. With the rapid advancement in CCD and CMOS image sensors, very compact and inexpensive lensless or lensfree systems for imaging cells in microchips have been developed recently. The integration of such lensless imaging configuration with miniaturized cell culture systems still need to be investigated in terms of biocompatibility, disposability and stability.

#### **1.3.1 Goal and objectives of the study**

The goal of this thesis is the conception, development and evaluation of an all-in-one microsystem with combined long-term animal cell culturing and real-time microscopy functions suitable for applications in cell biology and point-of-use diagnosis.

The study of the all-in-one cell culturing-imaging microsystem will be further specified by the following objectives:

1. Long-term incubation up to 2—4 days for mammalian cells in conventional culture medium without using laboratory incubators;
2. Real-time imaging of cell cultures and cells under microfluidic processing without using a standard low magnification optical microscope with optical resolution 3—4  $\mu\text{m}$ ;
3. On-line characterization of individual mammalian cells (with diameters around 10—15  $\mu\text{m}$ ) by the morphology, proliferation, as well as the colorimetric and fluorescence staining;
4. Compact and inexpensive, for example, a palm-sized device under 200,00 Euro;
5. Flexible temperature range of 4—45°C for the incubation of other types of animal cells with temperature stability comparable to commercial-grade incubators.

### 1.3.2 Working plan of the study

According to the objectives of the study, the all-in-one microsystem will include both a micro incubating module and a compact cell imaging module. Therefore, the working plan of the study will be as follows:

1. Firstly, the design principle will be investigated and a stand-alone micro-scaled incubating module will be established by using conventional culture medium running in the room environment. The design principle and the operational protocol will be evaluated and modified by the responses of mammalian cells in culture over several days.
2. Based on the standard optical microscopy principle, a compact and cost-effective automatic imaging module dedicated for the long-term time-lapse microscopy will be constructed and validated by the characterization of cells in culture. The emphasis of the evaluation will be on imaging quality and long-term running stability of the system.
3. In order to further shrink the imaging part, a more compact and cost-effective imaging module will be established based on the lensless or lensfree imaging method for the real-time imaging and characterization of growing cells. A disposable microchip suitable for the lensless imaging configuration will be developed for sustaining the cell culture under observation in a biocompatible environment. The imaging quality with cell cultures will be evaluated and compared with that of a low magnification optical microscope.
4. Finally, according to the design principle for the stand-alone micro incubator, a microfluidic culturing system will be developed for the selected compact imaging method. A complete cell culturing procedure: cell loading, long-term cell incubating, cell staining, cell passaging will be carried out under the real-time observation in order to evaluate the performance of the finished microsystem.

## 2 Theories and Analysis

According to the roadmap of this thesis, there are questions which need to be analyzed and verified theoretically before carrying out the materials preparation and experiments. In the following paragraphs of this chapter, the principle of sustaining the physiological microenvironment for cell culturing outside the incubator will be firstly analyzed. And then, related calculation methods for determining operational parameters of microfluidics will be presented. As to the imaging aspects, the standard microscopy imaging principle will be shortly introduced as the basis for the optical design of a compact imaging device. The principle of shadow imaging method will be thoroughly analyzed and quantitatively characterized, by which the opportunity of on-chip integrated imaging module capable of flexible cell imaging and characterization will be evaluated theoretically.

### 2.1 Sustaining physiological environment out of incubator

Cell cultures *in vitro* need to be immersed into liquid culture medium all the time. Through the liquid phase, soluble nutrients and gases can be exchanged and supplied to the cells. The gaseous and humidity environment inside an incubator is essential for keeping the medium with stable pH value, osmotic pressure, ample oxygen level and temperature. When the medium is exposed to the environment inside the incubator, the physical and chemical parameters of the liquid phase will be in equilibrium with the gaseous physical environment of the incubator. Therefore, the key to sustaining the physiological environment for cell culture *in vitro* is how to sustain these physical and chemical properties of the culture medium. More specifically speaking, the question is that how to sustain the culture medium at that equilibrated state as inside the incubator.

**Table 2.1 Physical and chemical environment comparison**

	<b>inside incubator</b>	<b>outside incubator</b>
<b>Temperature</b>	37°C	20 – 25°C
<b>Humidity</b>	≥ 90%	40 – 70%
<b>CO<sub>2</sub></b>	5 – 10%	0.03%
<b>O<sub>2</sub></b>	1 – 21%	20 – 21%

Climate parameters of inside and outside of an incubator are presented and compared in Table 2.1, in terms of temperature, humidity, CO<sub>2</sub> and O<sub>2</sub> concentrations. Generally, there are still quite a lot of incubators with no oxygen control, and the O<sub>2</sub> concentration is similar to that of air. Inside the body, the O<sub>2</sub> concentration is however from 1–14%, lower than that in the atmosphere. Some “tri-gas” incubators with oxygen regulation can provide lower oxygen level, enable mammalian cell culture with relative faster growth rate, longer lifetime and less stress reactions.

According to the differences between an incubator and room environment as shown in Table 2.1, if the equilibrium medium is taken out to the room atmosphere but still kept at 37°C, obviously, there will be a leaking trend of dissolved CO<sub>2</sub> in the medium to the air because there is much less CO<sub>2</sub> partial pressure in the air, and thus the pH value of the medium will increase. The O<sub>2</sub> dissolved in the medium can be kept stable because the O<sub>2</sub> partial pressure in the air is similar or higher than that of the incubator. Therefore, a gas- and water vapor-tight system is essential to keep the medium in the same equilibrium state. This principle will be used for establishing a stand-alone cell culturing microsystem without incubators.

## 2.2 Parameter calculations for operating stand-alone microfluidics

Compared to the conventional cell culturing with macro-scale vessels immersed in bulk medium in a static manner, the aim of microfluidic cell culture systems is to establish more controllable and reproducible *in vitro* cellular microenvironments. The determination of the geometry parameters of a microchip and the microfluidic parameters for operation is very important for the success of cell culturing, and here the stand-alone feature of the microsystem should be also considered. On one hand, the medium supply should provide enough nutrients and oxygen for cell culture within the microchip; on the other hand, the flow velocity should be slow enough without inducing cell injuries.

In conventional static culture, the medium is generally changed every 3 to 4 days ( $T_{macro}$ ), in contrast to this, microfluidic perfusion offers continuous fresh medium supply by convective flow. What should be the proper flow rate or how often the medium should be changed in the microfluidic system? To answer this question, a simple micro-channel model, with channel height  $h$ , width  $w$  and length  $L$ , is applied here. There are three time scales for cell culture: cell reaction or substance consumption time scale  $t_r$ , lateral (perpendicular to the flow direction) diffusion time scale  $t_d$  and convection flow (flow direction) scale  $t_c$ , the duration of the liquid flow from the inlet to the outlet. Inside the micro-channel, cells grow on the bottom floor with a density of  $\sigma$ ,  $\Delta S$  standing for a unit area on the bottom floor, and unit cellular mass consumption rate  $K_m$ . If the initial concentration of the substance is  $C_0$ , the diffusivity of the biological molecules is  $D$ , and the average flow velocity is  $\bar{v}$ , then the three time scales can be expressed as [8]:

## 2. Theories and Analysis

$$t_r = \frac{C_0 h \Delta S}{K_{m\sigma} \Delta S} = \frac{C_0 h}{K_{m\sigma}} \quad t_d = \frac{h^2}{2D} \quad t_c = \frac{L}{\bar{v}} \quad (\text{Equation 2-1})$$

In the micro-scale cell culture, the channel height  $h$  is much smaller than the medium thickness  $H$  in the conventional petri dish. Thus, the lateral diffusion process with time scale  $t_d$  ( $\sim h^2$ ) in the micro-channel happens much faster than the cell consumption process with time scale  $t_r$  ( $\sim h$ ) [8]. “The typical diffusivity of biological molecules in solution is between  $2 \times 10^{-5}$  cm/s (ion) and  $7 \times 10^{-7}$  cm/s (proteins). Plugging in a value of  $D = 10^{-6}$  cm/s gives a diffusion distance of 0.8 mm over 1 h. For a typical micro-channel with a 100  $\mu\text{m}$  width, the diffusion time is 50 s. To diffuse 3 cm (across a 60-mm culture dish), it will take 52 days. This means that diffusive transport of nutrients and wastes to/from cells is only responsible when the length scale is below 1 mm. In living tissues, an extensive blood capillary network delivers nutrients to within a few hundred microns of all cells [84].”

In a simple micro-channel shaped microfluidic cell culturing chip, the mass transportation is aided by the convective medium flow along the channel [8]. The continuous supply of fresh medium provides a concentration gradient sustaining the diffusion process [84].

With same cell type, same cell density and same medium or solution, the reaction time  $t_r$  is linear to the height of the channel  $h$ . Therefore, the maximum turnover time  $T_{micro}$ , which means for how long the medium inside the culture channel has to be totally replenished, can be deduced to as in Equation 2-2:

$$T_{micro} = \frac{h}{H} T_{macro} \quad (\text{Equation 2-2})$$

The turnover time is solely determined by the height of the micro-channel. The convection flow scale  $t_c$  is the time range when the fresh medium being introduced from the inlet until flowing to the outlet of the channel. If the convection flow scale is just equal to the turnover time [8]. Then, the average flow velocity and flow rate at supply-consumption balance status can be obtained as in Equation 2-3:

$$\bar{v} = \frac{HL}{T_{macro}h} \quad Q = \bar{v}hw = \frac{wHL}{T_{macro}} \quad (\text{Equation 2-3})$$

This means with a given channel height  $h$ , the average flow velocity  $\bar{v}$  and flow rate  $Q$  increases as the channel length  $L$ . If  $\bar{v}$  or  $Q$  is smaller than the value at balanced status as shown in Equation 2-3, then medium in the latter part of the channel has been already depleted by cells before the fresh medium has arrived.

What should be noticed is that, in a gas-tight microsystem, the oxygen level also has to be considered when determining the low limit of the flow rate. Conventional cell culturing vessels or cell culturing microchips are not gas-tight. The oxygen supply is not limited by the medium. However, in a gas-tight microsystem the oxygen is only supplied by the medium with dissolved oxygen. For the theoretical calculation, some experimental parameters should be used for the calculation in the material and methods chapter: The mean oxygen

consumption rates of one cell varies between  $10^{-17}$  for fibroblasts and  $10^{-16}$  for hepatocytes mole per second [85]. Under 37°C and oxygen partial pressure of 0.2 atm, there is 0.22 milli-mole oxygen dissolved in 1-liter equilibrium medium [86], corresponding a concentration of  $2.2 \times 10^{-7}$  mol/ml

With given micro-channel width  $w$  and length  $L$ , the flow rate is also determined at the supply-consumption balance status. As the thickness  $h$  of the micro-channel decreases, the average flow velocity increases resulting in a steeper parabolic shaped flow front as shown in Figure 2.2. Then the shear stress is much higher compared to microchips with a relative thicker medium layer above cells [87].

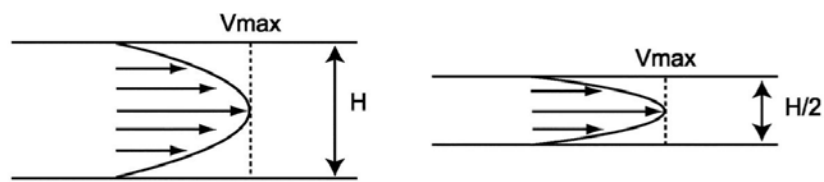


**Figure 2.2** Velocity profile for a channel of height  $H$  and another channel of height  $H/2$  with same maximum velocity  $V_{max}$ . The rate of change in velocity perpendicular to the flow direction is much greater in the lower channel [87].

The shear stress on the cell culturing substrate of a microfluidic chip with no cells can be represented mathematically with Newton's Law of Viscosity [88]:

$$\tau = -\mu \frac{dv}{dz}, \quad z = 0 \quad (\text{Equation 2-4})$$

where  $\mu$  is the viscosity of the liquid,  $v$  is the fluid velocity and  $z$  is the coordinate along the channel height. For the 2D Poiseuille microflow, when  $w \gg h$ , the parabolic flow profile can be simply estimated and the shear stress on the floor can be calculated by [89]:

$$\begin{aligned} \tau &= \frac{6\mu Q}{h^2 w} \\ \tau_{single} &= 2.95 \tau, \quad \frac{a}{h} < 0.25 \\ \tau_{population} &= \left(1 - 0.57 \left(\frac{a}{h}\right)\right) \tau, \quad \frac{a}{h} < 0.25 \end{aligned} \quad (\text{Equation 2-5})$$

The maximum shear stress experienced by one single cell  $\tau_{single}$  is multiplexed by a factor of 2.95 when  $a/h < 0.25$  ( $a$  is the cell diameter) [90]. If there are more cells adherent to the channel, because of the effect of neighboring cells, the shear stress on cell population  $\tau_{population}$  decreases and is approximated by a linear coefficient of  $1 - 0.57(a/h)$ . The effect can be ignored when cell radius is much smaller than the channel height [91].

## 2. Theories and Analysis

As for microchips of different geometrical designs, the velocity field  $v$  inside the microchip can be numerically resolved from Navier-Stokes equation with non-slip boundary condition by FEM (Finite Element Method) simulation software. Then the shear stress can be estimated and calculated according to Equation 2-4.

### 2.3 Optical configurations applied by standard microscopy

In order to design and establish a very compact imaging device for cell culture based on imaging principles of standard microscopes. The optical configurations and imaging principles are briefly introduced as follows:

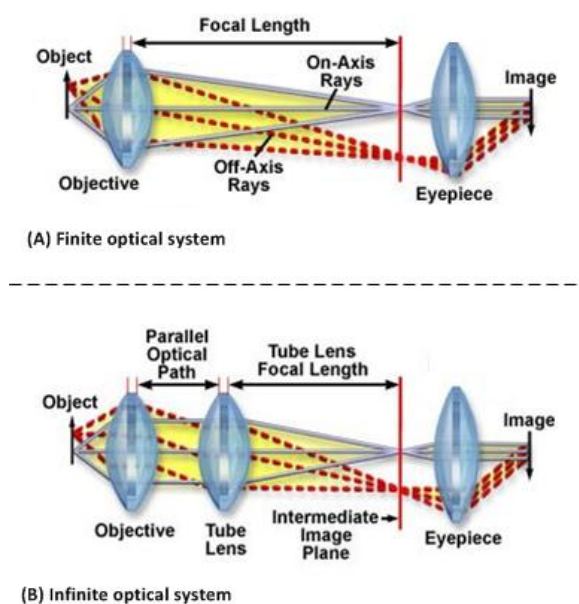


**Figure 2.3 (a) Optical paths of the finite optical system; (b) optical path diagram of the infinite optical system with an infinite-corrected objective and a tube lens** [<https://www.microscopyu.com/microscopy-basics/infinity-optical-systems>, 2011].

The simple compound microscope consists of an objective and an ocular or called eyepiece, and was first built by Robert Hooke in the 17<sup>th</sup> century [92]. The diagram of its optical path can be checked in Figure 2.3 (A) [93]. The image plane of the objective lens is at the front focal plane of the ocular. This intermediate image will be then magnified again and the final microscopy image will be formed in the human eyes. In such so-called “finite tube lens microscope”, the distance from the objective to the eyepiece has to be therefore fixed. The optical tube length varies according to different microscope manufacturers and models. For example, the standard tube length for Zeiss is 160 mm, for Olympus is 180 mm, and for Leica and Nikon is 200 mm [92]. However, if adding optical components into the light path the tube length has to be increased, thus introducing spherical aberrations.

Microscope objectives were then corrected in order to make its image to be formed into the infinity. Another tube lens was introduced into the optical light path to form the intermediate image. Such an “infinity-corrected optical system” is shown in Figure 2.3 (B). In the infinity region between the objective and the tube lens, optical components such as vertical illuminators, filter cubes, beam-splitters, polarizers, etc. can be simply inserted without bringing spherical aberrations [93]. The infinite optical system can make the design of the microscopy imaging system much more flexible. The transverse magnification of the infinite optical system is the ratio of the tube lens’s focal length to that of the objective [92]. The focal length of the tube lens of different microscope manufacturers varies For example, the standard focal length of tube lens of Zeiss is 164.5 mm, for Olympus is 180 mm, for both Nikon and Leica are 200 mm [92][94].

## 2.4 Theoretical resolution of “very near-field” shadow imaging

Lensless shadow imaging method will be introduced in order to further scale down the imaging module for cell culture in microchips. Therefore, the image forming mechanism of shadow imaging will be investigated and characterized theoretically.

The image-forming principle of shadow imaging is by light projection. The overall optical resolution of the system is determined by diffraction effect and pixelation (digitalization) effect from the imager. As reviewed in Chapter 1.2.3.1, “The Potential of contact/shadow imaging need to be developed for microchip applications”, the theoretical resolution of shadow imaging will be discussed here with regard to the distance from sample to the imager, as well as the possibility of inserting a microchip intermediating cell culture in an optimized culturing condition.

According to the Huygens-Fresnel principle, light diffraction is considered as a summation of spherical waves rather than a summation of plane waves. The amplitude at any later point is the superposition of the wavelets [15][95]. For a given aperture, the diffraction pattern of the light beam is determined by the distance from the aperture to the observation plane as shown in the diagram of Figure 2.4.

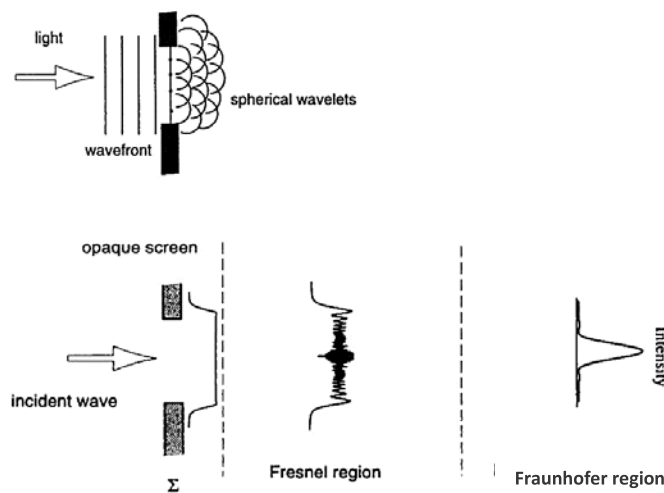


**Figure 2.4** Near-field and far-field diffraction regions [95].

An opaque screen containing a small aperture is illuminated by a plane wave. The diffraction patterns at a plane of observation change with the distance  $s$  between the aperture and the observation plane: (1) When  $s$  is very small, the diffraction pattern is almost a projection of the aperture with slight fringing around its periphery; (2) when  $s$  becomes intermediate, the fringes become more pronounced, and the diffraction pattern changes in structure as the distance increases. The diffraction in this region is known as the

Fresnel diffraction, which is also called near-field diffraction; (3) when  $s$  is very large, the pattern does not change in structure but merely changes in size. The diffraction in this region is known as the Fraunhofer diffraction or the far-field diffraction. The Fraunhofer diffraction pattern can be observed using a lens [15][95].

The shadow imaging obviously falls in the first type diffraction pattern. The samples are placed even closer than the near-field region, that the shadow image can be called “very-near field” diffraction. Due to the similarity of the configuration, the optical resolution of shadow imaging can be interpreted by the principle of optical lithography.

Lithography is the pattern transfer technique in the microfabrication. There are three types of photolithographic exposure techniques: contact printing, proximity printing, and projection printing. Contact and proximity printing, also called shadow printing, are the simplest and least expensive methods of imaging without any lens. In Proximity printing, the mask is kept away from the wafer with a small distance that minimizes defects resulted from contact. The optical resolution and image distortion are related to the distance  $s$  from the mask to the wafer surface (in proximity printing, the photoresist thickness can be ignored compared to  $s$ ). A typical intensity distribution of light incident on a photoresist surface after passing through a mask is illustrated in Figure 2.5. The mask contains a periodic grating consisting of opaque and transparent spaces of equal width  $b$  [96].

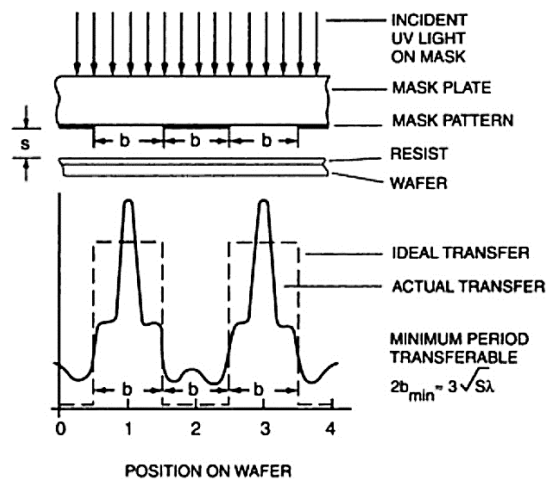


**Figure 2.5** Light distribution profiles on a photoresist surface after light passes through a mask containing an equal line and space grating [97] [98].

The resolution  $R$ , which is the minimum resolved dimension  $b_{\min}$ , under exposing radiation of wavelength  $\lambda$  and with mask-to-wafer distance  $s$  in the air, is given by [97] [98]:

$$R = b_{\min} = \frac{3}{2}\sqrt{\lambda s} \quad (\text{Equation 2-6})$$

## 2. Theories and Analysis

Based on Equation 2-6, for a gap of 10  $\mu\text{m}$  using 400 nm exposing radiation the resolution limit of proximity printing lithography is about 3  $\mu\text{m}$  [96].

In Equation 2-6,  $s$  is measured in the air (the refractive index of air  $n_{air} = 1$ ). If more condensed optical media, each with a thickness of  $d_i$  and refractive index of  $n_i$ , are interlayered in the space between, the resolution formula should be corrected as:

$$R = b_{min} = \frac{3}{2} \sqrt{\lambda \left( \sum \frac{d_i}{n_i} + s_{air} \right)} = \frac{3}{2} \sqrt{\lambda \left( \sum \frac{d_i}{n_i} \right)} \quad (\text{Equation 2-7})$$

When the intermediate layer is close in contact with the surface underneath, the thickness of air can be ignored. According to Equation 2-7, it means if the gap interlayered with transparent membranes of higher optical density, the resulting optical resolution can be further improved.

According to Equation 2-7, under averaged illumination wavelength of 550 nm, the corresponding theoretical thicknesses  $d_{max}$  of transparent materials are estimated with given resolution values as shown in Table 2.2. The selected materials are  $\text{Si}_3\text{N}_4$ , SU-8, Dry Film Resist (DFR),  $\text{SiO}_2$  and  $\text{TiO}_2$  with refractive index of 2.05 [99], 1.67 [100], 1.64 [101], 1.55 and 2.65 [102] respectively. All the materials have been proved with the biocompatibility when applied in biochips. The unfilled gap in the tablet thickness is due to the impossibility in process technologies for the corresponding materials.

**Table 2.2 Corresponding thickness of a transparent material for a given optical resolution**

	$n$	$R = 1 \mu\text{m}$	$R = 2 \mu\text{m}$	$R = 3 \mu\text{m}$	$R = 4 \mu\text{m}$
Air	1.00	0.80 $\mu\text{m}$	3.20 $\mu\text{m}$	6.40 $\mu\text{m}$	12.80 $\mu\text{m}$
$\text{Si}_3\text{N}_4$	2.05	1.66 $\mu\text{m}$	-	-	-
SU-8	1.67	1.35 $\mu\text{m}$	5.40 $\mu\text{m}$	12.15 $\mu\text{m}$	21.60 $\mu\text{m}$
DFR	1.64	-	-	11.93 $\mu\text{m}$	21.20 $\mu\text{m}$
$\text{SiO}_2$	1.55	1.25 $\mu\text{m}$	5.00 $\mu\text{m}$	-	-
$\text{TiO}_2$	2.65	2.14 $\mu\text{m}$	8.56 $\mu\text{m}$	-	-
Parylene C	1.64	1.33 $\mu\text{m}$	5.32 $\mu\text{m}$	11.93 $\mu\text{m}$	21.28 $\mu\text{m}$

( $n_i$  : refractive index;  $R$ : optical resolution; averaged illumination wavelength: 550 nm)

In order to observe the individual mammalian cells (with diameters around 10–15  $\mu\text{m}$ ) and cell culture, the overall optical resolution of the developed lensless system should be in the range of 3–4  $\mu\text{m}$ . From the theoretical calculation results shown in Table 2.2, with interlayered transparent biocompatible membranes within the thickness of 12  $\mu\text{m}$ , an optical resolution of the “very near-field” diffraction better than 3  $\mu\text{m}$  should be achieved. Therefore, it is possible to use a microchip designed with a very thin layer of a transparent membrane as an interface between the cell culture and the image sensor. Cells can be

sustained in an optimized physiological condition, and meanwhile, diffraction effect can be minimized to the most by the “very-near field” shadow imaging.

According to the “Nyquist sampling criterion”, the best spatial resolution that can be represented by an image sensor is doubled pixel pitch divided by magnification [103]. For the demand of the high definition imaging, the pixel size of a 1/3.2’ optical format (diagonal size) CMOS image sensor has been fabricated down to 1.1  $\mu\text{m}$  (Aptina Imaging, AR1230/1331CP, USA). As there is no magnification of shadow imaging or it can be considered as one, the pixelation (digitalization) limit by the image sensor should be down to double pixel size as 2.2  $\mu\text{m}$ . It means the imaging capability of the “very-near field” shadow imaging could be corresponding to that of a low-magnification microscopy.

As to fluorescent staining, the shadow imaging principle will not be applicable because the fluorescence emits in all directions. Interference fluorescence filter composed of alternating multi-layered materials such as  $\text{SiO}_2$  and  $\text{TiO}_2$  can be very thin with a thickness level of several micrometers in all. In the “very-near field”, the fluorescence of cells should be still imaged by the underneath image sensor, but should be more blurred. However, the fluorescence imaging could be interpreted with shadow imaging together in the aim of obtaining an improved resolution for stained cell culture.

## 3 Materials and Methods

In this chapter, related designs and developments preparing for the future experimental setups will be described. According to the theoretical analyses and calculations, following construction works will be carried out along the roadmap of the study: (1) a micro-channel based microfluidic system with good gas- and water vapor-tightness will be established and characterized in order to prove the concept of a stand-alone cell culture microsystem; (2) a compact automatic microscope of infinitive optical configuration will be designed and constructed as a flexible “desktop” imaging device for cell culture in stand-alone microchips, and the price list of its constructing parts will be presented; (3) according to the “very-near field” shadow imaging principle, a microchip with a transparent membrane bottom will be fabricated for sustaining the cell culture onto the image sensor. The image sensor is also modified to enhance its robustness or to alter its spectrum responsivity and make it suitable for the shadow imaging or the fluorescence imaging application. (4) The setup for the “very-near field” shadow imaging will be further integrated with microfluidic parts and temperature control module in order to realize the stand-alone cell culture and imaging functions in a room environment.

### 3.1 Establishing a stand-alone microfluidic incubating system for cell culture

In order to simply verify the principle of a stand-alone microfluidic system for mammalian cell culture without using any incubators, a commercially available plastic micro-channel slide optimized for cell culture is selected as the microchip. A transparent heating plate for microscopy use provides temperature control of the microchip. The slide is modified and connected with microfluidic parts of good air- and water vapor-tightness. The operational parameters will be calculated, and the resulting physiochemical parameters of the microenvironment will be characterized and verified according to the requirements of cell culture.

#### 3.1.1 Modification to a plastic micro-channel slide based setup

A flat-channel based flow chamber is the simplest microfluidic chip that has long been applied and characterized for cell culture. A commercially available ibidi plastic micro-channel slide  $\mu$ -slide VI<sup>0.4</sup> is employed (ibidi GmbH, Germany) here as the cell culture

microchip. The size of the plastic plate is 25 mm x 75 mm, on which 6 rectangular micro-channel each with a height of 400  $\mu\text{m}$  is engraved. Other dimensions of the micro-channel can be found in Table 3.1. The bottom is formed by thin film lamination, the material of which is a secret and protected by the manufacturer. It is claimed that the inner floor where cells will grow is tissue culture treated, and with very good optical quality comparable w glass.

**Table 3.1 Ibidi micro-channel specifications**

Dimensions	
Number of channels	6
Channel volume	30 $\mu\text{l}$
Channel length	17 mm
Channel width	3.8 mm
Channel height	0.4 mm
Adapters	female Luer
Volume per reservoir	60 $\mu\text{l}$
Growth area	0.6 $\text{cm}^2$ per channel
Coating area using 30 $\mu\text{l}$	1.2 $\text{cm}^2$ per channel
Bottom matches coverslip	180 $\mu\text{m}$

[[http://ibidi.com/fileadmin/products/labware/channel\\_slides/S\\_8060X\\_Slide\\_VI04/IN\\_8060X\\_VI\\_04.pdf?x5d9a3=3e4da32eb714ff7b39b3f63cd9550074](http://ibidi.com/fileadmin/products/labware/channel_slides/S_8060X_Slide_VI04/IN_8060X_VI_04.pdf?x5d9a3=3e4da32eb714ff7b39b3f63cd9550074), 2011].

The diagram of the micro-channel slide is shown as in Figure 3.1.1. It is designed that at each end there is a fixed female Luer adapter that can be simply connected with a male Luer barb adapter, the other end of which can be directly pressed into a flexible silicone tubing. The silicone tubing can be consequently pressed with other adapters or thinner tubings with 1/16" OD (outer diameter) and 0.25 mm ID (inner diameter). Translucent FEP (fluorinated ethylene propylene) or PFA (perfluoroalkoxyalkane) 1/16" tubings are common to be used because the material is easy to identify the inside liquid flow, also the material is not very rigid to handle during experiments (Upchurch Scientific, US).

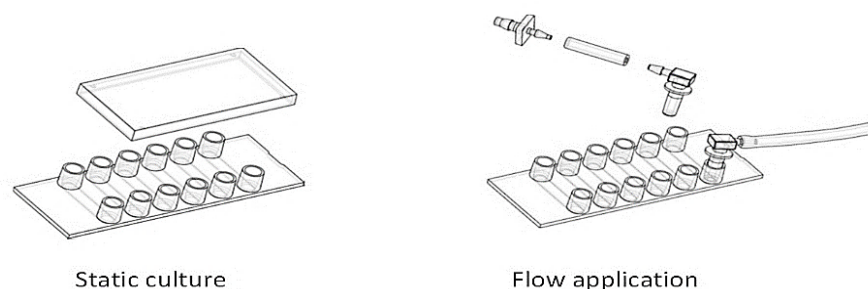


**Figure 3.1.1 Diagrams of ibidi  $\mu$ -slide VI <sup>0.4</sup> that will be used in static cell culture with a transparent click-on cover, and in cell culture with medium supply in perfusion mode**

[[http://ibidi.com/fileadmin/products/labware/channel\\_slides/S\\_8060X\\_Slide\\_VI04/IN\\_8060X\\_VI\\_04.pdf?x5d9a3=3e4da32eb714ff7b39b3f63cd9550074](http://ibidi.com/fileadmin/products/labware/channel_slides/S_8060X_Slide_VI04/IN_8060X_VI_04.pdf?x5d9a3=3e4da32eb714ff7b39b3f63cd9550074), 2011].

### 3. Materials and Methods

However, there are two problems about the ibidi microchip used in flow application as shown in Figure 3.1.1:

1. Commonly used tubing materials (Teflon and specially silicone) are with high gas and water vapor permeability, which is only suitable for using inside an incubator.
2. Inside each female-male Luer connection, the column space forms “big” reservoir as a dead volume at inlet or outlet of the flow channel compared to its small volume of less than 30  $\mu\text{l}$ . Every time when fresh medium or reagent is applied, the solution will firstly be diluted inside the reservoir. The application profile and duration of reagents under test will be hard to be controlled.

To solve the tubing problem, modifications are required to both tubing and connecting parts. PEEK tubing should be the best choice when a gas tight setup is required. But PEEK is very rigid and can hardly be processed and handled. As seen in Table 3.2, barrier properties of common tubing materials are summarized, and different units from different data resources are unified for easier comparison. Finally, the Tefzel tubing is chosen. Tefzel tubing is a fluoropolymer product that is 3 orders better than Teflon (FEP or PFA) tubing in barrier functions against gas and water vapor. Moreover, multi-layers of plastic tape are wrapped tightly onto the Tefzel tubing surface to further enhance its physical barrier properties. Tefzel tubings at inlet and outlet of the microfluidic system are connected to plastic syringes.

**Table 3.2 Barrier properties of materials for microfluidics**

	Permeability CO <sub>2</sub>	Permeability O <sub>2</sub>	Water Absorption	Moisture Vapor Transmission
	cm <sup>3</sup> ·mm/mm <sup>2</sup> ·hr·cmHg@25°C		%	g·mil/100 in <sup>2</sup> ·24hr@37°C, 90% RH
<b>Silicone</b>	6.5 x 10 <sup>-5</sup>	1.1 x 10 <sup>-5</sup>	0.1	4.4—7.9
<b>PDMS</b>	9.0 x 10 <sup>-6</sup>	1.7 x 10 <sup>-6</sup>		
<b>FEP</b>	3.6 x 10 <sup>-5</sup>	1.6 x 10 <sup>-5</sup>		
<b>PFA</b>	4.9 x 10 <sup>-5</sup>	1.9 x 10 <sup>-5</sup>		
<b>Tefzel</b>	5.4 x 10 <sup>-8</sup>	6.5 x 10 <sup>-9</sup>		
<b>Parylene C</b>	1.6 x 10 <sup>-9</sup>	1.5 x 10 <sup>-9</sup>	0.06	0.14

(Data source from Upchurch Scientific, Inc., US; V&P Scientific, Inc., US)

To solve the problem of both dead volume and gas permeable property at the joint part, firstly all the tubings are cut by a special tubing cutter (Upchurch Scientific, US) to ensure a smooth end surface smooth and with little deformation, and then the Tubing is inserted into the male Luer barb adapter with the tubing end in the same level as the outer rim of the adapter. The small upper round opening of the barb adapter holds the tubing very tightly, and then two separate parts become one plastic part. The space between the adapter and the tubing is filled with PDMS (Polydimethylsiloxane) fluid and cured for 24 hours in room temperature. In Figure 3.1.2, simplified diagrams showing that by this modification the “big” medium reservoir at each end is eliminated by supplying medium

from the thin Tefzel tubing directly to the micro-channel. The junction has been proved working well under a flow rate of several hundreds of micro-liters per hour without happening any leakage.

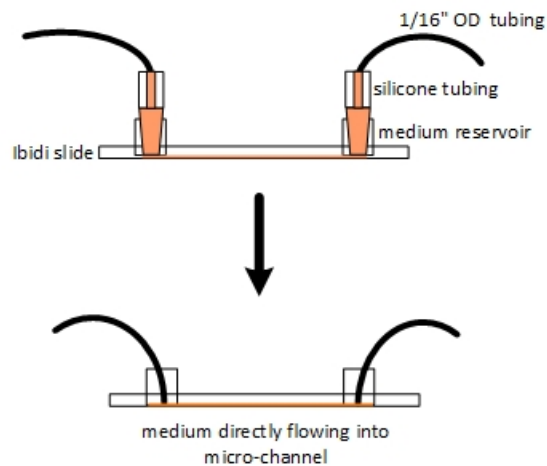


**Figure 3.1.2** Simple sketch showing the improvement achieved by filling the medium reservoir at each end of the micro-channel with PDMS polymer. The medium flow is directly guided by Tefzel tubing into the micro-channel. Orange shades represent the medium.

### 3.1.2 Flow rate determination for the established micro-channel slide based microfluidic system

The flow rate is a very important operational parameter for microfluidic systems. There are two aspects which need to be considered when determining the range of flow rate suitable for cell culture. The upper limit is determined by whether the shear stress experienced by cells is in the safe range; the lower limit is determined by whether there are sufficient soluble nutrients and oxygen supply for cells.

#### 3.1.2.1 Shear stress induced by microflow in the micro-channel

The shear stress in a rectangular flat micro-channel model has been theoretically characterized and can be directly calculated by Equation 2-5. Therefore, with a shear stress limit value, the corresponding flow rate in such a very flat-shaped channel can be calculated as:

$$Q = \frac{\tau h^2 w}{6\mu} \quad (\text{Equation 3-1})$$

### 3. Materials and Methods

For the viscosity value of the medium  $\mu$ , the value of water at 35 °C:  $0.7171 \text{ Pa} \cdot \text{s}$  [104] can be used.  $h$  (0.4 mm) and  $w$  (3.8 mm) are the height and width of the ibidi micro-channel in respective.

The shear stress *in vivo* experienced by interstitial cells is below  $0.1 \text{ dyn/cm}^2$  (corresponding to 0.01 Pa) [105]. In an ordinary microfluidic cell culture channel, the range of the shear stress is between  $0.5$  to  $10 \text{ dyn/cm}^2$  (corresponding to 0.05 to 1.0 Pa) [84]. Shear stress can have a range of negative effects on cells. Biased information on functional cellular analysis could be occurred even at a shear stress below  $10 \text{ dyn/cm}^2$  (corresponding to 1.0 Pa). For a non-mechano-sensitive cell type such as CHO (Chinese Hamster Ovary) cell line, when the shear stress value is as small as  $0.4 \text{ dyn/cm}^2$  (corresponding to 0.04 Pa), not only the viability is as that in the conventional cell culture condition, but also there is no shear-induced intracellular  $\text{Ca}^{2+}$  flux [46]. In reference [89], human fibroblast cells grew well under a shear stress value of no more than 20 mPa (corresponding  $0.2 \text{ dyn/cm}^2$ ) in a micro-channel bioreactor for 14 days. Epithelial cells *in vivo* are usually exposed to mechanical forces of different levels, the lower range of which is about  $0.2 \text{ dyn/cm}^2$  (corresponding to 0.02 Pa) during physiological processes [106]. In this micro-channel slide based microfluidic system, a shear stress level of  $0.2 \text{ dyn/cm}^2$  is corresponding to a flow rate of about  $10 \mu\text{l/h}$ .

#### 3.1.2.2 Soluble nutrients and oxygen supply provided in the micro-channel

For the conventional mammalian cell culture, a bulk medium layer with about 4 mm thickness can generally support a monolayer of cells for 4 days to grow into 90% confluence at 37°C. While in the situation of cell culture on the micro-channel microchip, the medium thickness of 0.4 mm is 10 times less. Therefore, according to Equation 2-2, the maximum turnover time, which means the time after which the medium inside the culture channel has to be totally replenished, should be 0.4 days or 9.6 hours. Then the flow rate has to be no less than  $3.1 \mu\text{l/h}$  for this micro-channel based system.

Furthermore, the dissolved oxygen supply needs to be considered. The mean oxygen consumption rates of one cell varies between  $10^{-17}$  and  $10^{-16}$  mole per second [85]. For a cell suspension with a density of 500,000 cells/ml, the  $30 \mu\text{l}$  medium inside the ibidi microchip contains 15,000 cells at the beginning. These cells will proliferate up to about 45,000 cells when they forming a confluence monolayer. The average oxygen consumption rate of cell population inside the micro-channel can be calculated as in the range of  $3 \times 10^{-13}$ – $10^{-12}$  mol/s. Under 37°C and 0.2 atm oxygen partial pressure condition, there is about 0.22 milli-mole oxygen dissolved in 1-liter equilibrium medium, i.e. the oxygen concentration is  $2.2 \times 10^{-7}$  mol/ml [86]. Therefore, by estimation, the lower limit of the flow rate of this micro-channel based system for different cell type varies from 5 to  $49 \mu\text{l/h}$  for providing enough oxygen supply to that amount cell population.

According to Equation 2-3, the nutrients concentration of medium decrease along the channel in the flow direction. If the observation point falls at the middle or first half part of the channel, then the flow rate lower limit for supporting the cell culture under observation

will be from 2.5 to 25  $\mu\text{l/h}$ . Therefore, if cells are not those high oxygen consumption types, for example liver cells, 10  $\mu\text{l/h}$  should be proper for most cell types that will be cultured in this established micro-channel based gas- and water vapor-tight microfluidic system.

### 3.1.3 Temperature control for the micro-channel based slide

A commercially available transparent hot plate with a controller as shown in Figure 3.1.3 (A) is applied here for keeping the slide bottom at a suitable temperature for cell growth. The main body of the hot plate (IX2 standard type-heating, Tokai Hit Co. Ltd, Japan) is made of hard glass, onto which transparent heating material is coated. The actual temperature field of this hot plate is verified by an IR (Infrared) camera (wavelength: 8–14  $\mu\text{m}$ , measuring range: 2–250°C, Pyroview 256CE, DIAS Infrared Systems, Augenamte Scientific GmbH, Germany). In order to properly position the hot plate under the IR camera, a cold metal block is employed as the initial positioning reference under the field of view. When the hot plate is set at 37°C, as shown in Figure 3.1.3 (C), the actual heating area (the middle rectangular area) provides a temperature accuracy of less than  $\pm 0.2^\circ\text{C}$ .

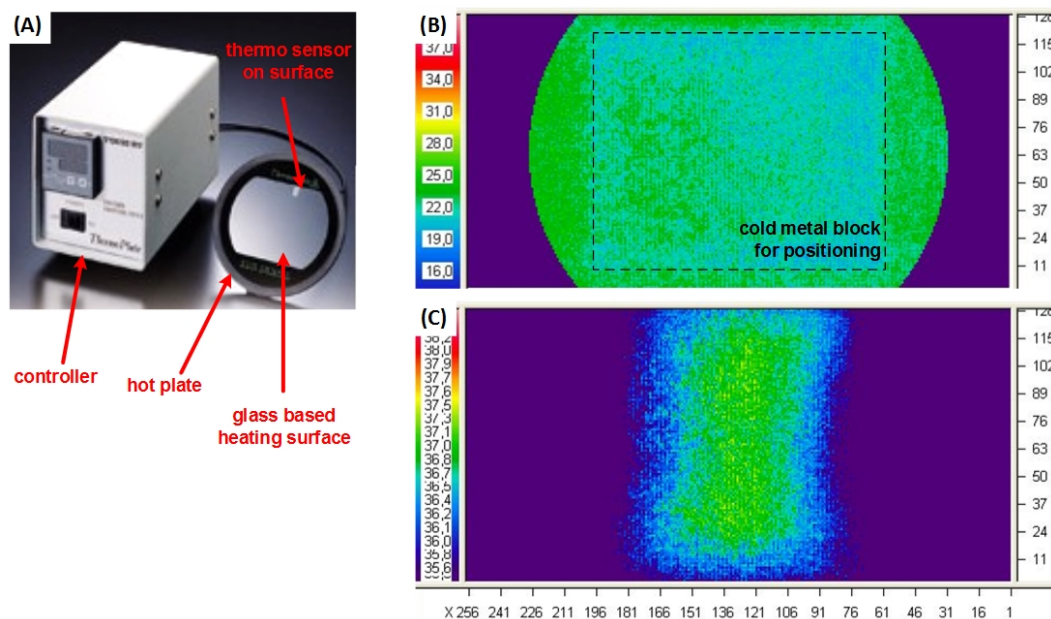


**Figure 3.1.3** (A) Photograph of the hot plate and its temperature controller; (B) Field of view of the IR camera, in which dashed lines represent the profile of a cold metal block used as a positioning reference under the IR camera; (C) The actual heating area of the hot plate are clearly represented by greenish color corresponding to  $37 \pm 0.2^\circ\text{C}$ .

As shown in Figure 3.1.3 (B), the flat heating surface is fixed and contacted tightly with the bottom side of the channel-based slide. All channels can be supported by the even heating surface. However, the actual temperature inside the channel should be lower than the set temperature of the hot plate. Therefore, another thermocouple tip is protected and isolated by parafilm and placed from the inlet onto the inner floor of a dummy channel,

### 3. Materials and Methods

which is next to the experiment channels. This dummy channel is filled with culture medium and then sealed. As the calculated flow rate will be in the range of 10–20  $\mu\text{l/h}$ , the turnover time of the medium will be several hours in such a 30  $\mu\text{l}$  micro-channel. Compared to the speed of the heat conduction process in such a thin layer medium, the medium flow is so slow that can be considered as “static”. The actual temperature of the experimental micro-channel can be therefore measured and adjusted by monitoring the temperature at the dummy channel inlet.

## 3.2 Constructing a compact “desktop” automatic microscope for time-lapse cell imaging

Dedicated to the long-term time-lapse imaging of multi-channel experiments, an economical and compact automatic “desktop” imaging device is developed according to the standard microscopy imaging principle. Compared to expensive and bulky live cell imaging microscopes, the aim is to provide a simplified but competitive imaging version suitable for stand-alone microfluidic cell culture chips or systems. The development includes: (1) optical and mechanical construction; (2) electronics and controllers; (3) supporting software

### 3.2.1 Optical and mechanical construction of the compact microscope

For the design flexibility, the infinite optical principle is employed in constructing this compact automatic microscope. The InfiniTube (Infinity photo-optical company, Göttingen, Germany) is a commercially available modular product that can be assembled by screwing the mechanical tubular package of each optical component to others provided to form the microscope optical train. With proper adaptors, it can be used with infinity-corrected objectives offered by main manufacturers. The InfiniTube optics is equivalent to a tube lens of 200 mm focal length, however, by complex optics design, it has a much more compact size of only 105 mm. The diagram of the InfiniTube optics module is shown in Figure 3.2.2. A variable Iris diaphragm installed after the tube lens module is used to alter and control the depth of field and/or the light throughput. Another focuser adjustment is at the end of the InfiniTube. The optical path from the back end of the microscopy objective to the front end of the infinite tube is considered as the infinite place. The compact microscope is designed as an inverted type for easy adapting to cell imaging from the bottom side of the cell culture. A RA (right angle) mirror is introduced in the infinite place just after the objective adaptor to bend the rest optical path in the horizontal direction. The optical train is positioned in a low-profile casting. Thus, higher mechanical stability can be obtained. The coaxial illuminator module situates between the RA mirror and the tube lens module. Inside the coaxial illuminator module, there is a dichroic beam splitter used for reflecting the excitation beam and transmitting the emission fluorescent beam at the same time. As a simplified microscope system dedicated for long-term experiment with specific fluorescence excitation and transmission bands, the filter cube and mechanical switch and shutter are eliminated. Fluorescence filters are inserted and fixed with the optical train.

Fluorescent and gray-scaled imaging of cells can be made alternatively with different LED illuminations.

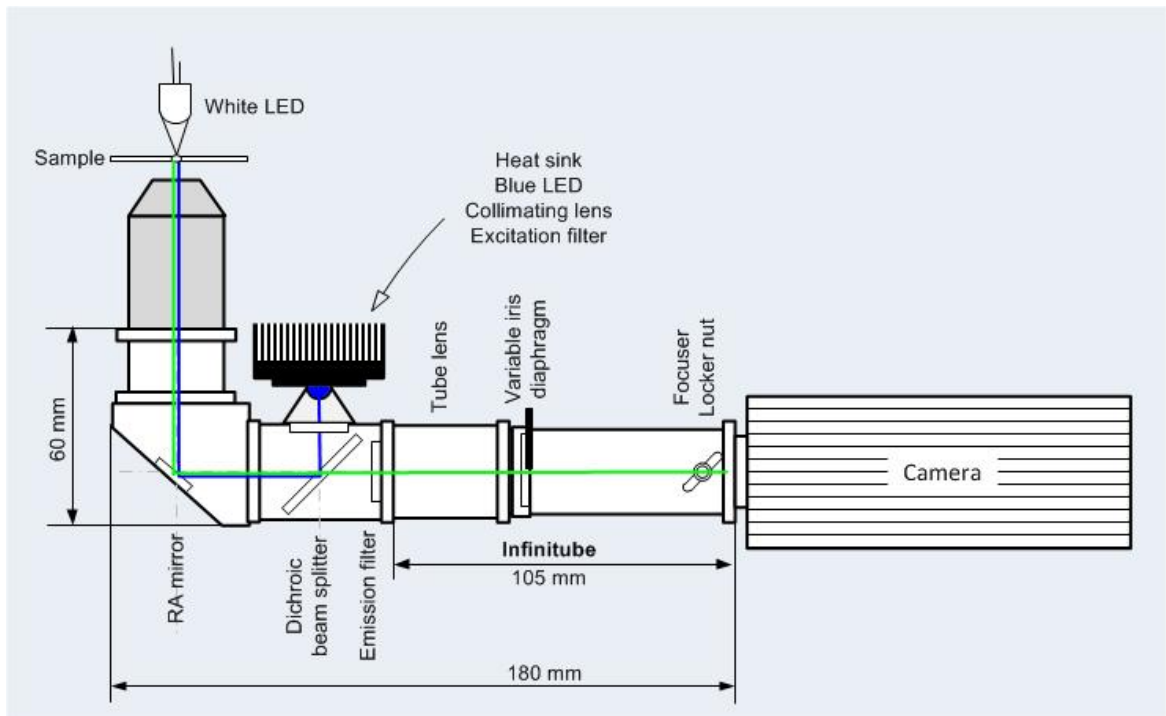


**Figure 3.2.2** Self-drawn sketch of the self-constructed compact “desktop” microscopy system, including infinite microscopic optics, illuminations and digital camera (not in scale).

The compact microscope consists of two types of illuminations. One is a white LED for the bright field cell imaging, and the other is a high-power blue LED for the epi-fluorescence microscopy. Both illuminations are capable of working in a strobe mode. One advantage is that the LED illumination will not produce as much heat as the conventionally used light bulb that will be working continuously as the microscope illumination. The electrical current through the PN junction of the LED can be considered constant, which means the output light flux can also be considered constant during each imaging process. Another advantage is that no mechanical shutter is required, and the shutter time can be simply set in the configuration of the digital camera. In this way, cells are only exposed to illumination for a couple of seconds while being taken one or two images at every time interval. Vibrations resulting from the shutter and filter cube movements are eliminated and specialized vibration resistance table is not required. The configuration and characterization of both illuminations are described as below:

**Bright field illumination:**

A 5-mm diameter LED with a wide emitting angle of  $120^\circ$  is positioned closely with a distance of 9 mm above the sample in order to simulate the Köhler illumination. The

### 3. Materials and Methods

sample can be illuminated with a uniform illuminator plate just from above. The field of view of the 10x or 20x microscopy objective is very small, therefore, the illumination field casted by the LED can be considered uniform when looking in the perspective of the sample spot. The numerical aperture (NA) of the illumination can be approximately calculated as the ratio of the LED radius (2.5 mm) to the distance above the sample plane. In the microscopy system, the NA of illumination should be adapted to the objective in order to get the optimal imaging quality. Under the Köhler illumination, the NA of the illumination should be opened approximately 70—80% of the objective NA [93][107]. For the most commonly used microscopy objectives, a 10x objective is usually with NA = 0.3 (Olympus CPLFLN 10x PH), and 20x objective with NA = 0.45 (Olympus LUCPLFLN 20x PH), and long working distance (LWD) 20x objective is with a relatively smaller NA = 0.4 (Olympus PLN 20x). The NA of the white LED illumination is about 0.27 by calculation, thus theoretically an objective with NA of 0.34—0.39 should be applied.

#### **Epi-fluorescence illumination:**

The fluorescent illumination is coupled from the port provided by the coaxial illuminator. The optics in the port is designed for those fiber optical illuminations (for example, Olympus X-Cite 120 light source). The original coupler at the port is disassembled in order to fit and position the LED collimating lens with a larger diameter in the center. Blue light exciting green fluorescence is one of the most commonly used spectrums of fluorescent dyes, such as FITC (Fluorescein Isothiocyanate), FDA (Fluorescein Diacetate), or cells transfected with GFP (Green Fluorescence Protein). High power LEDs (Luxeon K2, Lumileds of Phillips) are used as the excitation. The peak wavelengths of the two selected blue LEDs are 470 nm and 455 nm respectively. The corresponding light fluxes can be up to 46 lm for the 470 nm blue LED and 620 mW for the 455 nm royal blue LED (Lumileds of Philips), when the maximum allowed electrical current 1500 mA for both LEDs is applied. The excitation filter for blue LED 470 nm is BP (Band Pass) 472/30 (Peak wavelength/FWHM: nm) (25 mm diameter fluorescent interference filter, Edmond optics), and that for royal blue LED 455 nm is BP 440 (dissembled from Olympus microscope BH2). The emission filter for the greenish fluorescence is BP 520/35 (25 mm fluorescent interference filter, Edmond optics). The plastic TIR (total internal reflective) collimating lens (Carclo lens, Lumintronics LED-technik GmbH) specially designed for Luxeon K2 LEDs with plain and clear surface is clipped onto an adaptor and then glued on the LED base, which is six angle star shaped heat sink. The heat conducting glue is also electrically isolated. An even larger multi-pillar structured heat sink is further glued onto the backside of the LED base. The collimating angle is  $7.9^\circ$  and the total output efficiency is 80%—85%. The cross-sectional profile of the output light intensity is a single-peak steep shape with a FWHM (full width half maximum) of around 12 mm. The diameter of the coaxial illuminator port is 10 mm, by which the outer rim around the collimated light flux is shielded.

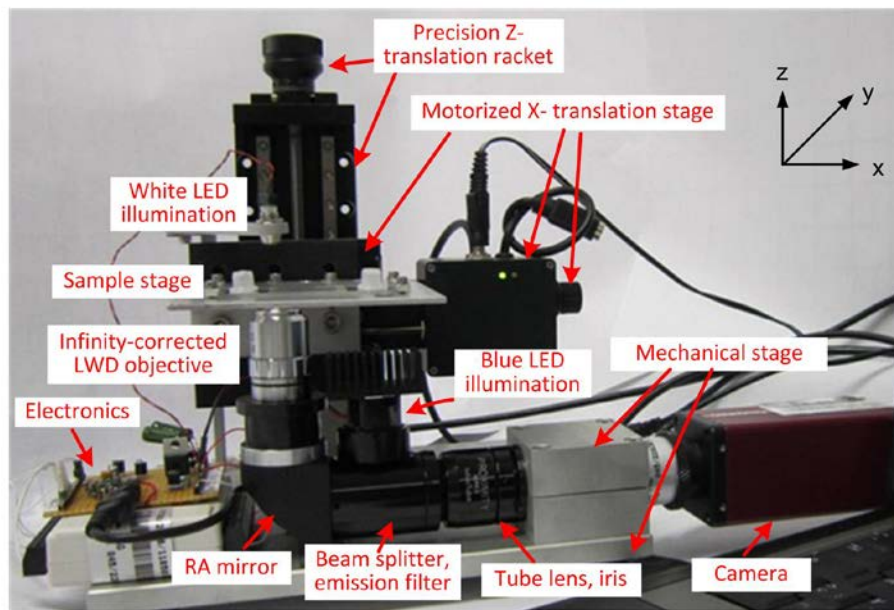


**Figure 3.2.2** Photograph of the finished mechanical and optical construction of the compact “desktop” microscope.

As a simplified version of conventional automatic microscopes, the compact microscope is only implemented with x-axis movement of the sample stage. The finished compact microscope is shown as in the Figure 3.2.2. The sample stage is fixed onto the x-axis of a motorized linear translation stage (Zaber Technologies Inc.) via an RA metal part, which is further connected to another z-axis precision translation racket (Ovis GmbH). The sample stage is connected with the RA metal part by screws and very hard springs, which are used for adjusting and retaining the horizontal level of the sample stage for long time. This linear translator can cover 4 parallel channels of an ibidi slide with its maximum moving distance of 28 mm. The infinite microscopy optics, electronics control module, and sample stage part are finally assembled together onto a homemade metal frame forming a whole concrete unit. At the bottom, 4 rubber nodes are situated at each corner to reduce mechanical vibrations of the whole frame. The footprint of the whole system is only of an A4 paper size. The components for constructing the compact “desktop” microscope are listed in Table 3.3. The cost of the whole system should be in the range of 5,000 – 10,000 Euro depending on different objective, camera and advanced LED illumination module selected.

### 3. Materials and Methods

**Table 3.3 Price list of the optical and mechanical components for constructing the “desktop” automatic microscope**

Parts	Specification	Manufacturer	Price (Euro)	Sum. (Euro)
Main optics	Infinitube standard RA	Infinity Photo-optical company	1372,50	1372,50
	coaxial illuminator		665,00	665,00
Excitation filter	25 mm GFP excitation filter 472/30	Edmond Optics	237,50	237,50
Emission filter	25 mm GFP Emission filter 520/35		237,50	237,50
Objective	LWD 20x		~ 500,00	500,00
LED blue	LUXEON K2 L XK2-PB14-P00, blau, 46 lm	Lumileds of Philips	5,88	5,88
LED royal blue	LUXEON K2 L XK2-PR14-Q00, royal-blue, 620mW		5,88	5,88
LED lens	Carclo Lens	Lumitronix LED-Technik GmbH	2,28	2,28
	Heat sink 38 mmx38 mm		5,54	5,54
	Heat conducting glue		8,90	8,90
LED white	LED plus housing		1,00	1,00
Camera	Dolphin F145 C	Allied Vision Technologies	2590,00 (17% off for institute)	2150,00
DAQ card	USB 6009 multifunctional DAQ card, 14 bit 48 KS/s	National Instruments	259,00	259,00
Electronics		Farnell	20,00	20,00
Linear translation stage	T-LS28M	Zaber Technologies Inc.	945,25	945,25
Linear precision stage	TL60-75 precision linear table	Ovis GmbH	380,70	380,70
Framework, adaptors	Homemade	Internal workshop	200,00	200,00
				6996,93

### 3.2.2 Electronics and controller for the hardware automation

To speed up the development process of the hardware automation of the compact microscope, all the hardware will be controlled by LabView program (V8.2, National Instruments, Austin, TX, USA). The system block diagram is shown in the Figure 3.2.3 (A), including a linear motorized stage (T-LS28M, Zaber Technologies Inc. Canada), a firewire digital camera (Dolphin F145C, Allied Vision Technologies Germany), a DAQ (Data Acquisition) card (National Instruments, Austin, TX, USA) and self-developed electronics for illuminations and temperature controlling (if required for cell culture microchips).

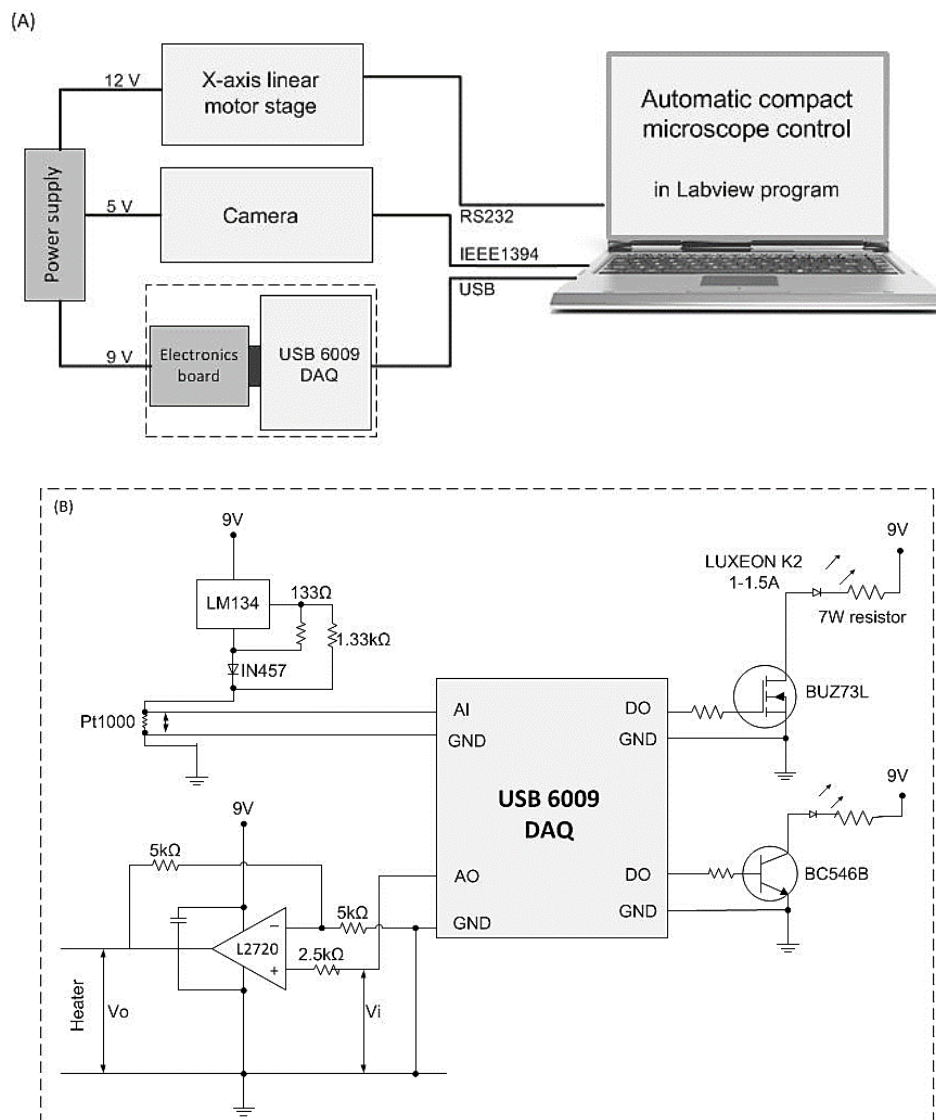


**Figure 3.2.3** (A) System block diagram of the automation components of the compact microscope; (B) Schematic diagram of the electronics of illuminations and temperature controlling modules connected with the DAQ card.

### 3. Materials and Methods

The core component of the motorized linear translation stage is a step motor with a mechanical accuracy of 4–5  $\mu\text{m}$  and a resolution down to 0.1  $\mu\text{m}$ . The motor is already integrated with a controller that provides both Visual Basics and LabView programming interfaces. The signal is transmitted via the series RS232 port of the computer. An external 12V power supply is used for the step motor. Digital cameras that support DCAM standard, including firewire cameras, can be programmed in LabView by default. The firewire color camera (Dolphin F145 C, Allied Vision Technologies, Germany) is connected via a mini 4-pin IEEE1394 (firewire) port, and another 5V external power supply is required. The DAQ (Data Acquisition) card USB 6009 is a multi-functional data acquisition device from National Instruments. It includes multiple digital (14-bit) and analog (12-bit) signals input and output that can be easily programmed by LabView. Both power and signal of the DAQ card are transmitted to the computer via a single USB port.

The DAQ card is used for intermediating self-made electronics to be controlled by the computer. The schematic diagram of the electronics can be checked in Figure 3.2.3 (B). LED illuminations are switched on/off by the DO (digital output) voltage from the DAQ card. There is also a close-loop temperature-controlling module for microchips. The module includes a temperature sensing circuitry that reads the temperature value into the AI (analog input) of the DAQ card. By the difference between the current temperature and the preset temperature value, the AO (analog output) of the DAQ card will generate a proper output voltage, which will be amplified by an OP (operational amplifier) and transformed into heating power.

#### **3.2.3 Control Software for the automated imaging functions**

The compact automatic “desktop” microscope is aimed to provide a flexible imaging device capable of both bright field and fluorescent time-lapse microscopy for long-term experiments. For cell culture and cell-based assays, it is favorable that the imaging system can address multiple channels, and at each testing point alternative bright field and fluorescent cell images can be captured. The finished program control panel is as shown in Figure 3.2.4. The programming behind each button or option will be described below, along with the time-lapse imaging procedure by the compact microscope.

##### **Step 1: Setting positions and imaging configurations of the testing points**

The Labview program for the movement functions was included in the bought linear translation stage (sample slider). These movement functions are placed at the upper block of the control panel. The sample stage is set to come “Home” (mechanical starting position) after every session so that the mechanical accuracy can be reserved for the next round. The selected positions will be saved and numbered. In the middle left block of the control panel, the white LED and blue LED can be switched independently by controlling the DAQ card’s digital outputs. Under each type of illumination, the real-time imaging of the firewire camera is checked in the MAX (Measurement & Automation Explorer), which is the

hardware management of LabView. Parameters for image acquisition by the firewire camera will be adjusted and saved respectively in the middle right block.

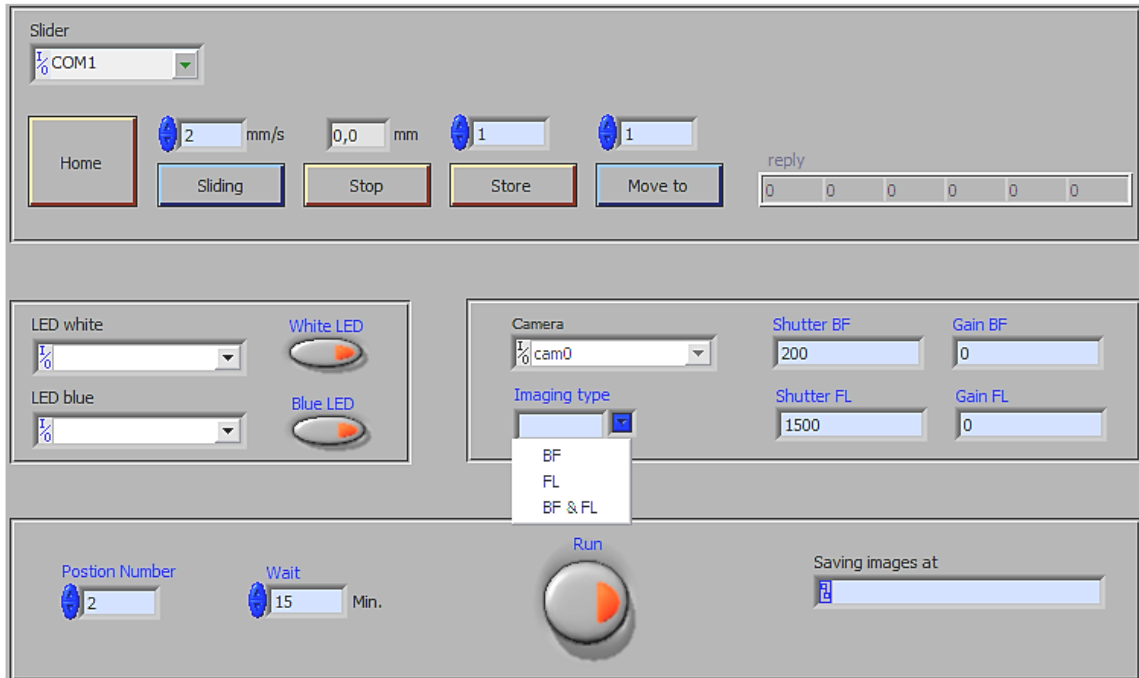


**Figure 3.2.4** Software Front panel of the controlling software for the compact automatic “desktop” microscope.

### Step 2: Setting imaging modes

There are three imaging modes that can be chosen for the time-lapse imaging by the compact microscope. They are BF mode (bright field imaging only), FL mode (epi-fluorescence imaging only) and alternative mode BF&FL (sequential bright field imaging and epi-fluorescence imaging). The camera configuration is adjusted and then saved in the MAX under a specific illumination condition. Like in the conventional automatic microscope, it is not easy to configure time-lapse imaging with two imaging methods of different image acquisition parameters. Here the problem is solved as follows: both bright field and fluorescence camera imaging parameters (shutter time, gain) are configured and saved respectively. Before each image acquisition, the corresponding camera configuration file will be written into the camera file (\*.icd) of LabView interface by the program [108]. In this way, the shutter time and gain settings can be changed by software for each imaging method in the alternative mode.

### Step 3: Timing of the time-lapse imaging procedure

After the setting of positions and imaging modes of testing points in the control panel, it is time to repeat the imaging procedure automatically by the program for the time-lapse

### 3. Materials and Methods

imaging. Sample slide, illumination, and camera are working together as in the time chart shown in Figure 3.2.5.

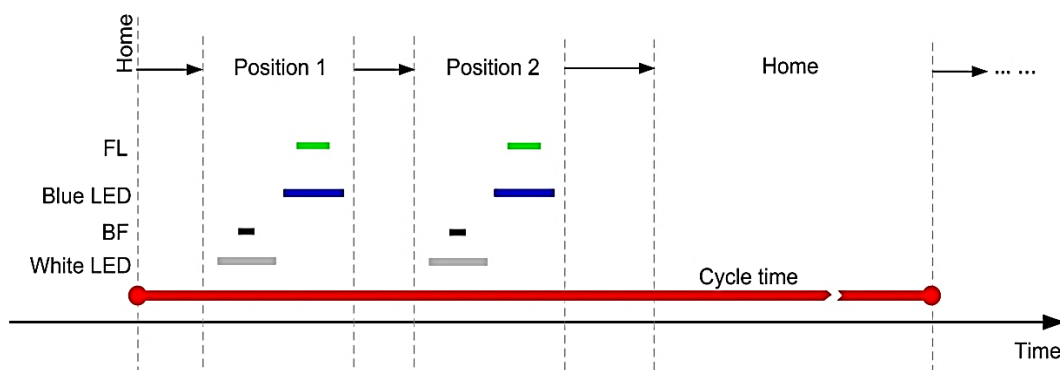


**Figure 3.2.5** Timing illustration of the program for time-lapse alternative bright field and epi-fluorescence imaging mode with 2 testing points.

For the simple illustration, only two testing positions are selected. In order to protect cells from light, the illumination will be only switched on for image acquisition. In each session, the sample stage starts from **Home**. After it reaches **Position 1**, the white LED is switched on, and then the camera snaps according to the imaging configuration file of BF. After the camera is closed, the white LED will be turned off. Then the blue LED is turned on, following the camera taking an image of the sample according to the camera configuration file of FL. After that, the blue LED is turned off. Then the sample stage slides to **Position 2**. The same imaging process repeats. Then, the sample stage will move back to **Home** and stands still. When the waiting time is up, the next round will start. Since the software is aimed for long-term running, a generic error resulted by AMD multi-core CPU should be noticed.

#### **!! Caution for running LabVIEW program with AMD multi-core CPU**

“Most multi-core and multi-processor AMD systems can cause unexpected behavior in NI driver software. This issue occurs when there is significant drift between the timestamp counters (TSCs) on the multiple cores. This TSC drift is often caused by power management features, which cannot be disabled in the BIOS. Many operating systems and applications (such as NI-DAQmx 8.5 or earlier) rely on the TSCs being synchronized. Specifically, this issue impacts AMD processors with an integrated memory controller (Family 0Fh). This problem has also been observed in the Intel E7500 processor [109].” Therefore, an “operating system patch” needs to be applied in the computer with AMD 64 Athlon dual-processor with Windows operating system. Otherwise, a generic error-50202 will appear when running LabVIEW program or its executive form after the experiment running for several hours.

### 3.3 Realization of the “very near-field” shadow imaging configuration

A compact automatic “desktop” microscope for time-lapse imaging has been constructed in Chapter 3.2 according to the standard microscopy imaging method. In order to achieve even higher miniaturization, the lensless “very-near field” shadow imaging method will be applied. In order to realize the “very-near field” optical configuration that has been proven by theoretical calculations and analysis in Chapter 2.3, a microchip with very thin and transparent membrane bottom is required as an interface between the cell culture and the image sensor. Moreover, the image sensor requires processing and modification in order to be deployed in the “very-near field” imaging configuration. In the following paragraphs, the microchip design, fabrication and image sensor processing will be described.

#### 3.3.1 MEMS microchips with transparent bottom membrane

The design and fabrication of microchips for the “very-near” field shadow imaging includes: (1) A MEMS microchip with a very thin transparent membrane bottom for supporting the cell culture inside an optimal environment while interfacing them in the proximity of the sensor surface. The membrane material must be suited for cell culture, i.e. adherent cells can grow and spread on it. All these requirements can be fulfilled by thin membrane made by silicon nitride ( $\text{Si}_3\text{N}_4$ ) [110]. The process used for depositing silicon nitride was already optimized in order to get a defined tensile stress and thus in a very flat strained surface, which provides excellent optical quality for microscopy. (2) Microchips with different thickness of transparent bottom layers. They will be used to check experimentally how the distance between the sample and the image sensor will affect the optical resolution of the shadow imaging method. (3) PDMS microfluidic parts integrated with the microchips for prolonged cell culture duration and as liquid handling interface.

##### 3.3.1.1 Fabrication of the $\text{Si}/\text{Si}_3\text{N}_4$ micro-cavity chip

Microchips with  $\text{Si}_3\text{N}_4$  bottom layers ( $\text{Si}_3\text{N}_4$ -chip) are fabricated by semiconductor process technology. In brief, the process starts with a 4-inch, 525  $\mu\text{m}$  thick, (100) orientated double-side polished silicon wafer. Then 1  $\mu\text{m}$  thick  $\text{Si}_3\text{N}_4$  layers are grown on both sides of the wafer using Plasma Enhanced Chemical Vapor Deposition (PECVD). A photoresist layer (SP2510, Rohm and Haas Electronic Material Deutschland GmbH, Birkenfeld, Germany) is spin coated on one side and patterned for square openings. It has been tested that at least up to a size of 2 mm x 2 mm a 1  $\mu\text{m}$  thick  $\text{Si}_3\text{N}_4$  membrane is mechanically robust and can be fabricated free of defects. However, a microchip with about 1 mm x 1 mm membrane bottom size is more robust when applied to practical operations. Reactive Ion Etching (RIE) is used to isotropically etch the silicon nitride down to the silicon. In this way, openings of 1.64 mm x 1.64 mm are formed in the 1  $\mu\text{m}$  thick silicon nitride. The exposed silicon is then wet etched anisotropically in 20% KOH at 80°C down to the other  $\text{Si}_3\text{N}_4$  layer. A funnel-shaped micro-cavity (volume: 0.85  $\mu\text{l}$ ) is formed in the silicon. Sidewalls of the micro-cavity

### 3. Materials and Methods

lie on four separate (111) crystal planes of the silicon, with an angle of  $54.7^\circ$  to the (110) plane. Considering the limited surface area of high-resolution image sensors, the wafer is diced into  $4.4 \text{ mm} \times 4.4 \text{ mm}$  chips bearing one single-cavity with a transparent bottom membrane as shown in Figure 3.3.1 (A).

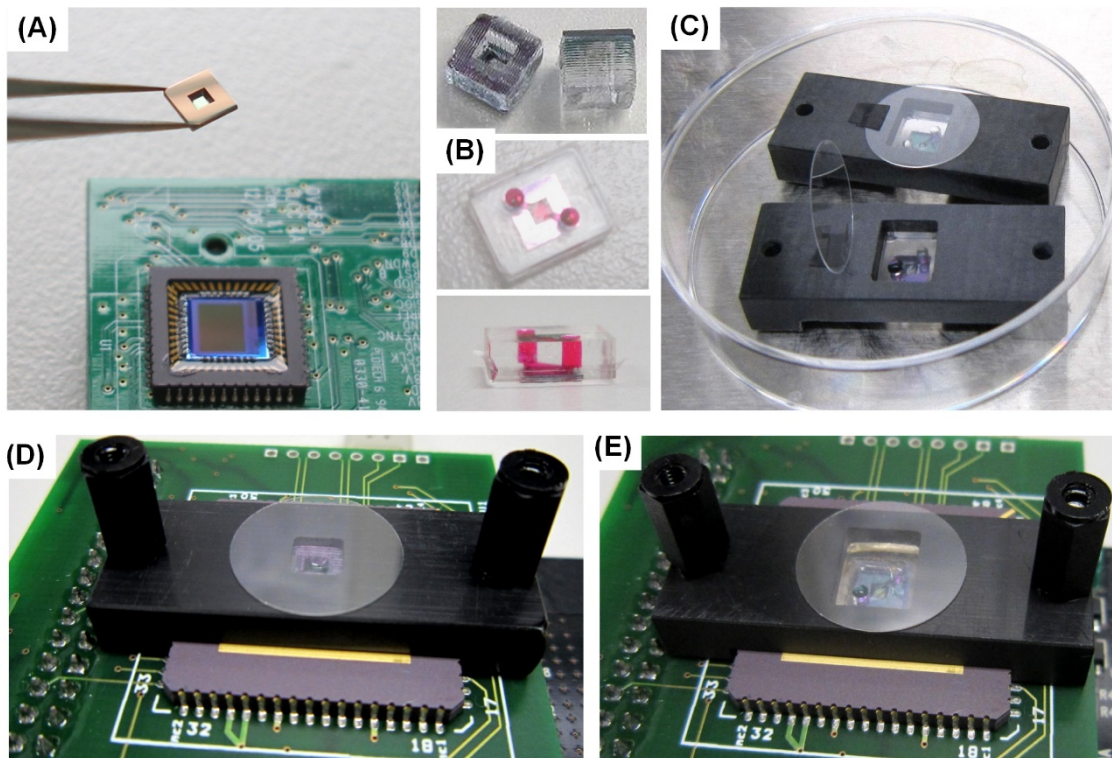


**Figure 3.3.1** (A) A  $\text{Si}/\text{Si}_3\text{N}_4$  micro-cavity chip and a prepared OV5620 image sensor; (B) Micro-cavity chips bonded with micro-well (upper) and micro-channel PDMS upper microfluidic parts (middle and lower); (C)  $\text{Si}/\text{PDMS}$  microchips inserted into plastic chip adaptors for the protection and easy handling of the cell culture either in the incubator or in the room atmosphere; (D) The micro-well chip and (E) the micro-channel chip are aligned and fixed in a good contact onto the self-made OV5650 image sensor board via microchip adapters.

#### 3.3.1.2 Fabrication of the $\text{Si}/\text{DFR}$ microchip

In order to check experimentally how the distance between the sample and the image sensor will affect the optical resolution of the shadow imaging method, microchips with different thicknesses of the thin bottom membrane are fabricated by replacing the above mentioned silicon nitride membrane by a photoresist layer. The dry film resist (DFR) (DuPont PerMX 3020, Micro Resist Technology GmbH, Berlin, Germany) exhibits good adhesion to Silicon and silicon nitride. The  $\text{Si}_3\text{N}_4$  layer is only deposited on one side of the silicon wafer. Funnel shaped wells without bottoms are obtained by using the same

lithography and etching procedures as mentioned above. Then the 20  $\mu\text{m}$  thick foil is laminated on the wafer at 75°C by a hot roll laminator. The procedure is repeated several times so that multilayer DFR with thicknesses of 20, 40 and 60  $\mu\text{m}$  are obtained. Then the laminated wafers are exposed to UV (UltraViolet) light and developed by PGMEA (1-Methoxy-2-propyl acetate) developer solution (mr-dev. 600, Micro Resist Technology GmbH, Berlin, Germany). The cured DFR membrane forms the transparent bottom layer of the micro-cavity chip.

### 3.3.1.3 Fabrication of the Si/PDMS microfluidic chips

The complete microchips used in practice are composed of two parts that are bonded together: the silicon-based micro-cavity chip providing the cell growing substrate and the PDMS parts providing the liquid conservation and exchange interface. Two kinds of PDMS components are fabricated, one is designed for the static cell culture with conventional operation style, and the other is especially designed for cell culture with microfluidic style:

(1) The first type PDMS component is bonded to the micro-cavity chip forming additional reservoir of the small cavity. Its bigger outer PDMS walls provide the possibility of an easier handling of the small silicon chip. For a quick and inexpensive fabrication, the simple casting mode for the “micro-well” shaped PDMS component is fabricated by 3D printing. The height of the outer walls is 5 mm, and the opening is 2 mm x 2 mm, resulting in additional volume of 20  $\mu\text{l}$  for medium conservation.

(2) The second type PDMS component is bonded to the micro-cavity chip forming a micro-channel over the cavity, and there are two openings on each end of the micro-channel (this chip is also called “single-channel” microfluidic chip with respect to the “dual-channel” microfluidic chip in the later chapter 3.4.1.1). Considering the 1 mm limit for the microchip scale [84], the height of the upper micro-channel is designed as 0.5 mm. Together with the height of the silicon micro-cavity chip about 0.5 mm, the 1 mm limit is reached. Going to this limit decreases the shear stress under a given flow rate to the minimum. Considering the limited area of the high-resolution image sensors, the margin area of the micro-cavity chip can only support a micro-channel in the diagonal direction over the micro-cavity. The PDMS component is designed to align the micro-cavity chip with a 300  $\mu\text{m}$  deep squared recess at the backside. A 4.0 mm long channel with the cross section of 500  $\mu\text{m}$  x 500  $\mu\text{m}$  is engraved inside this recess area in the diagnostic direction. An opening with a diameter of 1.5 mm is designed at each end of the channel in order to conveniently connect to the 1/16 inch OD Tefzel tubing. A two-part brass casting mold for the PDMS is fabricated by CNC (Computer Numerical Control) milling. After cleaning of the molds, two parts of the casting mold are fixed together by screws, and the pre-mixed PDMS pre-polymer is injected by a pump. Then the closed mold is heated on a hot plate at 120°C for 60 minutes. After the curing, the PDMS parts are released from the molds.

The cavity chip and the PDMS part are firstly cleaned using isopropyl alcohol and then glued with medical grade silicone-adhesive (MED-4013). The adhesive is cured at 80 °C for 2 hours. The finished Si/PDMS microchips are shown in Figure 3.3.1 (B). For a better

### 3. Materials and Methods

visualization, the micro-channel is filled with red dye solution. Since cross-lined PDMS is biocompatible and also can withstand temperatures from  $-45^{\circ}\text{C}$ – $200^{\circ}\text{C}$  (SYLGARD® 184 SILICONE ELASTOMER KIT, Dow Corning Corporation, US), the fabricated Si/PDMS chips are suitable for cell culture and can withstand autoclave and cryo-conservation.

To test the bonding strength of the finished chips, PEEK tubing (OD: 1/16") is connected to the chip by the compressed tension of the PDMS openings. One end is closed, and the other end is connected with a pressure-controlled airflow. The microfluidic chip is then emerged into a water bath. The air flow is switched on and the pressure is gradually increased. The air flow explodes out from the breaking  $\text{Si}_3\text{N}_4$  bottom membrane at a pressure of 0.65 bar. The bonding of the Si/PDMS microchip is therefore even stronger. As in the microfluidic experiment, the membrane bottom is supported by the image sensor surface underneath as presented in Figure 3.3.1 (D)-(E). The microchip should be applicable for the cell culture related microfluidic operations.

#### 3.3.1.4 Microchip adaptors for the easy and secured handling in practice

The finished microfluidic chips are relatively small and the thin bottom membrane is very fragile. A microchip adaptor is designed for the easy and secured handling. The microchips are inserted into the black plastic adaptors as shown in Figure 3.3.1(C). There is a cover slip on top to protect the biological sample cultured in a static manner from the outer environment. When the microchip is clamped in the adaptor, the bottom membrane is lifted from the floor. Thus, the membrane is well protected. Moreover, the Si/PDMS microchip is aligned and fixed by screws onto the image sensor board via the holes on the adaptor as shown in Figure 3.3.1 (D) and (E). This keeps the microchip bottom and the image sensor surface in a good contact by adjusting the screw but without lateral movement that could scratch or break both surfaces.

### 3.3.2 Processing and modifications to the image sensors

Besides of cells, the surface of the image sensor also needs protection in the shadow imaging configuration. The surface will be planarized by spin coating a very thin layer of SU-8 photoresist, which is transparent and hard after developing. In order to carry out fluorescence imaging under the "very-near field" shadow imaging configuration, an additional interference filter is deposited on the planar SU-8 surface. Details of the processing and modifications to the image sensor prepared for shadow imaging and on-chip fluorescence imaging will be described in the following paragraphs.

#### 3.3.2.1 Image sensor module and image sensor Die

A 1/2.5" 5-Megapixel color CMOS image sensor employed here is OV5620 from OmniVision. The pixel size is  $2.2\ \mu\text{m} \times 2.2\ \mu\text{m}$ . OV5620 is delivered in a 48-pin CLCC package and already soldered on an evaluation daughter PCB board. The daughter board needs to be plugged

into another evaluation mother PCB board that is controlled via USB port by a PC. Both of the daughter (OV05620-EAAA-AA0A) and mother (ECJA-BA0A) evaluation PCB boards are manufactured by OmniVision (ordered from Topas Electronic GmbH, Germany). The controlling software running under Windows is provided by OmniVision free of charge. The protective glass of this package format can be easily removed by heating the glass up to 300–400°C until the silicone glue melts. Then, the bonding wires are protected by biocompatible epoxy resulting in the form as shown in Figure 3.3.1 (A).

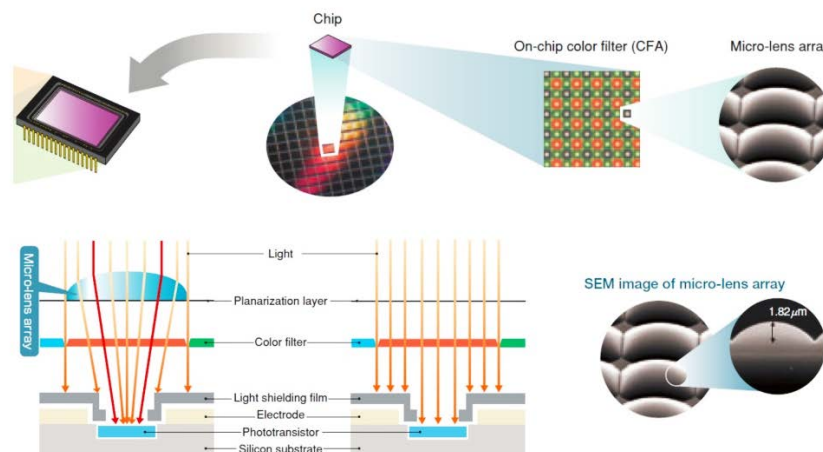


**Figure 3.3.2 The structure of an image sensor under microscope. It includes, from bottom to top, phototransistor, 2 pixels x 2 pixels Bayer patterned on-chip color filter array (CFA) and Micro-lens array for gathering more volume of incident light** [<https://www.photomask.com/products/on-chip-color-filters>, 2011].

The image sensor is fabricated with micro-lens on each pixel in order to collect more light in the active area of each phototransistor as shown in Figure 3.3.2. This layer of micro-lens array is very sensitive to scratching and contaminations. Therefore, the image sensor OV5620 has to be carefully protected and handled after the protective glass is removed. Between each micro-lens and phototransistor is a layer of color filters. A color filter with red, blue or green color is deposited over each pixel. These color filters are arranged alternately in the “2 x 2” Bayer pattern, which means that the smallest color spot that can be represented by the color image sensor is 2 x 2 pixels. Therefore, both the “color resolution” and the spatial resolution of the color image sensors can be considered the same as doubled pixel pitch.

In order to further improve the digital imaging quality, another image sensor OV5650 (supplied from OmniVision Co. Ltd., US) is employed here. OV5650 is a 1/3.2” 5-Megapixel color CMOS image sensor with a higher dynamic range of 69 dB. The pixel size is 1.75 μm x 1.75 μm. 69 pieces of OV5650 imagers are delivered as bare Dies (OV05650-G04A-1E-BUA4 5 MP COLOR CAMERA SENSOR DIE) on a blue membrane frame. Using bare Dies facilitates

### 3. Materials and Methods

the coating processes on the image sensor. Packaging and wire-bonding are performed by our in-house technician afterwards.

#### **3.3.2.2 Protective SU-8 coating on the image sensor Die**

Since the micro-lens array on top surface of the image sensor is very venerable to scratches, and the surface is too rough to be processed if additional fluorescence filter need to be deposited, it is favorable to have a hard and transparent coating on top. SU-8 photoresist is chosen as coating material for its very good transparency in the visible range and planarization capability in a couple of nanometers. Moreover, the SU-8 coating can withstand temperatures up to 200°C, which is compatible with subsequent coating processes like the interference filter deposition. For the spin-coating of the SU-8 on a single image Die, a PDMS adapter with a recess to retain the single Die is fabricated. This adapter levels out and extends the area of the imager Die, so that it can be fixed on the vacuum chuck of the spin coater. SU-8 2005 is spin-coated at 4500rpm for 40 seconds. Then the photoresist layer is baked for at 65 °C for 3 min and then at 95°C for 7 min. A low-cost film mask is aligned with the single Die and the resist is exposed to UV light. The coated Die is then developed with PGMEA (1-Methoxy-2-propyl acetate) developer solution to open the electrical connecting pads at the edges. The surface roughness of the SU-8 coated Die is measured with a confocal microscope (NanoFocus) across a step processed on the sensor surface. Results are shown in Figure 3.3.4. The roughness of the micro-lens array measured is about 300 nm. After SU-8 spin-coating, the roughness of the surface has been significantly improved from about 300 nm to a value of  $\pm 5.0$  nm. The roughness of the surface is greatly improved even at the coating edge. The resulting thickness of the SU-8 coating is about 4  $\mu\text{m}$ .

One of the chips with SU-8 coating is glued into a 68-pin CLCC (Ceramic Leaded Chip Carrier ceramic) chip carrier (68 LCC, .300 sq. cavity, Evergreen Semiconductor Materials, Inc., US), and then wires are manually bonded by an experienced technician. The wires are protected by biocompatible epoxy and further soldered onto the evaluation PCB board to check its working performance. The schematic of the daughter sensor head circuit is provided by OmniVision. The components arrangement is redesigned according to the size of the 68-pin CLCC chip carrier. The OV5650 daughter board is fabricated as a 4 layered PCB.

#### **3.3.2.3 Fluorescent Interference filter coating on the image sensor Die**

The advantages of the interference fluorescence filter have been reviewed in Chapter 1.2.4.3. The interference filter can achieve very high optical density ( $OD \geq 5$ ) while fabricated in a very thin layer (within 5  $\mu\text{m}$ ). Florescence light emits in all directions. therefore, a smaller distance between the sample and the image sensor surface leads to a better resolution of the fluorescence imaging. Image sensor Dies are firstly prepared with SU-8 coating for smoothing the surface, and then samples are placed on a silicon wafer. Each sample is fixed around the edges by Kapton tape, which can endure up to 400°C. The bonding pads are protected during the deposition process. The coating process of a

commercial grade interference filter is carried out by MSO Jena GmbH using Plasma-Ion Assisted Deposition.

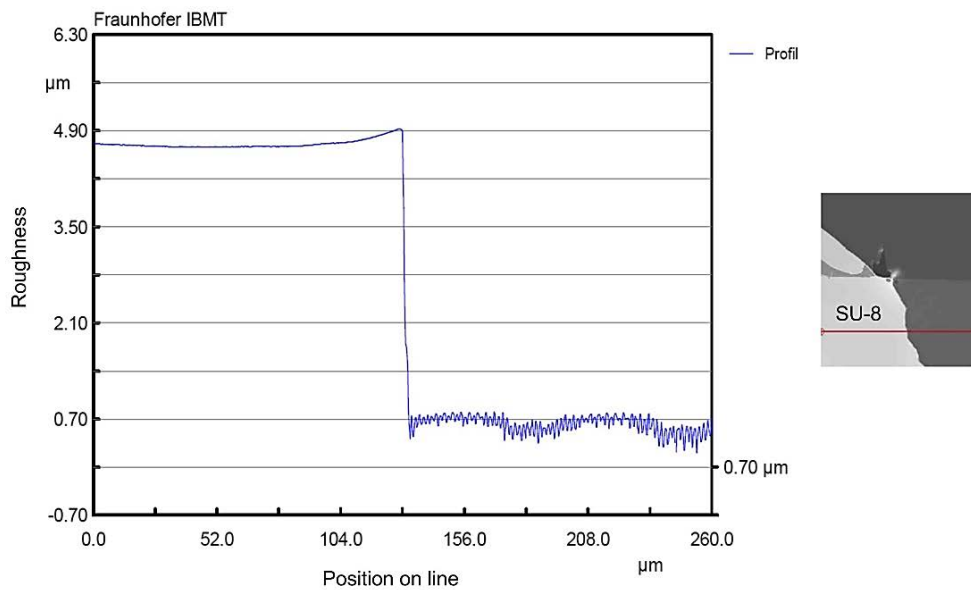
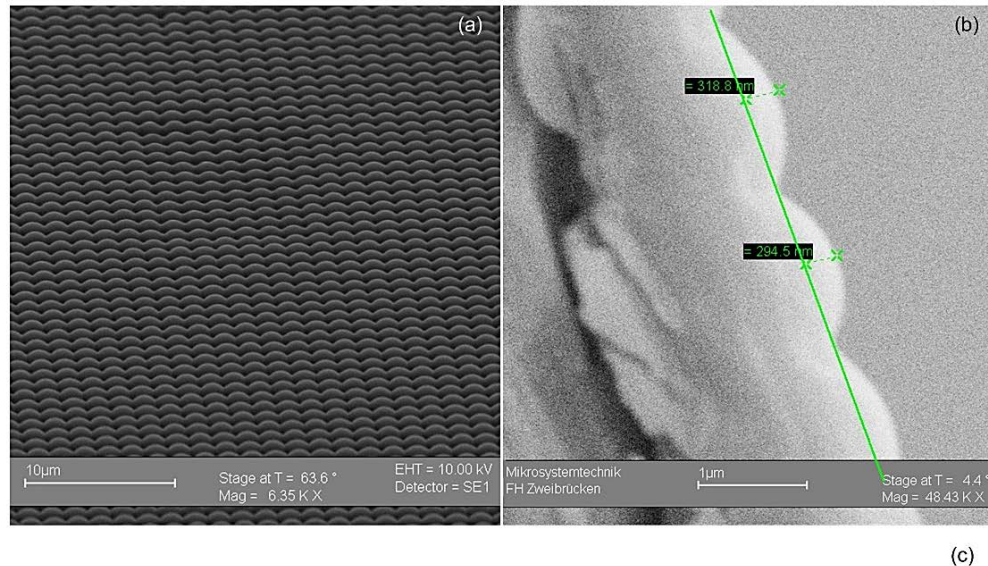


**Figure 3.3.4** (a) The SEM photo of the micro-lens array surface of the CMOS image sensor Die; (b) the image sensor is cut through and the SEM photo depicts its cross section; (c) the roughness profile around the edge between spin-coated SU-8 layer and bare sensor surface.

As the blue light exciting green fluorescence is one of the most widely used bands in life science detections with common fluorescent dye selections like FITC (Fluorescein

### 3. Materials and Methods

Isothiocyanate), FDA (Fluorescein Diacetate), or GFP (Green Fluorescence Protein), the interference filter is specified as below:

<b>Transmittance range (nm):</b>	<b>505 long pass (505 IF);</b>
<b>Transmittance:</b>	<b>90%;</b>
<b>Blocking range (nm):</b>	<b>450 – 490</b>
<b>Optical Density:</b>	<b>6</b>
<b>Tolerance (nm):</b>	<b>±5</b>

The graph below is the actual spectrum response of a 515-nm long pass filter optimized for the coating on a 4  $\mu\text{m}$  SU-8 layer, with less than 0.001% transmittance below 490 nm and with up to 80% transmittance above 510 nm. The interference coating is composed of multiple alternating  $\text{SiO}_2/\text{TiO}_2$  layers, consisting of 88 single layers. The total thickness is about 4.5  $\mu\text{m}$ . Since the actual coating on the Dies is not easy to be tested experimentally, the same coating layer is deposited on a standard B270 glass substrate as a reference and its transmittance is measured at 0° AOI (Angel of Incidence). Results are shown in Figure 3.3.5.

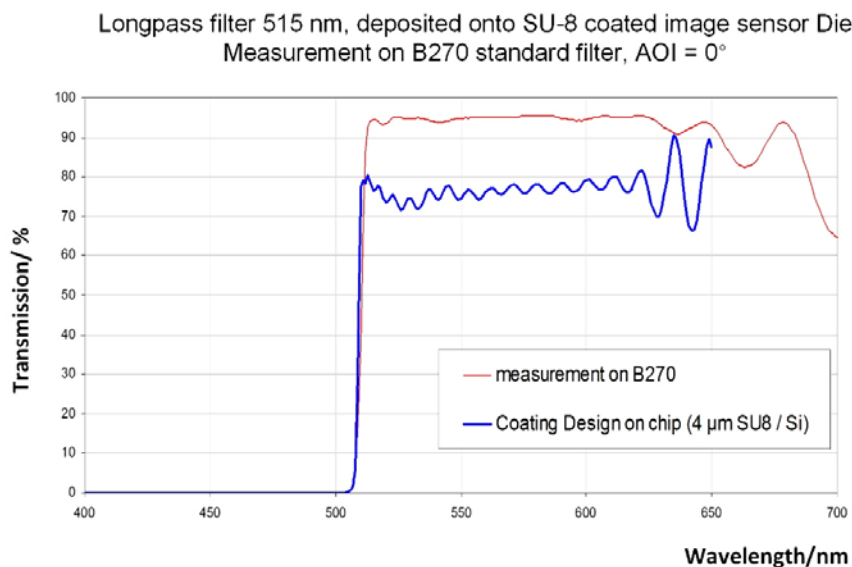


**Figure 3.3.5** Lower curve: the transmittance spectrum of the designed (calculated) interference filter to be coated on the surface of the CMOS image sensor with a thin layer of SU-8 photoresist on top; upper curve: The measurement of the designed coating on a standard B270 glass substrate.

### 3.4 Establishing a stand-alone cell culture microsystem adapted to the “very-near field” shadow imaging

Since the “very-near field” shadow imaging configuration has been realized, the immediate question comes to how to implement this imaging technique with cell culture microsystems. To upgrade the “very-near field” shadow imaging configuration into a stand-alone microsystem capable of cell culture in the room environment, following developments and modifications are required for both the micro-cavity chip and the image sensor module: (1) integration of microfluidics with the micro-cavity chip; (2) making the cell culture microsystem gas- and water vapor-tight; (3) integration of a temperature control system for the cell culture micro-cavity.

#### 3.4.1 Integration of microfluidics with micro-cavity chips

In order to integrate microfluidics with the shadow imaging configuration, PDMS parts with microfluidic channels and openings have been designed and fabricated to couple with the silicon based micro-cavity chips. The developed microsystem includes both single-channel and dual-channel geometries. The microfluidic flow inside the microchip is simulated by software. The shear stress at the culture substrate is estimated from the simulated results.

##### 3.4.1.1 Fabrication of single- and dual-channel Si/PDMS microfluidic chips

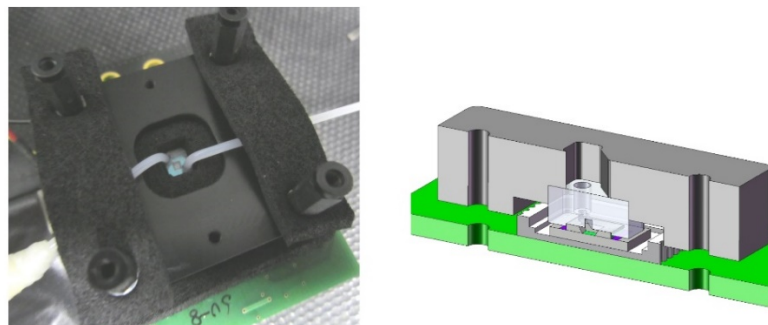


**Figure 3.4.1** (left) Experimental setup of the single-channel Si/PDMS microfluidic chip stacked onto the CMOS image sensor module; (right) Cross sectional view of the stacked components. Antistatic sponges will be used to stuff the gap layer around the microfluidic chip. (The illumination for shadow imaging is not shown)

The micro-cavity chip with transparent membrane bottom is not only suitable for the shadow imaging, but also in accordance with the “groove-structured” principle for microchip designs with low shear stress. In favor of different assay requirements, two types of microfluidic chips have been fabricated, “single-channel” and “dual-channel” microfluidic chips. The fabrication process of the single-channel (micro-channel Si/PDMS chip) microfluidic chip has been described in Chapter 3.3.3.3. As shown in Figure 3.4.1, the fluidic

### 3. Materials and Methods

openings with  $\varnothing$  1.5 mm ID can just fit tightly with 1/16" ( $\varnothing$  1.58 mm) OD Tefzel tubings. The upper microfluidic counterpart is lying in the diagonal direction.

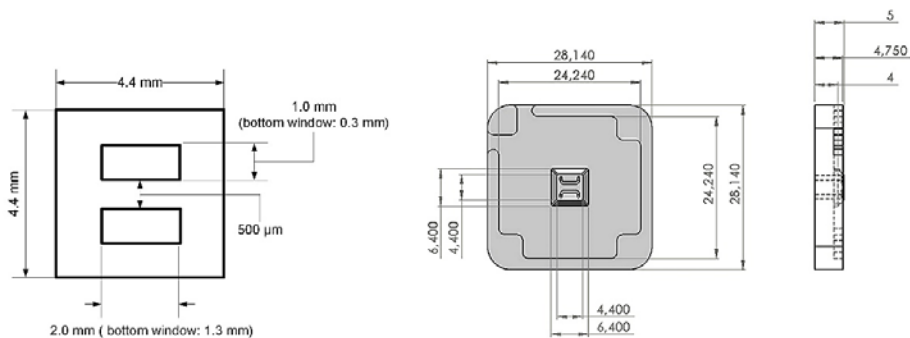


**Figure 3.4.2** (left) Dimensions of the upper surface of the Si/Si<sub>3</sub>N<sub>4</sub> dual-channel microchip and its optical window at the bottom side (in brackets); (right) Dimensions of the bottom and side of the PDMS microfluidic part. The cross section of the channel is 0.5 mm x 0.5 mm, each with two fluidic openings of  $\varnothing$  0.8 mm on the upper surface.

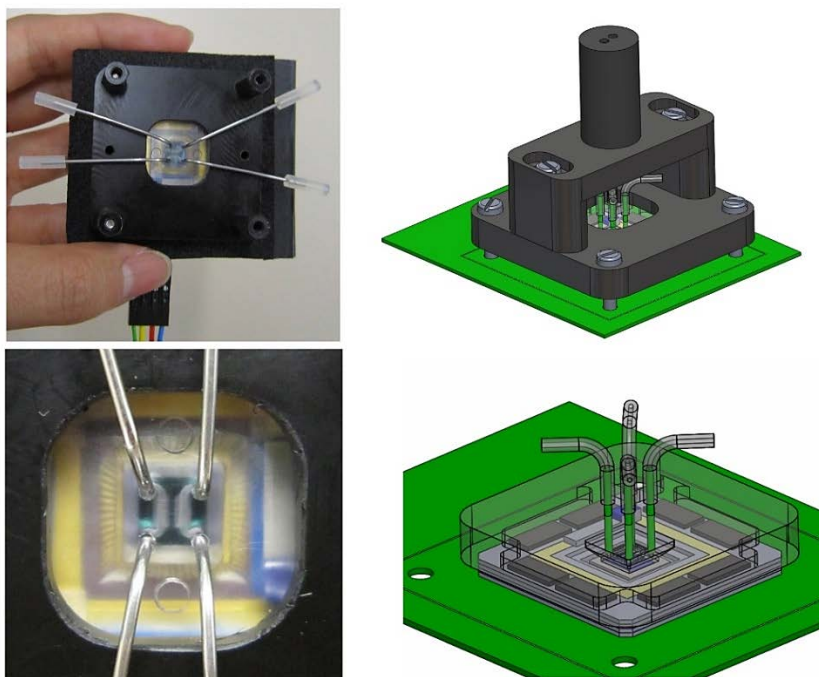


**Figure 3.4.3** (left) Experimental setup of the dual-channel microfluidic chip stacked onto the CMOS image sensor module. Blunt needle (OD:  $\varnothing$  0.82 mm, ID:  $\varnothing$  0.51 mm) is pressed into the microfluidic opening (OD:  $\varnothing$  0.8 mm) and is clamped tightly by the elastic PDMS material; (right) the perspective view of the stacked setup and a closer look underneath the chip adaptor. For the dual-channel microchip, illumination collimator with two adjacent columns is applied.

The dual-channel micro-cavity chip is fabricated with the same process, but the geometry is different. Two parallel channels, actually more like a “trench” shape, are engraved on one silicon chip. The dimensions for the “micro-trench” chip and upper PDMS microfluidic part are shown in Figure 3.4.2. The fabrication process of the PDMS part is as same as that described in Chapter 3.3.3.3. The volume of each micro-trench is 0.55  $\mu\text{l}$ , and plus the upper channel, the overall volume is about 1.0  $\mu\text{l}$ . The opening size is designed smaller than  $\varnothing$  0.8 mm. Blunt needles with  $\varnothing$  0.81 mm OD (ID F560089-1.5, Vieweg Dosier- und Mischtechnik GmbH, Germany) are modified into a right-angled shape. The end of the needle is pressed into the PDMS opening and is clamped tightly by the PDMS material as a tubing connector. The finished look and perspective view of the dual-channel microfluidic chip stacked onto the image sensor is shown in Figure 3.4.3. For the dual-channel illumination, a 25-mm long collimator with two adjacent empty columns spaced 0.5 mm from center is fabricated. Each column is with  $\varnothing$  2.0 mm ID.

### 3.4.1.2 Simulation of the microflow inside the single-channel microfluidic chip

Since in the dual-channel microchip, the microflow direction is along the micro-trench direction, the similar geometry has been simulated in pieces of literature and reviewed in chapter 1.2.3.2. The shear stress at the bottom of the upper rectangular micro-channel with a cross section of 0.5 mm x 0.5 mm is calculated as 0.96  $\text{dyn}/\text{cm}^2$  according to Equation 2-5 when the flow rate is 10  $\mu\text{l}/\text{h}$ . In such a groove-structured microchip, the shear stress at the bottom of the micro-cavity should be decreased by at least about 3 times according to the literature by Lindström [48]. Therefore, the shear stress value in the bottom of each dual-channel microchip should be no more than 0.22  $\text{dyn}/\text{cm}^2$  at 10  $\mu\text{l}/\text{h}$  medium flow.

For the single-channel microchip, the channel is oriented along the diagonal direction of the micro-cavity. In the case of this more complicated channel geometry, the flow inside the microchip needs to be characterized. The flow profile inside the micro-channel is simulated by FEM (Finite Elements Method) software (COMSOL Multiphysics 4.3 trial license, Comsol Inc. US). The velocity field  $v$  inside the microchip is numerically solved from the Navier-Stokes function with the following boundary conditions: Normal input velocity corresponds to a flow rate of 10  $\mu\text{l}/\text{h}$ ; output with pressure: 0 Pa; non-slip boundary conditions at walls, floor, and ceiling with zero velocity. Physical parameters of the fluid are set to those of water at 37°C for simplicity. Streamlines and velocity field of the microflow from different perspectives are shown in Figure 3.4.4. Parallel streamlines of the static velocity field along the channel direction (x) indicate that the fluid movement inside the micro-channel is laminar flow. As seen from the velocity field, the highest velocity appears in the center part of the microfluidic chip and gradually decreases outwards. The shear stress in such an irregular geometry cannot be calculated by Equation 2-5, but can be estimated by the velocity gradient  $\frac{dv}{dz}$  along the vertical direction (z). As calculated with the velocity curve of the xz-plane in the geometry center of the microchip, when under a flow rate of 10  $\mu\text{l}/\text{h}$ , at the microchip floor ( $z = 0, v(z) = v(0) = 0$ ),  $\frac{dv}{dz} = 0.04/\text{s}$  and therefore the shear stress value can be calculated by Equation 2-4 as 0.3  $\text{dyn}/\text{cm}^2$ .

### 3. Materials and Methods

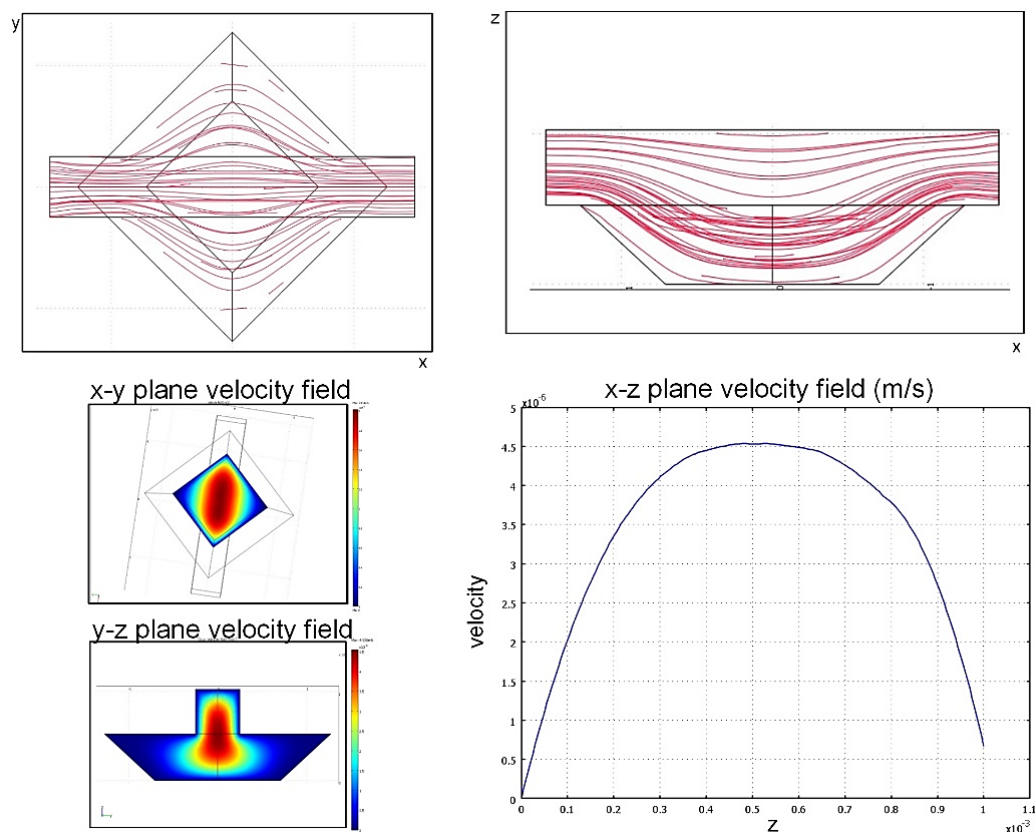


**Figure 3.4.4** (Upper) stream lines of the microflow from top and side views inside the single-channel microfluidic chip; (lower left) velocity fields of the microflow at the horizontal plane ( $z=50\ \mu\text{m}$ ) and diagonal sectional plane respectively; (lower right) the velocity profile (absolute velocity values simulated under a flow rate of  $10\ \mu\text{l/h}$ ) from the center point of the bottom along the height ( $z$  axial direction).

However, the volumes of both microfluidic chips are only  $1.0\ \mu\text{l}$  and  $1.4\ \mu\text{l}$  respectively, which means the actual flow rate proper for cell culture can be much less than  $10\ \mu\text{l/h}$ . If the medium inside need to be totally exchanged, for example in 1–2 hours, a flow rate around  $1.0\ \mu\text{l/h}$  should be applied. Therefore, the absolute values of the velocity field should also be linearly reduced by 1/10 under the same laminar flow pattern inside the microchip. Since the shear stress is proportional to the flow velocity at the floor where cells grow, according to Equation 2-4, the actual shear stress at bottom should be less than  $0.02$  and  $0.03\ \text{dyn/cm}^2$  respectively when the flow rate is at  $1.0\ \mu\text{l/h}$ . Under the safe range of shear stress for cells within  $0.2\ \text{dyn/cm}^2$ , the flow rate can be up to  $5.0\ \mu\text{l/h}$ .

#### 3.4.2 Parylene C coating on the Si/PDMS microfluidic chip

As has been discussed in Chapter 2.1, the physiological liquid microenvironment of a system used outside of the incubator needs to be kept inside a gas- and water vapor-tight

microchip with continuous flow of equilibrium culture medium. However, for the quick and cheap prototyped Si/PDMS microchips, the upper microfluidic part is made by brass-mold casted PDMS. The PDMS material is very gas and water vapor permeable. These problems can be solved in the future by using a plastic microfluidic upper part that will be fabricated in mass production. Here in the prove-of-concept stage, the PDMS part has to be modified for the cell culture practice in order to make it less permeable for gases.

Parylene (poly-para-xylylenes) coating can form a pin-hole free transparent film on the subject. It provides an excellent barrier function to both liquids and gases. The material is biocompatible and can harden the PDMS part [111] [112]. The coating process is carried out in the room temperature without other byproducts. The most commonly used type is Parylene C, which provides much better water vapor and gas barrier properties than Parylene N or Parylene D [113]. The values for the Parylene's barrier properties and comparison with other materials with unified unit can be found in Table 3.2 of Chapter 3.1.1.

The two types of microfluidic chips (single- and dual-channel) are placed inside the coating chamber and are placed upside-down with toothpicks inserted in the inlet and outlet holes. Then the toothpicks are fixed onto a substrate. "The coating process begins with the sublimation of the high purity crystalline dimer di-p-xylene at about 150°C. The vapor is pyrolysed at about 650°C to form the gaseous monomer which has an olefinic (any of a class of unsaturated open-chain hydrocarbons having at least one double bond) structure. The coating chamber is however at room temperature. The vapor condenses isotropically on all surfaces and can pass through very small holes of 1 µm. Then, the vapor spontaneously polymerizes to form a product with a high degree of crystallinity. The coating is absolutely conformal and can be laid down in the thicknesses from a few angstroms to 50 microns or more depending on the requirements of the application" [117]. The thickness of the coating here is about 3–4 µm on the outer surface of both the PDMS part and Silicon micro-cavity chip. Compared to the appearance of former Si/PDMS chips, the coated PDMS becomes harder and a little translucent. The treated PDMS part will become more transparent with the application of a thin layer of nail polish on the top surface after connected into the later working system. After coating, the PDMS/Si microchip is inserted into a black plastic adapter and only leaves a window on the top as shown in Figure 3.4.1 and 3.4.3. By this way, the permeability of the whole microchip can be further reduced. The adapter is used to fix and ensure the microfluidic chip bottom in a good contact with the image sensor surface by four adjustable screws.

#### **3.4.3 Temperature control for the cell culture inside the Si/PDMS microfluidic system**

Without using an incubator, temperature control and thermo-isolation for the cell culture inside the microchip are required. For example, the temperature of culturing mammalian cells should be kept at 37°C. Therefore, a heater and a temperature sensor are directly

### 3. Materials and Methods

integrated onto the image sensor module when the microchip is placed in the room environment. The temperature at the cell culture microchip is monitored and regulated by the close-looped PID controller. At the same time, black antistatic sponge materials are used for electronic, thermal and ambient light protection for the microchip.

#### **3.4.3.1 Construction of the on-chip heater and temperature sensor**

It has been found that, once the image sensor board is connected to the USB port of the computer, the image sensor will generate heat and thus cause temperature rise. Generally, at room temperature (21.7–21.8 °C), the upper and lower surface temperatures of the CMOS image sensor are equal. During a measurement running for 30 minutes by a commercial thermometer (K202, VOLTCRAFT, Conrad Electronic SE, Germany), the temperature of the CMOS image sensor was within  $32.0 \pm 0.1 - 0.2$  °C. For mammalian cells culture, 5 °C higher temperature is required. Therefore, additional heating elements are used. Based on the physical configuration of the image sensor PCB board, SMD ceramic resistors are chosen as heating elements because of their thin flat geometries. 8 x 1 Ohm resistors in series connection are mounted with thermo-conductive glue on the frame of the Alumina ceramic chip carrier which incorporated the SU-8 protected OV5650 image sensor (as indicated in Figure 3.4.5 upper). A Platinum thin film RTD (resistive temperature detector) Pt1000 is also mounted with thermo-conductive glue to monitor the temperature on the chip carrier. Pt1000 is of a thin flat geometry and is very long-term stable. Its output is relatively linear with respect to temperature. As the image sensor is placed inside the chip carrier, the three parts (image sensor, temperature sensor and the heating elements) can be quickly equilibrated and arrive at the same temperature because of the good heat conducting capability of the ceramic chip carrier.

The cell culture inside the Si/PDMS microfluidic chip is heated by the image sensor surface. Meanwhile, the Si/PDMS microchip is well thermo-isolated by black antistatic sponge layers, which are fixed onto the image sensor board by the chip adaptor. The sponge material can also protect the image sensor from static electronic shot, and shields the image sensor from ambient light. A small temperature gradient can still exist when the whole system is reaching a thermal equilibrium state. Therefore, the absolute temperature of the culture substrate needs to be carefully calibrated and verified with real cell culture trials.

#### **3.4.3.2 Characterization of the resolution of the temperature control**

The diagram of the temperature control system is shown in Figure 3.4.5 lower part. The heater and the thermal sensor are connected to the computer via a Low-cost multifunction DAQ card. The electronic circuit provides a constant current through the Pt1000. The current is set at 1 mA by the electronics configuration, but this value in practice is calibrated by inserting the sensor into a cup of ice and water mixture that is considered as the reference temperature of 0 °C. The actual current provided is 0.9145 mA. The current

passes through the Pt1000, and the voltage across the Pt1000 is measured and recorded via the analog input (AI) port of the DAQ card. All the calculations are processed with a self-developed LabView program.

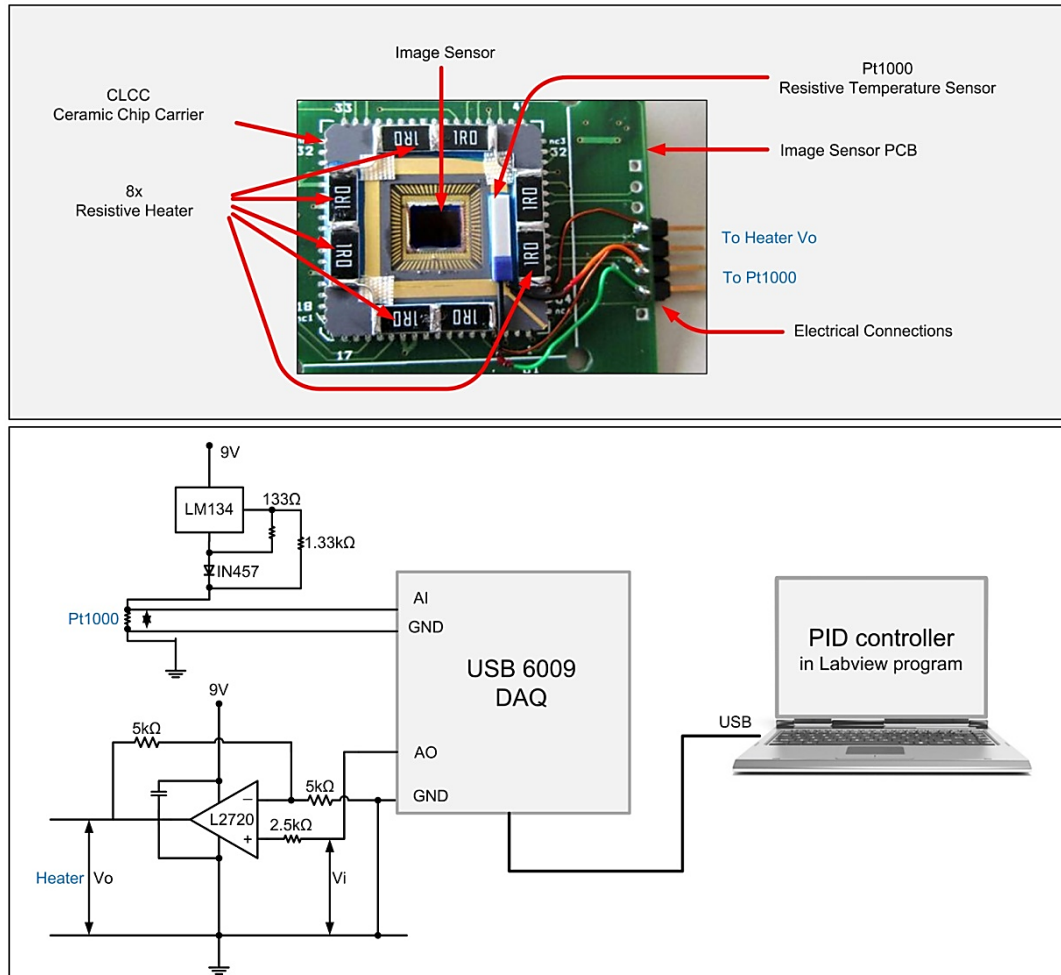


**Figure 3.4.5 (upper) photo of a SU-8 coated OV5650 image sensor board with a Pt1000 temperature sensor, heating elements of 8x 1 Ohm resistors, electronic connections; (lower) Diagram of the close-looped temperature control system (not in scale).**

The actual resistance of the Pt1000 can be simply calculated by its actual voltage divided by the constant current. Then the actual temperature measured by the Pt1000 is calculated by the Callendar-Van Dusen equation (as shown in Table 3.4) according to International Electrotechnical Commissions standard IEC751 Class B. This equation uses constants A ( $3,9083E-3$ ), B ( $-5,775E-7$ ) and C ( $-4.183E-12$ ), derived from resistance measurements at 0 °C, 100 °C and 260 °C. The results are fitted with a relative linear relationship as 3.85 Ohm per every centigrade change. As a feedback, the program will calculate the proper voltage to the heater with preset PID coefficients, according to the actual temperature deviation.

### 3. Materials and Methods

Because the output voltage (AO) of the DAQ card can be only up to 5V, a power circuitry with a voltage amplifier is designed. The data acquisition rate is 1000 Hz, but the measurements are averaged and the power supply for the heater is calculated for every one second because the reacting time of the Pt1000 is relatively slow, a couple of seconds.

**Table 3.4 Callendar-Van Dusen Equation (IEC751 Class B)**

<p><b>Callendar-Van Dusen Equation:</b></p> $R_T = R_0(1 + AT + BT^2 - 100CT^3 + CT^4)$ <p> <math>R_T</math> = Resistance (<math>\Omega</math>) at temperature T (<math>^{\circ}\text{C}</math>)  <math>R_0</math> = Resistance (<math>\Omega</math>) at <math>0^{\circ}\text{C}</math>  T = Temperature in <math>^{\circ}\text{C}</math> </p> <p>For <math>T &gt; 0^{\circ}\text{C}</math>, the quadratic formula can be used to solve for Temperature as a function of measured resistance with the result:</p> $0 = R_0BT^2 + R_0AT + (R_0 - R_T) \text{ implies...}$ $T_R = \frac{-R_0A + \sqrt{R_0^2A^2 - 4R_0B(R_0 - R_T)}}{2R_0B}$
---

The USB 6009 DAQ card has following configurations and resolutions of its analog I/O ports:

- 8 x Analog Inputs (AI)
  - 14-bit for differential measurements
  - 13-bit for single-ended measurements
- 2 x Analog Outputs (AO), 12-bit.

In this application, single-ended measurements are selected with a preset measurement range of 0–2.0 V. Therefore, the resolution of the AI is 0.244 mV, which corresponds to the resistance change of 0.244 Ohm with a constant 1 mA current. Compared to the linear resistance/temperature relationship of the Pt1000, the resolution of the temperature measurement should be less than 0.1  $^{\circ}\text{C}$ . With a preset voltage supply range of 0–2.5 V, the resolution of the AO is 0.61 mV. Because the output voltage is amplified by 2 times, the resolution of the voltage output to the heater should be 1.22 mV.

#### 3.4.3.3 Performance of the temperature control for the running microsystem

PID (Proportional-Integral-Derivative) method is applied in the close-looped temperature control. As in such a simple module, the integration function is not used, and the other two tuning coefficients are determined as 10 and 0.01 by experiment as shown in the self-made LabView control panel in Figure 3.4.6. The target temperature is primarily set at 37  $^{\circ}\text{C}$  for mammalian cells culture.

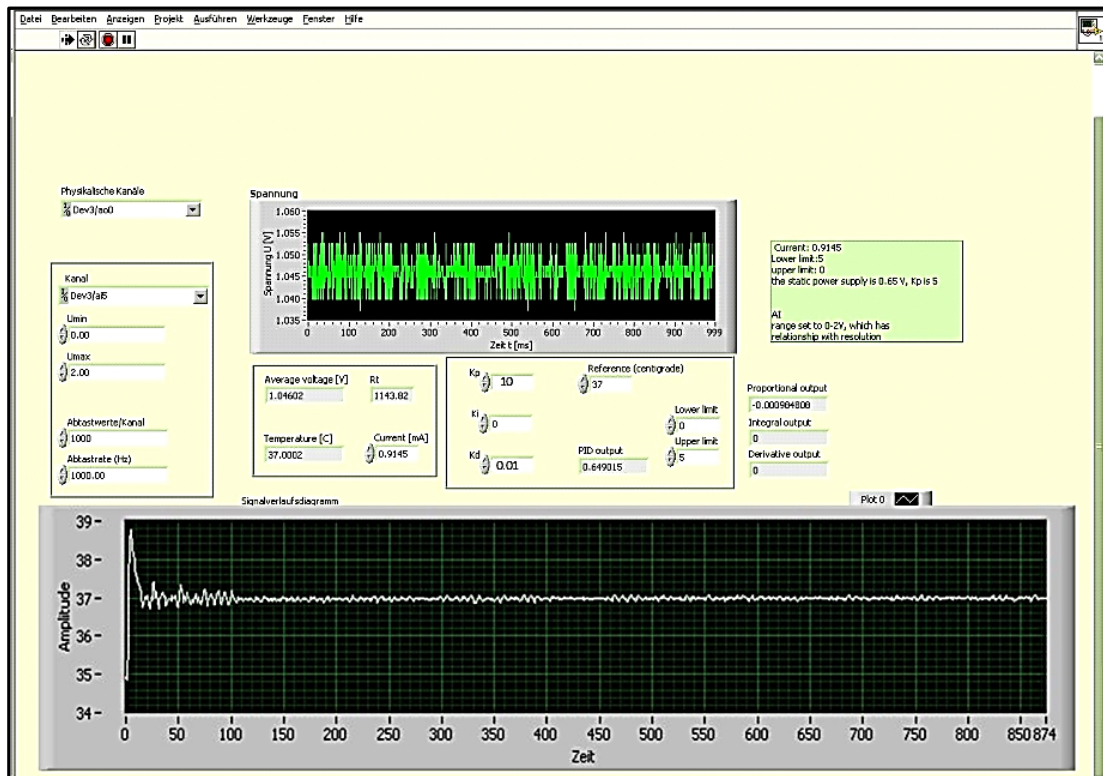


**Figure 3.4.6** Control panel of the LabView program for the close-looped temperature control system with a real-time log of temperature regulation on the lower part.

The temperature control system is experimentally tested with the whole microsystem placed in the room environment. The flow rate of the microfluidic chip is  $10 \mu\text{l}/\text{h}$ . Compared to the volume of the single-channel microchip  $1.4 \mu\text{l}$ , the flow is very fast and the turnover time is only about 7 minutes.

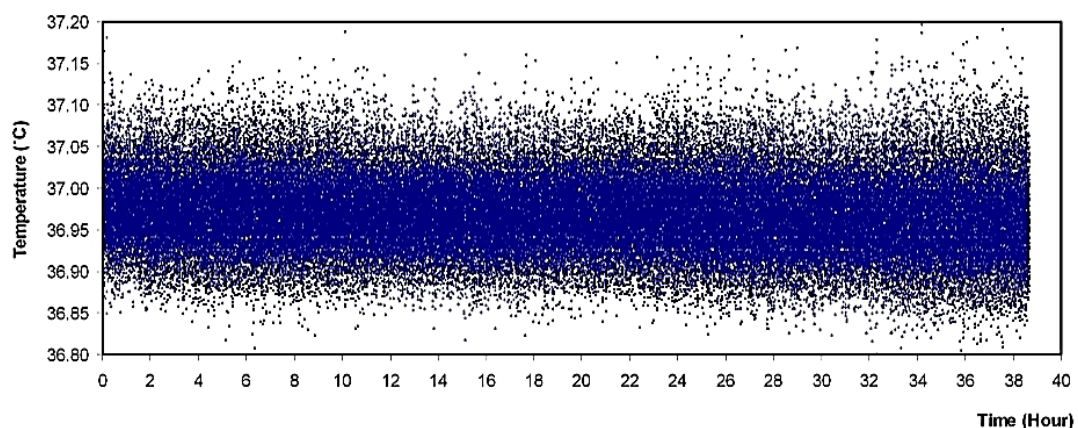


**Figure 3.4.7** 38 hour-temperature log of the culture microsystem with a flow rate of  $10 \mu\text{m}/\text{h}$  under the “very-near field” shadow imaging configuration.

### 3. Materials and Methods

The temperature measurements of the system continuously working for almost 40 hours is shown in Figure 3.4.7. It can be seen that the temperature of the whole system is very stable, fluctuating in a temperature range within  $\pm 0.2^{\circ}\text{C}$ . The stability is comparable to a commercial-grade incubator. For such a small system in room atmosphere and with so fast liquid changing rate, the performance of the temperature control for the microsystem is effective and secured for providing an ideal thermal environment for cell culture.

#### 3.5 Preparation of cell cultures

L929 (mouse fibroblast cell line), A549 (Human lung adenocarcinoma epithelial cell line) and T47D (human breast columnar epithelial tumor cells) are cultured in RPMI medium supplemented with L-glutamine (4 mM), penicillin (100 units/ml), streptomycin (100  $\mu\text{g}/\text{ml}$ ) (Invitrogen GmbH, Darmstadt, Germany) and 10% (v/v) fetal calf serum (PAA Laboratories GmbH, Germany). DG44 CHO (Chinese Hamster Ovary cell line) GFP (Green Fluorescence Protein) cells are cultured in CHO protein-free medium (Sigma-Aldrich Co., Germany) with L-Glutamine (2mM). Cells are kept in flasks and placed in an incubator (Heraeus BBD 6220, Thermo Scientific, Karlsruhe, Germany) with 5%  $\text{CO}_2$ , 97% humidified atmosphere at  $37^{\circ}\text{C}$ .

For culture cells inside the micro-channel slide, cells are harvested during the log phase of growth and re-suspended by fresh equilibrium medium in single cells suspension of 500,000 cells/ml. 30  $\mu\text{l}$  cell suspension is pipetted quickly from one opening of a micro-channel slide (ibidi GmbH, Germany), which is tissue culture treated by delivery. Then, its two reservoirs at ends are filled with medium. All the liquid handling and cell preparation are operated under a sterile bench. The micro-channel slide is covered and placed into an incubator for 2–4 hours before connecting to the microfluidics.

The Si/PDMS microchips are autoclaved before experiments with cell culture. During the log of growth, cells are harvested and re-suspended in single cells suspension. For the Si/PDMS micro-well chip, 20  $\mu\text{l}$  cell suspension (20,000 cells/ml) and for the Si/PDMS single-channel microchip, 10  $\mu\text{l}$  cell suspension (50,000 cells/ml) are respectively dispensed into the Si/PDMS microchip (with adaptor) quickly to avoid air bubbles. All the liquid handling and cell preparation are operated under a sterile bench. Microchips are then placed inside an incubator.

The equilibrium medium is prepared by firstly filling culture medium inside a covered petri dish. The petri dish with culture medium is placed inside a  $\text{CO}_2$  incubator for at least one hour before usage. The equilibrium medium is then aspirated by 1mm syringes to provide medium supply for cell culture in microsystems.

## 4 Experiments

Since technical developments and microchip designs have been presented, this chapter will focus on the experimental setups and protocols for working with real biological cells. Along the roadmap of the study, the stand-alone microfluidic system, the compact automatic “desktop” microscope, the “very-near field” shadow imaging configuration as well as the establishment of a stand-alone cell culture microsystem adapted to the “very-near field” shadow imaging will be one by one implemented into experimental setups suitable for practical cell culture and testing. Protocols for cell culture are adopted from the conventional cell culture, and adapted to those established microsystems.

### 4.1 Testing the stand-alone cell incubating system

#### 4.1.1 Micro-channel based stand-alone cell culture microfluidic setup

The complete micro-channel based cell culture experimental setup is shown in Figure 4.1.1. The stand-alone microfluidic system is provided with two independent microfluidic channels, and at each inlet a 4-port manual valve (Omifit manual small valve 001122, Diba Industries, UK) is introduced into the fluidic for a convenient fluidic traffic control. An automatic microscope (Olympus IX 81) is employed for the time-lapse imaging of cells cultured in the microsystem. The climate box of the automatic microscope is not used for the experiments, because it is really a hurdle for the practical handling and setting of the microfluidic system. So, as to not introducing any confusion to readers, the photo is taken by placing the microfluidic system on another microscope IX70 without climate box. The constant microflow is supplied by using a syringe pump with 6 cartridges (Razel Scientific Instruments, USA).

## 4. Experiments

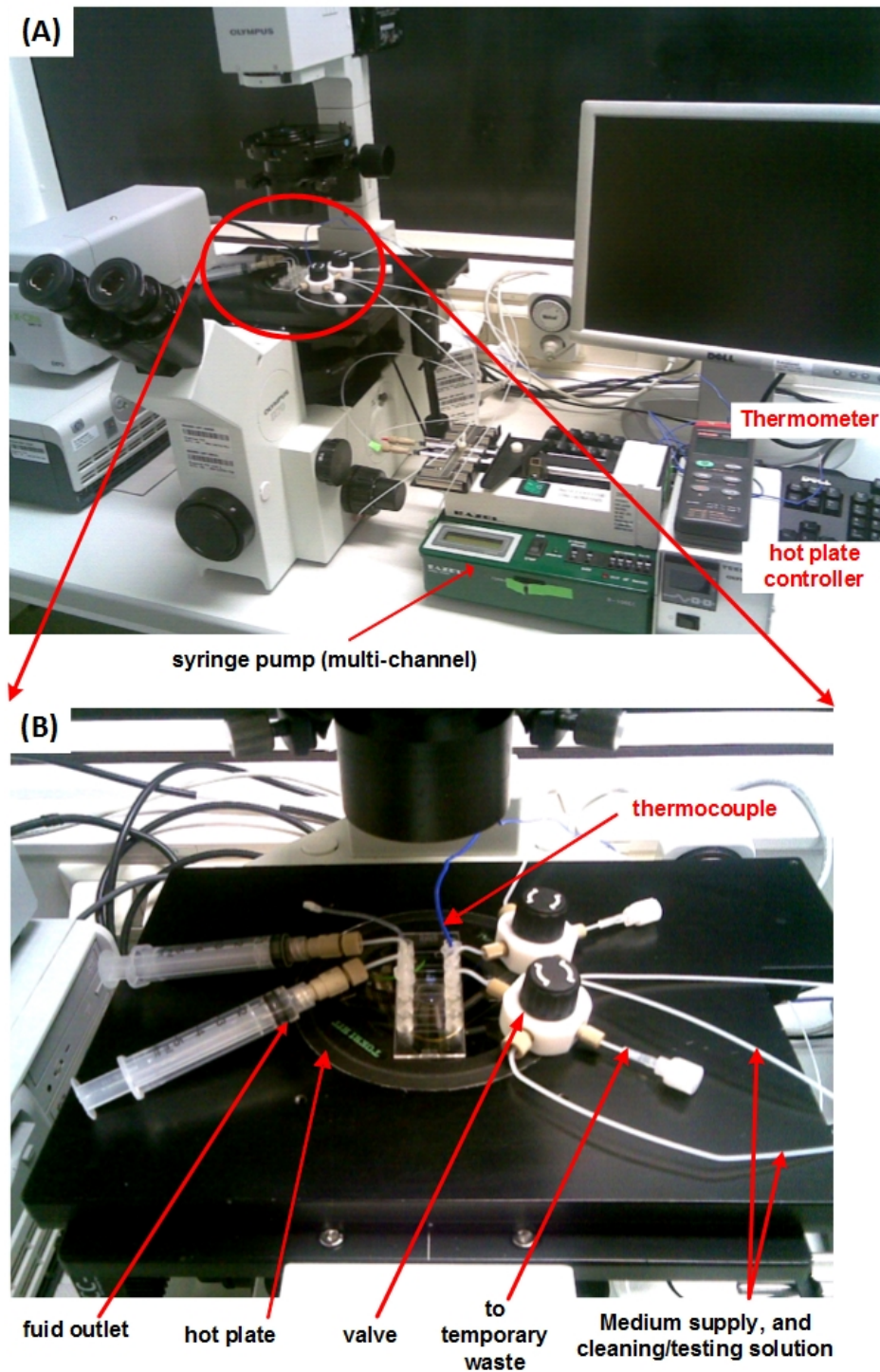


**Figure 4.1.1** Micro-channel slide based stand-alone cell culture microfluidic setup prepared with double channels for cell culture and testing. The microfluidic cell culture system is fixed onto the microscope plate for time-lapse imaging. (\* The actually used automatic microscope Olympus IX 81 is equipped with a climate box but the climate box is not used for this experiment)

The 4-port manual valve can be directly connected to the 1/16 inch OD tubings, and the valve is connected as close as possible to the channel inlet, thus resulting in a very small dead volume of fluid less than 5  $\mu\text{l}$  between the valve and the microchip inlet. The outlet of the channel is connected to a sterilized plastic syringe via Luer adapters and Tefzel tubing. A small amount of PBS is aspirated into the syringe for making the plug more lubricant before connecting to the fluidic path.

To test the barrier function of the microfluidic system, fresh equilibrium medium is purged into the whole system. The equilibrium medium is prepared by keeping the fresh culture medium in a petri dish and placed in an incubator for a couple of hours before use. The medium is therefore balanced with ideal pH value, temperature, osmotic pressure as well as plenty of nutrients and dissolved oxygen for culture cells. After 4 hours without fresh medium inflow, the equilibrium medium inside still keeps its orange color and no air bubbles appears. The static medium is then evaluated by pH testing paper showing the pH range of 7.2–7.4. It indicates that the entire microfluidic system is very well sealed from gas and water vapor. The system is ready for the culture of mammalian cells over extended period with continuous microflow of incubator equilibrium medium.

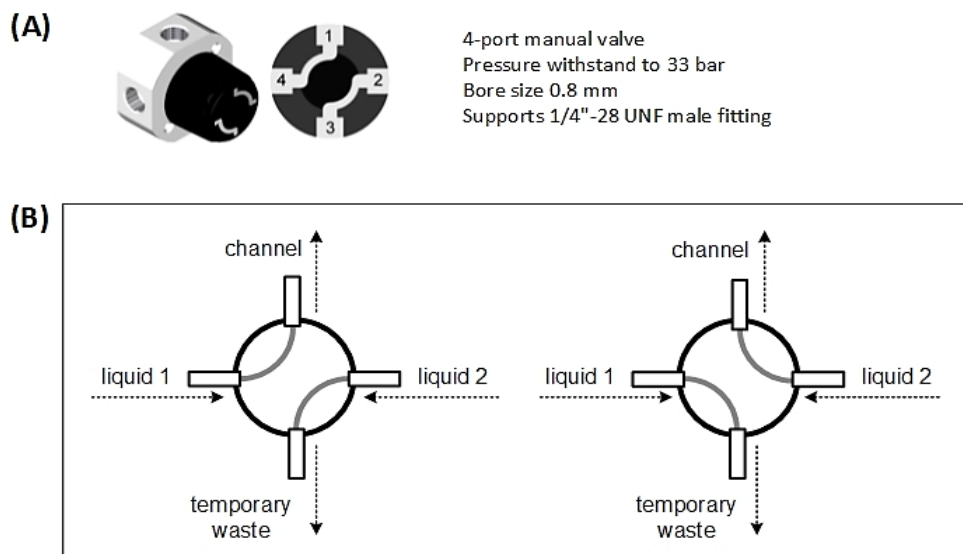


**Figure 4.1.2 (A) 4-port manual valve 3D sketch and the diagram illustrating its inner connections [http://www.c-h-m.de/shop/omnifit/OFTK\_Manual\_Valves.pdf, 2011]; (B) Traffic diagrams showing liquids change process without introducing air bubbles or contaminations.**

This 4-port manual valve (Figure 4.1.2 (a)) based liquid traffic design is very practical for changing liquid without introducing air bubbles or contaminations into the channel. The culture medium or a solution under test is kept in a sterilized 1 ml plastic syringe and is

## 4. Experiments

covered with a cap, while the Luer adapter at the tubing end is also inserted with a syringe filled with ethanol to protect any contamination from the air. The following procedure is used for changing the medium: A new syringe is connected to the tubing end and the frontier portion of the liquid inside the syringe is manually purged to the temporary waste. This ensures that, air bubbles or any other liquid residual are flushed away. Then the valve is turned to let the new liquid flow into the channel. The diagram of Figure 4.1.2 (B) shows how the liquid traffic is manipulated. The syringe with fresh medium or a solution under test is then installed onto a syringe pump (Razel Scientific Instruments, USA) providing continuous flow.

### 4.1.2 Preparation of the microfluidics

The whole microfluidic system is at first rinsed with isopropanol in order to flow out air easily, and then rinsed with 70% ethanol for sterilization. After that, the system is rinsed with equilibrium culture medium by a syringe pump. Because some soluble factors of the medium can be adsorbed onto the inner surface of the microchip, equilibrium medium is continuously flowed into the system for several hours at 100  $\mu\text{l}/\text{h}$  in order to enhance the biocompatibility of the inner surface of the whole system. The channel slide is meanwhile heated by the hot plate at 37°C.

### 4.1.3 Operations of cell culture with the microfluidic system

After 4 hours of incubation, cells inside the micro-channel slide are checked under the microscope. Cells are evenly distributed inside the micro-channel and already spread on the bottom surface. Then the empty micro-channel slide previously connected in the microfluidic system is replaced by the micro-channel slide with initial cell culture. The operation is carried out inside a sterile bench and needs to be very careful in order to avoid introducing air bubbles or contaminations. In the experiment, the hot plate and the micro-channel slide are fixed onto the motorized sample plate of an automatic microscope (Olympus IX81). The microscope is covered with a climate box. But the climate box is not used and the two small front doors are kept open. Although the microscope is equipped with a climate box, the cells are solely cultured inside the microfluidic system without using the climate box. According to the estimations and calculations related to the ibidi micro-channel slide in chapter 3.1.2, the flow rate used here for cell culture is 10  $\mu\text{l}/\text{h}$ .

The “time-lapse” function provided by the Olympus IX81 microscope software CellP cannot be used, because the captured images are saved in the memory but not in the hard disk, and this will lead to problems when the experiment takes several days. Therefore, the time-lapse imaging of the Olympus automatic microscope is configured like this: Phase-contrast images are taken every 5 minutes with auto-focusing function; the illumination level, exposure time are tested and set in advance; although the illumination is kept on all the time, the mechanical shutter of the microscope is configured that cells are only illuminated

when taking photos in order to protect cells from excess illumination; the captured images are saved in the computer hard disk.

In the first experiment, the growth of L929 cells is used to test the physiological environment provided by this microfluidic system. L929 cells are relatively easy to handle, and this cell line is one of the most widely used cell lines in biological laboratories.

In another experiment, cell cultures are carried in two parallel but independent micro-channels (double micro-channel) for an easy comparison. One channel is used as control and cells are cultured in a flow of the conventional medium. In the second channel, cells are cultured in a flow of medium with some reagent under testing.

Conventionally, the reagent under test is applied to the cell culture with a certain starting concentration in the whole culture medium. After some time, its effect on cells is characterized. By using this microfluidic system, the reagent is however applied to cell culture by a continuous microflow of culture medium with the same concentration. Moreover, the effect on cells is characterized along the experiment. To demonstrate the functionality of the double micro-channel system, a reagent with known toxic effect on cells will be chosen. For example, the silver nanoparticle is by far the most widely used nano-compound in products. Small silver nanoparticles (10 nm diameter) have been proven cytotoxic to human lung cells [114]. The colloidal solution of 10 nm Ag NPs (Plasma Chem GmbH) is diluted by the medium at a concentration of 10 µg/ml. It is continuously flowed into the second micro-channels to demonstrate its dynamic cytotoxic effects on cultured A549 cells and will be compared in real time with the cell culture in control. The automatic microscope is configured to take time-lapse images of both micro-channel alternately.

## 4. Experiments

### 4.2 Testing the compact microscope system

Both imaging quality and system stability are important for time-lapse imaging. Therefore, the constructed compact microscope is characterized not only by the bright field and fluorescence imaging of biological cells, but also by its stability of the long-term automatic microscopy operation. Moreover, the possibility of imaging GFP expressing cells is discussed and analyzed quantitatively.

#### 4.2.1 Imaging setup of the compact automatic microscope

The complete automatic compact microscopy system is shown in Figure 4.2.1. The microscope is simply manipulated by the front panel of the LabView program. Samples are loaded or cultured in ibidi micro-channel slides for the observation. Since the microfluidics and heating parts are not the focus of this chapter, they are not included in the setup.

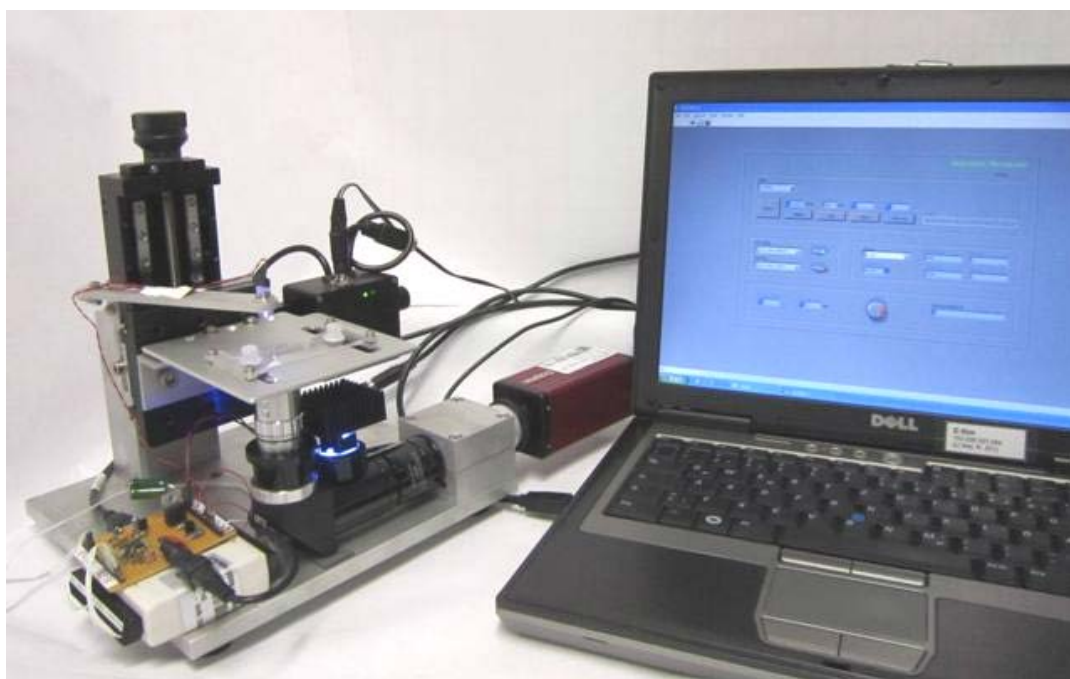


**Figure 4.2.1** Photograph of the compact automatic “desktop” microscopy (A4 paper sized footprint), including the constructed imaging device and a laptop computer with control program interface. All the samples are cultured or loaded in ibidi micro-channel slides for observation, heating elements and microfluidic parts are not included.

The real-time imaging of samples can be seen in the MAX control panel of the firewire camera. In this panel, Brightness, Gain and Shutter Speed can be configured manually (not absolute value). Via the rotary knob on the Z-translation racket and the two springs supporting the sample plate, the sample plate is adjusted along the x-axis horizontal

direction by focusing samples under the white LED illumination respectively in two parallel micro-channels spaced about 25 mm apart. Within the moving range of the translational slide, four independent micro-channels of the ibidi slide can be monitored.

#### 4.2.2 Test of the imaging ability of the “desktop” microscope

The imaging ability of the optical constructions of the “desktop” microscope is tested by imaging the microbeads with known diameters in both bright field and fluorescence modes. To represent the spreading morphology details of a mammalian cell of a 15–20  $\mu\text{m}$  size, fluorescent microbeads with diameters of  $1.88\pm 0.05 \mu\text{m}$ ,  $5.61\pm 0.32 \mu\text{m}$  (Polysciences Europe GmbH, Oppenheim, Germany) and  $15.0 \mu\text{m}$  (Molecular Probes, Invitrogen GmbH, Darmstadt, Germany) are chosen. Microbeads of the three different diameters are diluted by PBS and mixed together before loading into ibidi channel slide. The micro-slide is checked under conventional microscope in advance to make sure there are proper number of microbeads in the field.

After the above test by microbeads for an optimal optical construction, mammalian cell cultures L929 and A549 with different morphologies are then image by the compact microscope. The cells are cultured for 24 hours in a ibidi micro-slide before taking to the observation. To demonstrate the fluorescence imaging of cell cultures by the compact microscope, Fluorescein-diacetate (FDA) (excitation: 470 nm; emission: 520 nm), which is widely used for live cell staining, is chosen for the fluorescent staining reagent. Cell viability can be assessed directly through the presence of cytoplasmic esterase in living cells. The esterase activates the non-fluorescent cell membrane-permeable probe to a fluorescent product. This product is charged and well retained within cells of intact membrane function, producing intense uniform green fluorescence. Viable cells are with bright fluorescence and nonviable cells are dim or non-fluorescent. For the staining sample preparation, 5 mg/ml FDA in acetone solution was diluted 200 times in PBS solution and incubated with cells for 15 seconds at room temperature. Then the cells are washed once by PBS and covered with culture medium without pH indicator for the observation.

#### 4.2.3 Stability test of the “desktop” microscope for time-lapse imaging

The stability of the automated system includes focusing stability in the z direction and the scanning repetitiveness in the x direction in the whole operational period. An old micro-channel slide with scratches on the bottom side is used for testing the scanning repetitiveness. By imaging fluorescent microbeads the focusing stability is evaluated. Two testing points spaced with 28 mm are chosen in two different micro-channels (No.2 and No.5 of 6 micro-channels) and are imaged by both bright field and fluorescence microscopy with system running for 24 hours.

## 4. Experiments

### 4.2.4 Imaging GFP cells by the “desktop” microscope

The standard solution of fluorescein (Molecular Probes F-1300, extinction coefficient is  $90,000 \text{ cm}^{-1} \text{ M}^{-1}$  at 488 nm excitation, quantum yield = 85%) is usually used to quantify the imaging of GFP cells in spectroscopy and microscopy experiments. Its fluorescent brightness is  $76,500 \text{ M}^{-1} \text{ cm}^{-1}$ , which is 2.32 times brighter as compared to the EGFP (enhanced Green Fluorescence Protein) molecule [115]. Since the GFP cells are much less bright than the fluorescent staining, the possibility of imaging the GFP cells is dependent on the illumination intensity, filters selection, and camera sensitivity. Therefore, the camera (AVT), LED excitations (470 nm and 455 nm peaks), Band pass fluorescence excitation filters (BP472, BP440) and other optics of the “desktop” microscope are tested for the efficiency of fluorescence imaging, in reference to the Olympus CC-12 soft imaging system and Olympus X-Cite 120 light source of Olympus microscope IX70. Fluorescent microbeads and cells with FDA staining are imaged by both systems and images are compared. The intensities of the fluorescence excitation at the sample plane are measured by using a handheld power meter (LaserCheck, Coherent Inc., US).

All the related values are sorted in Table 4.1. The excitation (470 nm) intensity for FDA in IX70 is almost 2 times as that in the “desktop” microscope configuration. The excitation (450 nm) intensity for GFP in IX70 is even 7 times as that in the configuration of the “desktop” microscope. By using the “desktop” microscopy optics and the LED illumination, the fluorescence of the cultured GFP cells can be imaged by the CC-12 camera with an exposure time of 1000 ms, but is impossible to be observed by the AVT camera. Since the fluorescence excitation from the coupled LED illumination is very weak in this royal blue band, the Olympus X-Cite light source is coupled into the “desktop” microscope configuration instead of the LED illumination. The purpose of this is to see whether the GFP cells can be imaged by the optics of the “desktop” microscope and a common firewire camera.

Table 4.1 Calibration of the fluorescence imaging of the “desktop” microscope

	IX70		CAM						
Objective	10x	20x	10x	20x	20x LWD		20x LWD	20x LWD	
NA	0,3	0,45	0,3	0,45	0,4		0,4	0,4	
Excitation source	X-Cite (level 1, SERIES 120)		LED (470/ 25 nm, Lumitronics K2)					LED (455/ 20 nm, Lumitronics K2)	X-Cite (level 3, SERIES 120) plus collimating lens
Optical relaying system	Olympus		Infinity tube						
Filters (FDA)	WIB (BP460-495, BA510IF)		BP472/ 30 nm, BP520/ 35 nm		BP472/ 30 nm, BP520/ 35 nm		BP440, BP520/ 35 nm		
Filters (GFP)	425-475, 485-535								
470 nm Excitation Intensity (mW)		~ 3.2		~ 2	~ 1.7		~ 1.7		
455 nm Excitation Intensity (mW)		~ 2.6					~ 0.365		
Camera	CC-12		CC-12			CC-12	AVT Dolphin F145C	CC-12	AVT Dolphin F145C
Beads Exposure time (ms):	~ 5	~ 10	~ 10	~ 20	~ 20	Calibration: 200 ms ~ 1500 4000 ~ 400-500 ms, with gain=0			
Cell FDA Exposure time (ms):			~ 20-50 plus automatic gain	~ 20-50 plus automatic gain	~ 20-50 plus automatic gain		1500-2500 with gain=0 ~ 200ms		
CHO DG44 GFP Exposure time (ms):							~ 1000		

### 4.3 Testing the “very-near field” shadow imaging module

A simple LED collimated illumination module is designed and implemented with the “very-near field” shadow imaging configuration to form a very compact imaging setup.

Microbeads of different diameters and growing cells of different morphologies are imaged by the shadow imaging module. Both of colorimetric and fluorescent staining of cells are also tested by the system. The optical resolution, imaging quality and capability are evaluated.

#### 4.3.1 Lensless “very-near field” shadow imaging setup

The dimension of the imaging setup is only 40 mm × 40 mm × 50 mm as shown in Figure 4.3.1. It consists of a quasi-collimated LED illumination module, a 5-megapixel color CMOS image sensor module and a Si/PDMS microchip with transparent membrane bottom. The image sensor module is controlled with a desktop computer through the USB connection. Spaces between the collimator and the microchip adaptor are very well sealed from the ambient light.

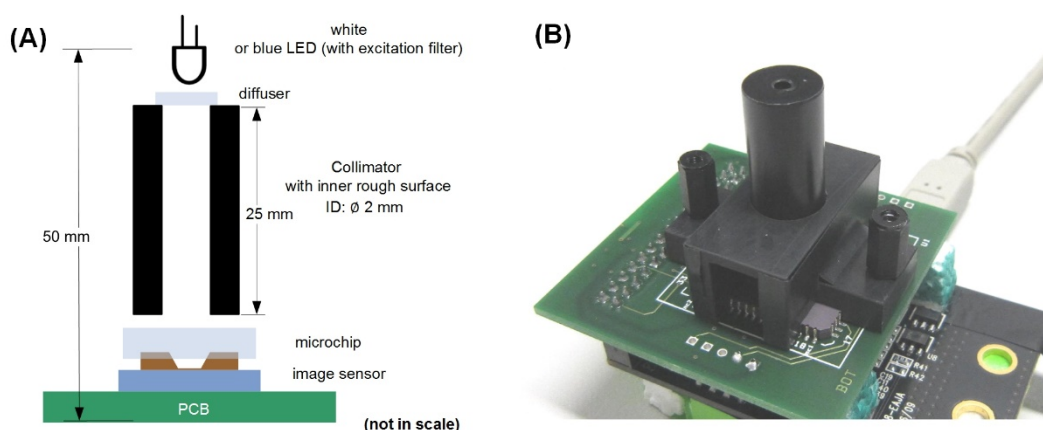


**Figure 4.3.1** (A) Diagram of the “very-near field” shadow imaging setup; (B) The photo of the experimental setup with the microchip adaptor and collimator part stacked onto the image sensor module.

The collimated illumination module is composed of a white LED ( $\varnothing$  5 mm, 60° angle) for bright field imaging or an ultra-bright blue LED ( $\varnothing$  5 mm, 50° angle, 470 nm) together with a band pass interference filter ( $\varnothing$  25 mm) for fluorescence imaging, a diffuser and a small tube (2 mm diameter and 25 mm length) with rough inner surface. For the dual-channel microchip, illumination collimator with two adjacent columns is applied. A variable resistor is in series connection with the LED for adjusting the light intensity. The uniformity and the collimation of the LED illumination is effectively improved with the diffuser and simple

collimator. The collimated illumination not only facilitates the shadow imaging but also fulfills the  $0^\circ$  incident angle of the interference filter.

Biological samples can be conveniently sustained and transported inside the microchip with an adaptor. All the liquid handlings are operated under a sterile bench. The microchip with the adaptor is placed inside an incubator and only stacked onto the image sensor when taking shadow images. Microscopy images are additionally taken under a converted microscope (Olympus IX70) as reference.

As it has been mentioned in Chapter 3.3.2.1, the preparation of an image sensor Die OV5650 requires much more work and effort than that of a packaged image sensor OV5620. Therefore, the OV5620 image sensor module is primarily used in the setup to prove the concept of the “very-near field” shadow imaging for cell cultures. Moreover, since there could be very slight shadows of the micro-channel when Si/PDMS micro-channel chips are applied, Si/PDMS micro-well chips are used in the tests of resolution and imaging capability. The descriptions of micro-channel chips and micro-well chips can be checked in Figure 3.3.1.

### **4.3.2 Testing the overall optical resolution of the “very-near field” shadow imaging system**

Theoretical resolutions of the two image sensors OV5620 and OV5650 are in respective  $4.4\ \mu\text{m}$  and  $3.5\ \mu\text{m}$  (dimension of 2-pixel size). As discussed in Chapter 2.3.1, interfacing samples with transparent membranes with very small thickness (for each single layered membrane of common transparent materials, the safe value is  $12\ \mu\text{m}$ ) will not impair the fine resolution provided by the image sensor. According to the Rayleigh criterion, the optical resolution of the “very near-field” shadow imaging system is tested by the PSF (Point Spread Function) of objects with sub-resolution size. Here microbeads of  $1.88\pm 0.05\ \mu\text{m}$  (Polysciences Europe GmbH, Eppelheim, Germany) in diameter are imaged in order to test the overall optical resolution of the configuration. Mammalian cells usually have a diameter of  $15\text{--}20\ \mu\text{m}$ . Thus, microbeads of  $15.0\ \mu\text{m}$  (Invitrogen GmbH, Darmstadt, Germany) are used to further test the diffraction effect on imaging qualities with increased DFR bottom thickness of 20, 40 and  $60\ \mu\text{m}$ . For this test, the OV5620 image sensor was used for imaging samples of different diameters inside Si/PDMS micro-well chips with different bottom thickness.

The Si/PDMS microchips are autoclaved before experiments with cell culture. In this experiment three types of cells with different morphology types are used. They are L929 (mouse fibroblast cell line), A549 (human lung adenocarcinoma epithelial cell line) and T47D (human breast columnar epithelial tumor cells). After the cells have sedimented onto the bottom membrane, the microchips are imaged by the “very-near field” shadow imaging setup and the bright field microscopy (Olympus IX71) for reference. Microchips are then

## 4. Experiments

placed inside an incubator (Heraeus BBD 6220, Thermo Scientific, Karlsruhe, Germany) maintained for 48 hours for the next imaging process of confluent cell layer.

OV5650 image sensor with and without the 4  $\mu\text{m}$  SU-8 coating are tested by imaging microbeads in Si/PDMS micro-well chip to check whether the SU-8 coating layer will affect the optical resolution. L929 cells are then cultured inside a Si/PDMS single-channel microchip in a static manner and are imaged by the SU-8 coated OV5650 image sensor and the Olympus IX70 microscope. The chip together with the adapter is placed into an incubator for half an hour. After that, an additional 5  $\mu\text{l}$  medium drops are pipetted on each opening. The cells inside the chip are cultured for 3 days in a conventional incubator with a coverslip on the chip adaptor. Due to the coverslip, almost no decrease of the liquid drops on the opening is observed during the 3 days.

### 4.3.3 Testing of the “very-near field” color shadow imaging of cells

OV5620 image sensor (no coating) module and Si/PDMS micro-well chips are used in the setup to figure out the image quality of morphologies and colorimetric staining of cell cultures.

For the sample preparation of colorimetric staining, A549 cells are used. After the seeded cells are deposited onto the bottom for a while, cells are fixed with 4% formalin (04003, Merck KGaA, Darmstadt, Germany) and made permeable with 0.2% Triton-X 100 (37240, SERVA Electrophoresis GmbH, Heidelberg, Germany) as the positive control. Then 0.05% (g/100 ml) Erythrosine B (Sigma-Aldrich Chemie GmbH, Schnelldorf, Germany) is applied for red staining in one chip and Trypan blue solution (VWR International GmbH, Darmstadt, Germany) is used for blue staining in another chip. After 5 min, cells are washed twice with phosphate-buffered saline (PBS) (20012, Invitrogen GmbH, Darmstadt, Germany) and observed with both the “very-near field” shadow imaging module and the microscope. The liquid operation is similar to the process for conventional 384 well-plate, but need more carefulness and faster piping and aspirating speed.

After preparing the positive control of live/dead colorimetric stained cells, as an example, the toxic effect of silver nanoparticles on A549 cell culture is stained and characterized in order to demonstrate the color shadow imaging. Small nanoparticle (10 nm silver nanoparticle) has been proved to be toxic to human lung cells [114]. The sample preparation simply goes as follows: The A549 cells are seeded inside a Si/PDMS micro-well chip and are cultured for 24 hours inside an incubator. After that, the medium is replaced by the medium with 5  $\mu\text{g}/\text{ml}$  10 nm silver nanoparticle and cultured for another 24 hours. The dosage and reaction time of nanoparticles with cell culture has been tested in advance in order to be sure that only a part of the cells will be killed and stained. The cell culture is then stained by Erythrosine B solution and is imaged with both imaging methods.

#### 4.3.4 Testing the “very-near field” fluorescence imaging of cells

The imaging capability of the interference filter (505 IF long pass) coated image sensor module OV5650 is evaluated by the “very near-field” fluorescence imaging of 15.0  $\mu\text{m}$  latex microbeads and FDA stained L929 cells cultured inside a Si/PDMS micro-channel chip. An ultra-bright Blue LED is collimated and the output spectrum is further shaped by an interference filter BP 472/30 (Band Pass filter, peak wavelength/FWHM in nm). Two kinds of microbeads are used: yellow-green colored microbeads (excitation/emission peak wavelengths in nm for fluorescence: 505/515) (F8844, Molecular Probes, Invitrogen GmbH, Darmstadt, Germany) and red colored microbeads (excitation/emission peak wavelengths in nm for fluorescence imaging: 565/580) (F21012, Molecular Probes, Invitrogen GmbH, Darmstadt, Germany). The L929 cells are firstly cultured for 24 hours and then stained with FDA (Fluorescein-diacetate). The staining mechanism and handling process can be checked on Chapter 4.2.2.

All the samples are observed as a reference by a conventional optical/fluorescence microscope (IX70, Olympus) with an objective of 4-times magnification. The filter cube of the fluorescence microscopy used is composed of a BP 460–495 nm (Band Pass filter, lower and upper wavelengths at half maximum in nm) for the excitation, and the BA 510 nm (Barrier filter at half maximum in nm for long pass) for the emission.

### **4.4 Testing the all-in-one cell culture-shadow imaging microsystem**

In the following paragraphs, the setup and operation of a stand-alone cell culture microsystem adapted to the “very-near field” shadow imaging configuration will be described. By using this all-in-one cell culture-imaging microsystem that is capable of stand-alone cell culture and real-time imaging without using conventional incubators or optical microscopes, complete cell culture and processing operations are carried out: cell seeding, cell incubating, and viability test by color imaging, cell passage, as well as 3D cell culture. Accordingly, the operational protocols of cell culture are also modified and adapted to this microfluidic system.

#### **4.4.1 All-in-one cell culture-imaging microsystem setup**

The practical experimental setup and its diagram of the “very-near field” shadow imaging configuration integrated microfluidic system are shown in Figure 4.4.1. A dual-channel Si/PDMS microfluidic chip is applied for demonstration. For the practical experiment, a 4-port manual valve and a syringe are also connected into each flow path as has been described in chapter 4.1.1. The computer programs control the temperature and image sensor modules by USB connections. The illumination is manually controlled with a variable resistor for the intensity level.

All the components of the complete experimental setup can be placed on a small roll trolley resulting in a simple and neat working environment as shown in Figure 4.4.2. A conventional incubator on the upper right part of the photo is used as a comparison for size. The optical window of the dual-channel microchip is shown on the computer screen in real time. The proper brightness and contrast of the imaging is adjusted with the controlling software of the image sensor. By using the white LED with a variable resistor, the illumination is adjusted very dim in order to protect cells from photo-damage. The exposure time and gain of the image sensor OV5650 are then adjusted to 160 ms and 2 respectively.

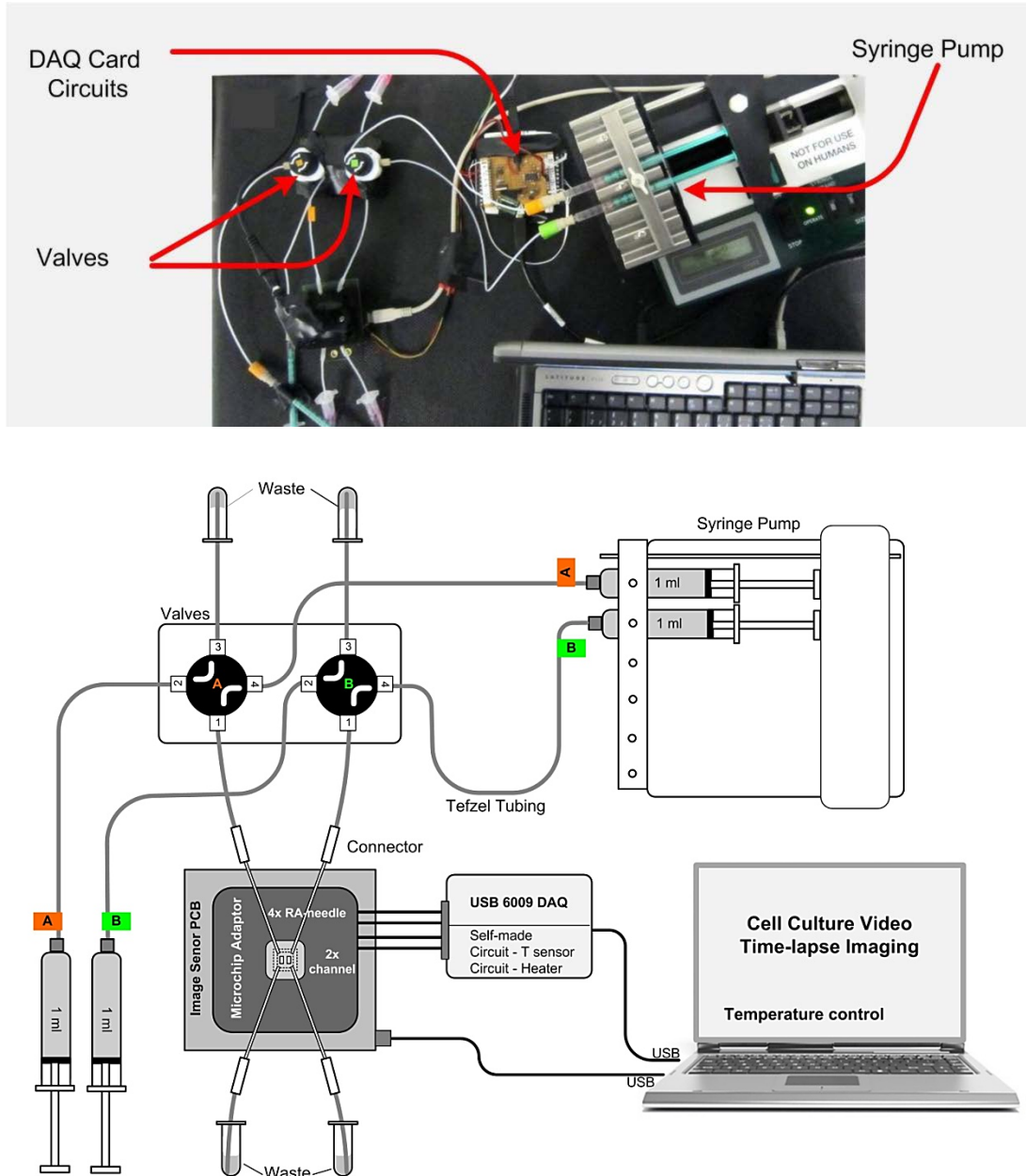


**Figure 4.4.1** (upper) Closer shot of the overall dual-channel cell culture and shadow imaging microfluidic setup; (lower) Diagram of the overall dual-channel cell culture and shadow imaging microfluidic setup. Two parallel microfluidic channels A and B, each is provided with two syringes for easy and secure medium exchange. Image sensor OV5650 is coated with a 4  $\mu\text{m}$ -thick SU-8 on top. Its image acquisition and temperature regulation are controlled by a laptop computer.

## 4. Experiments

### 4.4.2 Preparation of the microfluidics of the all-in-one microsystem

As has been tested in chapter 3.3.1.3, the bonding of the Si/PDMS micro-channel chip is strong and even the bottom membrane can withstand 0,65 bar air pressure. Since the microchip bottom is supported by the image sensor surface in this setup, the burst pressure will further increase and the washing process can be performed manually with a strong push of the syringe. It is very convenient that the filling process can be monitored in real time on the display: The interface between two different liquids is clearly visible due to the different refractive indices of different liquids. The channels are firstly rinsed with 99% isopropanol from port 2 to port 1. After the channels are completely filled as visualized in the display, the isopropanol is replaced by 70% ethanol in order to sterilize the microfluidic networks. After about 30 minutes, pre-balanced medium in a CO<sub>2</sub> incubator overnight is immediately flown into the microfluidics with a relatively high flow rate of 1.5 ml/h from valve port 4 to port 1. After about 20 seconds, the mixing of ethanol and medium is visible due to the changing of the refractive index. The medium delivery or exchange time from a syringe to a micro-channel can therefore be estimated as 20 seconds at a flow rate of 1.5 ml/h. Since the overall volume of the single- or dual-channel microchip is only about 1.0 µl, the flow rate is then turned down to 1.0 µl/h while the temperature control is kept on overnight.



**Figure 4.4.2** Photo of the practical stand-alone cell culture and shadow imaging experimental setup, comparing to the bulky conventional incubator on the upper right of the photo. The whole experimental components are placed on a roll trolley. Real-time imaging of the dual-channel is showing on the screen of the laptop, which is very intuitive for the operator.

### 4.4.3 Seeding cells into the all-in-one microsystem

To check the fast cell loading process into the all-in-one microsystem, both single-channel and dual-channel Si/PDMS microchips are tested. The cell suspension is prepared in warm equilibrium medium at a concentration of about  $1.25 \times 10^6$  cells/ml. The cell suspension is filled into a 1 ml syringe and connected to valve port 2. The suspension is firstly purged from port 3 to the waste until there is no air bubble in the flow, and then the cell suspension is directed from port 2 to port 1. In order to achieve a relatively even distributed cell seeding, the cell suspension has to be loaded into the micro-channel with a very quick speed by hand and then stopped to let cells gradually sediment onto the bottom of the microchip. In the single-channel microfluidic chip (1.4  $\mu$ l volume and 0.95 mm x 0.95 mm bottom area), about 750 cells are seeded onto the bottom window, and in the dual-channel microfluidic chip (1.0  $\mu$ l volume and 1.3 mm x 0.3 mm bottom area), generally less than 400 cells are seeded onto the bottom window.

The flow and sedimentation of cells can be visualized in the shadow imaging video at a frame rate of 3.75 fps from the transparent optical window. Once the streamlines of moving cells by the manual push become constant and stable, the loading process is immediately stopped by turning the valve from port 2–port 1 to port 4–port 1. After 15 min when the cells in the micro-channel have sedimented and adhered to the bottom, a very fast fresh medium flow of 1.5 ml/h is introduced into the microchip for 30 seconds to flush out excess cells left in the connecting tube between the manual valve and the microchip, while the adherent cells on the floor of the microchip are not moved or washed out. This flow rate has been practically tested and finally determined at 1.5 ml/h. The fast cells flow in the microchip is visualized with the underlined image sensor at a frame rate of 3.75 fps.

### 4.4.4 Incubating cells inside the all-in-one microsystem

#### 4.4.4.1 Flow rate determination for the cell culture in the all-in-one microsystem

To incubate cells in the single- and dual-channel microfluidic chips, the proper flow rate should be determined first. According to the theoretical calculations in chapter 3.1.2.1, the flow rate for the two kinds of microchips should be no less than 0.2–1.7  $\mu$ l/h (1500 cells in average), and 0.1–1.0  $\mu$ l/h (800 cells in average) respectively considering the cellular oxygen consumption. Since the height of the fluid above the sedimented cells in the microchannel is 1 mm for both microchips, according to the theoretical estimation in Chapter 2.2, the diffusion time of the soluble factors from the upper micro-channel to the cell layer at the bottom should be definitely over 1 hour. Therefore, the time for the total culture medium exchange does not necessarily need to be much faster than 1 hour, resulting in the flow rate of 1.4  $\mu$ l/h and 1.0  $\mu$ l/h respectively. According to the theoretical estimation in Chapter 3.4.1.2, shear stress values under those estimated flow rates would be in the safe range. If the cells are not those high oxygen consumption types, for example, liver cells, 1.0  $\mu$ l/h should be proper for most cell types that will be cultured in both single- and dual-channel gas- and water vapor-tight microfluidic systems.

## 4. Experiments

### 4.4.4.2 Cell culture operations in the all-in-one microsystem

Operations of cell culture in both single- and dual-channel microchips are as follows: After seeding cells in the microchip, cells will be initially incubated in a static manner for 2–4 hours. Then, a constant medium flow of 1.0  $\mu\text{l}/\text{h}$  is introduced into the microchip. In this experiment, L929 cells are cultured to demonstrate the ability of cell culture operations by using the microsystem.

According to the estimation in chapter 3.4.1.2, the flow rate can be up to 5.0  $\mu\text{l}/\text{h}$  while keeping cell culture on the bottom under a safe shear stress range in both single- and dual-channel microfluidic chips. Epithelial cells *in vivo* are usually exposed to mechanical forces of different levels. A549 cells are therefore cultured in the 1  $\mu\text{l}$ -volume microchip to test cellular responses under a normal as well as a relatively fast medium replenish rate as fast as 5 times per hour.

### 4.4.4.3 Temperature adjustment for the all-in-one microsystem

As it is shown in chapter 3.4.3.3, the temperature control module integrated on the all-in-one microsystem has been proved with a temperature stability of 0.02. Though the stability of the culturing temperature is very important, the absolute temperature value for the cell culture has to be also kept within a certain range. For instance, the absolute temperature for mammalian cell culture has to be regulated within the absolute temperature range of  $37\pm 0.5^\circ\text{C}$ .

As described in chapter 3.4.3.1, a Pt1000 is used as temperature sensor. It is located on the chip carrier. The temperature measured at this location could be slightly higher from that of the cell culture on the image sensor surface. As the microchip is very small, it is not easy to integrate a temperature sensor into the micro-cavity chip and to directly measure the absolute temperature on the cell culture substrate. Therefore, the exact temperature for practical cell culture is tested according to cell responses. The trial and error experiments have been performed at the following temperatures measured on the chip carrier: 38.5, 38.0, 37.5, 37.0.

### 4.4.5 Live-dead staining of cell culture in the all-in-one microsystem

To demonstrate the operating ability of a viability test by using this all-in-one microsystem, Erythrosine B solution is used for staining dead cells with compromised membranes. For making a positive control, A549 cell culture of 24 hours in one of the dual-channel microchip is treated with an air bubble manually introduced from the inlet syringe in order to kill cells by mechanical force. During the process, many cells could be stripped from the culturing substrate and flown away out of the microchip. The cells still remaining on the substrate could also be heavily injured with non-intact cell membranes.

The illumination is increased until the observing window appearing on the monitor changes from gray to white in order to clearly display the red color. 0.05% (g/ 100 ml) Erythrosine B solution is firstly introduced from valve port 2—port 3, and then directed to port 1 at a flow rate of 1.5 ml/h until the channel is totally filled with this red solution. Then the valve is switched to port 1—port 4, from which a medium flow of 1.5 ml/h is introduced to wash the cells in the micro-channel until the background becomes clear again. After this procedure, all dead cells will be stained with cherry red and it should be possible to clearly distinguish them from viable cells.

### **4.4.6 Passaging adherent cells cultured in the all-in-one microsystem**

Trypsin (EDTA) solution is introduced manually into the microchip, and then the cells in the micro-channel are incubated with trypsin solution statically for about 3 minutes. The real-time morphological changing of cells is imaged by the all-in-one microsystem and observed by the operator on the computer display. As it has been tested, cells can be washed out by PBS solution with a minimum flow rate of 6.0 ml/h. Then the cells suspension will be collected from the outlet.

### **4.4.7 3D cell culture by the all-in-one microsystem**

Besides of cell culture in the planar form, three-dimensional cell aggregates will be also carried out in the micro-cavity. The general principle is to decrease the cellular adhesion to the culturing substrate and thus to increase the possibility of cell-cell adhesion. From three aspects the operations in the all-in-one microsystem will be carried out in favor of forming cell aggregates: (1) the whole system is only rinsed by ethanol and then PBS solution, but will not be pre-treated with medium or serum in order to reduce the cell adherence on the bottom substrate; (2) compared with the cell numbers for culture in the planar form, single cells suspension of a higher concentration (2,500,000 cells/ml) is manually loaded to ensure there are excessive cells inside the micro-cavity; (3) after the cell seeding, the medium flow will be directly applied in the micro-cavity chip from the very beginning. Keeping the bottom shear stress in the safe range as estimated in chapter 3.4.1.2, the flow rate will be increased to 5.0  $\mu$ l/h in order to further reduce the cell adhesion to the cell culture substrate.

## 5 Results

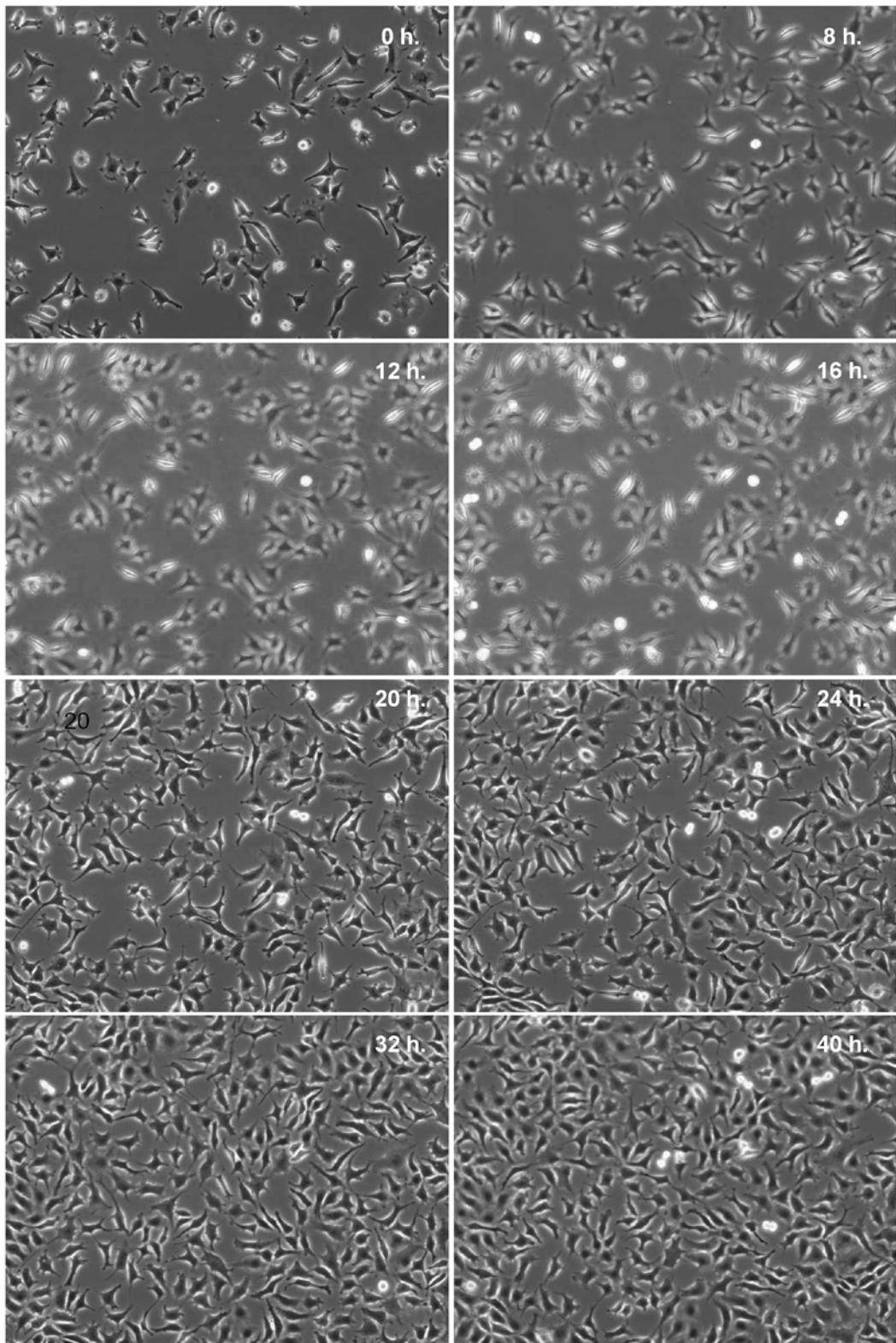
In this chapter, the experimental results of every stage towards the final goal of the study will be presented: (1) time-lapse microscopy imaging of cells cultured and tested in the stand-alone microfluidic system; (2) long-term automation stability and imaging capabilities of the compact automatic microscope for growing cells; (3) experimentally tested optical resolution of the “very-near field” shadow imaging configuration, and its bright field, color and fluorescence imaging capabilities for cells in culture and testing; (4) the complete cell culture, processing and on-line monitoring operated by the all-in-one microsystem. According to the results of characterizations and biological experiments, theories and methods applied and developed for the objectives of the study can be verified and evaluated.

### 5.1 Cells cultured in the stand-alone incubating system

Time-lapse imaging sequences and videos of cultured cells in the micro-channel based microfluidic system without using incubators are presented. The cellular healthy condition reflected by the morphology and proliferation rate of cultured cells can be used to evaluate the feasibility and effectiveness of the stand-alone cell culture concept.

#### 5.1.1 Time-lapse images of cell culture in a single channel

The time-lapse imaging sequence of L929 cells is taken every 5 minutes under the commercial automatic microscope (Olympus IX81) with a 10x optical objective. Some of these photos are presented in Figure 5.1.1. More detailed cell growth condition can be found in the video composed of all the images. In the stand-alone micro-channel based microfluidic system, cells are growing in a healthy state in respect of morphology, proliferation and finally forming a confluent layer. The number of cells at different points are manually counted and shown in Figure 5.1.2.



## 5. Results

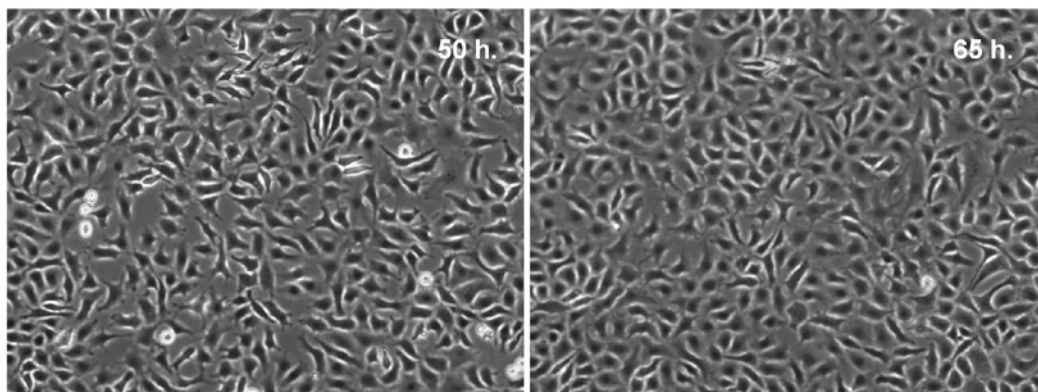


**Figure 5.1.1** Time-lapse images of L929 cell culture over 65 hours inside the stand-alone micro-channel based microfluidic system running in the room atmosphere.

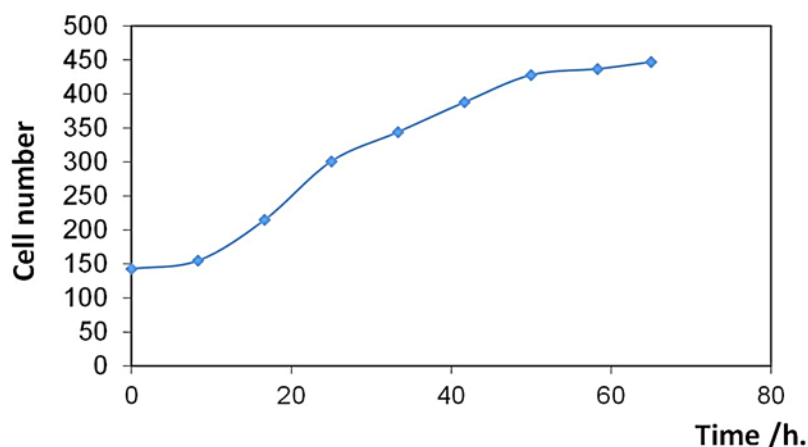


**Figure 5.1.2** Cell counts for the L929 cells cultured in the stand-alone microfluidic system. The doubling time of the fitted cell growth curve is about 24 hours.

From the fitted curve, the doubling time of the number of cells is about 24 hours, which is accordance with the value that is known for the conventional cell culture [116]. The stand-alone microfluidic system has proved its capability of running cell culture in room atmosphere without using incubators. The time-lapse imaging enables the evaluation of individual cells in the field of view.

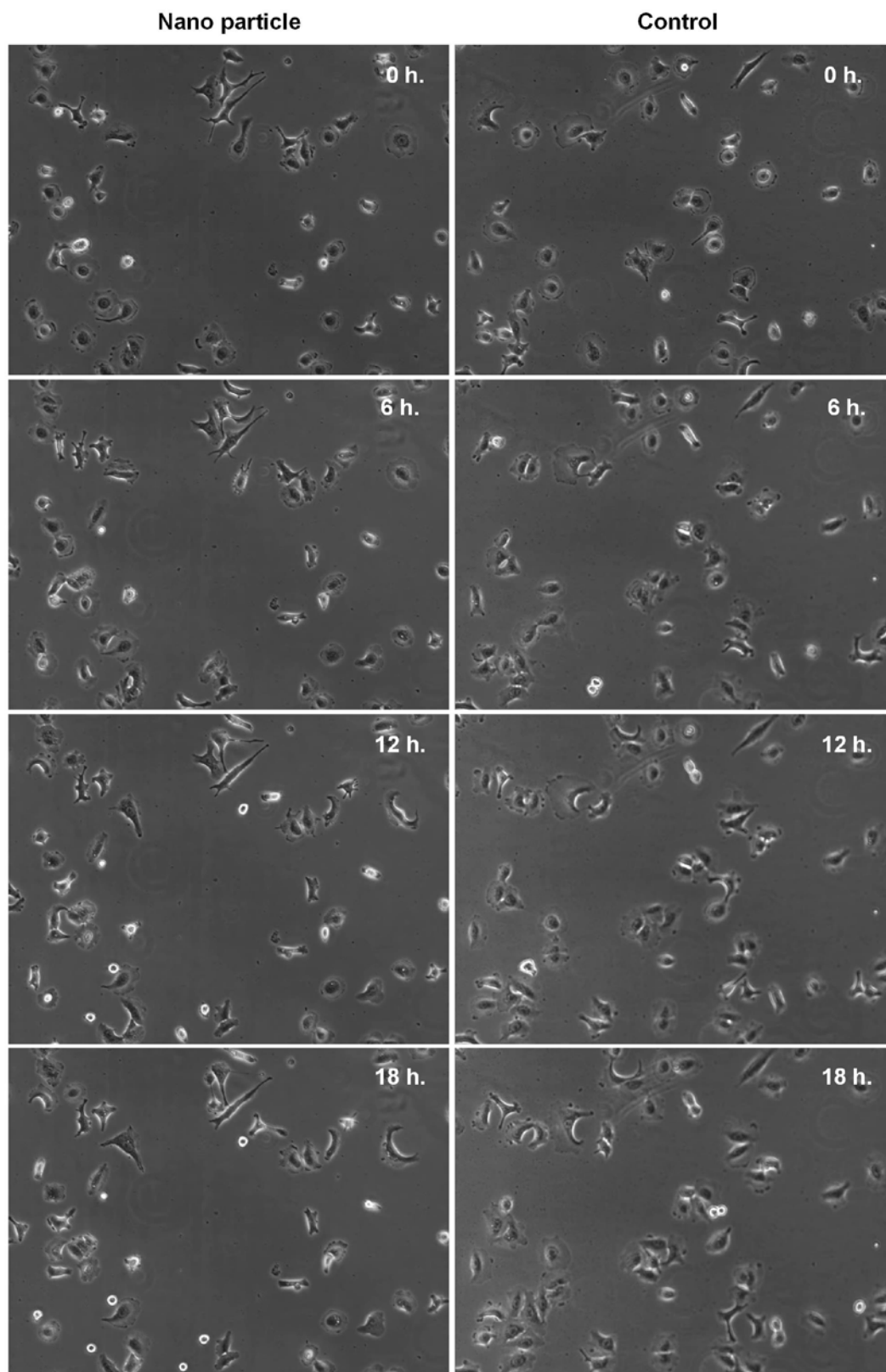
The images are out of focus from 8 hours to 16 hours due to the auto-focusing malfunction of the commercially automatic microscope. The auto-focusing function of the automatic microscope does not work well 100%, especially for such a long-term experiment up to 3 days of continuous running. Moreover, the sample plate for most automatic microscopes is

designed for conventional static culture containers. The complicated microfluidic connections and customized design could also cause malfunctions.

### **5.1.2 Time-lapse images of cell cultures in double channels**

Two parallel culture conditions are monitored at the same time by using this constructed stand-alone cell culture microfluidic system. The effect of 10 nm silver nanoparticles on A549 cells can be well presented and compared with the A549 cells cultured only with medium (control) by the results shown in Figure 4.1.3. Both cell culture is under identical culture and imaging conditions. The effect on individual cells can not only be tracked at refined time scale, but also can be carefully evaluated in respect of the reference individual cells in culture. Compared with the A549 cell culture in the normal state, the cell growth under the testing condition is obviously affected and interfered after culturing with nanoparticles for 24 hours.

## 5. Results



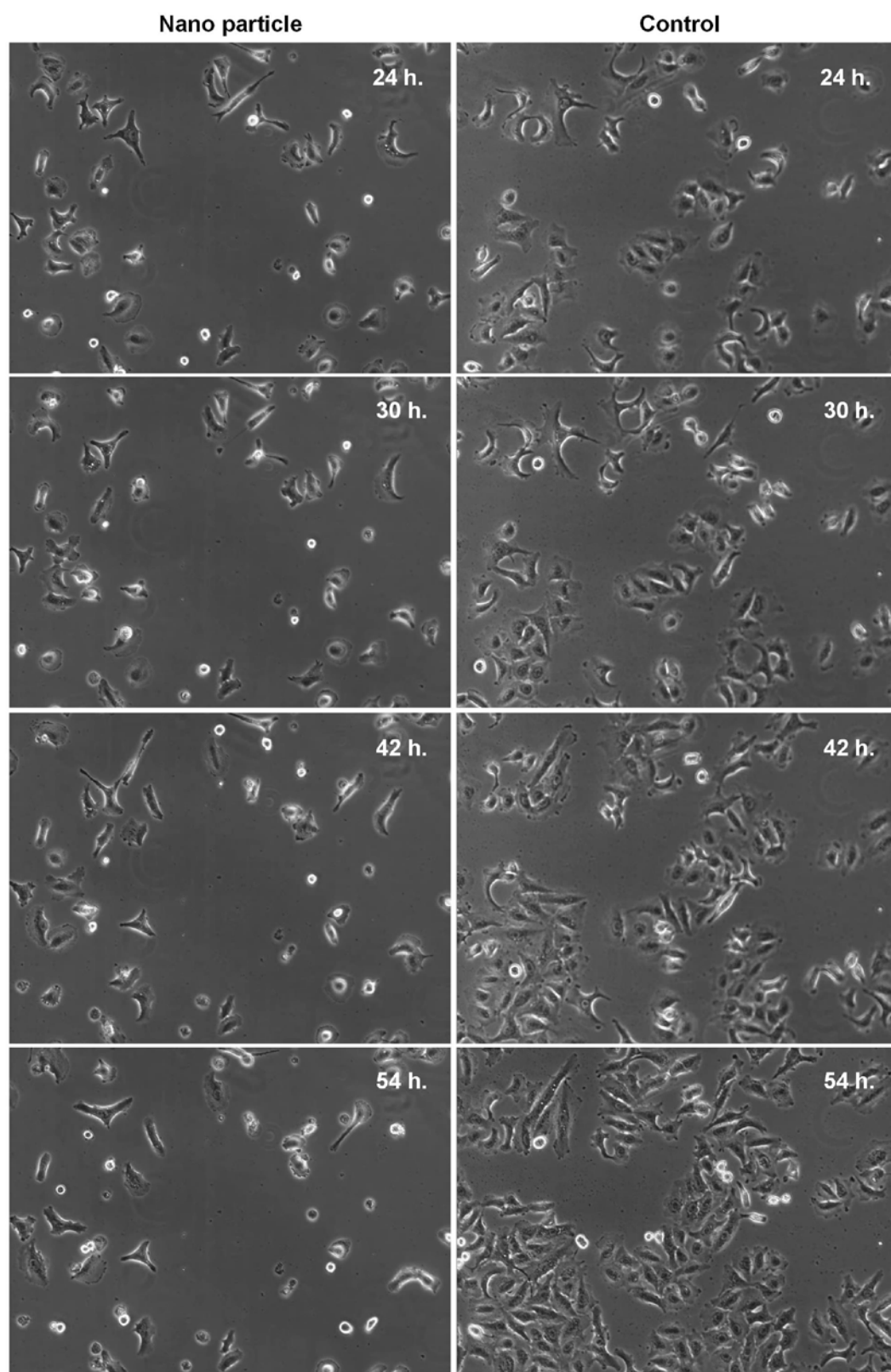


**Figure 5.2.3** Time-lapse images of A549 cell cultures in double micro-channels for 54 hours. (left) A549 cell culture with 10  $\mu\text{g}/\text{ml}$  10 nm silver nanoparticles contained in the continuous medium flow; (right) A549 cell culture flowed with medium is as the control.

## 5.2 Performance of the “desktop” automatic microscope

The compact automatic imaging device is specially designed for the long-term time-lapse imaging of cell culture for the stand-alone microfluidic system. The performance is presented by its imaging quality, the stability of the automatic microscopy operation and capabilities in the practical imaging of cell cultures.

### 5.2.1 Imaging quality of the “desktop” automatic microscope

Fluorescent microbeads of various diameters are imaged as shown in Figure 5.2.1. Although the objective (NA=0.45) from Olympus presents better contrast in the fluorescent image, there are shadows out of focus on the bright field image. This result is in accordance with the theoretical estimation in chapter 3.2.1, that the smaller NA (0.4) of the LWD objective better matches the NA (0.27) of white LED illumination for the bright field imaging.

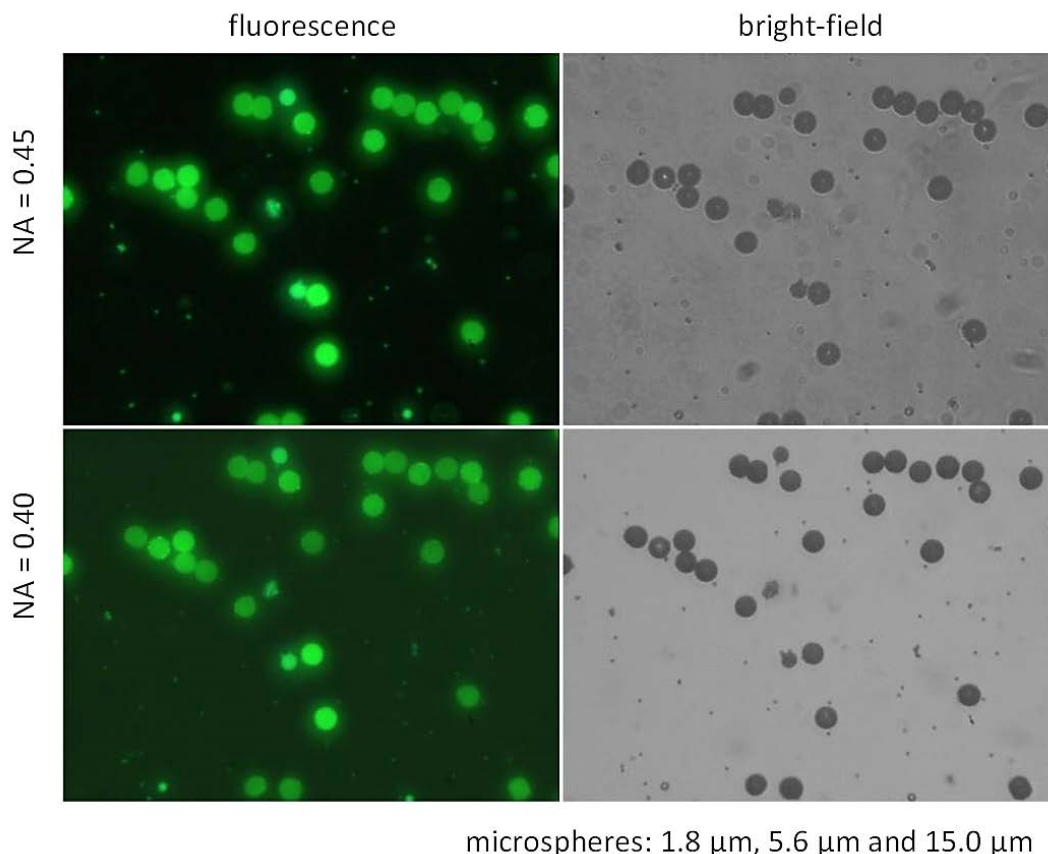


**Figure 5.2.1** Bright field and fluorescence imaging of various microspheres by the compact “desktop” automatic microscope using different objectives

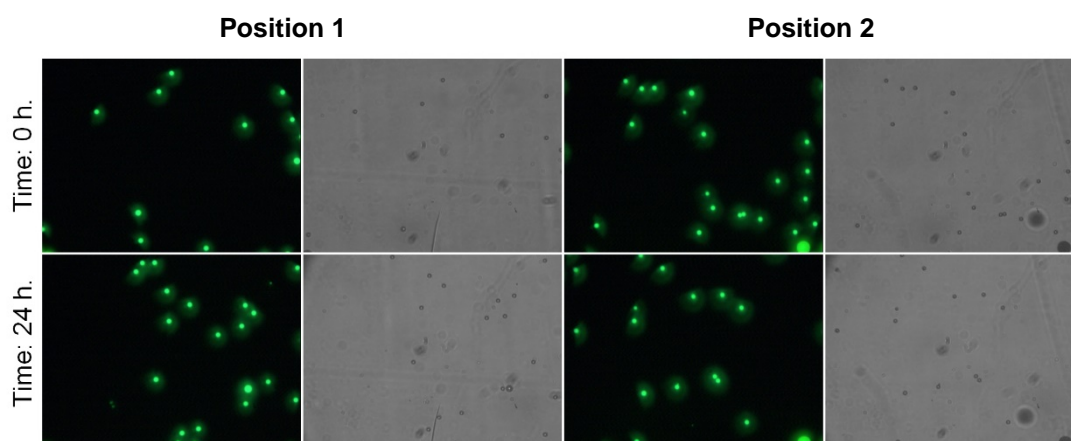
The compact imaging device is designed for alternating bright field and fluorescence time-lapse imaging. For this reason, the LWD 20x objective is more suitable than the Olympus 20x fluorescence objective for the application. When the LWD 20x objective is used in the

optical construction, the theoretical optical resolution of the compact imaging system can be calculated by the formula as  $0.6 \frac{\lambda}{NA} = 0.75 \mu\text{m}$  **[Min Gu, 2000]** under an illumination with averaged wavelength of 500 nm.

## 5. Results

### 5.2.2 Stability of the automatic microscopy operation

In order to test the stability and repeatability of the automatic microscopy operation, two independent channels spaced with 28 mm are imaged with this compact automatic imaging device continuously for 24 hours. The beginning and ending images under alternating bright field and fluorescence imaging mode are shown in Figure 5.2.2. Fluorescent microbeads in both channels are still kept in the focus plane of the fluorescence imaging after running for 24 hours. Meanwhile, the pattern on the bottom of each channel is the same under the bright field imaging. It means that the stability of the automatic imaging system is good enough to be applied for the long-term time-lapse imaging.



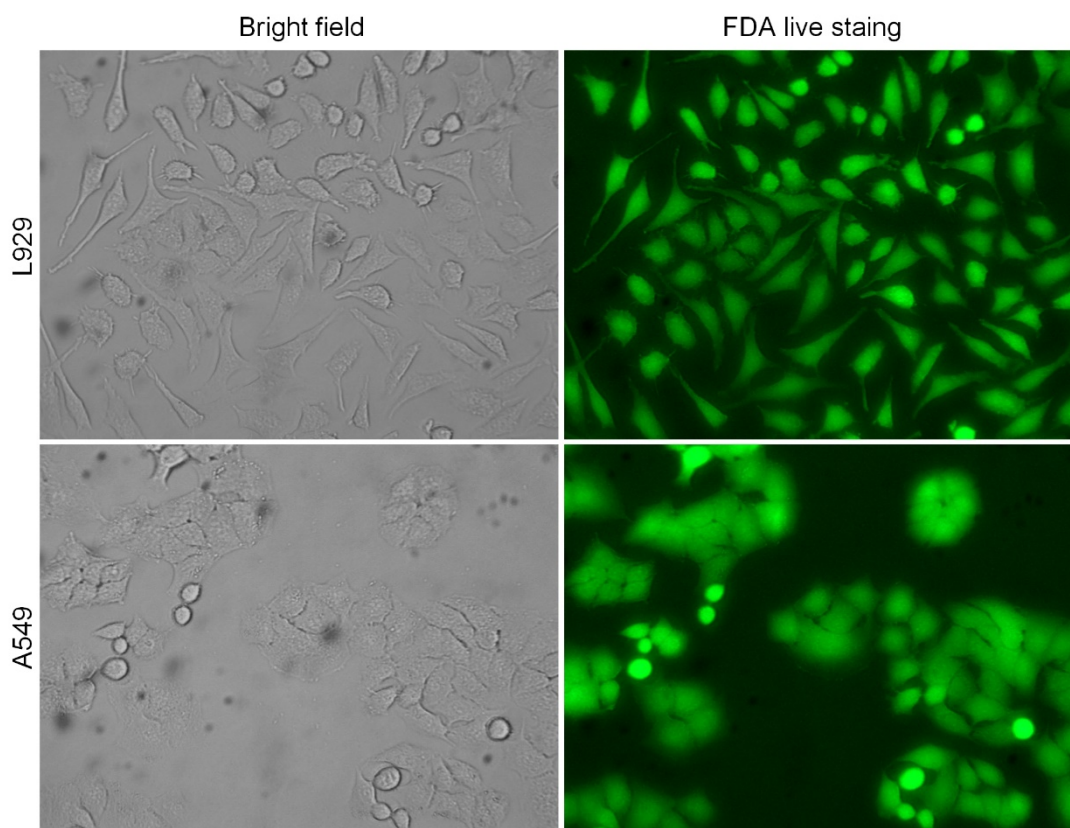
Compact microscope with a LW 20x objective, NA=0.4; Fluorescent microbeads 5.65  $\mu\text{m}$

**Figure 5.2.2** Stability of the “desktop” automatic imaging system in respect of focus plane and repeatability of two different testing points running for 24 hours.

### 5.2.3 Images of cell cultures by the “desktop” microscopic optics

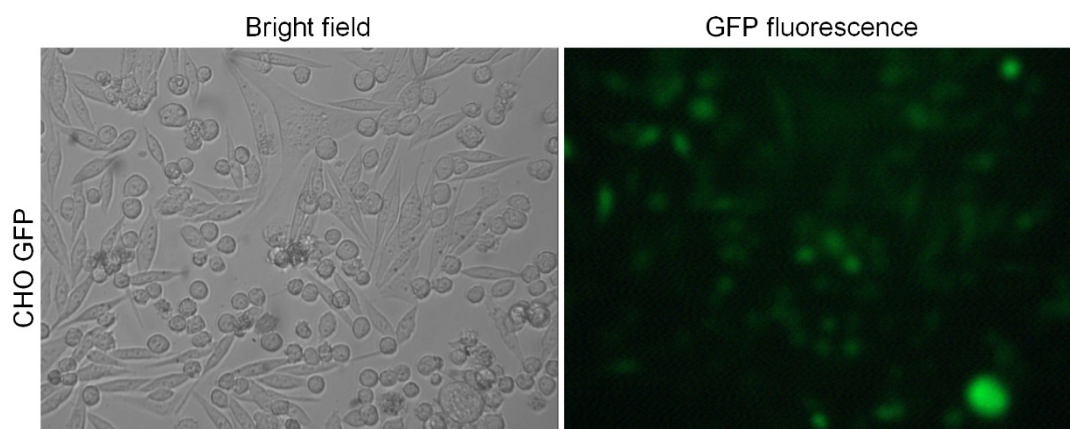
L929 and A549 cell cultures are both stained with FDA viability staining. The live cells are imaged with this compact imaging system respectively. Both bright field and fluorescent images are presented in Figure 5.2.3. In both imaging methods, morphologies of cells are well presented and also in a good contrast.

According to the measurement and estimation in chapter 4.2.4, the royal blue high power LED is not powerful enough for the imaging of GFP cells and therefore should be replaced by a commercial grade fluorescent light source Olympus X-cite 120. The fluorescence of CHO GFP cells is successfully imaged by this compact automatic microscopy optics as shown in Figure 5.2.4.



Compact microscope with a LW 20x objective, NA=0.4

**Figure 5.2.3** 20x Bright field and fluorescent images of L929 cells and A549 cells with FDA viability staining captured by the “desktop” automatic imaging system with LED illuminations.



Compact microscope with a LW 20x objective, NA=0.4

**Figure 5.2.4** 20x Bright field and fluorescent images CHO GFP cells by the “desktop” automatic microscope imaging system with white LED and X-cite 120 light source.

## 5.3 Imaging capabilities of the “very-near field” shadow

### imaging configuration

As an alternative imaging method with an even more compact size, the optical resolution of the “very-near field” shadow imaging will be estimated experimentally. Cell cultures of different morphologies, color and fluorescent staining of cells imaged by the “very-near field” shadow imaging configuration will be presented.

#### 5.3.1 Imaging quality of the “very-near field” shadow imaging

The sub-pixel sized  $1.88 \mu\text{m}$  microbeads in a Si/PDMS micro-well chip with  $1 \mu\text{m}$   $\text{Si}_3\text{N}_4$  bottom are imaged by the uncoated OV5620 image sensor module to experimentally test the optical resolution of the “very-near field” shadow imaging configuration. The shadow images of microbeads and the cross sectional intensity profile of one microbead are shown in Figure 5.3.1. Because the diameter of the sample is smaller than the pixel resolution, the cross sectional profile can be considered as the PSF (Point Spread Function) of the optical imaging system. The PSF is fitted by a Gauss function and its FWHM (Full Width at Half Maximum) is estimated to be about 2 pixel sizes.

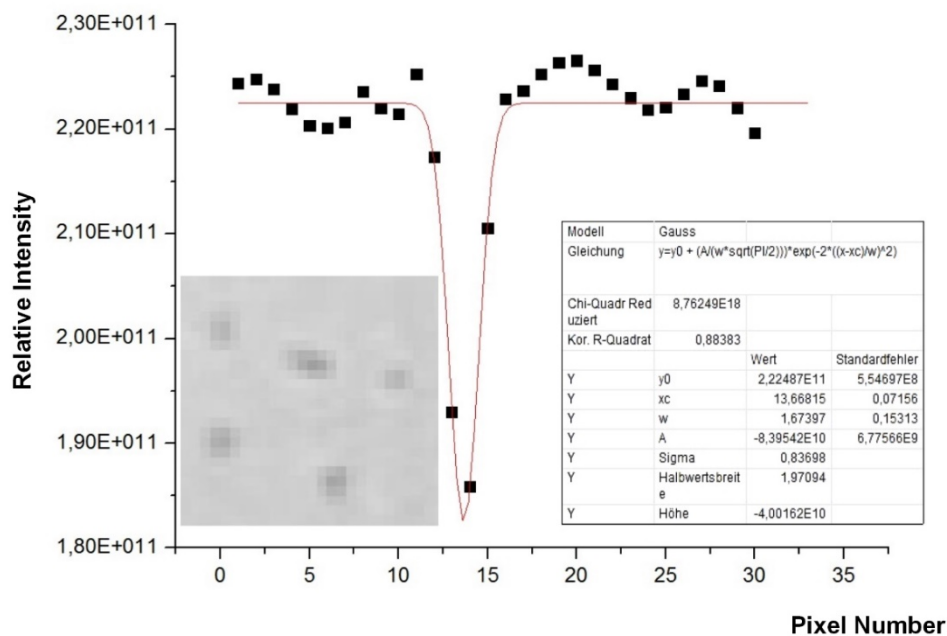


**Figure 5.3.1** Shadow images of  $1.88 \mu\text{m}$  microbeads on  $1 \mu\text{m}$  thick  $\text{Si}_3\text{N}_4$  membrane imaged by a  $2.2 \mu\text{m}$  pixel sized 5M CMOS image sensor (OmniVision OV5620 module) and the demonstrating intensity cross sectional profile of one microbead’s image.

According to Equation 2-6, the theoretical optical resolution of the diffraction pattern is only 780 nm if samples are interfaced by 1  $\mu\text{m}$   $\text{Si}_3\text{N}_4$  membrane and under the collimated illumination with averaged wavelength of 550 nm. Therefore, the pixelation effect overweighs the diffraction effect, and the resulting optical resolution of the “very-near field” shadow imaging system is determined by the resolution of the image sensor, which equals two pixel sizes according to the “Nyquist sampling criterion”. For the imager (OV5620) used here, two pixels correspond to 4.4  $\mu\text{m}$ . Since the theoretical diffraction limit is 780 nm, an image sensor with more refined pixel size could be applied in this “very-near field” shadow imaging configuration, e.g. 1  $\mu\text{m}$  pixel size with the digital resolution of 2  $\mu\text{m}$ .

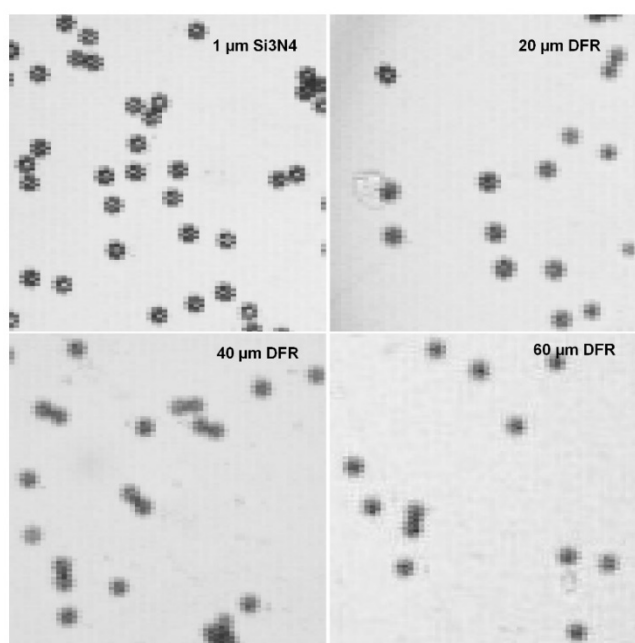


**Figure 5.3.2** Projected shadow images of 15  $\mu\text{m}$  microbeads interfaced by 1  $\mu\text{m}$  bottom thick  $\text{Si}_3\text{N}_4$ - and 20  $\mu\text{m}$ , 40  $\mu\text{m}$  and 60  $\mu\text{m}$  bottom thick DFR micro-cavity chips (Imager: OmniVision 2.2  $\mu\text{m}$  pixel sized 5M CMOS image sensor with no coating).

By using microfabricated chips, the image quality of shadow imaging with small distances from 1—60  $\mu\text{m}$  has been experimentally evaluated. Shadow images of 15.02  $\mu\text{m}$  microbeads, the size of which is equivalent to mammalian cells, interfaced by Si/DFR microchips and the cross sectional intensity profiles are shown in Figure 5.3.2 and Figure 5.3.3 respectively. As the thickness of the bottom layer increases, the contrast of shadow images decreases and the images become more blurred. Correspondingly in the figure of intensity profiles, the ratio of peak to background decreases. The steepness of profile edges, which indicates the fidelity quality of the projection, also decreases. The projection edges are sharp with bottom thickness of 1  $\mu\text{m}$   $\text{Si}_3\text{N}_4$ . Up to 20  $\mu\text{m}$ , the fidelity of the projection image is still good. When the thickness of DFR exceeds 40  $\mu\text{m}$ , the projection fidelity of 15  $\mu\text{m}$  microbeads is obviously degraded by diffraction effect.

## 5. Results

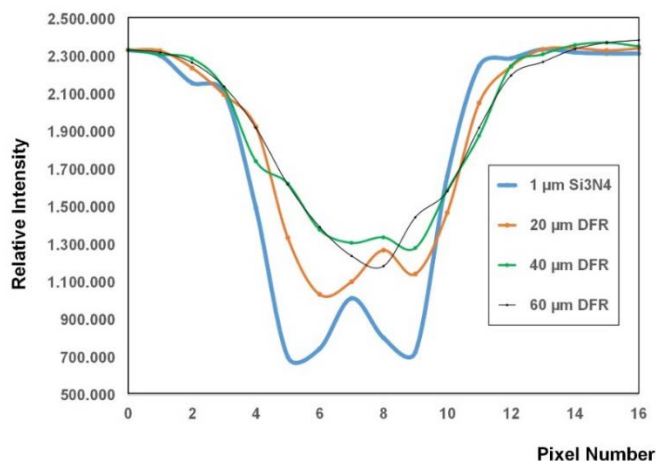


**Figure 5.3.3 Intensity cross-sectional profiles of 15  $\mu\text{m}$  microbeads interfaced by 1  $\mu\text{m}$  bottom thick  $\text{Si}_3\text{N}_4$ , 20  $\mu\text{m}$ , 40  $\mu\text{m}$  and 60  $\mu\text{m}$  bottom thick DFR micro-cavity chips (Imager: OmniVision 2.2  $\mu\text{m}$  pixel sized 5M CMOS image sensor with no coating).**

Similar to the contact imaging of 45  $\mu\text{m}$  transparent polystyrene microbeads by a 7  $\mu\text{m}$  pixel sized imager [57] as shown in Figure 1.2.11 of chapter 1, the shadow image of 15  $\mu\text{m}$  latex beads is also with a bright center but is smaller and more dimmed, which is presented in the intensity profile as double “peaks” (upside down). This bright center is probably due to the optical focusing effect of the sphere, which is similar as the imaging result presented in reference [57]. The microbeads used in the experiment are made of semi-translucent latex material, where the majority of the collimating light is diffused thus leaving a relatively darker projection. A small part of the collimating light transmits and is converged by the sphere shape forming a relatively brighter center. The bright center becomes even smaller and more dimmed until it disappears when the bottom thickness is increased up to 40  $\mu\text{m}$ , and here the intensity profile of the 15  $\mu\text{m}$  microbeads has been deformed by a more evident diffraction effect. The contrast and fidelity of 15  $\mu\text{m}$  shadow images decrease as the sample-imager distance increases. The best resolution and contrast of shadow imaging is obtained just below the substrate surface. The focus of the optical microscopy is confined to a very thin layer of the sample, while, the “depth of focus” of such shadow imaging is very long, more than several tens of micrometer.

According to Equation 2-6, the theoretical resolutions of the diffraction patterns by 20, 40 and 60  $\mu\text{m}$  DFR membranes are 3.89  $\mu\text{m}$ , 5.50  $\mu\text{m}$  and 6.73  $\mu\text{m}$  respectively. When the sample is interfaced by over 20  $\mu\text{m}$  thick DFR membranes, the diffraction effect already overweighs the pixelation effect of the image sensor. Though with up to 60  $\mu\text{m}$  thick DFR film 15  $\mu\text{m}$  microbeads can still be distinguished by the shadow imaging configuration, smaller features of cell morphologies will hardly be presented and identified.

### 5.3.2 “Very-near field” shadow images of different cell morphologies

The “very-near field” shadow images and 4x bright field microscopy images of L929, A549 and T47D cell lines cultured in the micro-well chips with 1  $\mu\text{m}$   $\text{Si}_3\text{N}_4$  membrane bottom are shown in Figure 5.3.4 (A)-(D) as comparisons.

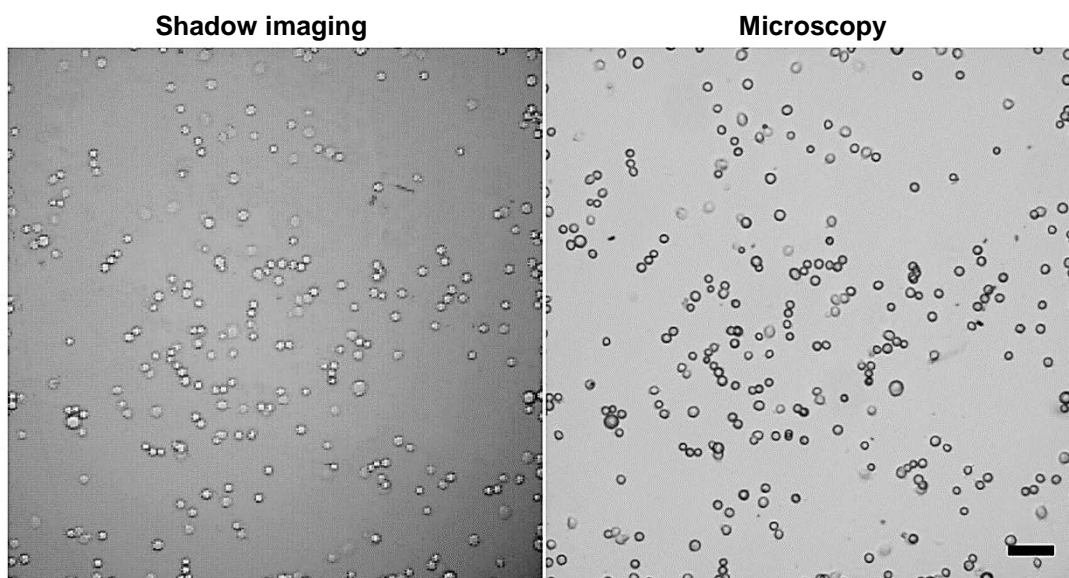


Figure 5.3.4 (A) “Very-near field” shadow imaging (Imager: OmniVision 2.2  $\mu\text{m}$  pixel sized 5M CMOS image sensor with no coating) and 4x bright field microscopy of A549 human lung carcinoma epithelia cells seeding in Si/PDMS micro-well chip with 1  $\mu\text{m}$   $\text{Si}_3\text{N}_4$  membrane bottom. Scale bar: 100  $\mu\text{m}$ .

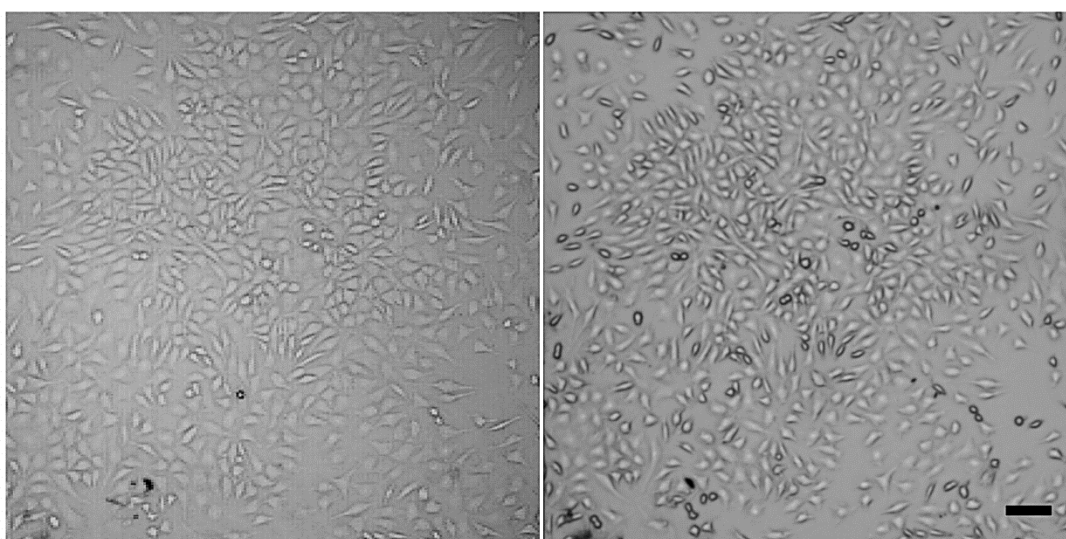
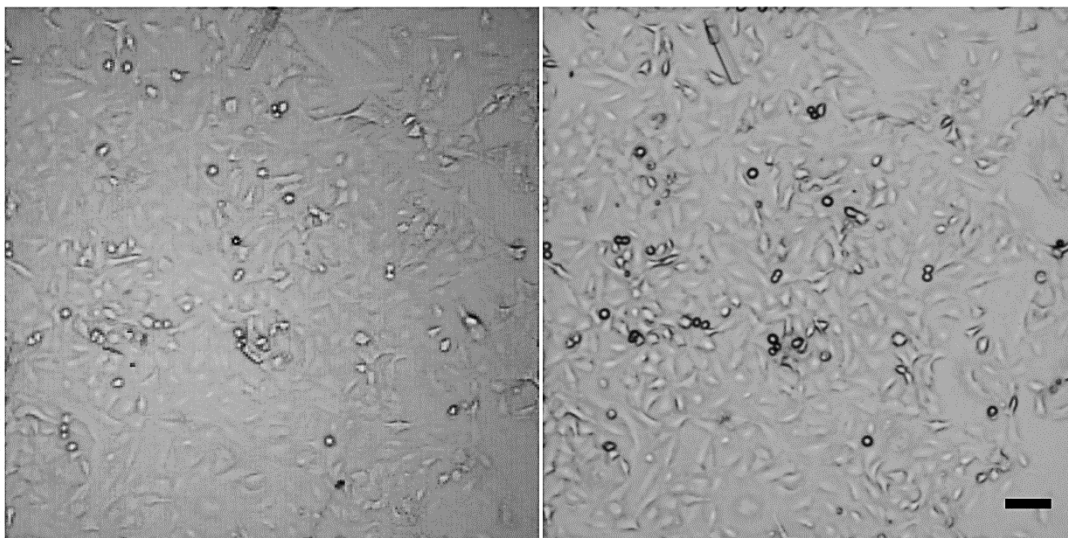
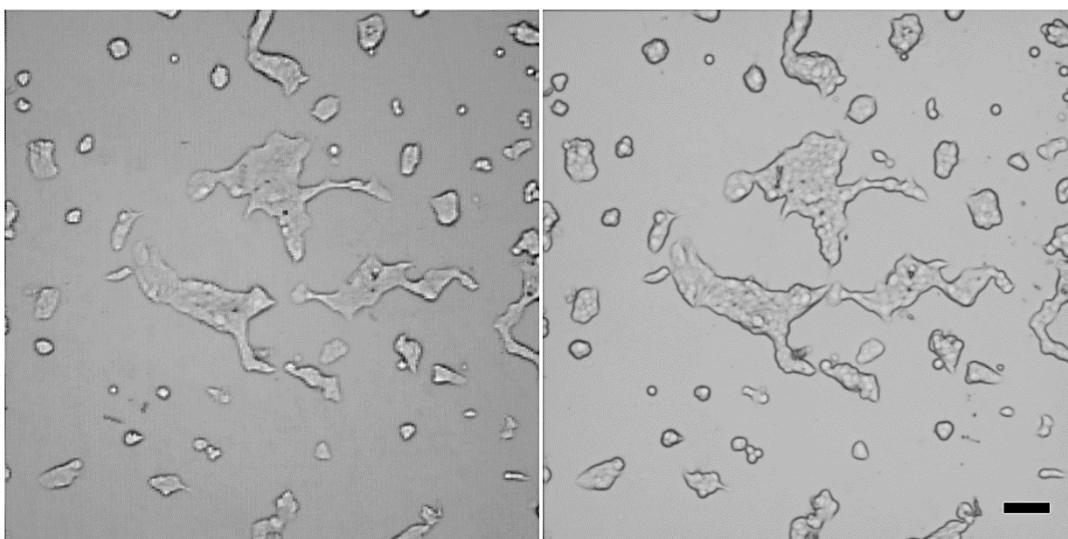


Figure 5.3.4 (B) “Very-near field” shadow imaging (Imager: OmniVision 2.2  $\mu\text{m}$  pixel sized 5M CMOS image sensor with no coating) and 4x bright-field microscopy of L929 mouse fibroblast cells layer cultured in Si/PDMS micro-well chip with 1  $\mu\text{m}$   $\text{Si}_3\text{N}_4$  membrane bottom. Scale bar: 100  $\mu\text{m}$ .

## 5. Results



**Figure 5.3.4 (C)** “Very-near field” shadow imaging (Imager: OmniVision 2.2  $\mu\text{m}$  pixel sized 5M CMOS image sensor with no coating) and 4x bright field microscopy of A549 Human lung adenocarcinoma epithelia cells layer cultured in Si/PDMS micro-well chip with 1  $\mu\text{m}$   $\text{Si}_3\text{N}_4$  membrane bottom. Scale bar: 100  $\mu\text{m}$ .



**Figure 5.3.4 (D)** “Very-near field” shadow imaging (Imager: OmniVision 2.2  $\mu\text{m}$  pixel sized 5M CMOS image sensor with no coating) and 4x bright-field microscopy of T47D human breast columnar epithelia tumor cells layer cultured in Si/PDMS micro-well chip with 1  $\mu\text{m}$   $\text{Si}_3\text{N}_4$  membrane bottom. Scale bar: 100  $\mu\text{m}$ .

For each type of cells, “very-near field” shadow images are showing high consistency with microscopy images on both cell morphologies and colonies. The “very near-field” shadow imaging quality is quite comparable to the low magnification microscopy. Since the cells are almost transparent, contrast produced in the specimen is by the diffraction, reflection and scattering of the incident light. Therefore, the contrast of the “very-near field” shadow

imaging should relate to the topography of the cell layers. Fibroblast cells are generally of a steeper topography than carcinoma epithelia cells at edges when they grow and spread on the substrate. From images of both imaging methods, L929 cells are indeed with higher contrast and clearer darker morphology outlines than A549 cells. The rounding cells when experience diving and just seeded cells of both L929 and A549 are all with high contrast and very clear dark outline and the inside is brighter than the background. The T47D are columnar cells, so the morphology of the grouping colonies is even steeper, which is reflected in the very dark and bold morphology outlines for the colonies by both imaging methods.

Since biological cells are almost translucent, parallel light passing through an adhered cell will experience a phase shift depending on cell thickness and refractive index. A part of the light will be scattered, some light will be reflected and, in the case of stained cells, the light will be absorbed. In the case of not completely adhered cells or dividing cells having a more or less spherical shape, the effect of cells on the parallel light that passing through is similar to that of a convex lens. Light passing through such a cell will be converged towards image sensor pixels that are located underneath the center of the cell. At the edge of the cell, the transition from the cell to the substrate is steeper resulting in a bigger light incident angle. Thus, more amount of incident light is reflected resulting in the darker and bolder edge in the shadow imaging. Most cells in the actual growing cell layer appear more complicated and diverse shapes and morphologies, resulting in a partly brighter and partly darker projection pattern. The “very-near field” shadow image of different cell type has different feature and contrast, which is consistent with that appears in the bright field image.

### 5.3.3 “Very-near field” shadow images of live-dead staining of cells

By using this “very near-field” shadow imaging module, color stained dead cells and non-stained live cells are presented at the same time under a simple collimated white LED illumination. According to chapter 3.3.2.1, the optical resolution of color shadow imaging is also 2 pixels, here corresponding to 4.4  $\mu\text{m}$ . Shadow images and microscopy images of fixed A549 cells as the positive control are presented in Figure 5.3.5. According to the description in chapter 4.3.3, these fixed cells are stained with Erythrosine B and Trypan Blue dead-staining solution respectively. The shadow images are in good accordance with microscopy images and no color aliasing effects are observed in the shadow images.

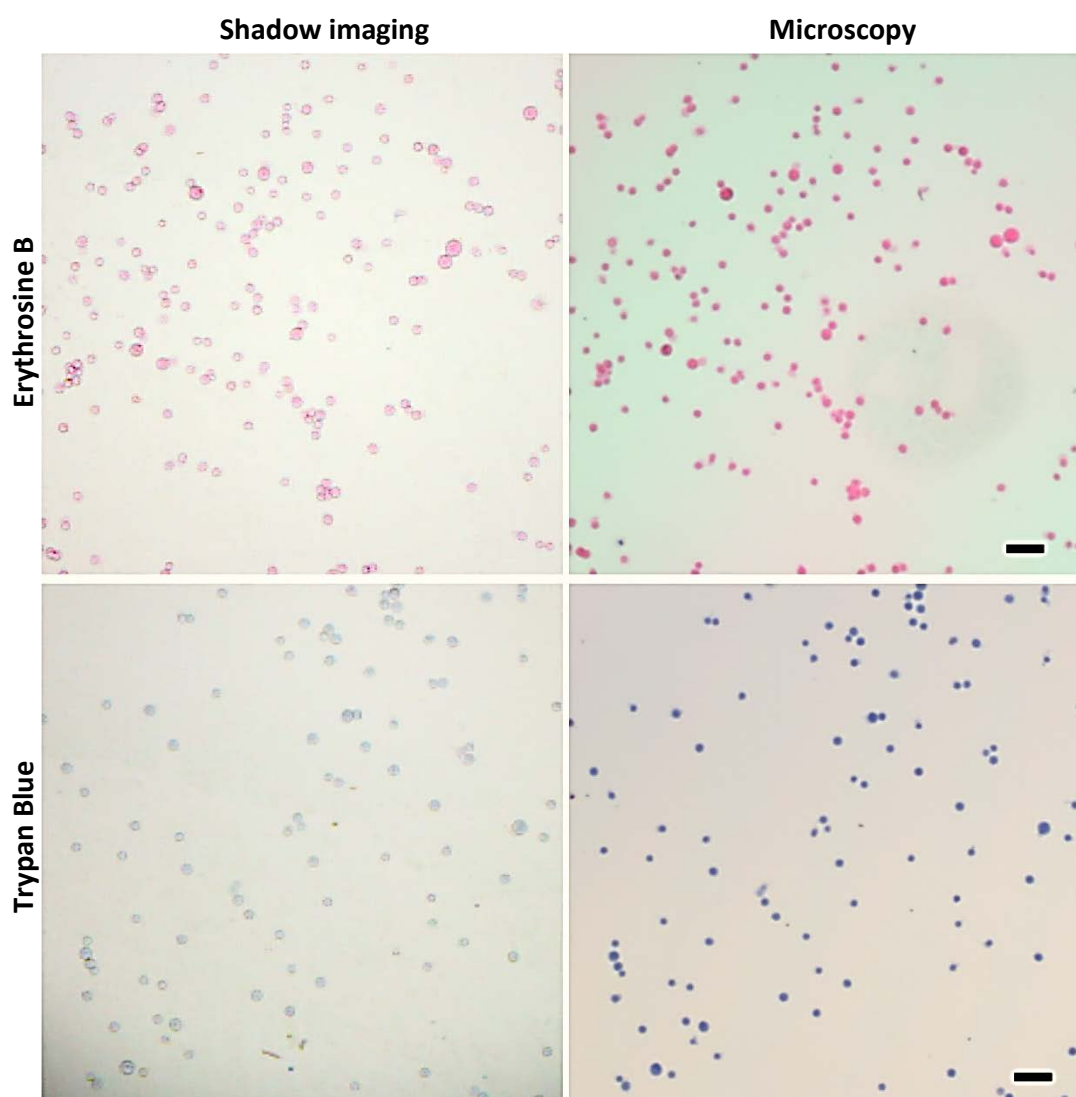


**Figure 5.3.5** Color “very-near field” shadow images (Imager: OmniVision 2.2  $\mu\text{m}$  pixel sized 5M CMOS image sensor with no coating) of fixed A549 cells in Si/PDMS micro-well chip stained by Erythrosine B and Trypan Blue staining solutions as positive control. Reference images are taken by a 4 $\times$  bright field microscopy. Scale bar: 100  $\mu\text{m}$ .

The white LED used here is actually a blue LED with yellow fluorescent powders covered on top and the resulting spectrum is with lower constituents in the red-light spectrum. Color shadow imaging is based on the absorbance of the illumination. Therefore, the imaging of cells stained by Trypan blue is with a poor contrast to the background because the blue light is dominant in the LED's light spectrum. To improve the color representation of both red and blue staining, a RGB white LED could be applied. In a practical live-dead test of cells cultured with silver nanoparticles, red Erythrosine B solution is used for the staining.

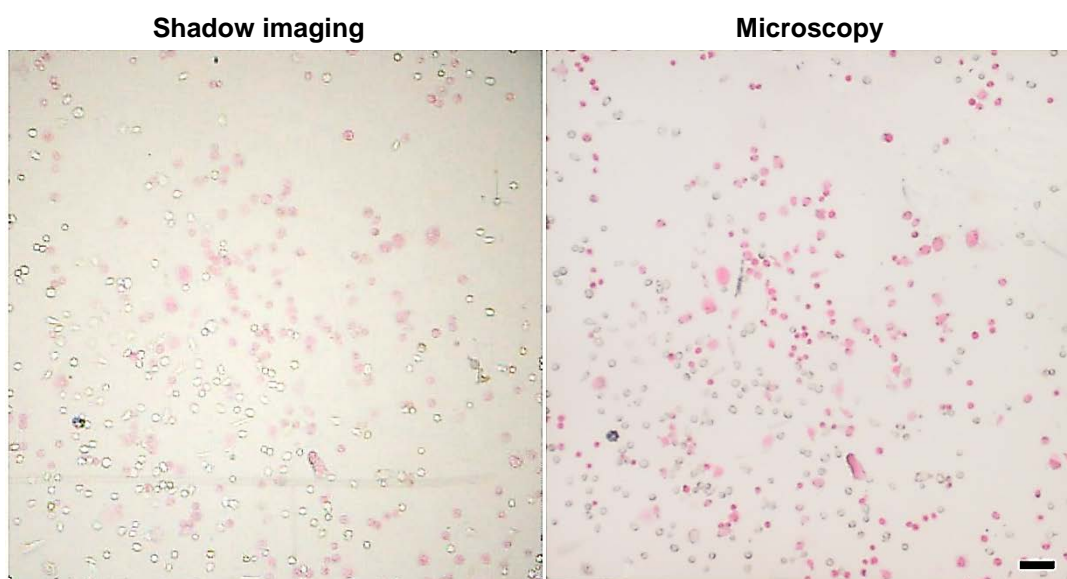


**Figure 5.3.6** Shadow image (Imager: OmniVision 2.2  $\mu\text{m}$  pixel sized 5M CMOS image sensor with no coating) and 4x bright field microscopy image of live-dead staining of A549 cells cultured in Si/PDMS micro-well chip. A549 cell culture has been incubated with 5  $\mu\text{g}/\text{ml}$  10 nm silver nanoparticle in the medium for 24 hours and then stained by Erythrosine B solution. Scale bar: 100  $\mu\text{m}$ .

According to the preparation of chapter 4.3.3, after the A549 cell layer cultured with 10 nm silver nanoparticles at 5  $\mu\text{g}/\text{ml}$  for one day, part of the cell culture is dead. The result can be checked in Figure 5.3.6. Unstained viable cells and dead cells with red staining are represented together in such a dense cell culture layer. The “very-near field” color shadow image is in a good accordance with the microscopy image. Single cells can be easily distinguished from each other no matter if stained or unstained. In the microscopy image, the viable cells are not very well presented. The reason could be that after the wash of cold PBS, viable cells tend to “stand up” from the substrate, while the dead cells with staining require the microscope to be focused closer to the substrate in order to achieve a better contrast of the staining. The shadow imaging, however, compared to microscopy is with a relative deeper “depth of focus”. Both viable and stained dead cells can be well presented at the same time. The “very near-field” color shadow imaging has been successfully applied in the live-dead staining test of cell culture.

### 5.3.4 “Very-near field” fluorescent images of viability test of cells

After the SU-8 spin-coating and lithography process, the electrically connected image sensor Die OV5650 functions well. With a 4  $\mu\text{m}$  SU-8 coating on top, the image sensor will be more robust compared to its previous vulnerable surface when used in combination with a micro-cavity chip. The micro-lens array on the image sensor surface is leveled by the SU-8 coating for the subsequent deposition process of the interference fluorescence filter. The “very-near field” shadow images taken by the image sensor with and without SU-8 coating, the “very-near field” fluorescent images of fluorescent microbeads and cell culture under fluorescent viability test will be presented.

#### 5.3.4.1 “Very near-field” shadow images by image sensor with and without SU-8 coating

According to Equation 2-7, the theoretical resolution of the diffraction pattern on the image sensor surface with 4  $\mu\text{m}$  SU-8 and 1  $\mu\text{m}$   $\text{Si}_3\text{N}_4$  membrane is 1.98  $\mu\text{m}$ . Compared to the pixel size of the image sensor OV5650 (pixel size: 1.75  $\mu\text{m}$ ), the diffraction effect will not impair the digital resolution of the OV5650 which amounts to 3.5  $\mu\text{m}$ . Its imaging performance is tested by using 15.0  $\mu\text{m}$  microspheres under a quasi-collimating white LED illumination, and the output images obtained with OV5650 image sensor with and without SU-8 coating on the surface are compared in Figure 5.3.7. For both images, 15  $\mu\text{m}$  microspheres are well presented with good contrast and smooth round shapes. Clustering microspheres are easily distinguished from each other. There is no obvious degrading of the image quality after the SU-8 layer has been coated.

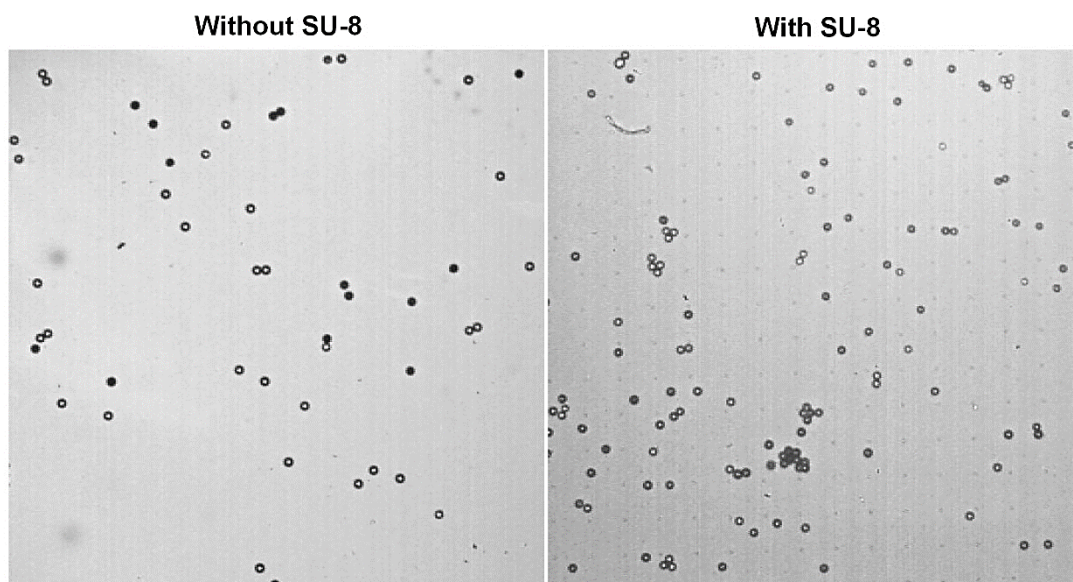


**Figure 5.3.7** Shadow images of 15.0  $\mu\text{m}$  microbeads interfaced by Si/PDMS micro-well chips imaged by OV5650 without and with the 4  $\mu\text{m}$  SU-8 coating on top.

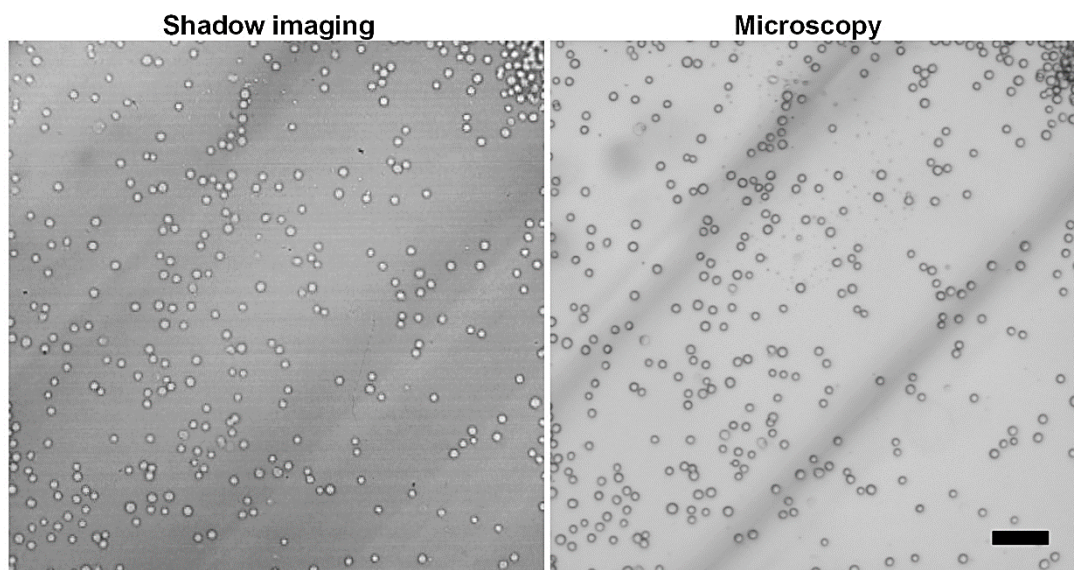


**Figure 5.3.8** L929 cells just seeded in a Si/PDMS micro-channel chip imaged by both OV5650 image sensor with SU-8 coating on top and by a 4x bright field microscope. Scale bar: 100  $\mu\text{m}$ .

L929 cells are observed by using the image sensor with SU-8 coating just after they are seeded inside a microfluidic chip as the image shown in Figure 5.3.8. As it is expected, the “very-near field” shadow image taken by OV5650 image sensor presents more refined imaging resolution compared to that taken by OV5620. A 4x bright field microscopic image is compared for the same field of view. The shadow image is in a good accordance with the microscopy image. Not only single cells but cells in dense clusters can be easily separated and distinguished from each other.

L929 cells are cultured inside a Si/PDMS micro-channel chip for 3 days in the incubator and then the chip is observed by both methods as shown in Figure 5.3.9. In the microscopy image, the cells have grown into a confluent layer with triangular morphology for most of the populations. A 10x microscopy image of the area of interest shows the cells cultured in the microchip are in a healthy state. Several pairs of rounding cells in the proliferation process disperse among the cells layer. In the shadow image, the morphology of cells is well presented and in a good accordance with the 4x microscopy image, and even the thin filaments of cells in such a condense population are very well presented. For the whole optical window, the shadow image qualities are the same even at corners regardless of the imaging methods (bright field, phase contrast and shadow imaging). The performance of “very near-field” shadow imaging is here comparable with a low magnification microscopy.

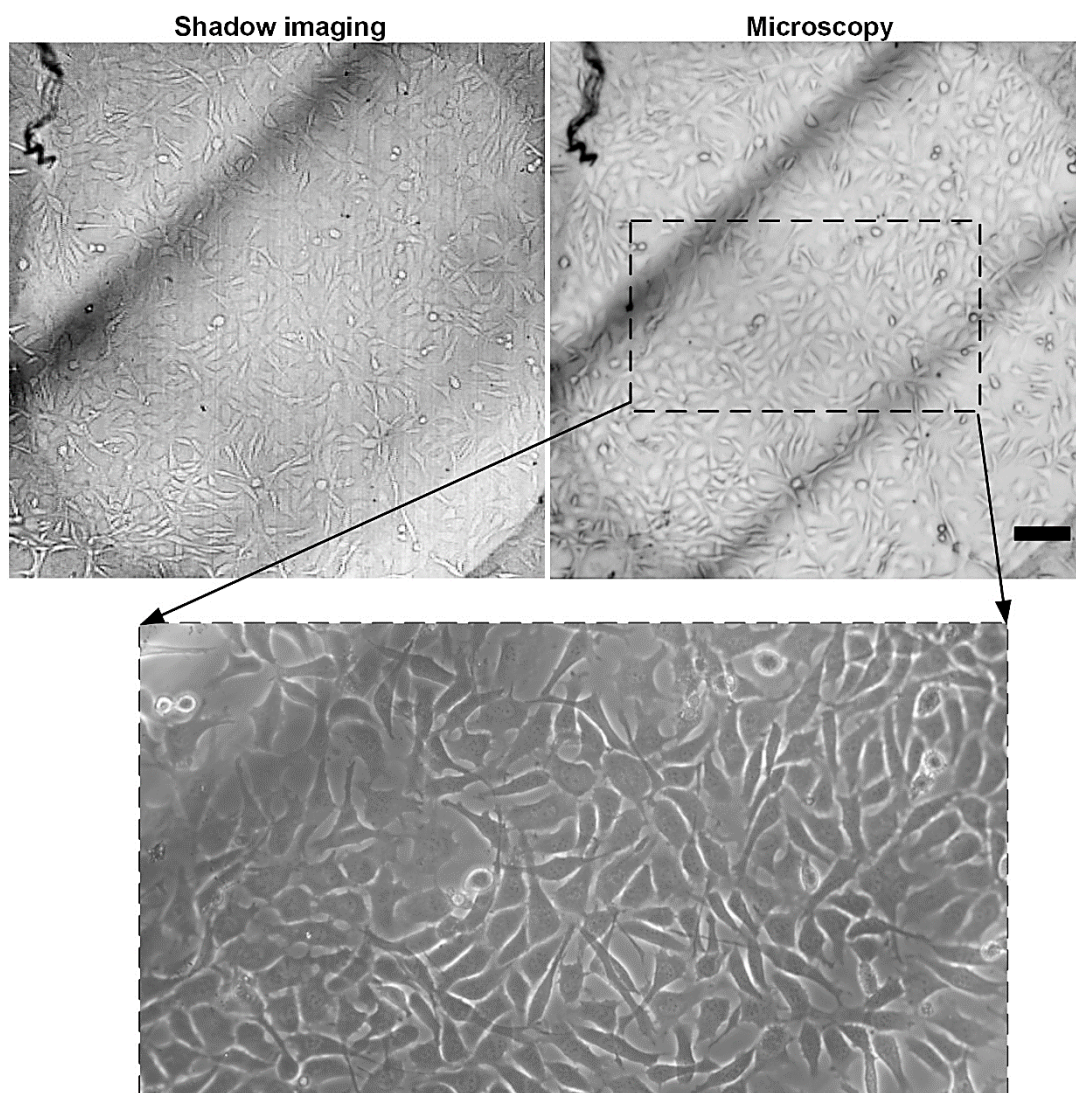


**Figure 5.3.9** Growing L929 cells in a Si/PDMS micro-channel chip imaged by both OV5650 image sensor with SU-8 coating and 4x bright field microscopy. Scale bar: 100  $\mu\text{m}$ . The lower enlarged rectangular is the 10x phase microscopy for the selected area.

#### 5.3.4.2 Optical resolution of the “very-near field” fluorescence imaging

In order to make it suited for fluorescence imaging, the OV5650 image sensor was additionally equipped with an interference filter. The sequence of coatings on the pixels of the imager is as follows: for the first step, a 4  $\mu\text{m}$  SU-8 coating and the second step a 4.5  $\mu\text{m}$   $\text{SiO}_2/\text{TiO}_2$  interference filter are consequently coated on top. Samples are interfaced with the Si/PDMS micro-well chip with a 1  $\mu\text{m}$   $\text{Si}_3\text{N}_4$  membrane bottom. According to Equation 2-7, the theoretical resolution of diffraction pattern under collimated illumination is 2.54  $\mu\text{m}$ . The resolution of the system for “very-near field” fluorescence imaging should be still determined by the digital resolution of the image sensor which amounts to 3.75  $\mu\text{m}$ . However, the fluorescence is emitted in all directions and the fluorescent light will be

refracted and reflected by multiple layers underneath. The resulting image quality and optical resolution will be estimated by experiment.

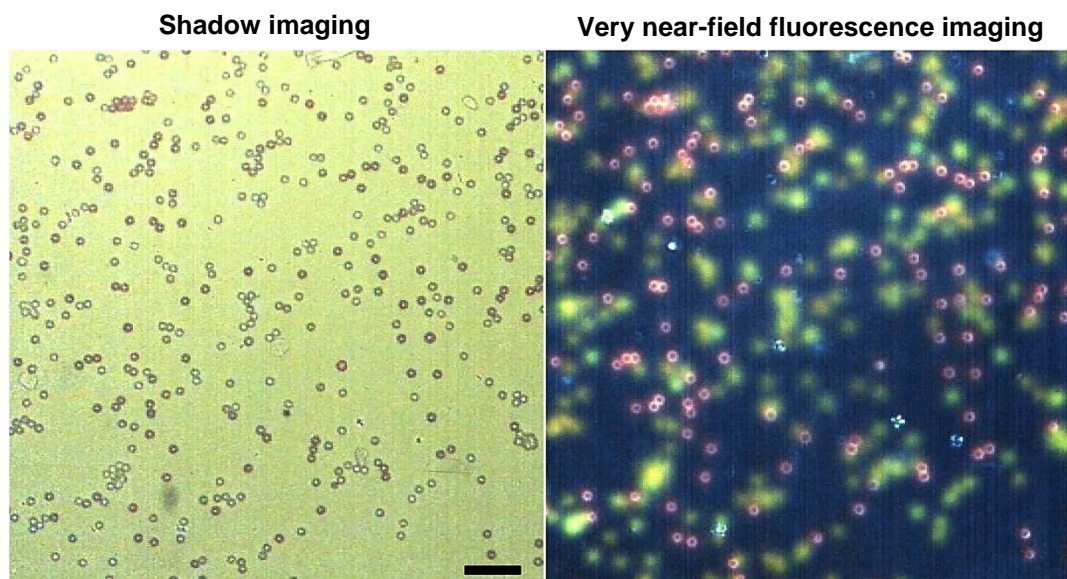


**Figure 5.3.10** “Very-near field” shadow image and fluorescent image of 15.0  $\mu\text{m}$  yellow-green and red fluorescent microspheres in a Si/PDMS micro-well chip (Imager: OV5650 image sensor with 4  $\mu\text{m}$  SU-8 coating and 4.5  $\mu\text{m}$  505 IF interference filter deposition). Scale bar: 100  $\mu\text{m}$

Fluorescent microbeads of 15  $\mu\text{m}$  are imaged by the “very-near field” shadow imaging setup under collimated white LED and blue LED respectively. Figure 5.3.10 show “very near-field” shadow images and fluorescent image for a mixture of 15  $\mu\text{m}$  yellow-green and red fluorescent beads diluted in water and kept in a Si/PDMS micro-well chip. When viewed in daylight the microbeads are translucent yellow-green colored and translucent red colored respectively. In the shadow image on the left of Figure 5.3.10, microbeads are well presented in morphology and dimension. The background becomes yellowish under the white LED illumination due to the coated 505 nm long pass filter. The yellow-green color microbeads appear as dark circles. Their yellow-green color is merged with the background. The red color microspheres appear as dark red translucent spots with darker outer rims. For the fluorescent image as shown on the right of the Figure 5.3.10, the exposure time is 3.0 ms under a collimated ultra-bright blue LED whose spectrum is further shaped with an interference filter of BP 472/30. The fluorescence is emitted at all directions. As it is expected, the yellow-green fluorescence from the yellow-green colored microbeads becomes blurred at edges and the beads appear greatly enlarged. Microbeads very closely spaced cannot be easily separated. A single yellow-green fluorescent microbead and two adjacent microbeads that can be just separated are analyzed in order to estimate the optical resolution of this fluorescence imaging configuration.

## 5. Results

From the cross-sectional intensity profiles (shown in Figure 5.3.11) of yellow-green fluorescent 15  $\mu\text{m}$  single microbead and two proximate microbeads that just can be separated in the “very near-field” fluorescent image, the FWHM of the single intensity profile and the distance between two peaks are all around 13 pixels. The expansion of the “very near-field” fluorescence imaging is about 50% under this optical construction. What should be noticed is that the resolution can be further improved by combining the shadow image with the fluorescent image as shown in Figure 5.3.12 of L929 cells with FDA viability staining. Adjacent spreading cells with fluorescence can be distinguished.

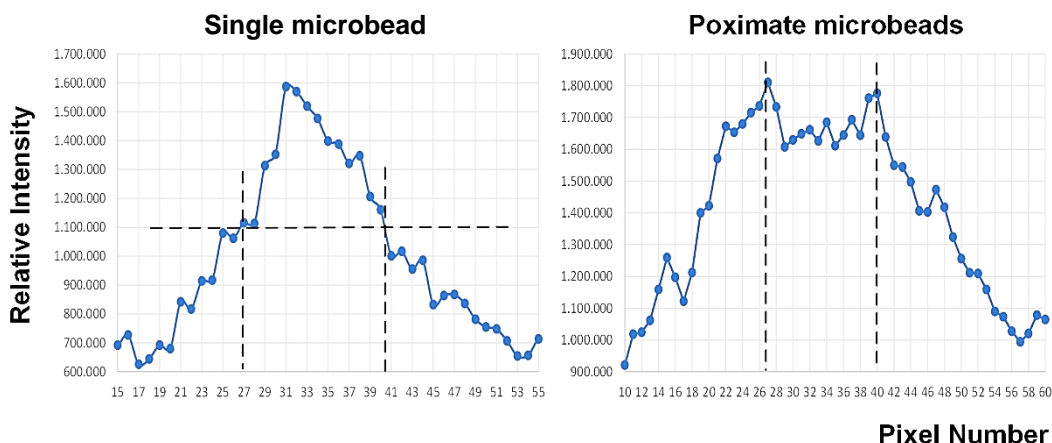
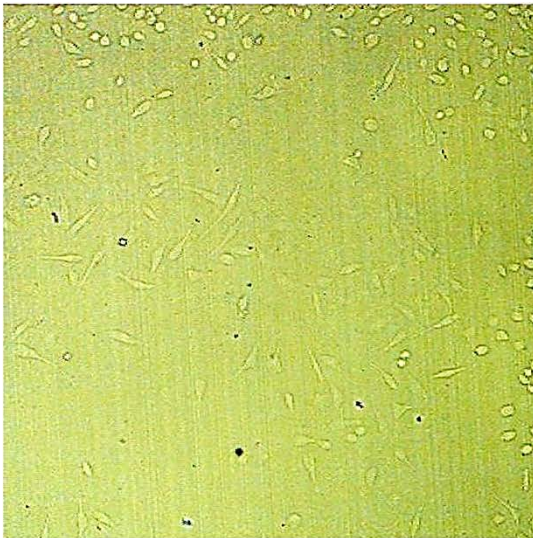


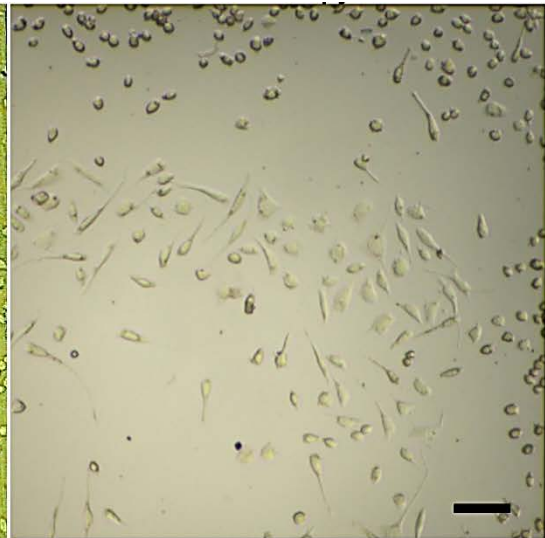
**Figure 5.3.11** Cross sectional intensity profiles of a yellow-green 15  $\mu\text{m}$  single microbead (left) and of two proximate microbeads (right). The “very near-field” fluorescent image is taken by OV5650 image sensor (pixel size 1.75  $\mu\text{m}$ ) with 4  $\mu\text{m}$  SU-8 coating and 4.5  $\mu\text{m}$  505 IF interference filter deposition under a collimated 470 nm LED illumination shaped by excitation interference filter of BP 470/30.

The excitation and emission peak wavelengths for the red fluorescent microbeads are 565 nm and 580 nm respectively, therefore the red fluorescence should not have appeared on the fluorescent image (Figure 5.3.10 right). However, the discussion of the appearance of the red fluorescent microbeads is not within the topic of this experiment. The red microbeads are presented with a brighter edge and darker center. The shape and dimension are not obviously expanded and clusters of multiple microbeads can be separated from each other. Only blue illumination is available; therefore, these red spots cannot be shadow imaging. The appearance of brighter edge is however similar to that of dark field imaging. The red microbeads could be probably excited by the surrounding yellow-greenish fluorescence from lateral directions, and at the same time, the yellow-greenish fluorescence is scattered at the edges of red microbeads. The red fluorescence emitted from the red microbeads is weaker and presents as the center of the red microbead. The scattered yellow-greenish light combined on the dark red fluorescence and appears yellow-orangish brighter outer circle.

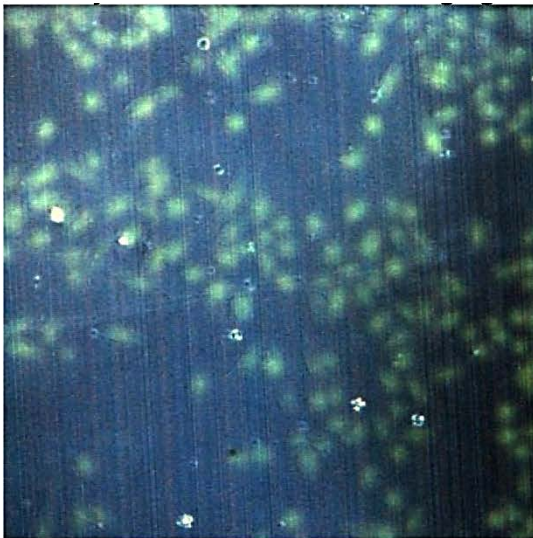
**Shadow imaging**



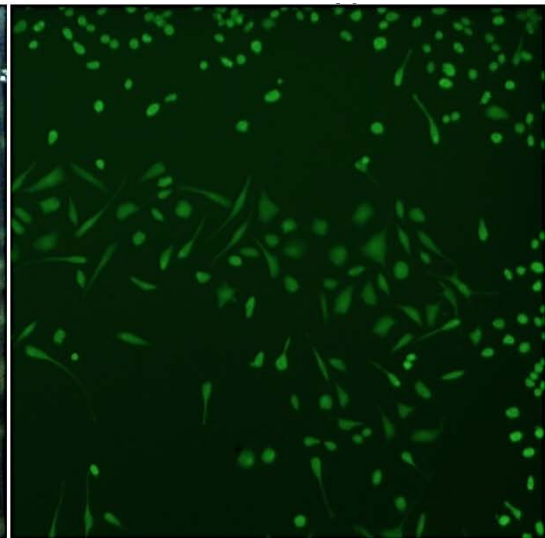
**Microscopy**



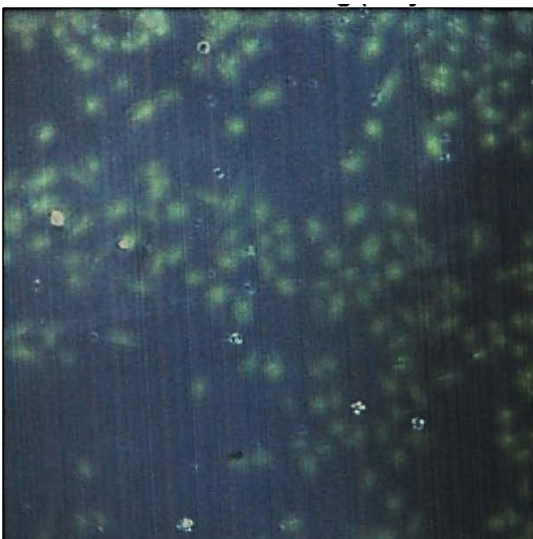
**Very near-field fluorescence imaging**



**Fluorescence Microscopy**



**Very near-field fluorescence image combined with shadow image**



## 5. Results

**Figure 5.3.12** “Very near-field” shadow image and fluorescent image of growing L929 cells and the same cell culture stained by FDA (Imager: OV5650 image sensor with 4  $\mu\text{m}$  SU-8 and 4.5  $\mu\text{m}$  505 IF interference filter coatings); Reference images taken by 4x bright field and fluorescence microscopy images for the same L929 sample. Scale bar: 100  $\mu\text{m}$ .

### 5.3.4.3 “Very-near field” fluorescent images of cell viability test

The “very-near field” shadow image and the fluorescent image of L929 cell culture stained with FDA are shown in Figures 5.3.12. As a reference, the sample is also checked under the 4x bright field and fluorescence microscopy (exposure time: 200 ms, excited by Olympus X-Cite 120 light source, level 1). It can be seen that the “very-near field” images of cells are in a good accordance with the microscopy images. The cells cultured in the Si/PDMS micro-well chip with 1  $\mu\text{m}$   $\text{Si}_3\text{N}_4$  membrane bottom are alive, which is represented by green fluorescence. Though the fluorescence from cells is not “in focus” (expanded 50%) by the “very-near field” imaging, the green fluorescence is still with a good contrast from the darker background (exposure time: 6 ms, excited by a simple blue LED with BP 470/30, 69 dB of sensor dynamic range). The “very-near field” fluorescence imaging method is with a much higher light collecting efficiency compared to the 4x fluorescence microscopy (excited by high power Xenon lamp). However, the background of “very-near field” fluorescence imaging of the cell culture is not as dark as its imaging of microbeads or under the microscopic image. One reason could be from the covered culture medium (as described in chapter 4.2.2), and one reason could be the temperature of the image sensor has increased after having been running for some time. Another reason could be that the microscopy image can be focused on a much thinner layer, but the “very-near field” imaging receives all the light from above layers.

However, it can be seen that most of the fluorescence blocks emitted from clusters of cells can still be separated. Since the corresponding shadow image presents a clearly morphology of individual cells, the resulting resolution of the “very-near field” fluorescence imaging can still be considered down to single cells level, by the simple and economical setup without complicated image processing. To reduce the background noise for fluorescence imaging, the temperature of the image sensor should be reduced. This requirement limits its application in the monitoring of cell culture, but might be used as a low-cost cytometer for the point-of-use application.

## 5.4 Cell culture and testing by the all-in-one cell culture-shadow imaging microsystem

The all-in-one cell culture-imaging system is designed and established with both stand-alone cell culture (liquid handling and incubating) and real-time shadow imaging functions. By this interactive cell culture-imaging platform, the operational parameters such as temperature and flow rate for the cell culture are calibrated. Complete cell culture and testing operations from cell seeding, cell incubating, to live-dead colorimetric staining, cell passage, and 3D cell culture have been carried out and the real-time or time-lapse images sequence of processed or cultured cells are presented.

### 5.4.1 Real-time shadow images of fast cell loading process

Cell loading is operated in both single-channel and dual-channel Si/PDMS microfluidic chips. The cell suspension is manually purged into the microfluidic port, and the fast process can be conveniently monitored by the real-time video captured by the image sensor (3.75 fps). Selected shadow images sequence of a cell loading process can be checked in Figure 5.4.1. The streamlines of cell flowing over the field of view are clearly visualized and are in accordance with the simulated results as shown in Figure 3.4.4 of Chapter 2.4.1.1. The loading operation begins with a strong manual purge, and then the flowing cells are recorded at different time points. After 1.5 seconds, the velocity of cells is reduced and cells gradually sink down to the bottom. By the comet flowing track of a cell, the flowing velocity can be calculated.

A screen shot of a dual-channel microfluidic chip is shown in the upper part of Figure 5.4.2. Each of the two independent cell cultures can be monitored on one microchip at the same time. This configuration is more favorable for cell-based testing with two different conditions in comparison, and in this way, subtle changes can be discerned more easily. In the lower part of Figure 5.4.2, selected shadow images sequence of the cell loading operation in one of the micro-channels is presented. As expected, the streamlines of cells flowing are in line shape along the channel orientation. From left to right, the velocity of cells flowing decreases and cells gradually sink to the bottom. It takes about 7 seconds for all the incoming cells sediment onto the bottom of the microchip with a total channel height of 1 mm.

At different height of the microchip, cells appear with different contrasts and fidelity in the shadow image. This diffraction effect and long “depth of focus” of the “very-near field” shadow imaging is intuitive and convenient for the operator working with cells in microfluidics.

## 5. Results

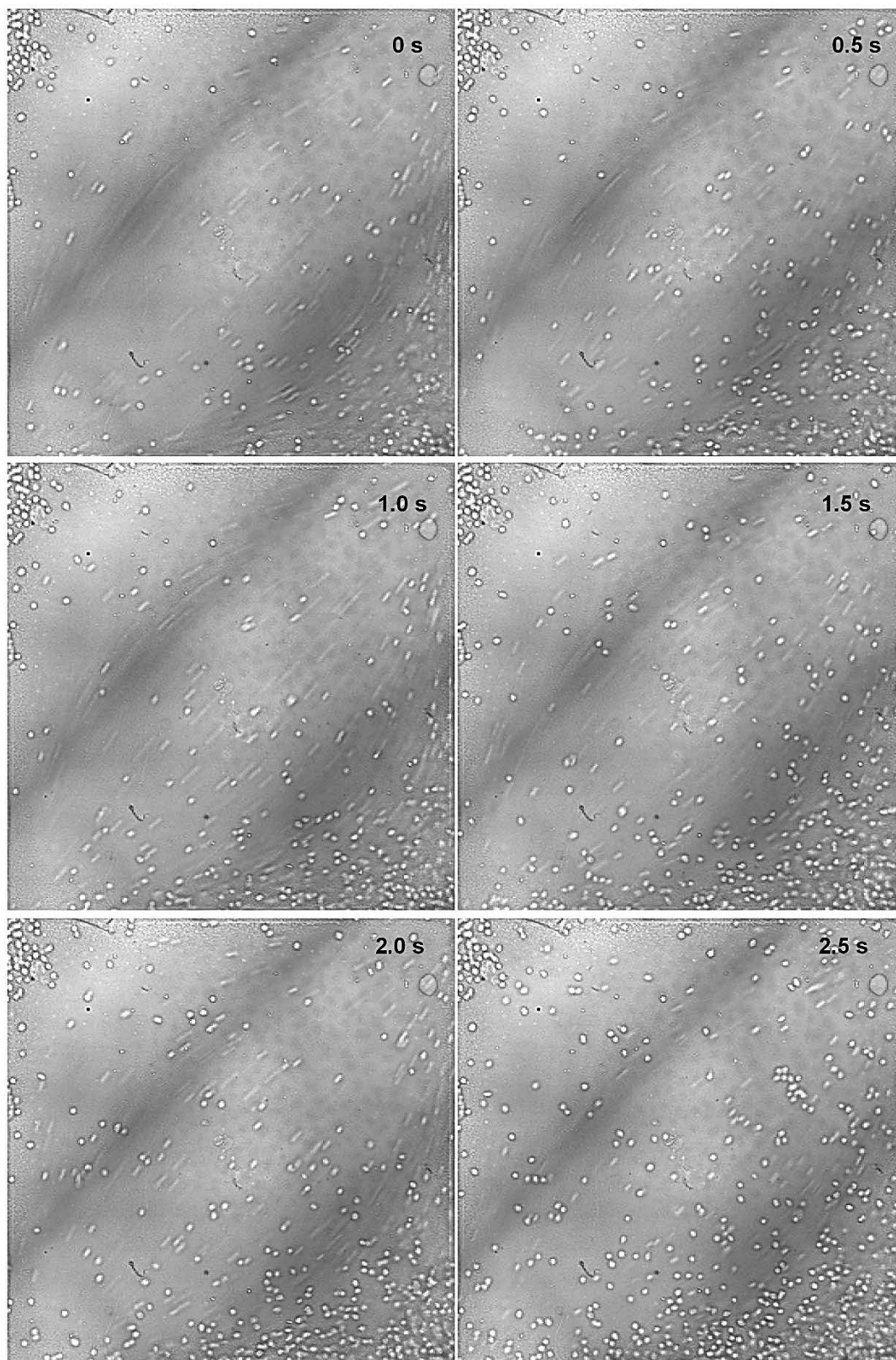


**Figure 5.4.1** Selected shadow images sequence of fast cell loading process into the single-channel Si/PDMS microchip of the all-in-one cell culture-imaging microsystem. The full optical window size is 1 mm × 1 mm.

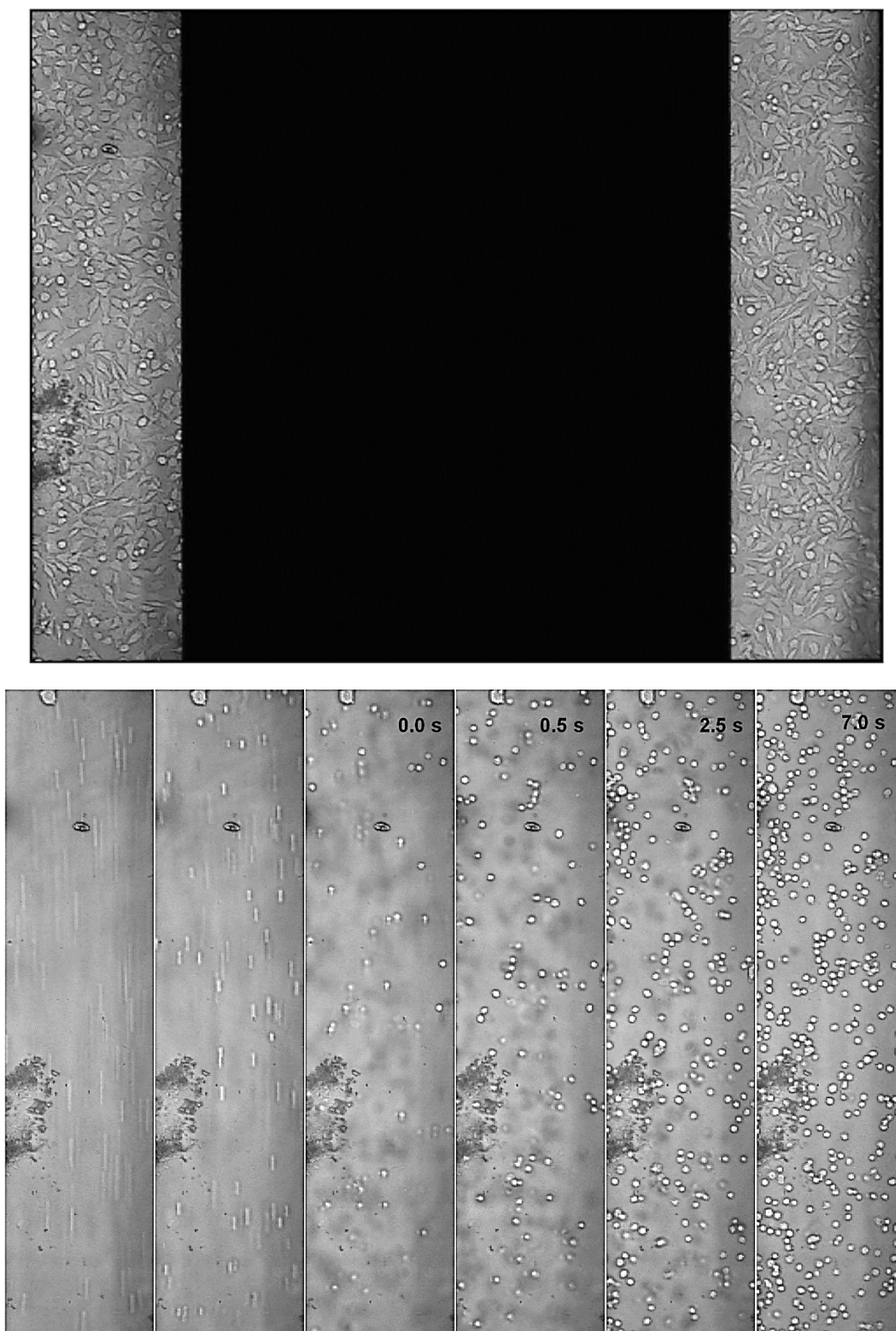


**Figure 5.4.2** (upper) The monitor screen showing a dual-channel Si/PDMS microchip of the all-in-one microsystem with growing cells in both micro-channels; (lower) selected shadow images sequence of cell loading process in one of the dual micro-channels. The dimension of the full optical window is 1.3 mm x 0.3 mm.

## 5. Results

### 5.4.2 Cell responses by temperature adjustment

In order to provide cells with optimal temperature, different targeting temperatures measured on the chip carrier has been tested according to the real cell responses under the real-time shadow imaging.

The trial and error experiments have been performed starting at 38.5°C for L929 cells culture. In this experiment a single-channel microfluidic chip is deployed and no microflow is applied after the cell loading. In Figure 5.4.3, the L929 cells adhere and spread only within half an hour, which is much faster than that in normal condition taking 3—4 hours. However, the cells begin to detach from the substrate at the time point 40 minutes, and after 90 minutes almost 90% of cells have detached from the substrate. The reason for such abnormal cellular response is probably because of the temperature is too high for cell culture.

For a sequence of experiments the targeting temperature was decreased in steps of 0.5°C down to a temperature of 37°C. For every experiment, the L929 cells were freshly prepared. When the targeting temperature is set at 37°C, the cells did not spread very well even after 4 hours. The targeting temperature of 37.5°C on the chip carrier is proved ideal for the mammalian cell culture. The cells adhere and spread normally during the first 4 hours like in the conventional cell culture. This means that the actual temperature on the bottom of the micro-cavity chip is in the range of 36.5—37.5°C, slightly lower than that measured on the chip carrier.

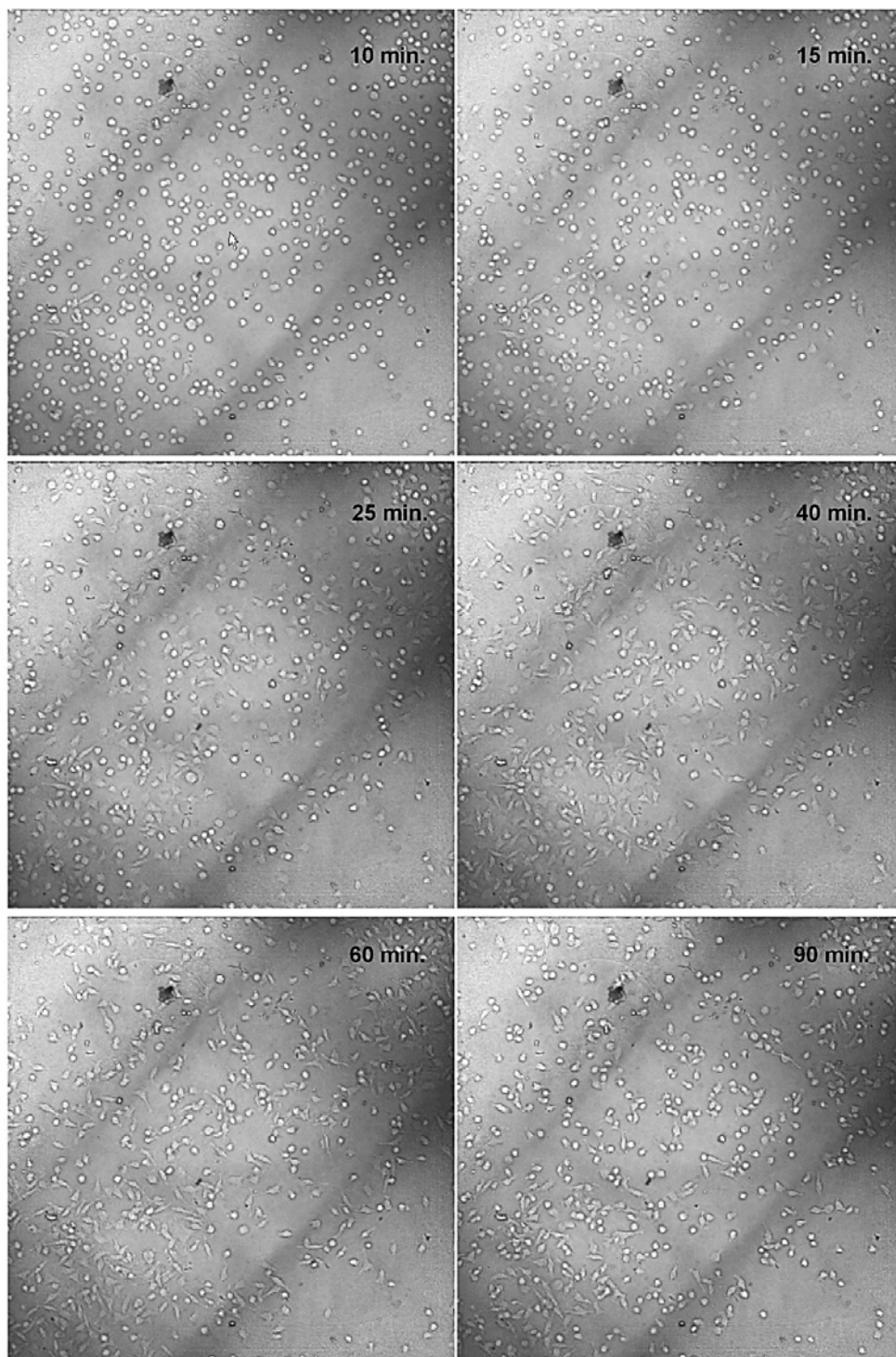


**Figure 5.4.3** Selected shadow images sequence of L929 cells culture in a single-channel microfluidic chip when setting the temperature of the chip carrier at 38.5°C. Cells attach and spread on the surface very quickly within half an hour but then begin to detach from the culture substrate since 40th minute because of the resulting inappropriate temperature on the culture substrate. The optical window size is 1 mm × 1 mm.

### 5.4.3 Real-time shadow images of live-dead colorimetric staining

The colorimetric live-dead staining process of the cell viability test has also been operated by controlled microflows on the all-in-one microsystem. The preparation of the positive control of cell culture has been described in chapter 4.4.5. The 0.05% (g/100 ml) Erythrosine B solution is introduced into the microchip at a flow rate of 1.5 ml/h. The mixing process of the red solution with the medium is clearly represented as shown in Figure 5.4.3 by the gradually changing color. At the time point of 3.95-second, the micro-channel is re-flushed by the medium with a flow rate of 1.5 ml/h. At the time point of 5.00-second, the staining result of individual cells is clearly visible: Dead cells are stained with cherry red and living cells are the brighter white dots.

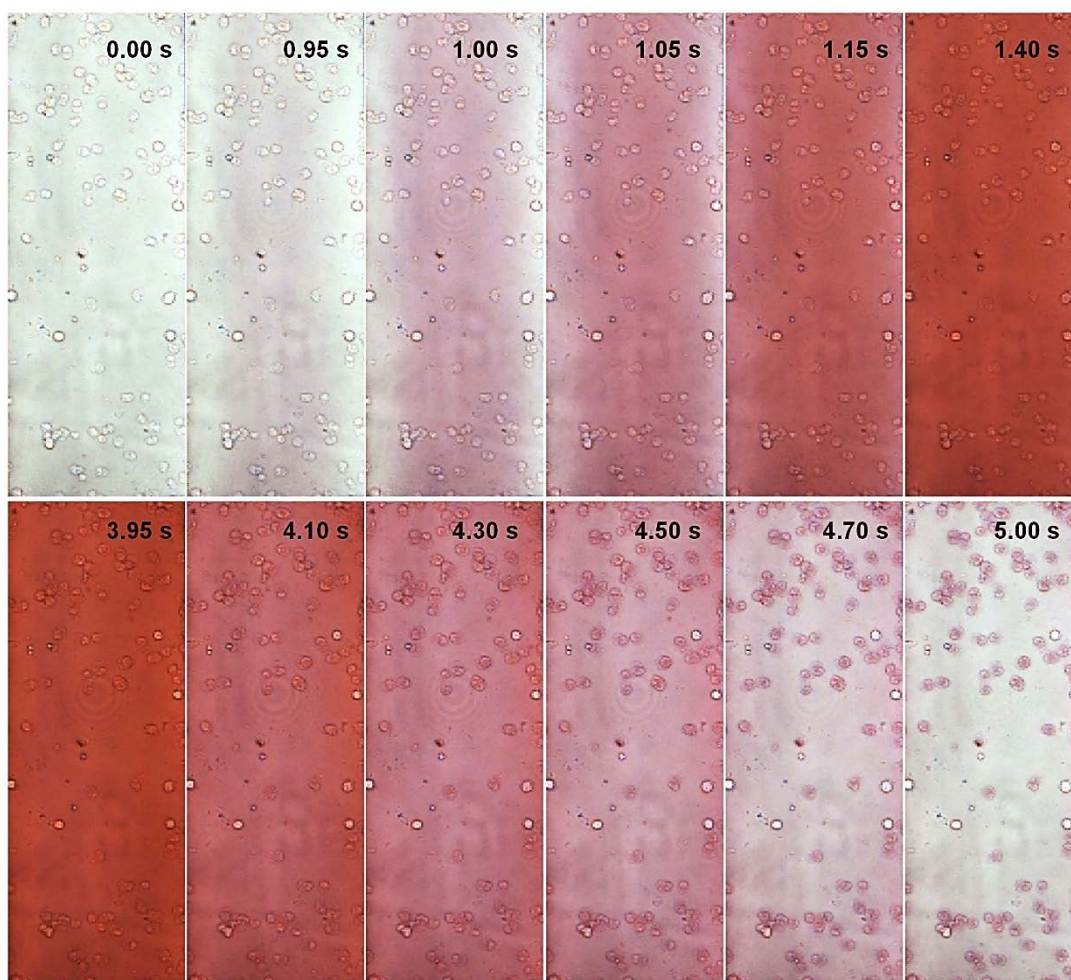


**Figure 5.4.4** Selected shadow image sequences of the live-dead colorimetric staining by flowing 0.05% (g/ 100 ml) Erythrosine B solution into one of the dual micro-channels containing dead cells. Since the time point of 3.95-second, the channel is flowed with medium again to wash the stained cells. Both liquids are purged with the syringe pump at a flow low rate of 1.5 ml/h. The field of the view is cropped by 0.8 mm x 0.3 mm.

## 5.4.4 Cell culture and harvesting by the all-in-one microsystem

### 5.4.4.1 Cell culture and imaging in the all-in-one microsystem

After the temperature of the all-in-one microsystem has been adjusted optimally for the mammalian cells culture, L929 cells are cultured inside the system for 20 hours at a flow rate of 1.0  $\mu\text{l/h}$  according to the procedure described in chapter 4.4.4.2. The time-lapse shadow images sequence of L929 cells in culture is shown in Figure 5.4.5. After cell seeding, the L929 cells are cultured without medium exchange for 4 hours. After 4 hours, the flow of fresh medium is started and is set to 1.0  $\mu\text{l/h}$  for the next 16 hours. The time-lapse images are taken every minute by the image sensor of the all-in-one microsystem. The images presented are all with good contrast. As shown in Figure 5.4.5, the morphology of L929 cells is also represented clearly even when the cells are growing into interlayered structures and even the very thin filaments of cells can be easily discerned. The imaging quality is quite comparable to a low magnification optical microscope. The time-lapse images indicate that, the cells are growing normally and in a very healthy state during the incubation of 20 hours.

Epithelial cells *in vivo* are usually exposed to mechanical forces of different levels. Cellular responses of A549 cells will be recorded when applying a relatively fast flow rate of 5.0  $\mu\text{l/h}$ , under which the estimated shear stress is still in the safe range. From 4—20-hour, the flow rate is still set at 1.0  $\mu\text{l/h}$ . At the time point of 20 hours, the flow rate is suddenly increased to 5.0  $\mu\text{l/h}$ . As shown in Figure 5.4.6, from the time point 20- to 60-hour, there is almost no growth and proliferation of the cell culture. Not until the time point 120-hour, the cells have grown into almost a confluent layer. The live-dead staining viability test operated on the microfluidic chip thereafter shows that there are no dead cells. The growth rate of the A549 cells under this experiment condition is obviously much lower compared to that in the normal culture condition. The reason could be the too fast medium replenish rate, almost 5 times per hour. Although plenty of nutrients have been supplied to cells, soluble factors from cellular secretion will be also taken away from cells around, and this probably will interference the growth of cells.

## 5. Results

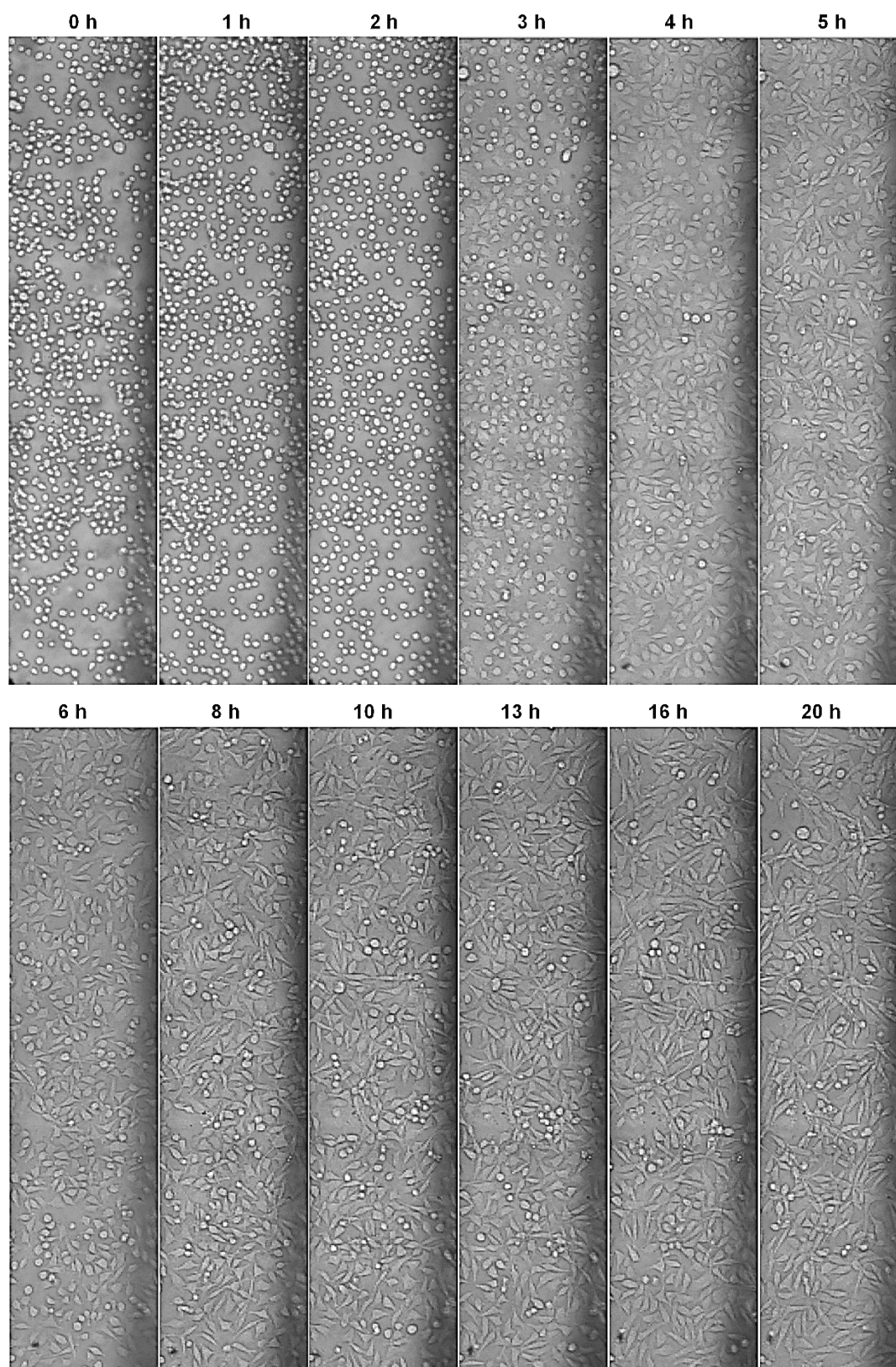


**Figure 5.4.5** Selected shadow images sequence of L929 cells cultured and imaged by the all-in-one microsystem. The flow rate is  $1.0 \mu\text{l/h}$  after static culture for 4 hours. The optical window size is  $1.3 \text{ mm} \times 0.3 \text{ mm}$ .

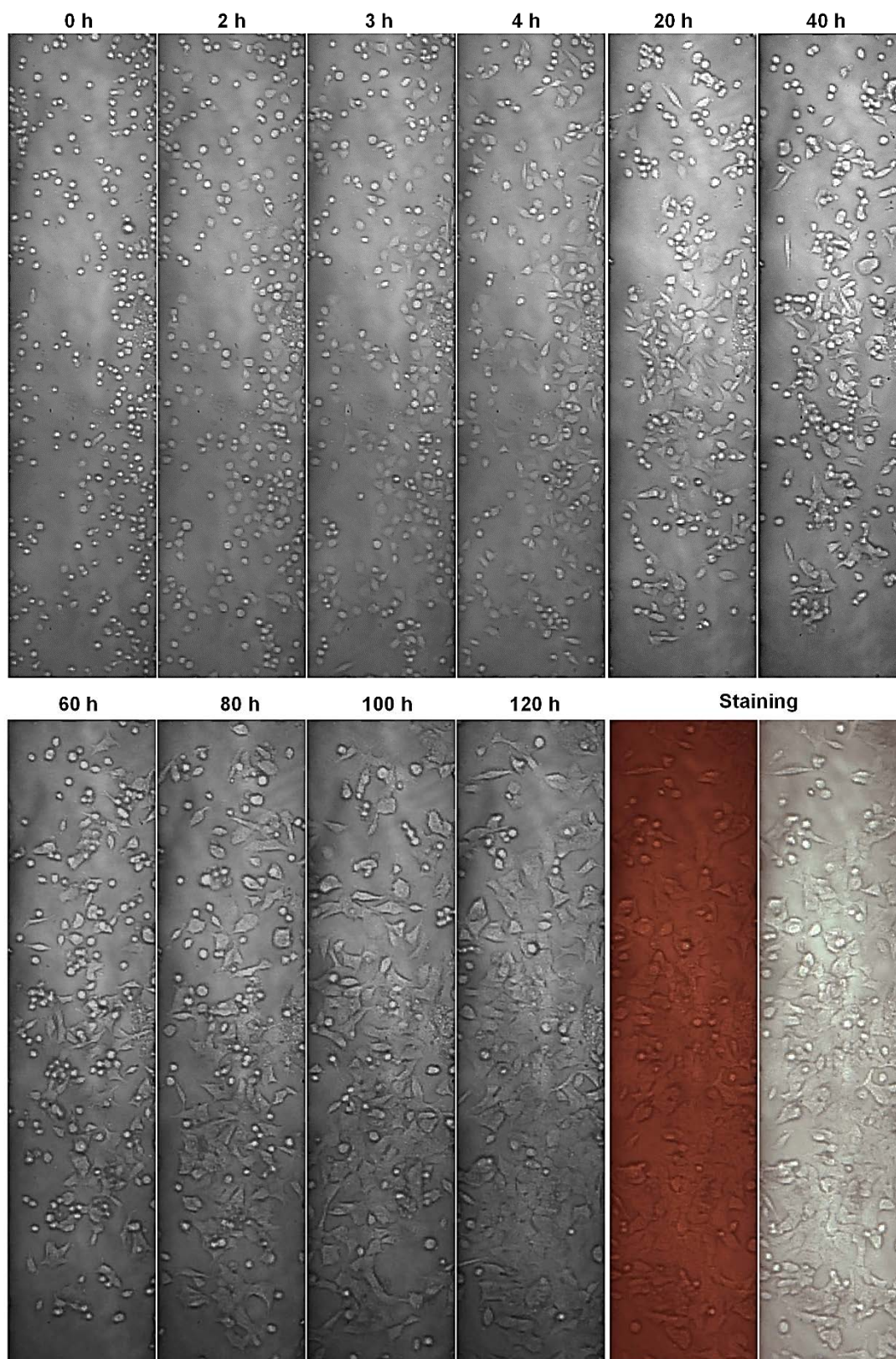


**Figure 5.4.6** Selected shadow images sequence of A549 cell culture and live-dead staining processes in one channel of a dual-channel microfluidic chip. The flow rate is increased to  $5.0 \mu\text{l/h}$  since the time point 20-hour. The finished culture is stained with Erythrosine B live-dead staining solution. The optical window size is  $1.3 \text{ mm} \times 0.3 \text{ mm}$ .

## 5. Results

### 5.4.4.2 Cell culture harvesting operation in the all-in-one microsystem

Cells of a L929 cell layer were harvested after 20 hours cell culture by adding conventional Trypsin (EDTA) solution after 20 hours' cell culture. The process is monitored in real time by the all-in-one interactive platform (3.75 fps). The morphological changes of cells during the harvesting process are very well presented by time as shown in Figure 5.4.7. During the 3 minutes of incubation, the cellular morphologies become smaller and brighter gradually. The cells are losing their attachment to the substrate. After 3 minutes (180 seconds) of incubation, PBS solution is flown into the microchip at a flow rate of 6 ml/h in order to wash the cells and then flush away cells losing attachment to the substrate. Under the PBS fast flow, the cells on the bottom window are still in the microchip until the time point 216-second. During that time, successively, cells are observed flowing fast across the window. These cells should be previously growing on the side walls. Then, the cells on the bottom window are suddenly flushed away within 0.27 second. It could be the sudden pressure change that the image at that time point 216.27-second is darker. An almost empty channel is presented at the time point 216.53-second.

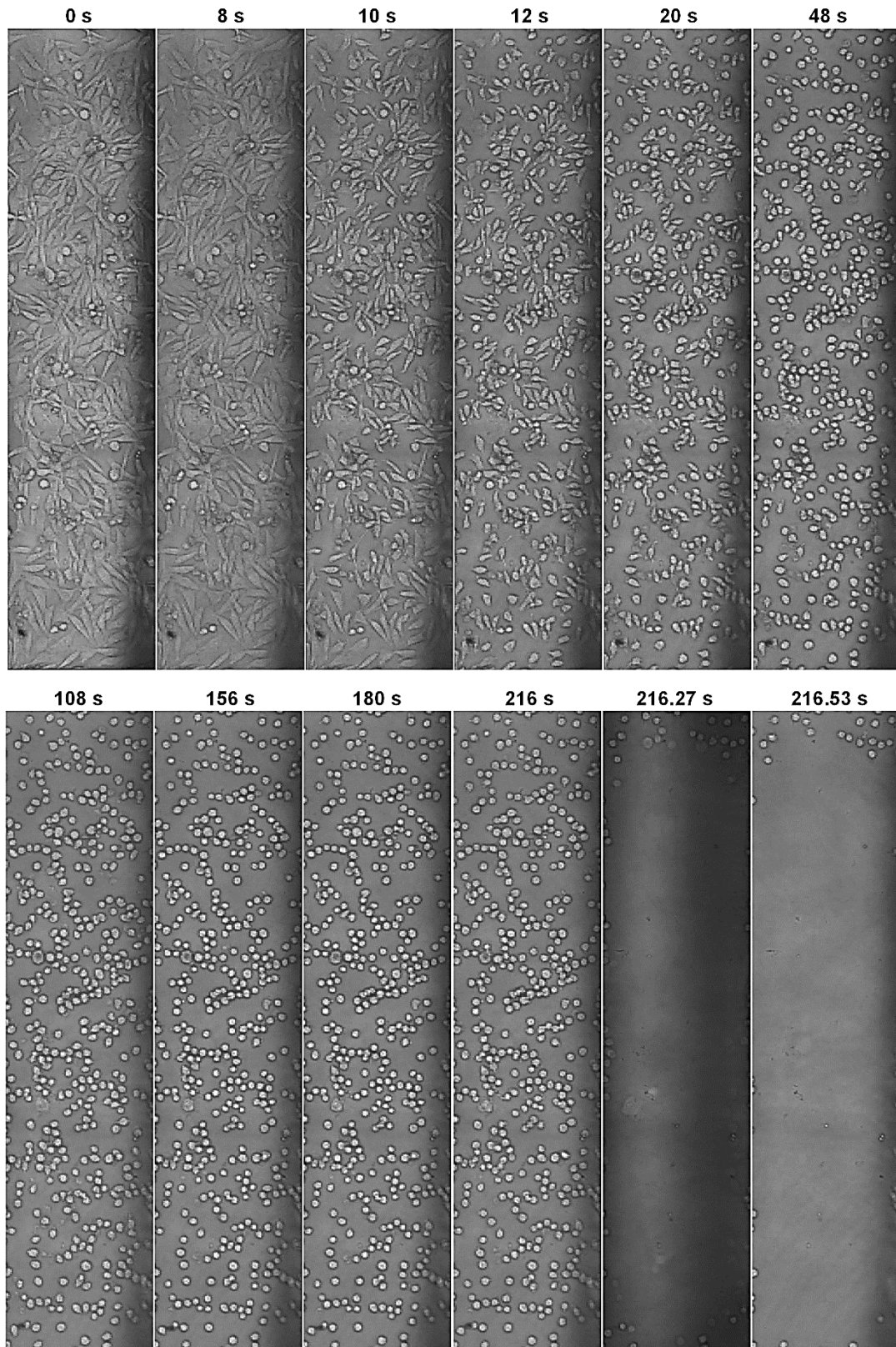
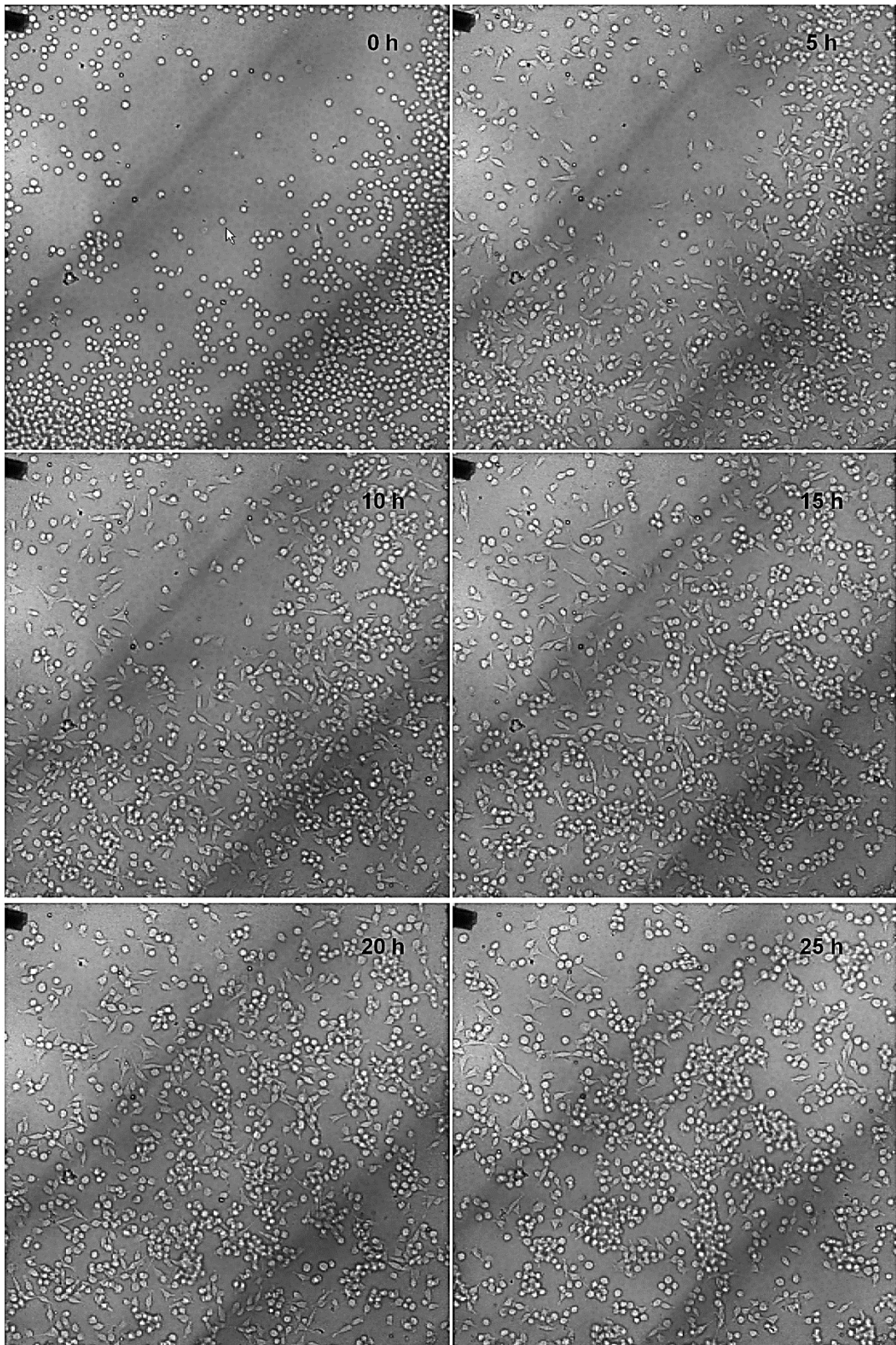


**Figure 5.4.7** Selected shadow images sequence of the L929 cell culture harvesting operation in the all-in-one microsystem after cells have been culture for 20 hours. The cell culture is incubated with Trypsin (EDTA) solution statically for 3 minutes. Since the time point 180 second, cells are washed and then flushed by the PBS solution at 6 ml/h.

### **5.4.5 3D cell culture and time-lapse imaging by the all-in-one microsystem**

3D cell clusters are successfully formed and the dynamic process is monitored by this all-in-one microsystem. The time-lapse imaging of the cell culture is captured every 1 minute as shown in Figure 5.4.8. The cells behavior during the aggregates-forming process can also be checked in the time-lapse video. Because of the long “depth of focus” in the “very-near field” shadow imaging method, the stacking process of cells can be recorded. At different heights, cells are presented with different contrasts in the “very-near field” shadow image. This diffraction effect captured by the “very-near field” shadow imaging is intuitive and convenient for the operator to judge the distribution of cells at different heights away from the bottom. The stacked or over-layered cells colony is presented as blurred appearance compared to the cells monolayer on the bottom window. Since the time point 20-hour, more and more colonies are formed and their volumes increase gradually. Within 45 hours, five 3D clusters of L929 cells have been obtained with lateral diameters of up to 150  $\mu\text{m}$ .



## 5. Results

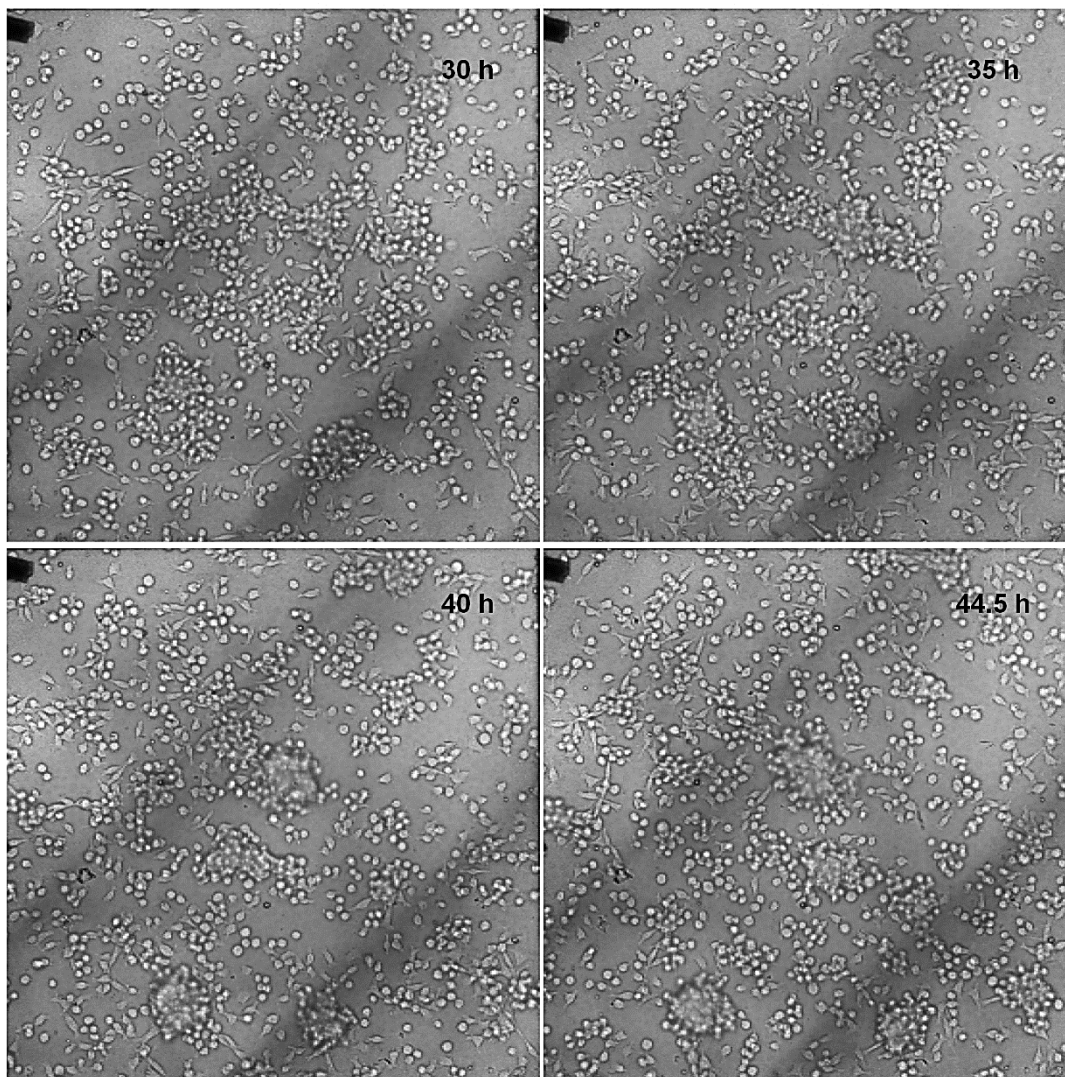


**Figure 5.4.8** The dynamic process of forming 3D cell clusters. Selected shadow images sequence of high concentrated L929 cells cultured and imaged by the all-in-one microsystem for 45 hours under a constant flow rate of  $5 \mu\text{l/h}$  from the cell seeding. There is no pre-treatment with serum or medium for the culture substrate in order to reduce cell adhesion on the bottom. The optical window size is  $1 \text{ mm} \times 1 \text{ mm}$ .

## 6 Discussions

In this chapter, achieved results will be discussed and compared with respect to the objectives of the study, the theoretical calculations, and commercial cell culture systems. The discussions will be organized by each technically developed and evaluated system.

### 6.1 “Micro incubator” or a stand-alone microfluidic cell incubating system

The perspective of this “micro incubator” is to transfer the conventional cell culture out of the conventional bulky incubators. Compared to many reported microfluidic cell culture systems using CO<sub>2</sub>-independent HEPES culture medium, the “micro incubator” is designed to deploy conventional culture medium, which is well accepted by the biological communities. The pH value of the preheated culture medium inside the microfluidic system keeps in the range of 7.2–7.4, and no air bubbles appear within a time period of 4 hours without fresh medium inflow. This indicates that the entire microfluidic system is very well sealed from gas and water vapor. The flow rate of the culture medium has been carefully calculated in advance according to the geometry of the micro-scaled culturing vessel and cell consumptions. The shear stress value at the bottom of the micro incubator has been assessed as a function of the microflow. The flow rate range leading to a shear stress below the cell sensible value has been determined. Without using a laboratory incubator, L929 cells and A549 cells are cultured in the “micro incubator” over days. The cell morphology, growth and behavior are observed under a commercial automatic microscope. Time-lapse image sequences show that the cells in culture are healthy and they behave like in conventional culture. The “micro incubator” concept has been achieved and fulfills the objectives.

An advantage of the “micro incubator” over conventional cell culture is that the application profile of a substance or a reagent under test can be better controlled, and cell responses in multiple micro-channels under test can be monitored and compared in parallel. As an example, A549 cell culture in two independent micro-channels respectively with conventional medium and silver nanoparticle dissolved medium are demonstrated by the “micro incubator” microfluidic system. The cell responses to the long-term low

## 6. Discussions

concentration silver nanoparticles have been monitored and synchronically compared with the normal cell culture at each time point.

### 6.2 Compact “desktop” automatic microscope

The imaging quality of the constructed “desktop” microscope has been evaluated by imaging the fluorescent microbeads and FDA stained biological cell cultures under both 20x bright field and fluorescence imaging modes. With a special program scheme, the “desktop” automatic microscope is capable of taking alternating bright field and fluorescent images at each testing point. This function is usually not included in a commercial automatic microscope. Instead, in order to have both cell morphology and fluorescence, a low intensity bright field illumination has to be kept on when taking the fluorescence imaging.

Compared to the commercial automatic microscope, the footprint of the finished imaging device is only of an A4 paper size, and the price for all the components is less than 7000 Euros.

The stability of the automation is evaluated by moving the sample plate and imaging two testing points spaced with 28 mm on a microchip. The reproducibility of both the lateral and vertical positions is very good during the 24 hour-continuous time-lapse imaging operations. Its vertical stability is even better compared to the commercial automatic microscope with an auto-focusing function used for the described experiments. Therefore, the compact “desktop” automatic microscope can be used for the long-term time-lapse imaging of multiple cell cultures under both bright field and fluorescence microscopy modes. The objective has been fulfilled.

### 6.3 Real-time chip-level lensless microscope

The best achievable optical resolution of the lensless shadow imaging is the digital resolution, which amounts to double pixel pitches of the image sensor. A distance between the object and the image sensor will also have an influence on the resolution. The best digital resolution of the image sensors on the market is about 2—3  $\mu\text{m}$ . In this study, the image forming mechanism of the lensless shadow imaging has been investigated and characterized when the distance between the object and the image sensor is in the “very-near field” range, which has not been theoretically addressed or experimentally demonstrated in other lensless imaging systems. According to the calculations, when an object is spaced with a transparent biocompatible material with a thickness less than 12  $\mu\text{m}$  or 5  $\mu\text{m}$  from the image sensor plane, the optical resolution of the shadow image will be better than 3  $\mu\text{m}$  or 2  $\mu\text{m}$  respectively. Therefore, interfacing cell culture by a microchip fabricated with a transparent bottom layer of several micrometers will not affect the overall resolution.

The disposable silicon-based microchip with a 1  $\mu\text{m}$  thick transparent  $\text{Si}_3\text{N}_4$  bottom has effectively and conveniently interfaced the cell culture onto the image sensor surface in the “very-near field”. The developed microchip adapter and the lid guarantees an easy handling of the microchip and the cell culture inside, e.g. when placing it inside a conventional incubator or when bring it in a good contact with the imaging sensor surface.

The lensless “very-near field” shadow imaging module is very practical compared to other reported lensless imaging configurations in the cell culture related experiments and operations. The silicon-based microchip is made of biocompatible materials suitable for cell cultures. Compared to the image sensor it can be fabricated at low cost and is obviously disposable. Therefore, the costly image sensor can be repeatedly used. This approach leads to a much lower price per test compared to other reported lensless imaging systems which perform the cell culture directly on the image sensor.

There are already many reports and demonstrations about lensless or lensfree imaging of cells. But in this study, both cell imaging and practical cell culture operations are considered at the same time. Biocompatibility and disposability for cell culture are carefully considered when developing this new lensless imaging configuration. Cell culture and cell-based assays often require flexible imaging capabilities for cell morphology visualization as well as colorimetric or fluorescent characterization down to single cells level. Compare to the high-resolution lensfree computational imaging, the real-time low-resolution imaging is more favorable for the practical operations, including not only the long-term time-lapse imaging of individual cells, but also the fast cell processing and microfluidic operations on microfluidic systems.

The “very-near field” shadow imaging configuration is successfully established in theory and evaluated experimentally by imaging the cultured biological cells at different growing stages without any imaging reconstruction process and delay. The imaging quality has been shown comparable with a 4x optical microscopy. Therefore, this “very-near field” shadow imaging configuration can be considered as a lensless chip-level real-time microscopy module suitable for applications in cell biology and point-of-use diagnosis.

#### **6.4 All-in-one cell culturing-imaging microsystem:**

The real-time chip-level lensless microscope and the “micro incubator” together make the realization of an all-in-one microsystem for cell culturing and real-time microscopy possible without using any conventional bulky incubator or optical microscope. A stand-alone microfluidic system has been developed based on the former disposable microchip fabricated for sustaining cell culture under the lensless imaging. An additional temperature control system is developed and is experimentally tested for its stability over 48 hours in the room environment. The “micro incubator” has been successfully constructed on top of the lensless “very-near field” shadow imaging configuration. The all-in-one microsystem has been established and characterized.

## 6. Discussions

Since the temperature of the working image sensor is at about 32°, the temperature control for mammalian cell cultures in the experiment is regulated around 37°C only with heating elements. It should be possible to control the temperature of the cell culture in the range of 4–45°C if integrating both heating and cooling elements onto the image sensor module. In this temperature range, all the animal cell types could be cultured in the optimal condition. This possibility makes the all-one microsystem much more flexible than the conventional large incubators that are optimized only at one temperature for example at 37°C.

For the all-in-one microsystem, dual-channel microchips are also available in favor of the comparison of cell responses under two different testing conditions at the same pace. The all-in-one microsystem can steadily fulfill the basic requirements of the complete cell culture operations and related experiments. It is competitive to the commercial live cell imaging system but with a much lower price and much smaller size.

Compared to the commercial live cell imaging system, there is no confinement from the climate box to the microfluidic operation. A dark room is also not required. No matter if in a lab or in the field, cells inside the interactive platform can be processed and characterized under real-time observation. This can be very intuitive and very convenient for the operators.

## 6.5 Outlooks of the study

If there would be more time and money for this study, the developments could be further improved in two directions:

### 6.5.1 Engineering works to the single all-in-one cell culture-microscopy device

Since the experimental setup in this study is still in the stage of a proof-of-concept, a lot of engineering and developmental work is still required to make a real robust handheld device. In the future, a compact cooler could be combined with the heating elements on the chip carrier of the image sensor module so that different types of animal cells could be cultured in the microsystem. The microchip could be re-designed and fabricated with a bigger transparent bottom for imaging more cells at the same time. A secured plug-and-play interface between the microchip and microfluidics could be designed in favor of an easy changing of the microchip sustaining the cell culture. All the physical components should be organized compactly into one housing as a compact device. A unified controller with memory cards would be developed for the image sensor, LED illuminations, micro valves and the syringe pump. In this way, the handheld device could be independently working without a computer. An integrated wireless communication module would be preferred for this all-in-one device, so that the configuration, manipulation and data

transfer could be realized from remote anytime anywhere to facilitate a more flexible and efficient working style for the operators.

### **6.5.2 Realization of an all-in-one cell culture-microscopy array-formed instrument**

Another direction for the development of the all-in-one cell culture-microscopy microsystem could in the high throughput operations of cell culture and cell-based assays. For the primary cell-based screening, many cell cultures and tests are required to be performed in parallel. The small field of view with serial mechanical scanning operations of the standard optical microscope limits the throughput, speed and stability of testing for cell cultures. Moreover, the automatic microscope is expensive and it is not very likely for a lab to employ multiple microscopes in parallel for the testing. Since by the “all-in-one” concept, each cell culture is equipped with a chip-level microscopy, multiple inexpensive and compact all-in-one cell culture-microscopy microsystems could be configured in array format to meet the high throughput demand. By each culture-microscopy “unit”, the flow rate, the temperature and the imaging type could be flexibly configured for different types of animal cells under different tests.

The array format concept should be realized by the current state of technologies, including the development of microfluidic networks and the electronic connection and control of multiple image sensors. The engineering work for the array-formed instrument also should include the physical design and a proper arrangement of all the components interlayered and interweaved together. Modular designs and secured interfaces could be the simple philosophy for the physical design.

## 7 Conclusions

In this thesis, an all-in-one cell culturing-imaging microsystem has been developed, characterized and evaluated by practical biological cell cultures and operations. The overall size of the all-in-one cell culture-microscopy system is within 40 mm x 40 mm x 50 mm and the whole system is running in the room atmosphere without using any optical lens or incubator. Along the roadmap of the study, concepts of a “micro incubator”, a compact “desktop” automatic microscope and a chip-level lensless microscope have been investigated in order to fulfill the final goal of the study.

The “micro incubator” or stand-alone microfluidic cell culture system is designed as a gas- and vapor-tight microfluidic system with a continuous flow of incubator conditioned culture medium. The microfluidic system is constructed based on a commercially available micro-channel slide and an external transparent hot plate for microscopy. The theoretically calculated optimal flow rate is 10  $\mu\text{l}/\text{h}$  in consideration of the nutrients, oxygen supply, shear stress and micro-channel geometry. L929 cells are successfully cultured for 65 hours at this flow rate. The estimated doubling time of the cell culture is 24 hours, which is consistent with that of the conventional cell culture. The cells are characterized by time-lapse 10x microscopy imaging under an automatic microscope in the room atmosphere. In two independent channels, A549 cells control and A549 cells flown with 10  $\mu\text{g}/\text{ml}$  10 nm silver nanoparticles in the medium are cultured for 54 hours. Cells under both conditions are imaged at the same time and their behavior can be easily compared.

Based on the classic infinite optical system, a compact “desktop” automatic microscope with the footprint of an A4 paper size has been established. It is dedicated to the stable long-term multi-channel time-lapse imaging of cell culture. The constructed compact “desktop” automated microscope is capable of taking alternating bright field and fluorescence images at each testing points under white LED and high-power blue LED illuminations. The imaging quality with a 20x LWD objective has been tested with fluorescent microbeads and FDA stained L929 and A549 cell culture. The stability and repeatability in focusing and scanning accuracy of the system have been proven for at least 24 hours. The system could be an inexpensive but also practical tool that costs 5,000—10,000 Euros depending on the selection of camera, illumination, and objective. If the fluorescence imaging of GFP cells is required, a more powerful fluorescent illumination must be developed

Based on the lensless imaging method, a much more compact chip-level real-time lensless microscopy module with a disposable microchip for sustaining cell cultures in a biocompatible environment has been developed. The disposable microchip for cell culture is composed of a polymer microfluidic interface and a silicon micro-cavity chip with a 1  $\mu\text{m}$  thick 1 mm x 1 mm transparent  $\text{Si}_3\text{N}_4$  bottom membrane, which is directly placed onto the image sensor surface. Under the collimated LED illumination, the optical resolution of the lensless “very-near field” imaging is only dependent on the digital resolution of the image sensor, which amounts to 3.5  $\mu\text{m}$  (double pixel pitches). A 4  $\mu\text{m}$  thick protective SU-8 layer and an additional 4.5  $\mu\text{m}$  thick long pass interference filter are deposited for the fluorescence imaging. The fluorescence collection efficiency is much higher than that of the corresponding 4x optical microscope, and a common blue LED is surely enough for the excitation. The expansion of the “very near-field” fluorescence imaging is about 50%. The resolution is further improved by combining the shadow image with the fluorescent image. Adjacent spreading cells with fluorescence can be distinguished. The imaging capability of the system has been verified by the real-time imaging of morphologies of different cell cultures, as well as colorimetric and fluorescent staining of cell cultures. The lensless “very-near field” shadow imaging requires no imaging reconstruction process or waiting time. It is really an imaging method that is “what you see is what you get”. The imaging quality has been shown consistent and comparable to a 4x optical microscopy.

The “very-near field” shadow imaging module and the “micro incubator” conception together make the realization of an all-in-one cell culture and microscopy microsystem possible without using any conventional bulky incubator or optical microscope. According to the “micro incubator” conception, a 3  $\mu\text{m}$  thick Parylene C layer is coated onto the entire surface of the PDMS/Si microfluidic chips to prevent gas and vapor permeability. Eight 1 Ohm resistors and a temperature sensor are directly glued on the imager’s chip carrier for the direct heating of the cell culture on the chip. The close-looped temperature control system has been proven as stable as a commercial incubator with  $\pm 0.2^\circ\text{C}$  variation day and night. Theoretically, different temperatures optimized for other animal cells culture can be realized by the same principle. The overall size of the all-in-one cell culture-microscopy system is within 40 mm x 40 mm x 50 mm and the whole system is running in the room atmosphere without using any lens or incubator. Cell cultures in both monolayer and 3D clusters are successfully cultured, processed and monitored. The fast operation process such as cell loading, staining and passaging have also been carried out and monitored in real-time by this interactive and intuitive platform. The all-in-one microsystem can fulfill the complete culturing operations for animal cells. Therefore, it could be further developed and engineered into a handheld cell culture device providing biologists a more flexible and efficient working style. Further, such cell culture-microscopy “units” could be arranged into an array format for cell cultures and cell-based assays regarding high throughput and flexibility.

## References

- [1] Bertrand Pain, M. E. Clark, M. Shen, H. Nakazawa, M. Sakurai, J. Samarut and R. J. Etches, "Long-term in vitro culture and characterization of avian embryonic stem cells with multiple morphogenetic potentialities", *Development*, Vol. 122, No. 8, 2339-2348, 1996.
- [2] Li Zhang, Yuanxing Zhang, Chun Yan and Jutang Yu, "The Culture of Chicken Embryo Fibroblast Cells on Microcarriers to Produce Infectious Bursal Disease Virus", *Applied Biochemistry and Biotechnology*, Vol. 62, 291-302, 1997.
- [3] Stephanie R. Dukovcic, Janine R. Hutchison, Janine E. Trempy, "Conservation of the chromatophore pigment response", *Journal of Applied Toxicology*, Vol. 30, Issue 6, 574-581, 2010.
- [4] Katsuyuki Kadoi, "Establishment of two chicken embryonic cell lines in a newly developed nutrient medium", *New Microbiologica*, Vol. 33, No. 4, 393-397, 2010.
- [5] John L. Fryer, C.N. Lannan, "Three decades of fish cell culture: a current listing of cell lines derived from fishes", *Journal of tissue culture method*, Vol. 16, Issue 2, 87-94, 1994.
- [6] Dwight E. Lynn, "Methods for Maintaining Insect Cell Cultures", *Journal of Insect Science*, Vol. 2, No. 9, 1-6, 2002.
- [7] Jamil El-Ali, Peter K. Sorger and Klavs F. Jensen, "Cell on chips", *Nature*, Vol. 442, 403-411, 2006.
- [8] Edmond W. K. Young, David J. Beebe, "Fundamentals of microfluidic cell culture in controlled microenvironments", *Chemical Society Reviews*, Vol.39, No.3, 1036-1048, 2010.
- [9] Frank B. Myers and Luke P. Lee, "Innovations in optical microfluidic technologies for point-of-care diagnostics", *Lab on a Chip*, Issue 12, 2015-2031, 2008.
- [10] Frances S. Ligler, "A Perspective on Optical Biosensors and Integrated Sensor Systems", *Analytical Chemistry*, Vol. 81, Issue 2, 519-526, 2009.
- [11] Matthias Mehling and Savas Tay, "Microfluidic cell culture", *Current Opinion in Biotechnology*, Issue 25, 95-102, 2014.
- [12] Elisabetta Primiceri, Maria Serena Chiriaco, Ross Rinaldi and Giuseppe Maruccio, "Cell chips as new tools for cell biology — results, perspectives and opportunities", *Lab on Chip*, Issue 19, 3789-3802, 2013.
- [13] Zoltan Göröcs and Aydogan Ozcan, "On-chip Biomedical Imaging", *IEEE Reviews on Biomedical Engineering*, 6, 29-46, 2013.

- [14] Alon Greenbaum, Wei Luo, Ting-Wei Su, Zoltan Göröcs, Liang Xue, Serhan O Isikman, Ahmet F Coskun, Onur Mudanyali and Aydogan Ozcan, "Imaging without lenses: achievements and remaining challenges of wide-field on-chip microscopy", *Natural Methods*, 9(9), 889-895, 2012.
- [15] Max Born and Emil Wolf, *Principles of Optics*, Cambridge University Press, UK, 1999.
- [16] Honghao Ji, David Sander, Alfred Haas and Pamela A. Abshire, "Contact Imaging: Simulation and Experiment", *IEEE TRANSACTIONS ON CIRCUITS AND SYSTEMS— I: REGULAR PAPERS*, Vol. 54, No. 8, 2007.
- [17] Alon Greenbaum, Alborz Feizi, Najva Akbari, and Aydogan Ozcan, "Wide-field computational color imaging using pixel super-resolved on-chip microscopy", *OPTICS EXPRESS*, Vol. 21, No. 10, 12469-12483, 2013.
- [18] Shuo Pang, Xiquan Cui, John DeModena, Ying Ming Wang, Paul Sternberg and Changhui Yang, "Implementation of a color-capable optofluidic microscope on a RGB CMOS color sensor chip substrate", *Lab Chip*, 10, 411-414, 2010.
- [19] Seung Ah Lee, Jessey Erath, Guoan Zheng, Xiaoze Ou, Phil Willems, Daniel Eichinger, "Imaging and Identification of Waterborne Parasites Using a Chip-Scale Microscope", *PLOS ONE*, Vol. 9, Issue 2, 1-5, 2014.
- [20] Ping Wang, Qingjun Liu, *Cell Based-Biosensors: Principles and Applications*, ISBN-13: 978-1-59693-439-9, Artech House, Boston/London, 2010.
- [21] Pratik Banerjee, Briana Franz, Arun K. Bhunia, Chapter 2: Mammalian cells-based sensor system, *Advances in Biochemical Engineering/Biotechnology: Whole Cell Sensing Systems 1*, Vol. 117, 21-55, 2010.
- [22] Paul A. Clemons, W. Frank An, Nicola J. Tolliday and Bridget K. Wagner, "Cell-Based Assays for High-Throughput Screening," *METHODS IN MOLECULAR BIOLOGY*, 486, 97-107, 2009.
- [23] *SIGMA: Fundamental Techniques in Cell Culture Laboratory Handbook 2nd Edition*.
- [24] Zigler JS, Lepe-Zuniga JL, Vistica B, Gery, "Analysis of the cytotoxic effects of light-exposed HEPES-containing culture medium", *In Vitro Cellular & Developmental Biology*, 21(5), 282-7, 1985.
- [25] Martin Oheim, "High-throughput microscopy must re-invent the microscope rather than speed up its functions", *British Journal of Pharmacology*, 152, 1-4, 2007.
- [26] Sungbo Cho, Sybille Becker, Hagen von Briesen, Hagen Thielecke, "Impedance monitoring of herpes simplex virus-induced cytopathic effect in Vero cells", *Sensors and Actuators B*, Vol. 123, Issue 2, 978-982, 2007.
- [27] Chang K. Choi, Chuck H. Margraves, Seung I. Jun, Anthony E. English, Philip D. Rack and Kenneth D. Kihm, "Opto-Electric Cellular Biosensor Using Optically Transparent Indium Tin Oxide (ITO) Electrodes", *Sensors*, 8(5), 3257-3270, 2008.
- [28] David J. Stephens and Victoria J. Allan, "Light Microscopy Techniques for Live Cell Imaging", *SCIENCE*, Vol. 300, 82-86, 2003.

- [29] Awanish Kumar and Dharm Pal, "Green fluorescent protein and their applications in advance research", *Journal of Research in Engineering and Applied Sciences*, Vol.1, Issue 1, 42-46, 2016.
- [30] Ben N. G. Giepmans, Stephen R. Adams, Mark H. Ellisman, Roger Y. Tsien, "The Fluorescent Toolbox for Assessing Protein Location and Function", *SCIENCE*, Vol. 312, 217-224, 2006.
- [31] Hongmei Yu, Ivar Meyvantsson, Irina A. Shkelab and David J. Beebe, "Diffusion dependent cell behavior in microenvironments", *Lab on Chip*, Issue 5, 2005, 1089–1095, 2005.
- [32] Clinton B Maddox, Lynn Rasmussen, and E. Lucile White, "Adapting Cell-Based Assays to the High Throughput Screening Platform: Problems Encountered and Lessons Learned", *JALA (Charlottesville, Va.)*, 13(3), 168–173, 2008.
- [33] OLYMPUS: ZDC-IMAGE live cell fluorescence imaging system specification.
- [34] Hiroshi Yamamoto, Masaki Harada, Ayako Michida, Mikio Houjou, Yassuhiko Yokoi, Akira Sakaguchi, Hajime Ohgushi, Akira Oshima and Sadami Tsutsumi, "Development of cell culture system equipped with automated observation function", *Journal of Biomechanical science and engineering*, Vol.2 No.3, 127-137, 2007.
- [35] Jamil El-Ali, Peter K. Sorger, Klavs F. Jensen, "Cells on chips", *Nature*, 442, 403-411, 2006.
- [36] Johan Pihl, Jon Sinclair, Mattias Karlsson, Owe Orwar, "Microfluidics for cell-based assays", *Materials Today*, Vol. 8, Issue 12, 46-51, 2005.
- [37] Petra S. Dittich, Andreas Manz, "Lab-on-a-chip: microfluidics in drug discovery", *Nature Reviews Drug Discovery*, 5, 210-218, 2006.
- [38] Hamish C. Hunt, James S. Wilkinson, "Optofluidic integration for microanalysis", *Microfluidics and Nanofluidics*, 4, 53-79, 2008.
- [39] Leslie Y. Yeo, Hsueh-Chia Chang, Peggy P. Y. Chan, and James R. Friend, "Microfluidic Devices for Bioapplications", *Small*, 7, No.1, 12-48, 2011.
- [40] Rafael Gomez-Sjoeberg, Anne A. Leyrat, Dana M. Pirone, Christopher S. Chen, and Stephen R. Quake, "Versatile, Fully Automated, Microfluidic Cell Culture System", *Analytical Chemistry*, 79, 8557-8563, 2007.
- [41] Paul J. Huang, Philip J. Lee, Poorya Sabounchi, Nima Aghdam, Robert Lin and Luke P. Lee, "A novel high aspect ratio microfluidic design to provide a stable and uniform microenvironment for cell growth in a high throughput mammalian cell culture array", *Lab on a Chip*, 5, 44-48, 2005.
- [42] Sarunas Petronis, Michael Stangegaard, Claus Bo Vöge Christensen, and Martin Dufva, "Transparent polymeric cell culture chip with integrated temperature control and uniform media perfusion", *BioTechniques*, 40(3), 368-376, 2006.
- [43] Michael Stangegaard, S. Petronis, A. M. Jørgensen, C. B. V. Christensen and M. Dufva, "A biocompatible micro cell culture chamber ( $\mu$ CCC) for the culturing and on-line monitoring of eukaryote cells", *Lab on Chip*, Issue 6, 1045-1051, 2006.
- [44] Chun-Wei Huang and Gwo-Bin Lee, "A microfluidic system for automatic cell culture", *Journal of Micromechanics and Microengineering*, Vol. 17, 1266-1274, 2007.

- [45] Todd M. Squires and Stephen R. Quake, "Microfluidics: Fluid physics at the nanoliter scale", *Reviews of Modern Physics*, 77, 977-1026, 2005.
- [46] Huabing Yin, Xunli Zhang, Nicola Pattrick, Norbert Klauke, Hayley C. Cordingley, Stephen J. Haswell, and Jonathan M. Cooper, "Influence of hydrodynamic conditions on quantitative cellular assays in microfluidic systems", *Analytical Chemistry*, 79, 7139-7144, 2007.
- [47] Amir Manbachi, Shamit Shrivastava, Margherita Cioffi, Bong Geun Chung, Matteo Moretti, Utkan Demirci, Marjo Yliperttula and Ali Khademhosseini, "Microcirculation within grooved substrates regulates cell positioning and cell docking inside microfluidic channels", *Lab on Chip*, Issue 8, 747-754, 2008.
- [48] Sara Lindström, Kiichiroh Mori, Toshiro ohashi, Helene Andersson-Svahn, "A micro-well array device with integrated microfluidic components for enhanced single-cell analysis", *Electrophoresis*, 30, 4166-4171, 2009.
- [49] Tobias Kraus, Elisabeth Verpoorte, Vincent Linder, Wendy Franks, Andreas Hierlemann, Flavio Heer, Sadik Hafizovic, Teruo Fujii, Nico F. de Rooija and Sander Koster, "Characterization of a microfluidic dispensing system for localized stimulation of cellular networks", *Lab on Chip*, Issue 6, 218–229, 2006.
- [50] Ke Liu, Rajasekar Pitchimani, Dana Dang, Keith Bayer, Tyler Harrington, and Dimitri Pappas, "Cell Culture Chip Using Low-Shear Mass Transport", *Langmuir*, 24, 5955-5960, 2008.
- [51] Yonathan Dattner and Orly Yadid-Pecht, "Low light CMOS contact imager with an integrated ploy-acrylic emission filter for fluorescence detection", *Sensors*, Vol. 10, Issue 5, 5014-5027, 2010.
- [52] Dirk Lange, Christopher W. Storment, Catharine A. Conley, Gregory T. A. Kovacs, "A microfluidic shadow imaging system for the study of the nematode *Caenorhabditis elegans* in space", *Sensors and Actuators B*, 107, 904-914, 2005.
- [53] Yoshiaki Mizukami, Daniel Rajiniak, Akiko Rajiniak, Masatoshi Nishimura, "A novel microchip for capillary electrophoresis with acrylic microchannel fabricated on photosensor array", *Sensors and Actuators B*, 81, 202-209, 2002.
- [54] Yahya Hosseini, Karan V.I.S. Kaler, "Integrated CMOS optical sensor for cell detection and analysis", *Sensors and Actuators A*, 157, 1-8, 2010.
- [55] SangJun Moon, hasan Onur Keles, Aydogan Ozcan, Ali Khademhosseini, Edward haggstorm, Daniel Kuritzkes, Utkan Demirci, "Integrating microfluidics and lensless imaging for point-of-care testing", *Biosensors and Bioelectronics*, 24, 3208-3214, 2009.
- [56] Xiaohui Zhang, Imran Khimji, Umut Atakan Gurkan, Hooman Safaee, Paolo Nicolas Catalano, Hsan Onur Keles, Emre Kayaalp and Utkan Demirci, "Lensless imaging for simultaneous microfluidic sperm monitoring and sorting", *Lab on Chip*, Issue 11, 2535-2540, 2011.
- [57] Marianna Beiderman, Terence Tam, Alexander Fish, Graham A. Jullien and Orly Yadid-Pecht, "A low-light CMOS contact imager with an emission filter for biosensing applications", *IEEE Transactions on biomedical circuits and systems*, Vol. 2, No. 3, 2008.

- [58] Honghao Ji, David Sander, Alfred Haas, Pamela A. Abshire, "A CMOS contact imager for locating individual cells", IEEE International Symposium on Circuits and Systems ISCAS, 3357-3360, 2006.
- [59] Honghao Ji, Pamela A. Abshire, "CMOS contact imager for monitoring cultured cells", IEEE International Symposium on Circuits and Systems, Vol. 4, 3491-3494, 2005.
- [60] Ulrich Ch. Fischer and Hans P. Zingsheim, "Submicroscopic pattern replication with visible light", Journal of Vacuum Science & Technology, Vol. 19, Issue 4, 881-885, 1981.
- [61] Ulrich Ch. Fischer and Hans P. Zingsheim, "Submicroscopic contact imaging with visible light by energy transfer", Applied Physics Letters Vol. 40, Issue 3, 195-197, 1982.
- [62] Guoan Zheng, Seung Ah Lee, Yaron Antebi, Michael B. Elowitz, and Changhui Yang, "The ePetri dish, an on-chip cell imaging platform based on subpixel perspective sweeping microscopy (SPSM)", Proceedings of National Academy of Science (PNAS), Vol. 108 No. 41, 16889-16894, 2011.
- [63] Seung Ah Lee, Xiaoze Ou, J. Eugene Lee, and Changhuei Yang, "Chip-scale fluorescence microscope based on a silo-filter complementary metal-oxide semiconductor image sensor", OPTICS LETTERS, Vol. 38, No. 11, 1817-1819, 2013.
- [64] Chao Han and Changhuei Yang, "Viral plaque analysis on a wide field-of-view, time-lapse, on-chip imaging platform", Analyst, Issue 15, No. 139, 3727-3734, 2014.
- [65] Xiquan Cui, Lap Man Lee, Xin Heng, Weiwei Zhong, Paul W. Sternberg, Demetri Psaltis, and Changhui Yang, "Lensless high-resolution on-chip optofluidic microscopes for Caenorhabditis elegans and cell imaging", Proceedings of National Academy of Science (PNAS), Vol. 105, No. 31, 10670-10675, 2008.
- [66] Jigang Wu, Xiquan Cui, Lap Man Lee and Changhui Yang, "The application of Fresnel zone plate based projection in optofluidic microscopy", Optical Express, Vol.16, No.20, 15595-15602, 2008.
- [67] Waheb Bishara, Uzair Sikora, Onur Mudanyali, Ting-Wei Su, Oguzhan Yaglidere, Shirley Luckhart and Aydogan Ozcan, "Holographic pixel super-resolution in portable lensless on-chip microscopy using a fiber-optic array", Lab on Chip, Issue 11, 1276-1279, 2011.
- [68] Aydogan Ozcan, "Mobile phones democratize and cultivate next-generation imaging, diagnostics and measurement tools", Lab Chip Frontier, DOI: 10.1039/c4lc00010b, 2014.
- [69] Ahmet F Coskun, Aydogan Ozcan, "Computational imaging, sensing and diagnostics for global health applications", Current Opinion in Biotechnology, Vol. 25, 8-16, 2013.
- [70] Seung Ah Lee 2 and Changhuei Yang, "A smartphone-based chip-scale microscope using ambient illumination", Lab Chip, 14, 3056-3063, 2014.
- [71] Ritu Raj Singh, Derek Ho, Alireza Nilchi, Glenn Gulak, Patrick Yau, and Roman Genov, "A CMOS/thin-film fluorescence contact imaging microsystem for DNA

analysis," IEEE TRANSACTIONS ON CIRCUITS AND SYSTEMS—I: REGULAR PAPERS, Vol. 57, No. 5, 1029-1038, 2010.

- [72] Honghao Ji 2, Marc Dandin, Pamela Abshire, "Integrated fluorescence sensing for lab-on-a-chip devices," Proc. IEEE/NLM Life Science Systems and Applications Workshop, 1-2, 2006.
- [73] Claude Weisbuch, M. Rattier, L. Martinelli, H. Choumane, J.-C. Avarre, Y. Marcy, G. Cerovic, M.-L. Miramon, G. O. Reymond, H. Benisty, "Towards portable, real-time, integrated fluorescence microarray diagnostics tools," ITBM-RBM (Journal), Vol. 28, 216–223, 2007.
- [74] Khaled Salama, Helmy Eltoukhy, Arjang Hassibi, Abbas El Gamal, "Modeling and simulation of luminescence detection platforms," Biosensors and Bioelectronics, Vol. 19, 1377–1386, 2004.
- [75] Marc Dandin, Pamela Abshire and Elisabeth Smela, "Optical filtering technologies for integrated fluorescence sensors," Lab Chip, 7, 955–977, 2007.
- [76] Mark L. Adams, Markus Enzelberger, Srephen Quake, Axel Scherer, "Microfluidic integration on detector arrays for absorption and fluorescence micro-spectrometers," Sensors and Actuators A, Vol. 104, 25-31, 2003.
- [77] Charles Richard, Alan Renaudin, Vincent Aimez and Paul G. Charette, "An integrated hybrid interference and absorption filter for fluorescence detection in lab-on-a-chip devices," Lab Chip, 9, 1371–1376, 2009.
- [78] Oliver Hofmann, Xuhua Wang, Alastair Cornwell, Stephen Beecher, Amal Raja, Donal D. C. Bradley, Andrew J. deMello and John C. deMello, "Monolithically integrated dye-doped PDMS long-pass filters for disposable on-chip fluorescence detection," Lab Chip, 6, 981–987, 2006.
- [79] Ahmet F. Coskun, Ikbal Sencan, Ting-Wei Su, and Aydogan Ozcan, "Lensless wide-field fluorescent imaging on a chip using compressive decoding of sparse objects," OPTICS EXPRESS Vol. 18, No. 10, 10510-10523, 2010.
- [80] Ansuman Banerjee, Andrea Pais, Ian Papautsky, and David Klotzkin, "A polarization isolation method for high-sensitivity, low-cost on-chip fluorescence detection for microfluidic lab-on-a-chip," IEEE SENSORS JOURNAL, Vol. 8, No. 5, 621-627, 2008.
- [81] Georg J. Ockenfuss, Robert B. Sargent, "Optical interference filters for fluorescence spectroscopy and microscopy," BIOPHOTONICS INTERNATIONAL Vol. 14, No. 8, 34-37, 2007.
- [82] Ikbal Sencan, Ahmet F. Coskun, Uzair Sikora & Aydogan Ozcan, "Spectral Demultiplexing in Holographic and Fluorescent On-chip Microscopy", Scientific Reports, Vol. 4, No. 3760, 1-9, 2014.
- [83] Shuo Pang, Chao Han, Jesse Erath, Ana Rodriguez, and Changhui Yang, "Wide field-of-view Talbot grid-based microscopy for multicolor fluorescence imaging", Optics Express, Vol. 21, Issue 12, 14555-14565, 2013.
- [84] Zbigniew Darzynkiewicz, Elena Holden, Alberto Orfao, William Telford, Donald Wlodkovic, Recent Advances in Cytometry, Part A, Instrumentation, Methods, fifth edition, Elsevier Academic Press, ISBN:9780123749123, USA, 2011.

- [85] Jared W. Allen, Salman R. Khetani, and Sangeeta N. Bhatia, "In vitro zonation and toxicity in a hepatocyte Bioreactor", *Toxicological Sciences*, Vol. 84, 110-119, 2005.
- [86] Johnson Mark, André Gerald, Chavarie Claude, Archambault Jacques, "Oxygen transfer rates in a mammalian cell culture bioreactor equipped with a cell-lift impeller", *Biotechnology and Bioengineering*, Vol. 35, Issue 1, 43-49, 1990.
- [87] Glenn M. Walker, Henry C. Zeringue and Davide J. Beebe, "Microenvironment design considerations for cellular scale studies", *Lab on a Chip*, 4, 91-97, 2004.
- [88] William. M. Deen, *Analysis of transport phenomena*, Oxford University Press, New York, 1998.
- [89] Natanel Korin, Avishay Bransky, Uri Dinnar and Shulamit Levenberg, "A parametric study of human fibroblasts culture in a microchannel bioreactor", *Lab on Chip*, Issue7, 611-617, 2007.
- [90] Donald P. Gaver 3rd, and Stephanie M. Kute, "A Theoretical Model Study of the Influence of Fluid Stresses on a Cell Adhering to a Microchannel Wall", *Biophysical Journal*, Vol. 75, 721-733, 1998.
- [91] Masako Sugihara-seki, "Flow around cells adherent to a microvessel wall III. Effects of neighboring cells in channel flow", *JSME International Journal, Series C*, Vol. 44, No. 4, 2001.
- [92] Tomasz S. Tkaczyk, *Field Guide to Microscopy*, SPIE Field Guides, Volume FG13, John E. Greivenkamp, Series Editor, ISBN: 9780819472465, SPIE PRESS, Bellingham, Washington USA, 2009.
- [93] Nikon MicroscopyU: The source for microscopy education, <http://www.microscopyu.com>.
- [94] ZEISS Microscopy Online Campus: Education in Microscopy and Digital Imaging, <http://zeiss-campus.magnet.fsu.edu/tutorials>.
- [95] Min Gu, *Advanced Optical Imaging*, ISBN: 3540662626, Springer-Verlag Berling Heidelberg, 2000.
- [96] Marc J. Madou, *Fundamentals of microfabrication: the science of miniaturization*, 2nd ed., ISBN: 0849308267, CRC Press LLC, US, 2002.
- [97] Stein K. U., Widmann D., "Semiconductor Technologies with Reduced Dimensions, Solid State Circuits Conference", 1976.
- [98] Larry F. Thompson, C. Grant Willson, Murrae J. Bowden, *Introduction to Microlithography*, American Chemical Society, Washington, D.C., 1994.
- [99] Badih El-Kareh, *Fundamentals of Semiconductor Processing Technologies*, ISBN: 0792395344, Kluwer Academic Publishers, US, 2002.
- [100] MEMS Cyclopedia, "SU-8: Thick Photo-Resist for MEMS", <http://memscyclopedia.org/su8.html>, 2013.
- [101] OCG Microelectronic Materials NV, HPR-504 Data Sheet: HPR 500 safer solvent positive resist series.
- [102] Mikhail Polyanskiy, *Refractive Index Database*, <http://refractiveindex.info/>, 2014.

- [103] "Optical system and detector requirements for live-cell imaging", Introduction to Live-cell imaging technique, Nikon MicroscopyU, the source for microscopy education, 2000-2013.
- [104] Joseph Kestin, Mordechai Sokolov and William A. Wakeham, "Viscosity of Liquid Water in the Range -8°C to 150°C." Journal of Physical and Chemical Reference Data, Vol. 7, No. 3, 1978.
- [105] Rutkowski JM, Swartz MA, "A driving force for change: interstitial flow as a morphoregulator", Trends of Cell Biology, Vol. 17, Issue 1, 44-50, 2007.
- [106] Mike Althaus, Roman Bogdan, wolfgang G. Clauss and Martin Fronius, "Mechano-sensitivity of epithelial sodium channels (ENaCs): laminar shear stress increases ion channel open probability", The FASER Journal, Vol. 21, No. 10, 2389-2399, 2007.
- [107] Mortimer Abramowitz, Michael W. Davidson, "Köhler Microscope Illumination", Molecular Expressions website, <http://micro.magnet.fsu.edu/primer/anatomy/kohler.html>, 1998-2005.
- [108] NI Developer Zone "Changing Camera Configuration Programmatically".
- [109] National Instruments Knowledge base 4BFBEIQA: AMD umlti-core/CPU systems can cause unexpected behavior in NI driver software.
- [110] Hagen Thielecke, Thomas Stieglitz, and Hansjoerg Beutel, Till Mtthies, Hans Heinrich Ruf, Joerg-Uwe Meyer, "Fast and Precise Postioning of Single Cells on Planar Electrode Substrates," IEEE Engineering in Medicine and Biology Magazine, Vol. 18, No. 6, 48-52, 1999.
- [111] Young Shik Shin, Keunchang Cho, Sun hee H. Lim, Seok Chung, Sung-Jin Park, Chanil Chung, Dong-chul Han and Jun Keun Chang, "PDMS-based micro PCR chip with Parylene coating", J. Micromech. Microeng., Vol. 13, 768-774, 2003.
- [112] James J. Licari, AvanTeco, Whittier, "Coating materials for electronic applications", Springer, Noves Publications, CA, US, June 2003.
- [113] V&P Scientific Inc., "Parylene properties & characteristics", [http://vp-scientific.com/parylene\\_properties.htm](http://vp-scientific.com/parylene_properties.htm), 2010
- [114] Anda R. Gliga, Sara Skoglund, Inger Odnevall Wallinder, Bengt Fadeel and Hanna L Karlsson, "Size-dependent cytotoxicity of silver nanoparticles in human lung cells: the role of cellular uptake, agglomeration and Ag release", Particle and Fibre Toxicology, Vol. 11, No. 11, 1-17, 2014.
- [115] Shelley R. McRae, Christopher L. Brown and Gillian R. Bushell, "Rapid purification of EGFP, EYFP, and ECFP with high yield and purity", Protein Expression and Purification, Vol. 41, No. 1, 121-127, 2005.
- [116] Iloki Assanga, S. B., Gil-Salido, A. A., Lewis Lujan, L. M., Rosas-Durazo, A., Acosta-Silva, A. L., Rivera-Castaneda, E. G. and Rubio-Pino, J.L., "Cell growth curves for different cell lines and their relationship with biological activities", International Journal for Biotechnology and Molecular Biology Research, Vol. 4, No. 4, 60-70, 2013.
- [117] Para Tech Coating, UK Limited, "What is Parylene", <http://www.Paratechcoating.co.uk/what-is-parylene.asp>, 2010.